Cellular Metabolism in B cells: Roles of AMP-activated Protein Kinase, Glutamine, and Glucose Metabolism in Humoral Immunity

By

Shawna Kailee McLetchie Brookens

Dissertation

Submitted to the Faculty of the

Graduate School of Vanderbilt University

in partial fulfillment of the requirements

for the degree of

DOCTOR OF PHILOSOPHY

in

Cancer Biology

August 31, 2021

Nashville, Tennessee

Approved:

Mentor, Mark R. Boothby, M.D. Ph.D.

Committee Chair, Jeffrey C. Rathmell, Ph.D.

Committee Member, Barbara M. Fingleton, Ph.D.

Committee Member, Mary Philip, M.D. Ph.D.

Committee Member, James W. Thomas, II, M.D.

DEDICATION

This dissertation is dedicated to my parents, Roxanne and Nicholas McLetchie, to my grandmother Ortiz McLetchie, and to my husband, Bradley Brookens, for their unwavering patience, love, and support.

ACKNOWLEDGEMENTS

The initiation and completion of the research thesis project presented in this dissertation would not have been possible without many mentors, family, and friends. I would like to express my gratitude here.

First, I wish to express utmost appreciation and gratitude to my thesis advisor and mentor Mark Boothby MD PhD. He is an excellent example of a rigorous and critical scientist. As a mentor, he was undeniably committed to my success as evident by his constant and thorough feedback on my oral and written skills, which has given me a greater respect for the nuances in science and research. Dr. Boothby struck a fine balance between pushing me to reach my limits while still giving me the freedom to grow in independence. On a personal level, I have appreciated his many anecdotes that he has shared with me, which are sprinkled with many life lessons. I am very thankful to have worked for my doctorate under the guidance of someone who has heightened my resilience and not complained about how messy I keep my bench.

I would like to thank my thesis committee members, who have been positive role models to me as scientists. To Jeff Rathmell PhD, for chairing my committee, setting an excellent example of leadership in the Vanderbilt community, teaching the instrumental classes that introduced me to the Immunometabolism field, and for generously donating the $Gls1^{f/f}$ and $Glut1^{f/f}$ used in Chapter 5. To Barbara Fingleton PhD for her excellent course in Advanced Concepts in Cancer, which greatly increased my confidence in giving presentations, and for her questions and comments during committee meetings, which have forced me to more accurately plot and describe my data. To Mary Philip MD

PhD, who has mastered the unique ability to ask some of the toughest questions and comments, which have led to improvements in the way I conducted experiments, while still remaining very personable and approachable. To Tom Thomas MD, who has been extremely helpful in sharing his plethora of knowledge on B cells and whose suggestions during meetings have given me interesting new directions to follow.

I would like to express sincere gratitude to the members of the Boothby lab who have been crucial to my progress and success. A year prior to my joining the lab, Sung Hoon Cho, PhD made the first observations on the essential role for AMPK in B cell memory, which has been the foundation of my thesis and led to the funding that has partially financially supported me. Dr. Cho has been my go-to to bounce new ideas, perfect techniques, help solve problems, and even just to laugh/vent about life. His commitment to solving problems and reliable kind and positive temperament is one I have always aspired to emulate. Ariel Raybuck's ability to wear many hats is unmatched as she always took the initiative to address problems both experimentally and administrative-related. I will be forever grateful for her willingness to conquer and divide long harvest days with the lung inflammation studies as well as other helpful inputs she has suggested along the way. Discussions with Paulo Basso PhD, a visiting graduate student from Brazil, were integral for me to build confidence in myself and in my data. Dr. Basso was fun to bounce ideas off of and extremely generous with his time as he was always offering help with experimental harvest days. Jennie Hamilton, PhD and Jessica Li have laid down a lot of the foundational groundwork for the glutaminase studies and have both been a joy to discuss both science and non-science topics. I am

also grateful to Edna Kemboi, who was an excellent teacher in training me how to run a Seahorse assay and whose personality made everyday positive and fun.

In addition to the Boothby lab members, a lot of work in this thesis would not be possible without the help of Core personnel and Vanderbilt staff. Lan Wu MD has been key to maintaining the FACS BD Cantos machine, which I have used in almost every experiment. The Flow Cytometry Shared Resource Core assisted in the occasional flow sort. Jenny Schafer PhD in the Cell Imaging Shared Resource Core, Marjan Rafat PhD, and Anne Kenworthy PhD have all extended help to enable me to prepare quality immunofluorescent images. I am appreciative of the work and the clear communication I receive from the Animal Care Facility. I am grateful to many of the custodial and delivery staff who joked with me during the day and in the evenings, and without knowing it, greatly improved my morale and kept me from dropping everything and going home towards the end of long experimental days.

I have immense gratitude to mentor Janice Blum PhD at Indiana University Medical School who has contributed to my previous scientific development. I am extremely lucky that she took a chance on a Middle School science teacher with virtually zero research experience into her lab. It is because of her attentiveness and my experiences with her two post doctoral fellows, Liliana Pérez PhD and Crystal Walline PhD that I was motivated to pursue a PhD in the biomedical sciences.

I would also like to thank the Initiative for Maximizing Student Diversity (IMSD) team, specifically its leadership Linda Sealy PhD, Roger Chalkley DPhil, and Christina Keeton PhD. IMSD, where I did my first Journal Club presentation and memorably received a high level of critical feedback, prepared me for what was to come. IMSD was

also an outlet and the means to which I have met my closest friends in graduate school. I am also grateful to the T32 Microenvironmental Influences in Cancer Training Program (MICTP), spearheaded by Jin Chen MD PhD, which not only was a source of funding, but also consisted of seminars that have contributed to my professional development.

Of course nothing would be possible without financial support, namely IMSD (R25-GM062459), MICTP (T32 CA009592-29), a diversity supplement to NIH grant Fit to Remember? (AI113292), and P.M.I. departmental funds. The last two listed sources together with HL106812, funded experimental work. I am personally grateful for Vanderbilt's Provost Graduate Fellowship Award, which has supplemented my stipend for 5 years and improved my personal finances during graduate school.

I cannot express enough gratitude towards my family who often came to visit me in Nashville--even coming to lab to keep me company on weekends. To my brother Sheldon McLetchie, for being a study buddy in times when it was hard to focus. To my mother, Roxanne McLetchie for instilling high work ethic in me, grounding me, providing direction, and being an excellent role model. To my father, Nicholas McLetchie for dragging me to lab before I can even remember during his own journey through graduate school, for instilling in me the love for biology at a young age, and for talking to me through the good and bad times. To my grandmother, Granti, whose immigration to the United States was integral for anyone in my family to pursue this path, and who still reminds me of the important things in life. Lastly, I must thank my husband, Bradley Brookens for deciding to make me Mrs. Brookens before I got a chance to be Dr. McLetchie. I am forever grateful for the all-nighters he pulled with me on those long harvest days, for listening, being interested in my science, and so much more.

TABLE OF CONTENTS

LIST OF TABLES

Table **Page**

LIST OF FIGURES

Figure **Page**

Figure **Page**

Figure **Page**

Figure **Page**

LIST OF ABBREVIATIONS

AMPK – adenosine monophosphate (AMP)-activated protein kinase

ATP – adenosine triphosphate

PPP – pentose phosphate pathway

TCA – tricarboxylic acid

α-KG -- alpha-ketoglutarate

NADH – nicotinamide adenine dinucleotide (NAD) + hydrogen (H)

$FADH_2$ – flavin adenine dinucleotide

OXPHOS – oxidative phosphorylation

NT – nucleotides

UDP-GlcNAc -- uridine diphosphate N-acetylglucosamine

NEAA – non-essential amino acids

PHD – prolyl hydroxylase domain

HIF – hypoxia inducible factor

mTORC1 – mechanistic target of rapamycin complex 1

TSC2 – tuberous sclerosis complex 2

ROS – reactive oxygen species

Ig – immunoglobulin

SARS-CoV-2 – severe acute respiratory syndrome coronavirus 2

BCR – B cell receptor

VDJ – variability diversity joining

GC – germinal center(s)

GCB – germinal center B cell(s)

MBC – memory B cell(s)

ASC – antibody secreting cell(s)

SLPC – short-lived plasma cell(s)

LLPC – long-lived plasma cell(s)

SHM – somatic hypermutation

DZ – dark zone

LZ – light zone

FDC – follicular dendritic cells

Tfh – T follicular helper cells

Ab – antibody

NP-KLH – 4-Hydroxy-3-nitrophenylacetyl hapten conjugated to keyhole limpet hemocyanin

ASCT2 – alanine-serine-cysteine transporter 2

ECAR – extracellular acidification rate

OCR – oxygen consumption rate

LKB1 – liver kinase B1

ER – endoplasmic reticulum

CaMKKβ -- Ca^{2+}/calmodulin-dependent protein kinase kinase

ACC – acetyl-CoA carboxylase

T-ALL – T cell acute lymphoblastic leukemia

ELISA – enzyme-linked immunosorbent assay

ELISpot – enzyme-linked immunosorbent spot

2-NBDG – 2-(*N*-(7-Nitrobenz-2-oxa-1, 3-diazol-4-yl)Amino)-2-Deoxyglucose

NP-ova – 4-Hydroxy-3-nitrophenylacetyl hapten conjugated to ovalbumin

MFI – mean fluorescence intensity

FSC – forward scatter

mtROS – mitochondrial ROS

LPS – lipopolysaccharide

BAFF – B-cell-activating factor

Ag – antigen

Ova -- ovalbumin

NAC – N-acetyl cysteine

PGC1α -- peroxisome proliferator-activated receptor gamma coactivator 1-alpha

Q – glutamine

MT – mitotracker

GSH – glutathione

CHAPTER 1

INTRODUCTION

The work presented in this chapter provides an introduction on common themes throughout the thesis and gaps in knowledge

I. Overview

Cellular metabolism sets the foundation of many biological processes. The exploitation of metabolic pathways has been used to treat cancers, diabetes, and immune pathologies. The dynamic life of the B lymphocyte lineage provides a good model for studying the regulation of metabolic pathways critical for proliferation, long-term survival, and biosynthetically demanding functions like antibody production. Metabolic sensor and orchestrator of a plethora of metabolic programs, AMP-activated protein kinase (AMPK), is critical for metabolic adaptation to stressful nutrient-limiting conditions in multiple cell types and settings. Many cells rely on glucose and glutamine as fuels for metabolic pathways. However, whether AMPK is critical for the B lymphocyte lineage was not clear at the time of starting my thesis. Additionally, how glucose and glutamine metabolism influence germinal center outcomes was not fully elucidated. Here in Chapter 1, I provide a general overview of metabolism and B cell responses and introduce gaps in knowledge at the time of embarking my thesis work.

II. Cellular metabolism is a highly regulated network of biochemical reactions critical for many biological processes

Cellular metabolism encompasses all the biochemical reactions necessary to sustain life and pervades many aspects of biology (DeBerardinis et al., 2012). Metabolic pathways are the means that cells generate energy, synthesize macromolecules, regulate genes, eliminate toxins, adapt to environmental conditions, and ultimately die (**Fig 1.1**).

Energy metabolism refers to all the reactions involved in the release of adenosine triphosphate (ATP) during degradative, or catabolic pathways. In contrast, biosynthetic metabolism, or anabolism, often requires energy input and results in the generation of complex macromolecules deemed necessary for survival, proliferation, and function. Aside from catabolic and anabolic pathways, metabolic enzymes and metabolites have functions in signal transduction and gene regulation via epigenetic modulation of chromatin (Wang et al., 2020; Li et al., 2018). Additionally, it is through metabolic pathways that excess cellular content and molecules are maintained, for instance regulation of autophagy and antioxidant systems intersect with metabolic processes (Rabinowitz et al., 2010; Foyer, 2005). Furthermore, regulation of metabolic pathways is integral for a cell's ability to respond and adapt to environmental signals and nutrients (Yuan et al., 2013). Lastly, apoptosis, necrosis, and ferroptosis modes of cell death involve multiple mitochondrial proteins and lipid metabolites with dual roles in metabolism (Green et al., 2013; Lee et al., 2021). Collectively, metabolism is involved in many biological activities of the cell.

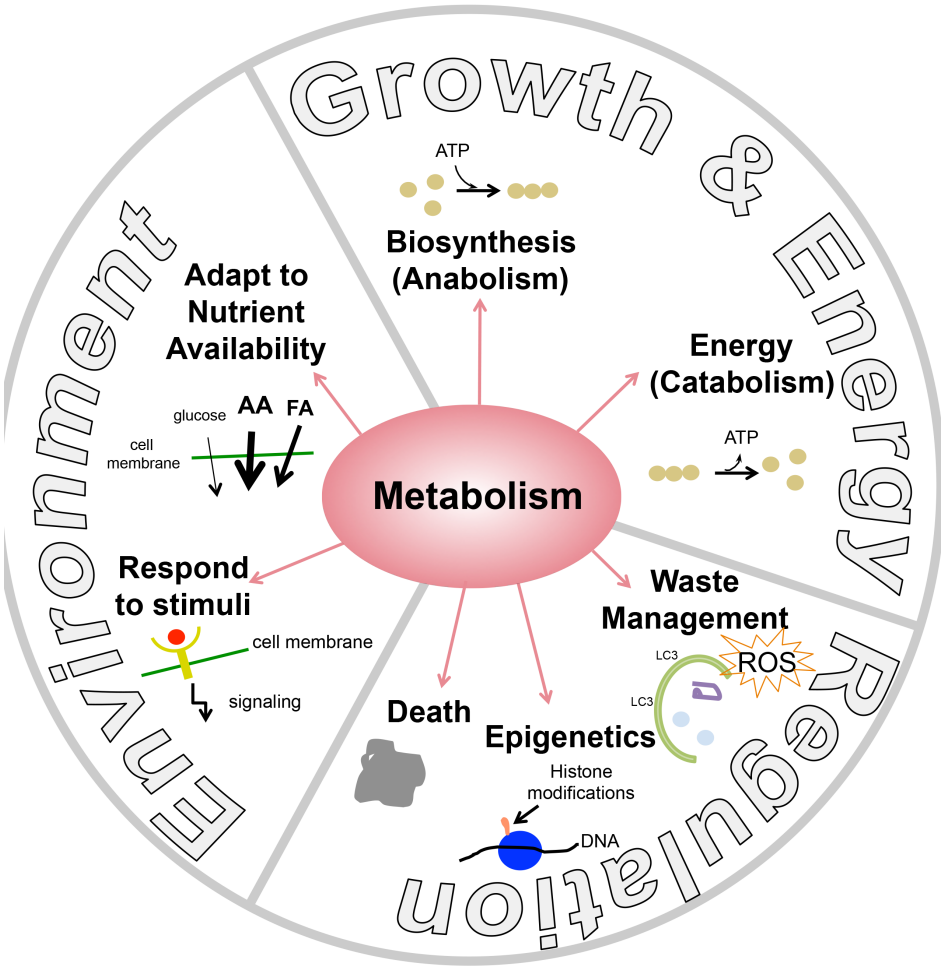

Figure 1.1 Cellular metabolism is the foundation of many biological processes. Cells use metabolic pathways to support the synthesis and break-down of macromolecules promoting growth, proliferation, storage and energy generation. Metabolism regulates many cellular processes including redox pathways, autophagy, epigenetics, and cell death pathways. Metabolic sensors allow cells to adapt and respond to environmental stimuli and nutrient availability. Figure loosely inspired after reading Pavlova et al., 2016.

Metabolism is composed of an interconnected biological network of pathways involving metabolites, enzymes, and cofactors to catalyze reactions in subcellular locations (**Fig. 1.2**). Most pathways cannot function independently. For instance, glucose-6-phosphate, generated in the first step of glycolysis, is a precursor of the pentose phosphate pathway (PPP). Additionally, multiple substrates can be used as a carbon or nitrogen source to fuel a given pathway. Fatty acids, carbohydrates, and proteins can all be oxidized in the tricarboxylic acid (TCA) cycle after initial processing. Metabolites can also be generated from multiple sources. For example, pyruvate, which enters the TCA cycle and used for gluconeogenesis among other fates, can be generated from both the oxidation of glucose and the transamination of alanine. These are just a few of the multitude of examples illustrating the interconnectivity of metabolic pathways.

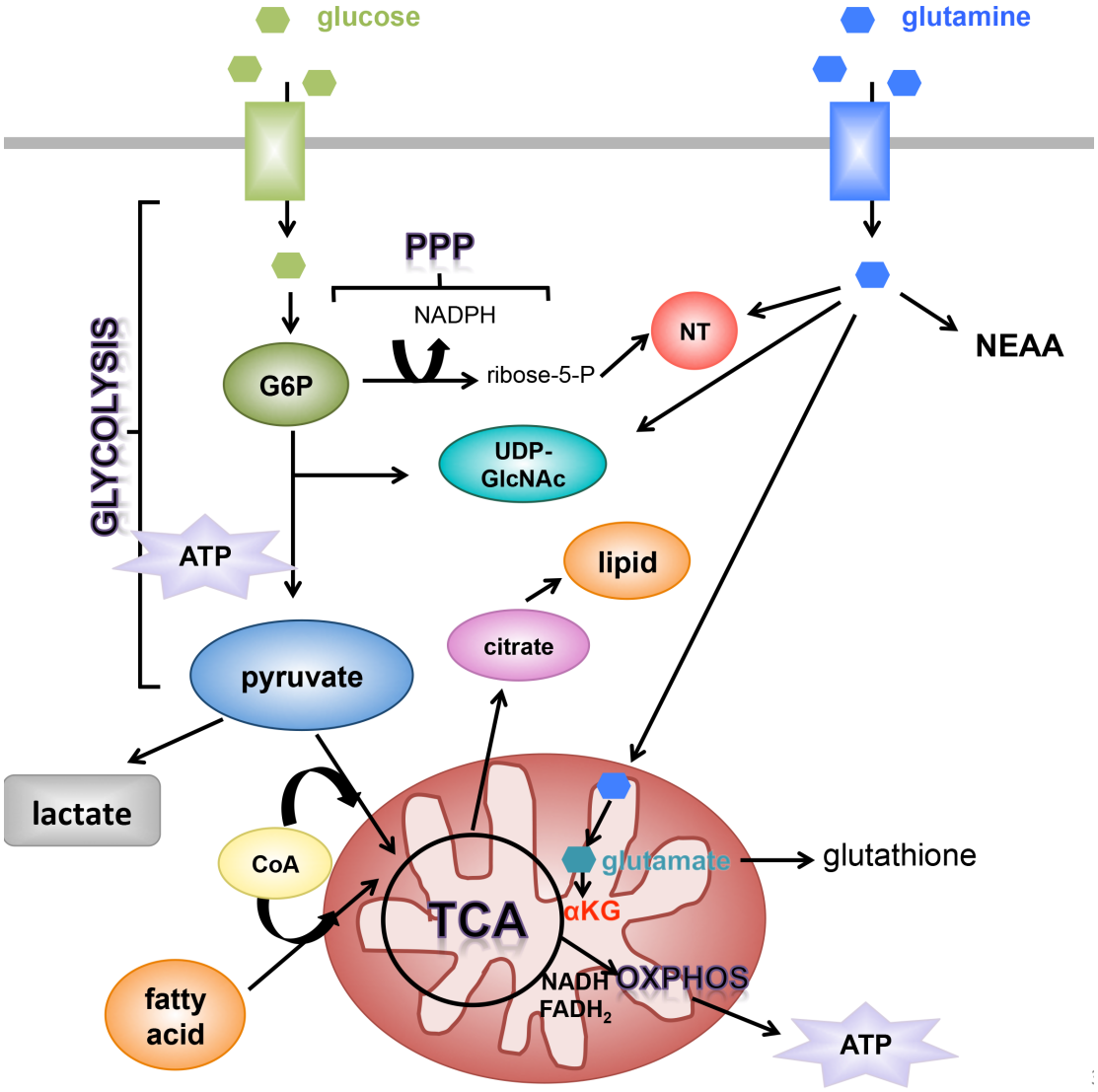

Figure 1.2 Cellular metabolism is an interconnected network (simplified cartoon). Glycolysis involves the oxidation of glucose into pyruvate and the generation of ATP. Pyruvate and fatty acids can fuel the tricarboxylic acid (TCA) cycle after activation with coenzyme A (CoA). Glutamine can also fuel the TCA cycle after conversion to glutamate followed by conversion to TCA intermediate alpha-ketoglutarate (α-KG). NADH and $FADH_2$, produced during the TCA cycle, are used during oxidative phosphorylation (OXPHOS), generating ATP. TCA metabolites such as citrate can be used for fatty acid synthesis. Glutamate is a precursor for glutathione, critical for redox homeostasis. Glucose-6-phosphate (G6P), the first metabolite generated in glycolysis can also be shunted to the pentose phosphate pathway (PPP) leading to the generation of ribose-5-phosphate, a precursor for nucleotides (NT). Glycolytic intermediates and glutamine can also be shunted into the synthesis of nucleotide sugar uridine diphosphate N-acetylglucosamine (UDP-GlcNAc), a key substrate for protein glycosylation via the hexosamine biosynthetic pathway. Besides fueling the TCA cycle and contributions to nucleotide and UDP-GlcNAc, glutamine can also serve as a nitrogen donor for *de novo* synthesis of non-essential amino acids (NEAA) like alanine and aspartate. Figure loosely inspired from Liu et al., 2019.

Metabolic reactions are driven by enzymes and non-protein cofactors to facilitate the flux of metabolites through pathways. The ability to sense fluctuations in nutrients, ATP/ADP/AMP, oxygen, and other metabolites in a timely and accurate manner and link those to cellular pathways is critical for proper function (Efeyan et al., 2015; Wang et al., 2020; Yuan et al., 2013). There are several conserved nutrient and oxygen sensors that orchestrate metabolic pathways to promote optimal fitness. For example, when sugars, amino acids, and lipids are abundant, nutrient sensing pathways promote anabolism and storage. In contrast, during times of low nutrient availability, sensors enable catabolism and pathways like autophagy to obtain energy and nutrients from non-essential cellular content. Similarly, during hypoxic conditions, oxygen-dependent prolyl hydroxylase domain (PHD) proteins no longer target transcription factor hypoxia inducible factor (HIFα) for proteasomal degradation (Yuan, et al., 2013). Instead, HIFα stabilization and accumulation leads to activation of a transcriptional program that assists the cell in adaption to low oxygen tensions. Specifically, HIFα induces expression of glycolytic genes to induce oxygen-independent glycolysis and limit reliance on oxygen-dependent oxidative phosphorylation (OXPHOS) (Gordon et al., 2007). Thus, metabolic sensors are critical for responding to environmental limitations and stressors.

In addition to the influence and importance of nutrient sensing in the environment on metabolism, cell type also dictates dominant metabolic pathways utilized to accomplish cell function. Lineage-specific networks of metabolic enzymes and higher-level regulation promote tissue-specific functions (Metallo et al., 2013). For instance, glycogen synthesis dominates metabolic pathways in skeletal muscle cells compared to

triacylglycerol synthesis primarily employed by adipocytes (Ivy, 1991; Ahmadian et al., 2007). Different tissues may also experience different microenvironments and nutrient availability due to their location. The portal architecture of the liver results in a gradient of venous nutrient supply available to hepatocytes (Puchowicz et al., 1999). Thus, both lineage-restricted genetic programs and environmental nutrients factor into metabolism of various cells and tissues.

A complete overview of metabolism includes addressing the existence of regulatory mechanisms and feedback loops among nutrient sensors, which together orchestrate multiple signaling events. Most notably, master metabolic regulators AMP-activated protein kinase (AMPK) and mechanistic target of rapamycin complex 1 (mTORC1) promote catabolic and anabolic pathways, respectively. AMPK negatively regulates mTORC1 both indirectly through the activation of TSC2 and directly by an inhibitory phosphorylation of Raptor, an essential component of mTORC1 (Gwinn et al., 2008). Recent evidence in yeast reveals that mTORC1 reciprocally downregulates AMPK by phosphorylation of a conserved residue (Ling et al., 2020). Though they do not interact directly, cross-talk between energy sensor AMPK and HIF signaling pathways has also been observed in a few settings (Salminen et al., 2016). Reciprocal regulation between multiple major metabolic signaling networks ensures a balance between anabolic and catabolic processes.

III. Exploitation of metabolism as a therapeutic approach in cancer

Many human diseases, including cancer, diabetes, and obesity, involve mutations in key metabolic enzymes and processes leading to alterations in normal physiology (Pavlova et al., 2016; Le et al., 2019). Understanding the mechanisms driving metabolic dysfunction and identifying vulnerabilities in disease is at the forefront of current research and has given rise to therapeutic targets in the clinic (Tripathi et al., 2018; Wolpaw et al., 2017; Pircher et al., 2016; Montero et al., 2011; Stuani et al., 2019; Pålsson-McDermott et al., 2020).

Malignant cells often have a heavier reliance on specific metabolic pathways compared to normal tissues. Otto Warburg discovered that cancer cells exhibited substantially more glucose uptake and lactate production compared to normal tissue even in the presence of oxygen; this observation later became known as the Warburg Effect and coincided with fully functioning mitochondria in many settings (Warburg, 1956; Porporato et al., 2017). It has been proposed that the Warburg effect provides glycolytic intermediates for biosynthesis supporting the high demand for growth in tumor cells and disrupts the microenvironment by the production of lactate (Liberti et al., 2016). Since the discovery of the Warburg effect, much attention has been given to glucose metabolism. The importance of glutamine in cancer metabolism has garnered later recognition (DeBerardinis et al., 2010; Yoo et al., 2020; Wise et al., 2010); glutamine uptake in many cell lines is up to ten-fold higher compared to any other amino acids (Eagle, 1955).

Glutamine acts as a nitrogen source for both nucleotide and non-essential amino acid synthesis, critical for proliferating tumor cells. Glutamine, after conversion to glutamate, is a precursor to glutathione synthesis critical for redox homeostasis in normal and cancer cells (Balendiran et al., 2004). Many cancer types also rely on glutamine

to fuel the TCA cycle via glutaminolysis and subsequent conversion to TCA substrate α-ketoglutarate (α-KG) (Altman et al., 2016). Glutaminase, which catalyzes the glutaminolysis reaction of glutamine to glutamate is highly expressed in some tumor cell types especially those driven by oncogenic cMyc (Mafra et al., 2019) Targeting glutamine metabolism in tumors with glutamine analogs was efficacious in decreasing tumor growth but also had significant cytotoxic effects in healthy tissues (Ahluwalia et al., 1990). However, specific inhibition of glutaminase with small molecule CB-839 has potent anti-tumor activity and currently has shown favorable outcomes in clinical trials (Gross et al., 2014; Meric-Bernstam et al., 2019; Guerra et al., 2019; Cohen et al., 2020). Other agents that have been approved in clinical trials include those targeting other metabolic enzymes such as isocitrate dehydrogenase (IDH1/2), mitochondrial complex I, fatty acid synthase among others (Luengo et al., 2017; Tripathi et al., 2018). Thus, targeting enzymes that catalyze essential metabolic reactions for tumor cells has shown great promise.

In addition to targeting critical metabolic enzymes like glutaminase for tumor cells, metabolites and nutrient sensors have also been effective targets. Agents that degrade circulating amino acids arginine and asparagine have been critical in limiting a nutrient supply crucial for some renal cell cancers and lymphomas respectively (Luengo et al., 2017). Furthermore, several rapamycin analogs that target metabolic regulator mTOR, frequently upregulated in cancer, have been developed and approved in the clinic (Hua et al., 2019). Though many cancer types have elevated reactive oxygen species (ROS) as a consequence of altered metabolism, antioxidant supplementation and therapeutic targets of ROS have been a controversial strategy with mixed results in combatting malignant cells (Fuchs-Tarlovsky, 2013; Ghoneum et al., 2020). Collectively,

targeting metabolic enzymes, metabolites, and metabolic regulators that are uniquely altered and relied upon by malignant cells continues to have potential in therapy either alone or in combination with other agents for the treatment of cancer and other metabolic diseases.

IV. Lymphocytes as a model for studying metabolism

Similar to his seminal observation in cancer cells, Warburg discovered that leukocytes also exhibited aerobic glycolysis upon activation (Warburg et al., 1958). These observations have relatively recently been recapitulated to some extent in both myeloid and lymphoid lineages of immunity and reviewed in several publications (Kelly et al., 2015; O'Neill et al., 2016; Pearce et al., 2013; Boothby et al., 2017). Heightened interest in the metabolic pathways that support immune cell activation, proliferation, function, and survival has exploded in the last 10-15 years. Analogous to the cancer metabolism field, this sector, coined "immunometabolism", aims to target key metabolic pathways with the possibility of modulating immunity during vaccination, immune pathologies, or in tumor infiltrating immune cells (Patel et al., 2019).

Understanding the metabolic factors that generate efficacious tumor infiltrating immune cells converge both realms of tumor and immune cell metabolism. Immune cells infiltrate in the tumor microenvironment where they can respond to tumor-specific antigens. One perspective is that both cancer cells and activated lymphocytes co-exist in crowded microenvironments competing for limited nutrients (Chang et al., 2015). However, recent evidence indicates that variations in nutrient acquisition between

immune cells and cancer cells are due to cell-intrinsic differences in metabolic wiring leading to distinctions in fuel preference (Reinfeld, Madden et al., 2021). This genetic vs. environmental dichotomy in determining dominant metabolic pathways is a recurring theme in both cancer and immune cells.

The lymphoid lineage, consisting of B and T lymphocytes and their progeny are unique in their high specificity for antigen and make up the two branches that generate immunological memory. Though B and T lymphocytes are distinct from tumor cells in that lymphocytes are not malignant and usually exhibit more metabolic plasticity, they provide a good model for studying metabolic changes in various settings (Macintyre et al., 2013; Franchina et al., 2017). After receiving appropriate activation signals, both naïve B and T lymphocytes undergo a period of proliferation, differentiation, and contraction requiring tightly regulated metabolic programming to support the fluctuating energy and metabolite demands at different stages (Akkaya et al., 2019; Pearce et al., 2013). The immunometabolism field has grown exponentially, however the B lineage is relatively less investigated. In the year 2020, for every one publication concerning metabolic regulation of B lymphocytes there were roughly seven publications on T lymphocytes. Both lymphocyte lineages have comparable phases of development, activation, expansion, contraction, and memory where educated hypotheses about critical metabolic pathways in T cells could be extrapolated to parallel B cell subsets. However, recent reports indicate distinctions in B and T cell metabolism with the former having greater levels of protein synthesis, reliance on OXPHOS, and equitable increases in ECAR and OCR upon activation (Khalsa et al., 2019; Caro-Maldonado et al., 2014). Additionally

specialized functions like class-switching, affinity maturation, and antibody production are exclusive to the B lineage and likely have distinct metabolic demands.

V. B cells confer humoral immunity

Prior to introducing current understanding about B cell metabolism, I will next give a foundation of B cell activation and differentiation. The B lineage is at the center of the adaptive humoral immune system and is responsible for mediating protection usually against non-self pathogens and their endotoxins via the production of antigen-specific immunoglobulins (Ig), otherwise known as antibodies. Currently, monoclonal antibodies for the treatment of severe acute respiratory syndrome coronavirus 2 (SARS-CoV-2), which has caused the worldwide pandemic respiratory disease COVID-19, has been the center of public interest (Wang et al., 2020; Chen et al., 2021). Antibodies have multiple applications including in biomedical research techniques, cancer checkpoint blockade, treatment of autoimmune disorders, among others and are derived from the B lymphoid lineage. *In vivo*, antibody functions include antigen neutralization, recruitment of the complement system to destroy antigens, antibody-dependent cellular cytotoxicity, and opsonization (Forthal, 2014). In addition to humoral-mediated protection via the production of antibodies, B cells also have cellular functions including antigen presentation to T cells and the production of regulatory and effector cytokines that influence other immune cell functions (Hoffman et al., 2016).

B cells develop in the bone marrow where they rearrange immunoglobulin gene segments generating a diverse repertoire of B cell receptors (BCR) (theoretically in

humans at least 10^{12} possible unique variants) in a process called VDJ recombination (Briney et al., 2019; Schatz et al., 1989). Mature B cells then emigrate from the marrow and traffic through lymphatic tissues. Initiation of B cell responses occur predominately in secondary lymphoid structures (spleen, lymph node, Peyer's patches) where rare-antigen reactive B cells encounter cognate antigen. B cell responses have broadly been characterized into T-dependent germinal center (GC) responses and T-independent extrafollicular responses (Elsner et al., 2020). In many settings, GC are proceeded by a short extrafollicular phase of proliferation and differentiation (MacLennan et al., 1991). The dominant viewpoint in the field is that class-switched affinity matured B cells that confer immunological memory are predominately derived from GC responses. However, evidence indicates that many of these processes are also observed in extrafollicular reactions, blurring conventional distinctions (Bortnick et al., 2013; Takemori et al., 2014; William et al., 2002). Notwithstanding, much of the thesis work here uses T-dependent antigens and therefore the focus taken will be on outcomes of the GC. Additionally, the focus will be on the fates of follicular B cells rather than marginal zone and B-1 B cells in the peritoneal cavity which both straddle the innate immune system and act as a first line of defense (Cerutti et al., 2013; Baumgarth 2017).

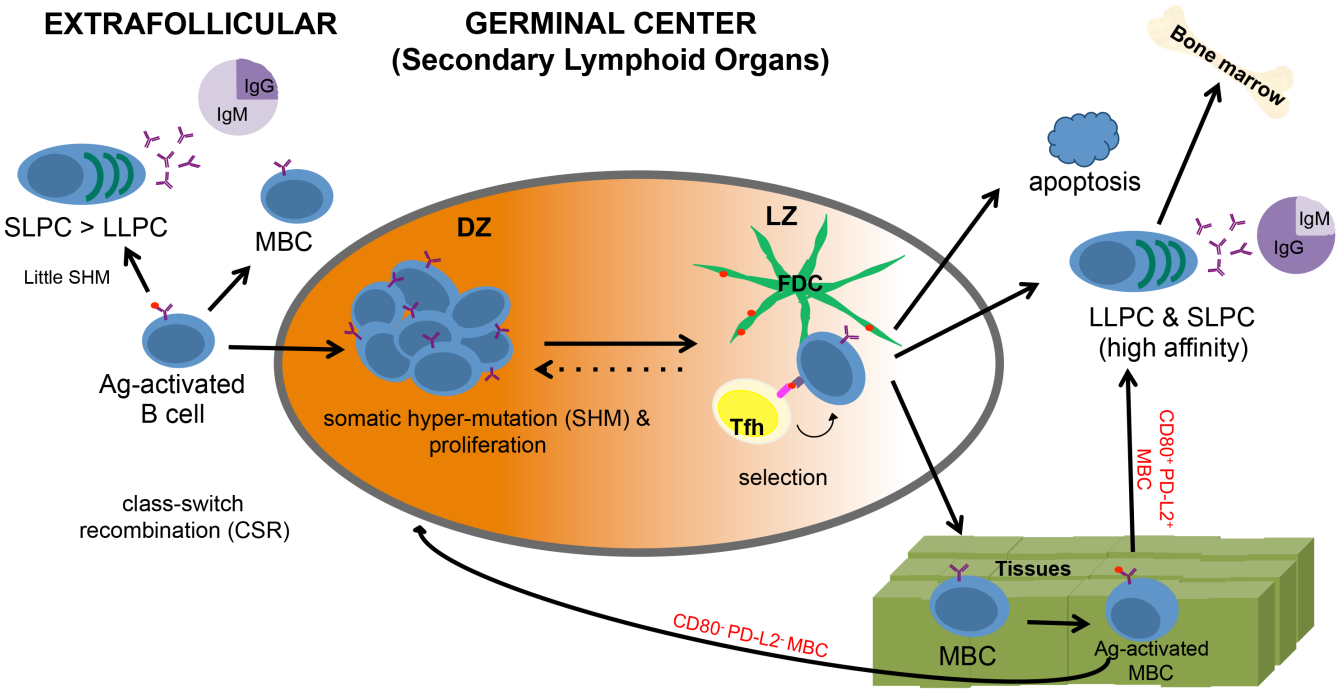

Figure 1.3 Extrafollicular and germinal center reactions. Upon encounter with antigen, B cells proliferate and can differentiate into memory B cells (MBC) or antibody secreting cells (ASC), composed of proliferating plasmablasts or terminaly differentiated plasma cells. Plasma cells may be short-lived (SLPC) or long-lived (LLPC). Extrafollicular responses are T-cell independent and predominately lead to SLPC that are of low affinity and the IgM isotype. Germinal centers produce more robust responses where B cells (GCB) undergo rapid proliferation and somatic hypermutation (SHM) in the dark zone (DZ). GCB traffic to the light zone (LZ) where B cells expressing receptors with appropriate affinity for antigen are selected for differentiation or apoptosis. LZ resident follicular dendritic cells (FDC) and T follicular helper cells (Tfh) assist in selection. Positively selected GCB cells differentiate into MBC or ASC, which can be LLPC or SLPC, the majority producing class-switched antibodies with higher affinity than those produced in extrafollicular responses. A portion of LLPC traffic and reside in the bone marrow where they continuously produce antibody into the sera. MBC migrate through the tissues. Upon rechallenge, $CD80^+$ $PD\text{-}L2^+$ MBC rapidly differentiate into ASC and the $CD80^-PD\text{-}L2^-$ MBC population can reseed a GC for further bouts of proliferation and SHM.

Germinal centers (GC) are dynamic sites of rapid proliferation, somatic hypermutation (SHM), selection, and differentiation of activated B cells (Victora et al., 2012; Cyster et al., 2019) (**Fig. 1.3**). The transcriptional regulation that underlies activation and differentiation of GCB has been well studied (Song et al., 2018). Within two days of exposure to antigen, B and T cells are observed at the T cell border in follicles. Some B-T interactions will result in proliferation and B cell differentiation into antibody secreting cells (ASC), also known as plasma cells, in extrafollicular regions. These extrafollicular ASC secrete mostly IgM with low affinity for antigen before undergoing apoptosis ~6 days after immunization. Other B-T interactions migrate to B cell follicles and commit to the germinal center fate. Germinal center B cells (GCB), which persist for ~3 weeks (MacLennan, 1994), traffic between so called dark and light zone regions where they undergo iterative rounds of proliferation/SHM in the dark zone (DZ) and selection in the light zone (LZ). SHM involves the introduction of point mutations in variable regions of immunoglobulin genes resulting in a pool of B cells expressing BCRs with minor variations and affinities for the antigen (Teng et al., 2007). Importantly, VDJ recombination during B cell development together with SHM during B cell activation allows for the expression of BCR and production of antibodies that can recognize virtually a limitless number of antigens. Additionally, diversification among BCR can increase the chances of being able to respond to epitope drift, for example to SARS-CoV-2 variants.

In the LZ of the GC, B cells are selected for or against survival and differentiation depending on many factors including the affinity for antigen (Shlomchik et al., 2012). Iterative rounds of SHM and selection results in the survival of B cells expressing BCR with increased affinity for antigen, a process known as affinity maturation. The degree of

affinity and other factors determine GCB fate. GCB can differentiate into either memory B cells (MBC) or ASC, though most GCB, which have undesirable BCR affinity to the antigen, are fated for cell death. Each ASC secretes the soluble form of the BCR of a single affinity and isotype. ASC, composed of plasmablasts and terminally differentiated plasma cells, can live and function for either days and called short-lived plasma cells (SLPC) or months to years, termed long-lived plasma cells (LLPC).

Humoral memory is conferred by two durable, mostly GC-derived populations: MBC and LLPC. Both populations have been observed to live for decades in humans long after antigen clearance (Crotty et al., 2003; Slifka et al., 1998). Similar to naïve B cells, MBC, migrate through lymphatic tissues. Upon encounter with cognate antigen, MBC are fated to either rapidly differentiate into ASC with robust kinetics or re-enter GC for further iterations of selection and SHM. Most LLPC traffic to and reside in the bone marrow where they continuously secrete antigen-specific antibody in the sera independent of the presence of either antigen or MBC (Manz et al., 1997). Gut-resident IgA secreting LLPC have also been reported (Landsverk et al., 2017). Achieving robust humoral immunological memory is key for the development of vaccines.

Class-switch recombination is the process in which the constant region of the antibody is replaced by another isotype through DNA recombination. Depending on the nature of the antigen and the cytokine milieu, class-switching results in a switch from an IgM BCR to one of the following BCR: IgG1, IgG2, IgG3, IgA, IgE, each eliciting unique downstream signaling as a BCR and distinct effector functions as a secreted antibody (Wan et al., 2015; Higgins et al., 2019). Recently, a widely accepted case has been made that activated B cells are programmed for class-switching prior to entry into the GC (Roco et

al., 2019). IgM responses peak a week after immunization and class-switched responses temporally lag behind. However, IgG1 antibody responses remain at relatively high levels in the sera for several weeks likely due to IgG1 secreting LLPC. An example of the kinetics of IgM and IgG1 antibody responses after immunization and later re-challenge with antigen is illustrated and taken from my experimental results in **Fig. 1.4**.

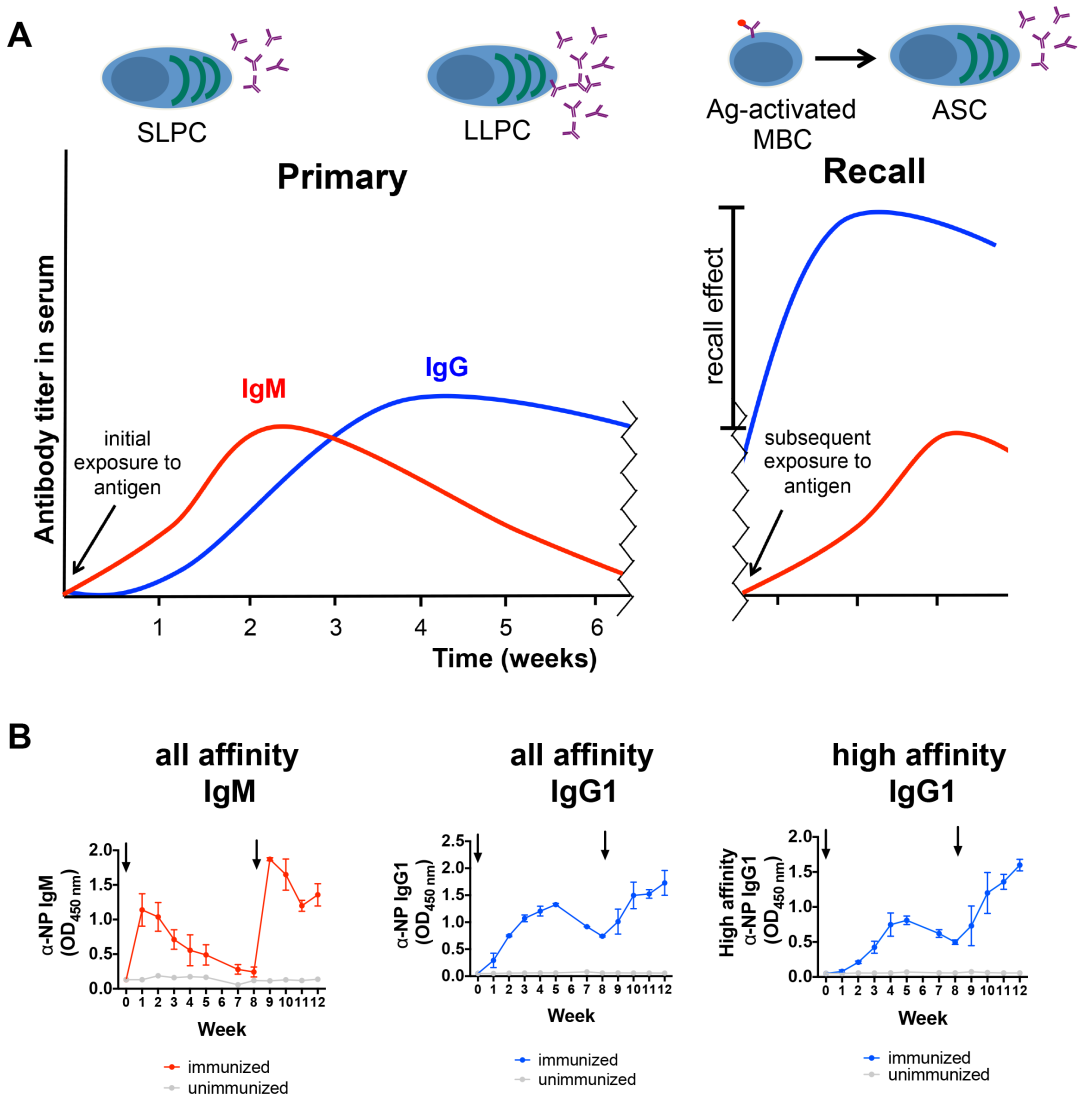

Figure 1.4 An example of antibody responses over the course of immunization. (A) After exposure to antigen, extrafollicular and germinal center responses lead to the generation of antigen-specific IgM followed by antigen specific IgG1. IgM secreting SLPC make up the majority of initial antibody (Ab) responses. After the germinal center wanes (~3 weeks post antigen exposure), LLPC and MBC remain. Ab titers remain in the sera due to the activity of continuously secreting LLPC. IgG titers remain higher than IgM due to the longer half-life of IgG and the composition of the LLPC population (IgG secretors > IgM secretors). Upon secondary exposure to antigen, Ab titers increase with robust kinetics due to the rapid differentiation of cognate MBC into ASC. The recall effect, or the functional capacity of MBC, is calculated as the difference in Ab titer immediately before and after exposure to antigen. (B) Weekly relative NP-specific IgM, IgG1 of all affinity, and IgG1 of high affinity after I immunized and later rechallenged wildtype mice with NP-KLH. Arrows indicate time of immunization.

VI. Immunometabolism of B cells

Through the lens of metabolism, the biology of the B lymphocyte lineage involves exclusive functions in antibody synthesis, SHM, and class-switching and therefore must have tight metabolic programming and regulation to support each process. For the past ~10-15 years the elucidation of the mechanisms critical for B lymphocyte lineage have accelerated (Boothby et al., 2017, Jellusova et al., 2020). A simplified cartoon of metabolic demands in different B cell subsets is illustrated in **Fig. 1.5**.

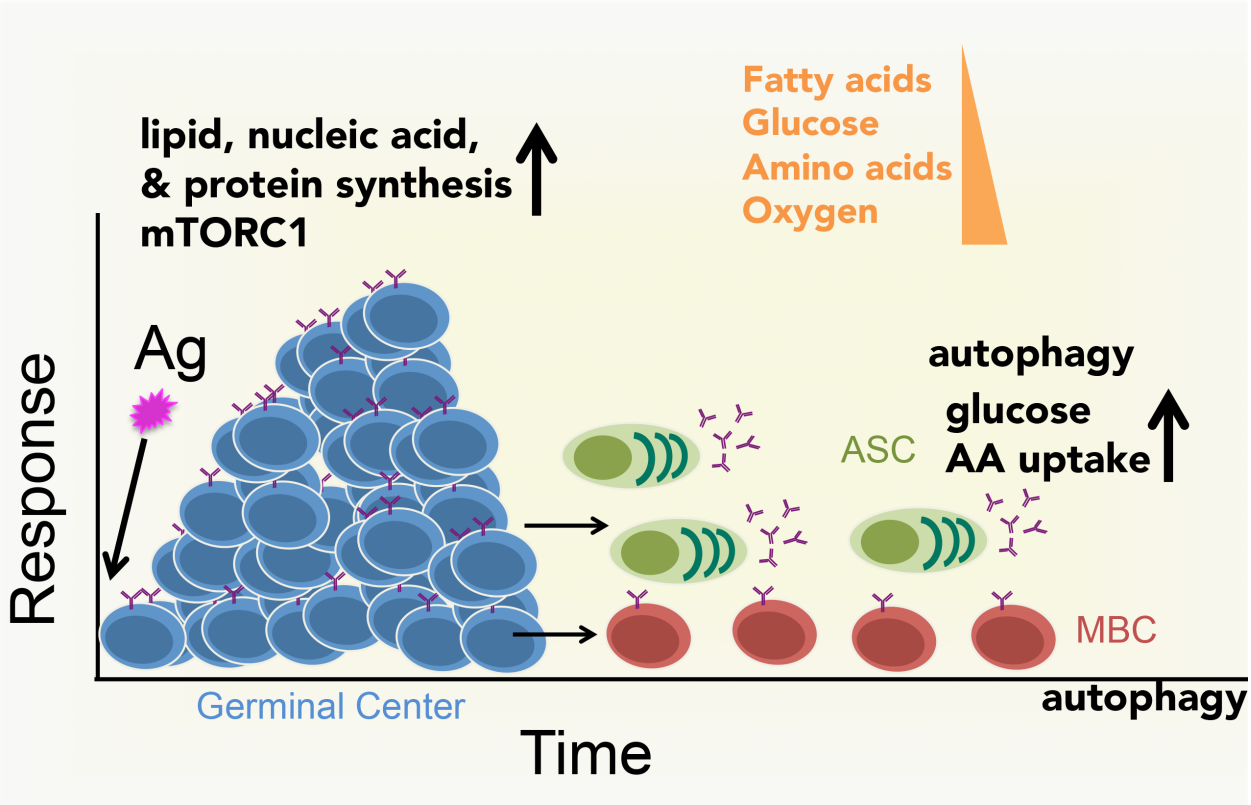

Figure 1.5 Metabolic processes and demands of B lymphocyte lineage cells (simplified cartoon). Activated B cells and GCB have increased uptake of glucose, AA, and fatty acids to support proliferation. Autophagy is critical for MBC and LLPC persistence. LLPC have increased glucose and amino acid uptake compared to SLPC. All B lymphocyte lineage cells must have the metabolic machinery and regulation to adapt to various environmental stimuli and nutrient availability.

Several activation stimuli including IL-4, anti-CD40, CpG, lipopolysaccharide (LPS), and anti-BCR lead to increased expression of glucose transporter Glut1 and increased glucose uptake in B cells (Woodland et al., 2008; Blair et al., 2012; Caro-Maldonado et al., 2014; Doughty et al., 2006; Waters et al., 2018; Cho et al., 2011; Dufort et al., 2007; Jayachandran et al., 2018; Akkaya et al., 2018). Activated B cells also exhibit increased expression of glutamine transporter ASCT2 and enhanced glutamine uptake as well as an increase in fatty acid uptake (Heyse et al., 2015; Masle-Farquhar et al., 2017; Waters et al., 2018; Brand et al., 1989; Dufort et al., 2014). In activated B cells, two groups used glucose tracer experiments to show that most of the glucose is shunted into the PPP for nucleotide synthesis while glutamine largely feeds the TCA cycle in anaplerotic reactions. (Waters et al., 2018, Doughty et al., 2006). However, other groups discovered substantial amounts glucose-derived carbons in TCA cycle intermediates suggesting that both glutamine and glucose contribute to mitochondrial metabolites (Le et al., 2012; Dufort et al., 2014). In fact, glucose in activated B cells was found to be critical for ATP-citrate lyase-mediated *de novo* lipogenesis where glucose-derived lipids are used for organelle membrane structures in proliferating and differentiating cells (Dufort et al., 2014). Extracellular acidification rate (ECAR) is a surrogate measurement of lactate production, one of the multiple fates of glycolytic end-product pyruvate. ECAR and oxygen consumption rate (OCR), as a measurement of mitochondrial function, increased proportionally with LPS, IL-4, and anti-BCR treatment, suggesting that activated B cells upregulate glycolytic and mitochondrial pathways equitably (Caro-Maldonado et al., 2014; Cho et al., 2011). Balanced metabolic pathways observed in resting and activated B cells contrasts to T cells, which preferentially skew towards expression of glycolytic genes and ECAR (Khalsa et al., 2019; Caro-Maldonado et al. 2014). Levels of ROS, which are byproducts of metabolic flux and

NADPH oxidase, are linked to B-cell fate determination (Jang et al., 2015). ROS^{lo} LPS activated B cells differentiate into plasma cells, whereas ROS^{hi} are more likely precursors to IgG1 class-switching (Jang et al., 2015).

Though there is less data on metabolism in *in vivo* GCB compared to B cells activated *in vitro*, GCB similarly exhibit elevated glucose uptake, mitochondrial content, and the expression of panels of genes encoding enzymes involved in glycolysis, TCA cycle, the electron transport chain, and fatty acid oxidation increased (Jellusova et al., 2017; Ersching et al., 2017; Diaz-Muñoz et al., 2015; Cho et al., 2016). GCB have increased HIF1α expression and hypoxic regions promoting a pro-glycolytic signature (Cho et al., 2016; Abbott et al., 2016; Jellusova et al., 2017; Boothby et al., [under review 2021]). In contrast to the prior evidence of increased glucose utilization in GCB, a recent paper provided evidence that GCB neither increased glucose uptake nor exhibited a hypoxic/glycolytic signature (Weisel et al., 2020). In this setting, rather than glucose, GCB exhibit strong appetite for fatty acids, which were oxidized in mitochondria (Weisel et al., 2020). In brief, divergence in reports on the major metabolic pathways employed by GCB may be due to the differences in interpretation, experimental models, and immunization strategies used (Boothby et al., [under review 2021]). GCB are a heterogeneous population and therefore genetic models and antigens that skew the characterization of the GC may shift dominant pathways observed. In addition to glucose and fatty acids, GCB may also rely on glutamine metabolism as treatment of mice with a glutaminolysis inhibitor, severely impaired the formation of GC (Choi et al., 2018). The relative contribution and fates of glucose, glutamine, and fatty acids needs to be dissected further for a better understanding of the metabolic demands in GCB.

Concerning metabolic regulation of B cell activation and GCB formation, metabolic sensors liver kinase B1 (LKB1) (Walsh et al., 2015), and glycogen synthase kinase 3 (GSK3) (Jellusova et al., 2017) have been shown to maintain metabolic quiescence in naïve B cells. Other signaling molecules like R-Ras2 (Mendoza et al., 2018), protein kinase Cβ (PKCβ) (Tsui et al., 2018), mechanistic target of rapamycin 1 (mTORC1) Raybuck et al., 2018), tandem PH domain containing proteins (TAPP) (Jayachandran et al., 2018), and transcription factors cMyc (Ersching et al., 2017; Tesi et al., 2019), RNA-binding protein HuR (Diaz-Muñoz et al., 2015), and epigenetic regulator enhancer of zest 2 (EZH2) (Guo et al., 2018) among others have all been implicated in regulating metabolism in activated B cells and GCB. However, metabolic regulators that enable B cells to adapt to stressful conditions like low nutrient availability are undetermined. Additionally, there is very limited literature establishing metabolic regulation governing processes exclusive to B cells, like SHM and class-switching. Furthermore, at the time of embarking my thesis, little was known on the metabolic regulation of differentiated B cells like ASC and MBC. Autophagy was reported to be critical for the longevity of MBC and the maintenance of mitochondrial homeostasis (Chen et al., 2014; Chen et al., 2015). How ROS is regulated in MBC and other subsets has been understudied.

Plasma cells are an assorted population and vary in terms of lifespan, antibody secretion rate, isotype secreted, and tissue of residence (Boothby et al., 2019). ASC have an expansive endoplasmic reticulum (ER) network to support the synthesis of immunoglobulin. It has been proposed that enhanced lipid synthesis in activated B cells is in anticipation of expanding the ER membrane in differentiated plasma cells (Dufort et al., 2014). ASC have extraordinary demand to synthesize glycosylated antibodies at an

impressive rate of up to 10^4 antibody molecules per cell per second (Nguyen et al., 2019). Highlighting their high rate of protein synthesis, plasma cells have increased expression of amino acid transporters and enhanced glucose uptake compared to naïve or activated B cells (Tellier et al., 2016; Vijay et al., 2020; Haniuda et al., 2020). Though LLPC and SLPC are transcriptionally indistinguishable (Lam et al., 2018), LLPC have enhanced Glut1 expression, glucose uptake, spare respiratory capacity, and rates of antibody synthesis compared to their short-lived counterparts (Lam et al., 2016). Over 90% of imported glucose in LLPC is used for the glycosylation of antibodies with a small fraction fueling the TCA cycle (Lam et al., 2016). Though a fraction of glucose fuels the TCA cycle in LLPC, long chain fatty acids are the preferred carbon choice (Lam et al., 2016). In addition to glucose and fatty acids, differentiation to the plasmablast stage after malaria infection led to increased appetite for glutamine (Vijay et al., 2020). Consistent with this observation, in *in vitro* cultures, glutamine in the media was critical for plasma cell differentiation (Crawford et al., 1985). Increased use of glutamine in plasma cells is necessary for amino acid synthesis and NADPH production likely used for redox balance (Garcia-Manteiga et al., 2011; Bertolotti et al., 2010; Lam et al., 2018). In sum, similar to GCB and activated B cells, the literature indicates that ASC use multiple fuels for different functions. At the initiation of my thesis, questions remain concerning how flexible ASC are in choosing carbon sources used for specific functions like plasma cell differentiation and antibody production. Additionally, whether rates of antibody synthesis can be regulated was unknown. As for metabolic processes, autophagy was critical for maintaining ER stress in plasma cells and was essential for LLPC persistence in vivo (Pengo et al., 2013). However, the metabolic factors that promote autophagy in LLPC was unknown.

B lineage subsets must undergo metabolic rewiring to meet the demands of their function while also adapting to varying nutrient conditions. In addition to antigen, GCB may be competing for limited nutrients. LLPC tend to reside in specific niches in the bone marrow whereas IgA plasma cells densely populate the gut (Manz et al., 1997; Landsverk et al., 2017). Accordingly, distinct subsets of cells along the B lineage must cope with changing and distinct metabolic demands, potentially in nutrient-limited microenvironments. This implies that sensors of metabolic status need to regulate multiple cellular mechanisms for B cells to adapt, survive, and function. Furthermore, both MBC and LLPC demand pro-survival wiring, however antibody synthesis in LLPC would require different metabolic programs than metabolically quiescent MBC. Discovery of the metabolic regulation that promotes longevity in these distinct populations is warranted.

VII. AMP-activated protein kinase (AMPK) is a master regulator of energy homeostasis

Most cellular processes require energy generated by the hydrolysis of ATP into ADP and phosphate or alternatively into AMP and pyrophosphate. Cellular ATP levels are re-generated by catabolic processes that include glycolysis, aerobic respiration, and fatty acid oxidation. Adenosine monophosphate (AMP)-activated protein kinase (AMPK) plays a crucial role in sensing the energy status of a cell (due to sensitivity of intracellular AMP concentrations) and subsequently balancing ATP-generating and ATP-consuming processes (**Fig. 1.6A**). AMPK was first described as an enzyme inactivated by increasing concentrations of ATP (Beg et al., 1973). AMPK has since been

discovered to be a highly conserved heterotrimeric kinase complex composed of a serine/threonine catalytic α subunit as well as regulatory β and γ subunits. In mammals, there are two isoforms of α (α1 and α2), two of β (β1 and β2) and three of γ (γ1, γ2, and γ3) (Stapleton et al., 1996; Cheung et al., 2000; Thornton et al., 1998). The expression and combinations of particular isoforms are tissue restricted with potentially tissue-specific functions. B and T lymphocytes express only the α1 isoform of the catalytic subunit, which is encoded by *Prkaa1* and denoted as AMPKα1 (Tamás et al., 2006; Mayer et al., 2008).

When activated, AMPK phosphorylates downstream targets which function to stimulate ATP generating pathways while simultaneously inhibiting ATP consuming pathways in order to maintain energy homeostasis (**Fig. 1.6B**). AMPK activation can also be achieved by decreasing concentrations of glycolytic intermediate fructose-1,6-bisphosphate (Zhang et al., 2017). Phosphorylation of AMPKα1 at the Thr-172 residue is essential for AMPK activation (Hawley et al., 1996). In most tissues, this phosphorylation can be carried out by upstream kinase liver kinase B1 (LKB1), a tumor suppressor linked to Peutz-Jeghers syndrome (Hawley et al., 1996; Shaw et al. 2003). Alternatively, phosphorylation of the Thr-172 residue on AMPKα1 can occur independently of LKB1 and metabolic stress in response to calcium flux via upstream Ca^{2+}/calmodulin-dependent protein kinase kinase (CaMKKβ) in T lymphocytes (Tamás et al., 2006).

AMPK activation induces a plethora of downstream metabolic pathways favoring catabolism and energy conservation (Mihaylova et al., 2011). Pharmaceutical activation of AMPK leads to increased expression of glucose transporters, GLUT4 and GLUT1 as well as glycolytic enzyme, hexokinase 2 (Zheng et al., 2001; Stoppani et al., 2002; Wu et al.,

2013). AMPK signaling also indirectly promotes GLUT4 trafficking to the cell membrane, which enhances glucose uptake (Webster et al., 2010; Yamaguchi et al., 2005; Taylor et al., 2008). Simultaneously AMPK inhibits ATP-consuming processes such as glycogen synthesis and gluconeogenesis by directly targeting glycogen synthase or indirectly by influencing epigenetic factors and inhibition of transcription factors (Bultot et al., 2012; Mihaylova et al., 2011; Koo et al., 2005; Leclerc et al., 2001). AMPK expression has also been associated with increased expression of genes encoding glutamine-processing enzymes like glutaminase in T cells (Blagih et al., 2015). In addition to glucose metabolism, AMPK regulates both protein and fatty acid metabolism. The first described AMPK target, acetyl-CoA carboxylase (ACC) promotes fatty acid synthesis. An inhibitory phosphorylation of ACC by AMPK promotes fatty acid oxidation (Munday et al., 1988; Fullerton et al. 2013). AMPK also negatively regulates protein synthesis by an inhibitory phosphorylation of Raptor, a subunit of mammalian target of rapamycin complex 1 (mTORC1) (Gwinn et al., 2008). In addition to inhibiting protein and lipid biosynthesis, AMPK also stimulates canonical autophagy and mitochondrial homeostasis by targeting Unc51-like kinase1 (ULK1), mitochondrial fission factor (MFF), and mitochondrial biogenesis activator PGC-1α (Herzig et al., 2018). Many studies elucidate a role for AMPK in lymphocyte energy metabolism, function, survival, and ultimately immunity.

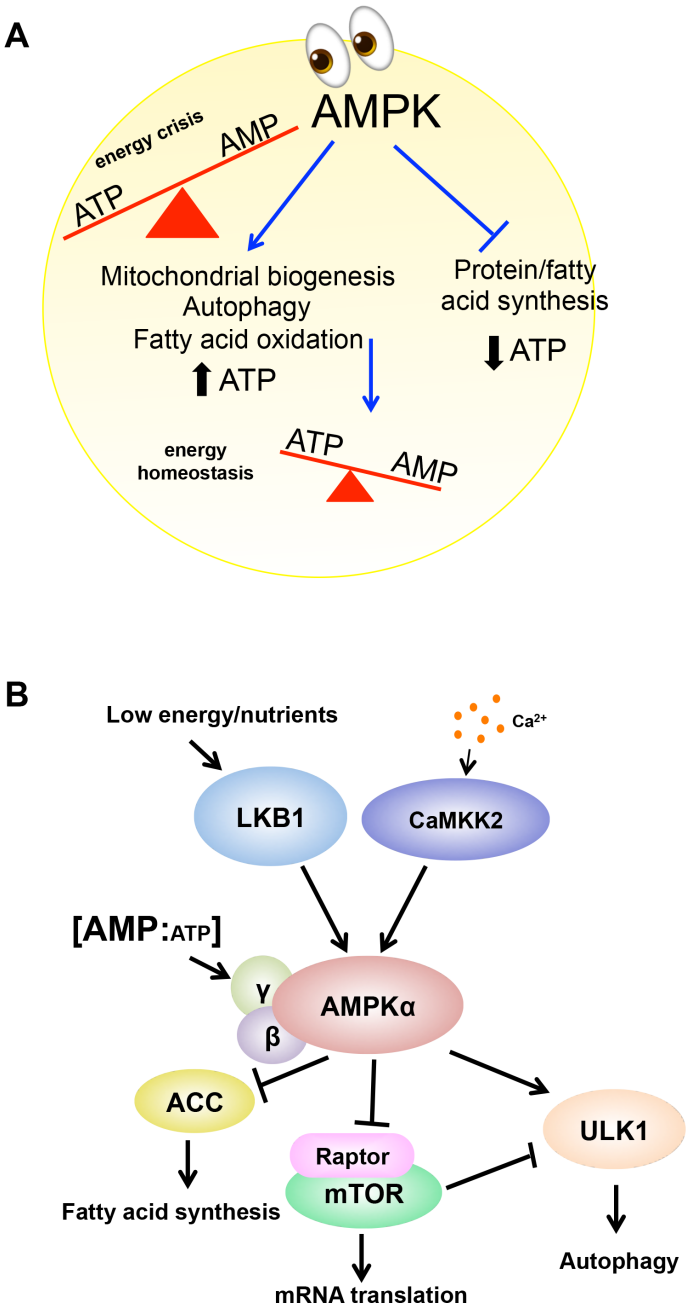

Figure 1.6 AMPK is a metabolic sensor that promotes energy homeostasis by regulating multiple downstream pathways and tilting the balance towards catabolism. (simplified cartoon) (A) AMPK can sense increased intracellular AMP:ATP ratios. Once activated, AMPK promotes pathways that lead to ATP generation like mitochondrial biogenesis, autophagy, and fatty acid oxidation while simultaneously inhibiting ATP consuming processes such as fatty acid and protein synthesis thereby restoring energy homeostasis. (B) AMPK can be activated via liver kinase B 1 (LKB1) in low nutrient or energy conditions. AMPK can also be activated independent of metabolic stress through CaMKK2. Once activated AMPK targets multiple targets including downstream inhibitory phosphorylation of acetyl-CoA carboxylase (ACC) and mechanistic target of rapamycin complex 1 (mTORC1), and activating phosphorylation of Unc-51 like autophagy activating kinase 1 (ULK1).

VIII. The role of AMPK in primary T cell responses in controversial but AMPK is critical for promoting T cell memory

AMPKα1 had been shown to be largely dispensable for B and T cell development (Mayer et al., 2008, Rao et al., 2015). There are conflicting reports on the role of AMPK in primary T cell immune responses. Global genetic knock out of AMPKα1 led to normal IFNγ responses of Th1 $CD4^+$ T cells after T cell activation *in vitro* (Mayer et al., 2008). Similarly, T cell intrinsic depletion of AMPKα1 by CD4cre*Prkaa1*$^{fl/fl}$ did not alter secretion of IFNγ from OT1 CD8 T cells in response to SIINFEKL peptide (Rolf et al., 2013). However, $CD8^+$ T cells from globally AMPKα1-deficient mice secreted elevated levels of IFNγ after anti-CD3/CD28 activation (MacIver et al., 2011; Blagih et al., 2015). A third phenotype was reported with T cell-intrinsic deletion of AMPKα1 leading to a decrease in IFNγ secretion after anti-CD3 and anti-CD28 activation of sorted naïve $CD8^+$ T cells (Rao et al., 2015). This discrepancy of whether AMPKα1 promotes, inhibits, or is dispensable for T effector cytokine responses may vary depending on experimental settings. *In vivo*, AMPKα1-deficient T cells had reduced glucose uptake and mitochondrial function, which resulted in reduced primary T effector responses to viral and bacterial pathogens (Blagih et al., 2015). However, Rolf *et al*. and Mayer *et al*. report that loss of AMPKα1 in $CD8^+$ T cells led to normal activation, proliferation, and effector function of antigen specific cytotoxic T cells in response to OVA-expressing Listeria monocytogenes (LmOVA) infection or ova peptide itself (Rolf et al., 2013; Mayer et al., 2008). Discrepancies again may be due to the different model systems (for instance, T cell intrinsic deletion vs. global deletion of AMPKα1). Although the role of AMPK in primary immune responses is unclear, previous studies have collectively shown the importance of AMPK in promoting T cell memory. Mice treated with metformin, a pharmaceutical

associated with increased AMPK activity, or rapamycin, which inhibits mTOR had higher frequencies of $CD8^+$ T memory cells that enhanced protective immunity after infection with LmOVA (Pearce et al., 2009). Consistent with this finding, increased expression of memory markers were observed in human CD4+ T cells after genetically inducing AMPK expression (Braverman et al., 2020). Additionally, genetic ablation of AMPKα1 in $CD8^+$ T cells led to diminished survival of antigen-specific CTLs memory cells after ova immunization (Rolf et al., 2013).

IX. Evidence for a role of AMPK in the B lineage is limiting

At the time of embarking my thesis, few studies showing a role for AMPK in B function had been reported. LPS-activated B cells treated with increasing concentrations of metformin secreted fewer antibodies despite similar cell numbers suggesting that AMPK might negatively regulate IgG secretion *in vitro* (Lee et al., 2017). However, globally AMPKα1-deficient mice were capable of mounting a normal T-dependent humoral response 2 weeks after immunization suggesting that AMPKα1 may be dispensable for the primary B cell response (Mayer et al., 2008). LKB1, an upstream activator of AMPK, is important for counteracting NF-κB-driven B cell activation and spontaneous germinal center formation *in vivo* (Walsh et al., 2015). It remains to be determined if the hyperactive phenotype of B cells observed in LKB1-deficient animals is AMPK-dependent since LKB1 has multiple downstream targets apart from AMPK including SADs and MARKs which play roles in cell polarity (Shackelford et al., 2009). There are few reports of AMPK activity in memory B cells, but one human study demonstrated

that AMPK phosphorylation is elevated in sorted memory B cells from elderly individuals compared to IgM^+ cells (Frasca et al., 2017). Whether AMPKα1 plays a role in memory B lymphocyte or T-independent humoral responses needed to be elucidated. Furthermore, whether AMPK plays a role in the function or survival of the ASC compartment is unknown. In considering the disparate findings among reports, it is vital to note that observations made from global genetic knockouts of AMPKα1 or systemic activation of AMPK by pharmaceuticals such as metformin may be due to extrinsic factors resulting from changes in AMPK activity of other cell types and to issues of acute vs. chronic inhibition with potential counter-regulation. Therefore, care should be taken before making conclusions about the function of lymphocyte-intrinsic AMPK in these studies.

X. AMPK enables lymphocytes to adapt to metabolic stress and has varied activity in different T subsets

Naive lymphocytes remain in the G_0 phase of the cell cycle and primarily use oxidative phosphorylation to generate the energy needed for maintaining membrane potential and migration (Waters et al., 2018; Caro-Maldonado et al., 2014). When the ATP synthase inhibitor oligomycin in naïve B and T cells block mitochondrial function, AMPK is essential for switching from oxidative metabolism to glycolysis in order to maintain ATP levels (Mayer et al., 2008). Additionally, IL-4-induced glycolysis of naïve B cells was supported by AMPK expression indicated by improved B cell survival (Cho et al., 2011). Therefore, the downstream functions of AMPK to promote different metabolic programs are flexible and depend on the metabolic needs of the cell. T-cell receptor activation

leads to transient activation of AMPKα1 through CaMKKβ independent of metabolic stress (Tamás et al., 2006). It has been hypothesized that production of ATP through AMPK activation via CaMKKβ immediately following T-cell receptor activation prepares the T cell for the energetic demands of subsequent cell proliferation. Whether B cells also activate AMPK via CaMKKβ downstream of the B-cell receptor has not been tested but it has long been known that B cell size increases substantially in response to BCR and/or IL-4 in a pre-proliferative period prior to onset of S-phase (Berton et al, 1992).

While naïve T lymphocytes primarily exhibit mitochondrial oxidative phosphorylation, newly activated and proliferating lymphocytes rely heavily on glycolysis which generates building blocks to support forming cell membranes, nucleic acids, and protein for the rapidly dividing cells. Once activated, T cells up-regulate mTORC1 activity, which promotes protein translation and cell growth (Waickman et al., 2012). AMPK activity counteracts the biosynthetic activities of rapidly proliferating T cells by negative regulation of aerobic glycolysis and mTORC1, which ultimately promotes long-term T cell survival and function *in vivo* (Rolf et al., 2013; MacIver et al., 2011; Blagih et al., 2015). Consistent with the view that AMPK activation inhibits the glycolytic profile of effector cells, inhibition of glycolysis with 2-deoxy-glucose in $CD8^+$ T cells correlated with increased AMPKα1 T-172 expression and decreased expression of various glycolytic enzymes (Sukumar et al., 2013). One potential role for AMPK signaling in effector cells is to limit mTORC1 activity, thereby preventing superfluous growth and cytokine secretion after antigen-induced activation.

In addition to the role of AMPK in dampening T cell activation, AMPK allows lymphocytes to respond and adapt to the microenvironment. Lymphocytes constantly

migrate through various microenvironments with a range of available nutrients from oxygen and glucose rich blood to nutrient-poor lymphatic tissues. It is therefore likely that metabolic profiles of lymphocytes adjust in response to the microenvironment for survival (Boothby et al., 2017). AMPK signaling was evident in activated T cells after glucose or glutamine deprivation suggesting that AMPK allows lymphocytes to adapt to limited nutrient availability in the microenvironment (Blagih et al., 2015; Rolf et al., 2013). It remains to be determined how naïve and activated lymphocytes adapt metabolically *in vivo* as they migrate through different tissues. AMPK activity in lymphocytes may prevent superfluous effector cell proliferation and growth, especially in low nutrient conditions, and the switch to oxidative metabolism may promote the survival of long-lived memory lymphocytes (Rolf et al., 2013).

AMPK has differential activity in different subsets of the T cell lineage. T regulatory cells have more AMPK activity and fatty acid oxidation than T effector cells (Michalek et al., 2011). AMPK inhibition of its downstream direct target ACC favored T regulatory cell differentiation over a T effector phenotype (Berod et al., 2014). One potential explanation for how AMPK activity is differentially expressed in different lymphocyte subsets is asymmetrical cell division of cytosolic contents during differentiation. Metabolic regulators such as mTORC1 and c-Myc as well as mitochondria are reported to distribute asymmetrically during cell division of differentiating B and T lymphocytes, generating metabolically distinct daughter cells (Verbist et al, 2016). Observations regarding cell-specific metabolic profiles have led to therapeutic strategies involving skewing T lymphocytes to a certain subset by activating specific metabolic pathways (Braverman et al., 2020).

XI. AMPK in B and T cell cancer malignancies

AMPK signals in and may affect transformed lymphocytes as well. Although this issue is beyond the scope of my thesis work, here I will give a brief overview of literature published at the initiation of my thesis work regarding the role of AMPK in transformed cells. Cancer cells have altered metabolic programming that promotes uncontrolled cell proliferation. As a metabolic sensor that promotes catabolic and anti-proliferative cellular pathways, AMPK and upstream tumor suppressor LKB1 have been investigated as molecular targets in tumors (Shackelford et al., 2009). Most evidence for the anti-tumor role of AMPK is seen in solid tumors. However, there is recent evidence for the protective role of AMPK in lymphomas. A genetic association study revealed that overexpression of AMPK subunits α1, β1 or β2 correlated with longer survival in Non-Hodgkin Lymphoma patients (Hoffman et al., 2013). Clinical and basic science studies reveal the anti-tumor effect of AMPK on hematological malignancies including diffuse large B-cell lymphoma (DLBCL) (Alkhatib et al., 2017; Singh et al., 2013) where metformin treated diabetic patients newly diagnosed with DLBCL had better overall survival than other DLBCL patients. Acadesine, another pharmaceutical that activates AMPK, induced apoptosis in B-cell chronic lymphocytic leukemia cells (Campàs et al., 2003). AMPKα1 was shown to suppress Myc-induced B-cell lymphoma progression and the Warburg effect in mice (Faubert et al., 2013). Regulatory subunits of AMPK also play a role in minimizing tumorigenesis in lymphomas. Germ-line genetic deletion of the AMPKβ1 isoform accelerated p53-driven T cell lymphoma via ACC activation, which promoted lipogenesis necessary for membrane synthesis of proliferating cells (Houde et al., 2017).

Though there are many examples of AMPK having anti-tumor effects detailed

above, AMPK can also promote cancer cell survival by allowing cells to adapt to stressful conditions (Jeon et al., 2015). T cell acute lymphoblastic leukemia (T-ALL), associated with Notch signaling pathway mutations, drives AMPK activation which promotes OXPHOS and T-ALL cell viability (Kishton et al., 2016). Discrepancies for whether AMPK plays a protective role against tumorigenesis or promotes tumor survival may reflect the differentiation state at which the lymphocyte transformed into malignancy.

XII. Summary and Thesis Projects

Metabolism underpins many processes in cellular biology. Many diseases including cancer often involve aberrant metabolic pathways with altered reliance on metabolites, metabolic enzymes, or metabolic regulators. B lymphocytes are a good model for studying metabolism because they have multiple differentiation states with dynamic energy and biosynthetic requirements. AMPK is a metabolic sensor shown to be critical for T cell metabolic plasticity supporting primary and recall T-cell mediated immune responses. Whether AMPK has similar functions in the B lymphocyte lineage, which has exclusive functions including antibody production and class-switching, is unknown. AMPK regulates a plethora of downstream metabolic pathways including glucose and glutamine metabolism. Glucose and glutamine have been shown to be critical fuels for B cell activation, differentiation, and antibody synthesis. However whether these fuels have specific functions in SHM or class switching are unknown. Additionally, the amount of flexibility that B lymphocytes exhibit in fuel choice to support functions like antibody production are not clear. Understanding critical metabolic pathways of different cell types can lead to therapeutic targets for effective vaccine development, immune pathologies, and cancers.

In **Chapter 2**, I include all the materials and methods used during this thesis work and include figures to show details on mouse genotyping and optimization strategies for pulse-chase experiments. Chapters 3, 4 and 5 are data chapters where each chapter begins with a brief introduction and ends with a discussion section. Chapters 3 and 4 consist of data modified from a publication in Journal of Immunology integrated with additional data not included in the publication (Brookens et al., 2020). **Chapter 3** details

preliminary data revolving around metabolic profiles of B lymphocyte lineage and then proceeds to focus on the role of AMPK in B cell activation and GC reactions. The majority of Chapter 3 focuses on AMPK function in the formation, maintenance, and function of the MBC compartment. In **Chapter 4** I shift focus to the role of AMPK in the ASC population. I show evidence illustrating the importance of AMPK in fine-tuning Ab synthesis by dampening mTORC1 activity. AMPK has been shown to regulate both glutamine and glucose metabolism. Therefore, in **Chapter 5**, I present novel but unpublished data focusing on how glucose and glutamine metabolism synergistically affect B cell antibody responses. Finally, in **Chapter 6** I discuss limitations, implications, and future directions of this thesis work.

CHAPTER 2

MATERIALS AND METHODS

In this Chapter, I detail all methods used for my thesis work. I also include here descriptive supplemental data regarding each genetic mouse model and optimization of pulse-chase analyses.

Animals

All animal protocols were in compliance with the National Institutes of Health guidelines for the Care and Use of Experimental Animals and were approved by Vanderbilt University Institutional Animal Care and Use Committee. *Prkaa1 flox* mice were purchased from the Jackson Laboratory and were crossed with mice harboring Cre recombinase under the control of three types of control element: tamoxifen-inducible *Rosa26*-CreER^{T2} and *huCD20*-CreER^{T2}, or *mb1*-Cre. To control for Cre toxicity in B cell responses (Schmidt-Supprian et al., 2007; Becher et al., 2018), age-matched *Prkaa1*$^{+/+}$ mice with the corresponding Cre transgene were used as wildtype controls and co-housed with *Prkaa1*$^{f/f}$ mice. Mice were housed in pathogen-free conditions and both male and female mice, aged 6-10 weeks, were used.

Unless otherwise indicated, all *in vitro* studies in Chapters 3 and 4 were done using purified B cells from tamoxifen-inducible *Rosa26*-CreER^{T2} knock-in mice (**Fig 2.1A**). For tamoxifen-inducible models, *Rosa26*-CreER^{T2} and *huCD20*-CreER^{T2}, mice were injected intraperitoneally with three doses of 3 mg tamoxifen dissolved in 200 µL of safflower oil every other day with the last dose concluding 5-10 days prior to the harvest time point (or immunization time point with huCD20-CreER^{T2} mice). Cre recombinase under the control of the ubiquitous promoter, *Rosa26*, led to >75% deletion of *Prkaa1* alleles in both CD19^{+} purified B cells and CD138^{+} bone marrow cells after tamoxifen regimen (**Fig 2.1B,C**). However, as observed in AMPK full-body knock-outs (Wang et al., 2010; Mayer et al., 2008; Foretz et al., 2010), ubiquitous loss AMPK led to splenomegaly (**Fig. 2.1D**). Elevated cell numbers in *Prkaa1*$^{f/f}$ *Rosa26*-CreER^{T2} mice after tamoxifen treatment was not due to increases in the CD19^{+}, CD4^{+}, or CD8^{+} populations (**Fig**

2.1D), and instead may be consistent with elevated erythroid precursors observed in AMPK-deficient animals (Wang et al., 2010; Mayer et al., 2008).

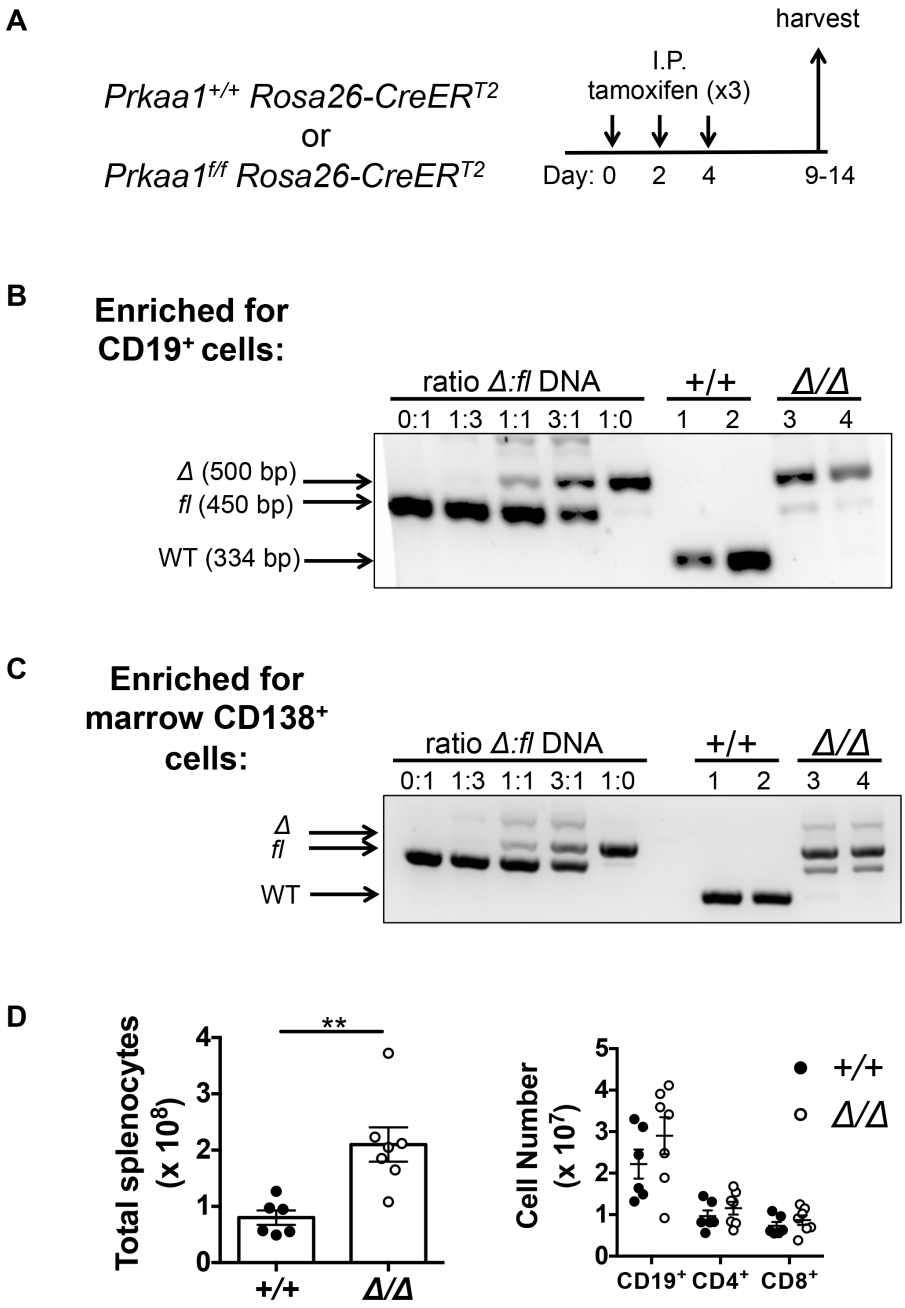

Figure 2.1 *Prkaa1*$^{f/f}$ *Rosa26*-CreER^{T2} knock-in mice have >75% tamoxifen-induced deletion of *Prkaa1* alleles in B cells and bone marrow plasma cells but lead to splenomegaly. (A) Tamoxifen regimen to activate Cre recombinase and target *Prkaa1* loxP sites for deletion. Mice were injected 3 times with 3 mg in 200 µL safflower oil once every other day. Mice were harvested nine to fourteen days following the initial tamoxifen injection. (B,C) PCR of *Prkaa1* deletion from genomic DNA of *Prkaa1*$^{+/+}$*Rosa26*-CreER^{T2} and *Prkaa1*$^{f/f}$ *Rosa26*-CreER^{T2} (B) splenic CD19^{+} B cells and (C) bone marrow CD138^{+} plasma cells after tamoxifen regimen; Wildtype band = 334 bp, *Floxed* band = 450 bp, Δ band = 500 bp. (D) Total number of splenocytes, B cells, CD4^{+}, and CD8^{+} T cells in *Rosa26*-CreER^{T2} mice (*Prkaa1*$^{+/+}$ and *Prkaa1*$^{\Delta/\Delta}$).

To test B cell-intrinsic AMPK on humoral immunity, without the confounding variable of loss of AMPK in non-B lineage populations, I crossed *Prkaa1*$^{f/f}$ mice to mouse lines with B cell-restricted promoters: tamoxifen-inducible *huCD20*-CreER^{T2} or constitutively active *mb1-Cre*. The *huCD20* promoter is active from the pre-B cells to mature B cell stage (Ahuja et al., 2007). CD19^{+} B splenocytes of tamoxifen treated *Prkaa1*$^{f/f}$ *huCD20*-CreER^{T2} had more than 50% deletion of *Prkaa1*; no deletion of *Prkaa1* was observed in the CD19^{-} fraction (**Fig 2.2**). Due to technical issues related to new B cell generation after tamoxifen treatments in the huCD20-CreER^{T2} model, in longer term experiments, I used the potent B lineage-specific tamoxifen independent *mb1*-Cre transgene which is active as early as the pro-B cell stage during B cell development (Hobeika et al., 2006). I confirmed that loss of *Prkaa1* by *mb1*-Cre did not alter the pre-immune B cell repertoire in the periphery (**Fig. 2.3 A,B**). Flow sorted memory B cells (MBC) and antibody secreting cells (ASC) from *Prkaa1*$^{f/f}$ mb1-Cre mice had nearly 100% deletion efficiency of *Prkaa1*.

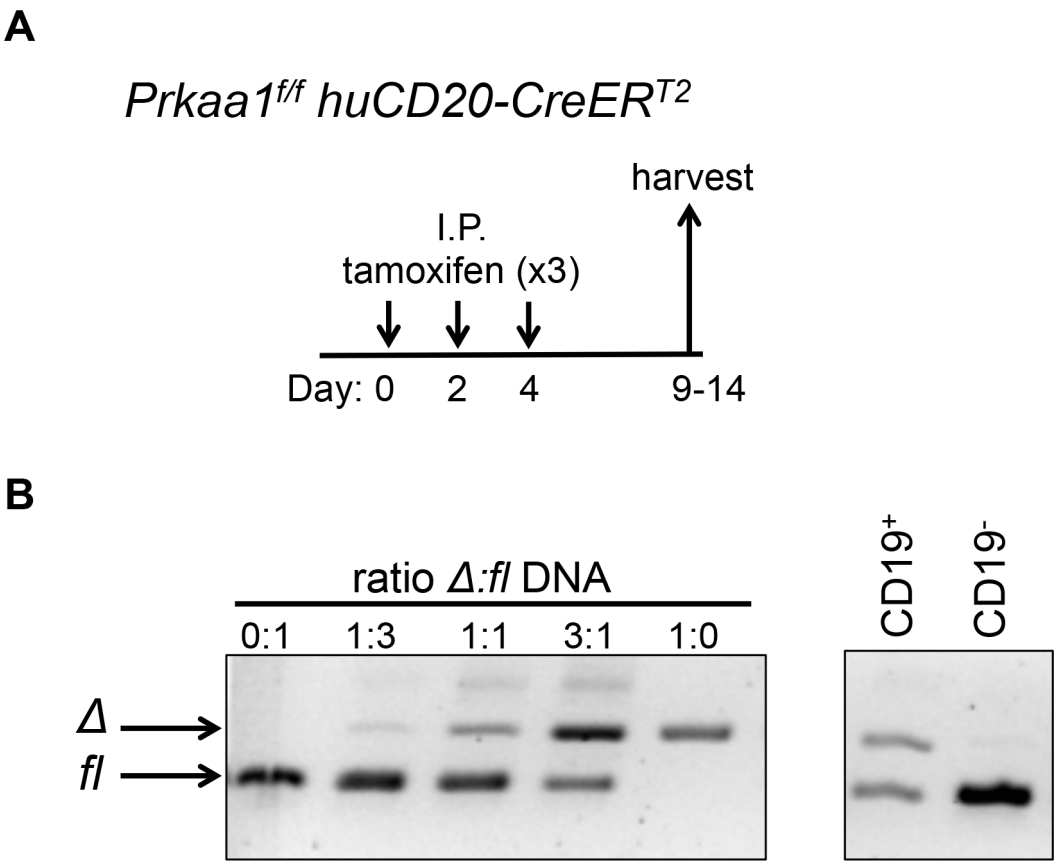

Figure 2.2 *Prkaa1*$^{f/f}$ huCD20-CreER^{T2} mice have B cell restricted Prkaa1 deletion after tamoxifen regimen. (A) Tamoxifen regimen to activate Cre recombinase and target *Prkaa1* loxP sites for deletion in mature B cells. (B) PCR of *Prkaa1* deletion from genomic DNA of *Prkaa1*$^{f/f}$ *huCD20*-CreER^{T2} splenic CD19^{+} B cells and CD19^{-} cells after tamoxifen regimen. Samples were on the same gel but cropped to show lanes of interest.

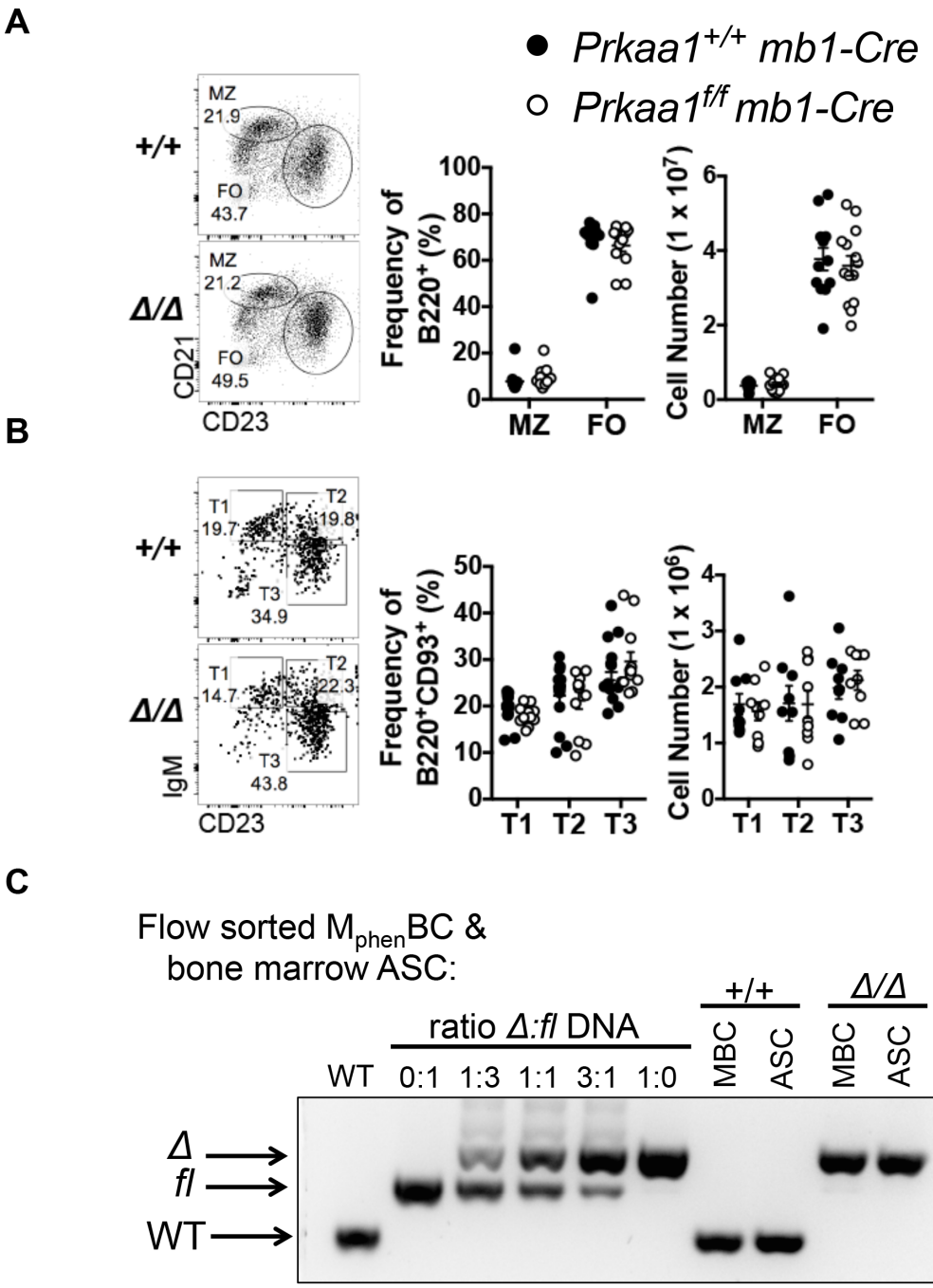

Figure 2.3 *Prkaa1*$^{f/f}$ *mb1*-Cre mice efficiently excise Prkaa1 from the B lineage and have normal pre-immune B cells in the periphery

. (A,B) Frequencies and numbers of (A) marginal zone, follicular, and (B) transitional B cells in the spleen of *mb1*-Cre mice (*Prkaa1*$^{+/+}$ or *Prkaa1*$^{f/f}$). Data are representative of eight vs. nine mice in 4 independent experiments. (C) PCR of *Prkaa1* deletion from genomic DNA of flow sorted splenic memory B cells (MBC: B220^{+} CD38^{+} IgD^{-}) and bone marrow antibody secreting cells (ASC: CD138^{+} TACI^{+}) in *Prkaa1*$^{+/+}$ *mb1-Cre* and *Prkaa1*$^{f/f}$ *mb1-Cre* mice.

For reversion assays in Chapter 4, *Raptor*$^{f/f}$ mice, purchased from Jackson, were bred with *Prkaa1*$^{f/f}$ huCD20-CreER^{T2} and *Prkaa1*$^{f/f}$ *Rosa26*-CreER^{T2} to generate *Prkaa1*$^{f/f}$ *Raptor*$^{f/+}$ huCD20-CreER^{T2} and *Prkaa1*$^{f/f}$ *Raptor*$^{f/+}$ *Rosa26*-CreER^{T2} mice respectively. In Chapter 5, *Gls1*$^{f/f}$ and *Glut1*$^{f/f}$ mice, a generous gift from Dr. Jeffrey Rathmell, were crossed with huCD20-CreER^{T2} mice to induce B cell-specific tamoxifen-inducible deletion. *Gls1*$^{f/f}$*Glut1*$^{f/f}$ huCD20-CreER^{T2} mice were also generated to test synergistic humoral effects of doubly-deficient animals. For transfer experiments in Chapter 3, CD45.1^{+} IgH^{a} recipient mice were generated by crossing CD45.1^{+} IgH^{b} and CD45.2^{+} IgH^{a} mice; both lines were purchased from Jackson Laboratory (stock # 002014 and 008341, respectively). OT-II transgenic mice, which have CD4^{+} T cells that recognize chicken ovalbumin peptide residues 323-339 when presented by MHC-II, were purchased from Jackson.

PCR

For genotyping, ~0.5 cm of tail tissue was homogenized in 0.5 mL tail lysis buffer (50 mM Tris Base, 100 mM EDTA, 100 mM NaCl, 1% SDS, pH 8.0) and proteinase K prior to DNA extraction. Genotyping of mice tail DNA was done using primers listed in **Table 2.1**. To test deletion efficiency of *Prkaa1* post experiments, genomic DNA was extracted from purified or sorted cells using cell lysis buffer (1% SDS, 50 mM Tris Base, 10 mM EDTA pH 8) and proteinase K. One hundred nanograms of genomic DNA were used as a template for *Prkaa1* and CreER^{T2} amplifications using primers listed in Table 2.1.

For real time quantitative PCR in Chapter 5, mRNA was isolated from 2-day LPS blasts using TRIzol reagent following manufacturer's instructions (Life Technologies).

RNA concentration was measured using NanoDrop software and used to synthesize cDNA using Promega AMV Reverse Transcriptase kit. cDNA templates were amplified using SYBRGreen Power UP Master Mix (ThermoFisher). All mRNA levels were calculated relative to actin using the $2^{-\Delta\Delta CT}$ method and normalized to wildtype. Primer pair sequences to detect Gls1, Slc2a1, and actin mRNA sequences are listed in Table 2.1.

	Sequence (5' → 3')
ER^{T2}-Cre	F- CCGGAGATCTTAATGTCCAATTTACTGACCGTA R- GCTAGAGCCTGTTTTGCACGTT
HuCD20 Exon 2	F- CACAAGGTAAGACTGCCAAAAATC R- ATATACAAGCCCCAAAACCAAAAG
Mb1-Cre	F- CCCTGTGGATGCCACCTC R- GTCCTGGCATCTGTCAGAG
Prkaa1	F- CCCACCATCACTCCATCTCT R- AGCCTGCTTGGCACACTTAT Δ- CCCACATAGGAAAGCGTGTT
Raptor	F- CTCAGTAGTGGTATGTGCTC R- GGGTACAGTATGTCAGCAC
Glut1	F- CTGTGAGTTCCTGAGACCCTG R- CCCAGGCAAGGAAGTAGTTC
Gls1	F- TAAGATCTGTGGCTGGTCTTCCAGG R- ACAATGTACCTGAGGGAGTTGACAGG
C4	F- TCCCTATGCAGGTGTGCATG R- CCCACCTCACATGCATGAAG
Slc2a1 (Real-Time PCR)	F- CAGTTCGGCTATAACACTGGTG R- GCCCCCGACAGAGAAGATG
Gls1 (Real-Time PCR)	F- GGGAATTCACTTTTGTCACGA R- GACTTCACCCTTTGATCACC
beta-actin (Real-Time PCR)	F- CATCCGTAAAGACCTCTATGCCAAC R- ATGGAGCCACCGATCCACA

Table 2.1 Primer sequences used for genotyping, deletion efficiency, and real time quantitative PCR.

Immunizations

For immunizations in Chapters 3 and 4, mice with B lineage-specific loss of AMPKα1, driven by huCD20 and *mb1* promoters, were immunized intraperitoneally with hapten carrier protein, 4-hydroxy-3-nitrophenylacetyl hapten (NP) conjugated to keyhole limpet hemocyanin (NP-KLH), emulsified in Imject Alum (50 μg NP-KLH in 50 μL alum per mouse) (Lalor et al., 1992). Recall responses were induced with 100 μg NP-KLH in 100 μL alum per mouse.

For transfer experiments in Chapter 3, $CD45.2^+$ IgH^b B cells (10^7) purified from *Prkaa1*$^{+/+}$ *Rosa26*-$CreER^{T2}$ and *Prkaa1*$^{f/f}$ *Rosa26*-$CreER^{T2}$ mice, polyclonal wildtype $CD4^+$ T cells (4 x 10^6), and $CD4^+$ T cells from OT-II transgenic mice (10^6) were transferred into each allotype-disparate $CD45.1^+$ IgH^a mice pre-conditioned with sub-lethal irradiation (split dose of 3.5 Gy x 2) two days prior to transfer. After irradiation and transfer of donor B and $CD4^+$ cells, recipient mice were immunized with NP_{16}-ovalbumin (NP-ova) emulsified in Imject Alum (100 μg in 100 μL).

For immunizations in Chapter 5, mice were immunized with 100 μg NP-ova emulsified in 100 μL Imject Alum. For lung inflammation models in Chapter 5, mice were immunized and boosted one week later with 100 μg of either NP-ova or ovalbumin emulsified in 100 μL of Imject Alum. Three weeks after the initial immunization, mice received daily inhalations of 50 μg ovalbumin dissolved in 20 μL PBS for seven consecutive days. Mice were harvested within twelve hours of the seventh inhalation.

Serum and peripheral blood collection

To track circulating memory B cells in Chapter 3, approximately 100 µL of blood was collected from the tail veins of mice in 200 µL ACK lysis buffer (150 mM NH_4Cl, 10 mM $KHCO_3$, 0.1 mM EDTA) in the presence of heparin before flow cytometry. For the collection of serum, used to screen for circulating antibodies by ELISA in Chapters 3-5, approximately 100 µL of blood was collected from the tail vein and left to clot. Serum was separated from the blood clot by centrifugation.

Flow cytometry

Unless otherwise specified, all mAbs were from BD Pharmingen, Life Technologies, eBiosciences, or Tonbo Biosciences. For detection of GC- and memory-phenotype B cells, splenocytes (3×10^6) were stained with anti-B220, -GL7, -Fas, -IgD, -CD38, NP-APC and a dump channel containing anti-CD11b, -CD11c, -F4/80, -Gr-1, and 7-AAD in 1% BSA and 0.05% sodium azide in PBS. To phenotype different memory B cell subsets, a second panel consisted of anti-B220, -CD38, -CD80, -PD-L2, -IgG1, NP-APC and the aforementioned dump channel with the addition of anti-IgD, -CD4, -CD8, -GL7. In analyses of transfer experiments, allotype-specific antibodies were used to distinguish donor (CD45.2) and recipient (CD45.1) B cells as described (Lee et al., 2013).

For flow analyses of mitochondria, $1\text{-}3 \times 10^6$ cells were washed in PBS and stained with 200 nM MitoTracker Green, 50 nM MitoTracker Deep Red, and Ghost-780 in PBS for 20 min at 37˚C, then washed again (1% BSA in PBS) and further stained with anti-B220, anti-IgD, anti-GL7, -CD138, or -CD38. MitoSox (5 µM) and Bodipy C-11

581/591 (1.25 μM) staining were performed similarly. For 2-NBDG uptake analysis, 3 x 10^6 cells were stained for 20 min with 60 μM 2-NBDG and Ghost-510 after an hour incubation in PBS to deplete intracellular glucose stores. 2-NBDG stained cells were then stained with anti-B220, -CD138, -TACI, -NP, -GL7, and -CD38. For intracellular phospho-flow analysis, cells were fixed with 4% PFA followed by methanol permeabilization. Anti-phospho-S6 (Cell Signaling Technologies) staining was performed was as described (Raybuck et al., 2016). Samples were analyzed using a FACSCanto flow cytometer driven by BD FACS Diva software and were processed using Flow-Jo software (FlowJo LLC).

Preparative sorting

Starting from single-cell suspensions of splenocytes, memory-phenotype B cells ($M_{phen}BC$) were enriched by depleting IgD^+ and $Thy1.2^+$ cells using biotinylated antibodies followed by BD IMag™ streptavidin particles on an IMag™ Cell Separation Magnet (BD Biosciences). Cells were stained as described for flow cytometry and dump negative, IgD^- $CD38^+$, $B220^+$ cells were sorted into 10% FBS in PBS for downstream applications. To sort for ASCs cells in the bone marrow, $CD11b^+$ cells were similarly depleted from the single-cell suspension from flushed femur bones. The remaining cells were stained as described for flow cytometry and dump negative, $CD138^+TACI^+$ cells were collected.

ELISA

For detection of circulating antigen-specific antibody of all- and high-affinity after immunization with NP-KLH or NP-ova in alum adjuvant, serial dilutions of sera were added to NP_{24}-BSA (all-affinity) or NP_2-PSA (high affinity) (Biosearch Technologies) coated (0.1 μg/well) 96-well plates and incubated overnight at 4˚C followed by incubation with either HRP-conjugated anti-IgM or -IgG1 (Southern Biotech). For transfer experiments, NP-specific donor vs. recipient derived antibody were distinguished by detecting with either biotinylated anti-$IgG1^a$ or -$IgG1^b$ (BD Biosciences), followed by Streptavidin-HRP (R & D Systems). ELISA plates were developed using Ultra TMB Substrate (Thermo Scientific) and optical densities at 450 nm were measured. To compile results across biologically independent experiments, optical densities within the linear range of serially diluted sera were pooled. In Chapter 5, ovalbumin-specific antibodies were screened for by incubating serial dilutions of sera onto ovalbumin (1 μg/well) coated 96-well plates at 4˚ overnight followed by HRP-conjugated anti-IgM or –IgG1 incubation and development using Ultra TMB Substrate.

The recall effect in Chapter 3 was calculated as the difference between the OD value generated from sera collected one day prior to rechallenge subtracted from the OD value generated from sera seven days post rechallenge. OD values from a dilution in the linear range of the curve were used to calculate recall effects.

For detection of secreted antibody after *in vitro* studies in Chapter 4, supernatants from cultured cells were added to anti-Ig(H+L) (Southern Biotech)-coated 96 well plates before detection with HRP-conjugated antibodies. Normal mouse IgG

(Thermo Scientific) was used as a standard to interpolate concentrations of IgG for tissue culture supernatants.

ELISpot

To detect antigen-specific antibody secreting cells (ASCs) after immunization in Chapters 4 and 5, 96-well high protein binding membrane plates (Millipore) were coated with 1 μg/well NP_{24}-BSA, NP_2-PSA, or ovalbumin. Splenocytes or bone marrow cells (5 – 20 x 10^5) were added and plates were incubated at 37˚ overnight followed by incubation with biotinylated anti-IgM, -IgG1, -$IgG1^a$, or -$IgG1^b$ antibodies prior to incubation with VectaStain ABC kit (Vector Laboratories) and development using 3-amino-9-ethylcarbzole (Sigma, St. Louis, MO). ASCs were quantified using an ImmunoSpot Analyzer (Cellular Technology).

Tissue culture

Splenic naïve B cells were purified by negative selection using biotinylated anti-CD43, -Thy1.2, and -F4/80 (>85% $CD19^+$) followed by streptavidin particles and IMag™ Cell Separation Magnet (BD Biosciences). To induce plasma cell differentiation, B cells were seeded at 5 x 10^5 per mL and treated with 5 μg/mL LPS (Sigma), 10 ng/mL BAFF (AdipoGen), 10 ng/mL IL-4 (Peprotech), 5 ng/mL IL-5 (Peprotech), and 50 nM 4-hydroxy-tamoxifen (4-OHT) (Sigma). For cross-linking the B cell receptor in Chapter 3, α-IgM F(ab')2 (Southern Biotech) was used at 10 ng/mL. To culture cells in hypoxic conditions in Chapter 3, cells were transferred for 24h to a 37˚C CO_2 incubator where P_{O2} of 1% is maintained by nitrogen gas. For proliferation analysis in Chapter 5, two

million purified B cells were labeled with 5 μM Cell Trace Violet (Invitrogen) before seeding cells at 5 x 10^5 per mL with 1 μg/mL anti-CD40 (Tonbo), BAFF, IL-4, and IL-5. Cells were cultured for 2-8 days in RPMI-1640 supplemented with 10% FBS (Peak), 100 U/mL penicillin (Invitrogen), 100 μg/mL streptomycin (Invitrogen), 3 mM L-glutamine (Invitrogen), and 0.1 mM 2-mercaptoethanol (Sigma). B cells were also expanded on the NB.21-2D9 feeder line as previously described (Nojima et al., 2011; Kuraoka et al., 2016) in Chapter 4. Every three days, supernatants were frozen for further analysis and the expanded B cells were reseeded on fresh NB21 feeder cells in new media, IL-4, and 4-OHT.

For spontaneous antibody secretion in Chapter 4, day 7 LPS cultures were subjected to Ficoll step gradient centrifugation (Invitrogen) to eliminate dead cells and debris. Cells were then washed and 5 x 10^4 cells were seeded in 100 μL of fresh media in a 96 well plate for 8 hours. Supernatants were frozen and levels of secreted IgG1 were determined by ELISA. Secreted IgG1 was detected as early as 30 minutes after seeding and continued to increase linearly for up to 8h (**Fig. 2.4A**).

Pulse-chase analyses of antibody production

In Chapter 4, after 7 days of culture with LPS, BAFF, IL-5, IL-4, and 4-OHT as above, viable cells were recovered after Ficoll step gradient centrifugation, rinsed, and recounted. To determine the appropriate pulse and chase times, equal numbers of cells were pulsed for 0.5, 1, or 6 hours with 2 μCi [^{3}H]-leucine (Moravek, 60 Ci/mmol) per 2 x 10^6 cells per mL of arginine-, lysine-, and leucine-deficient RPMI (Sigma) supplemented back with complete RPMI levels of L-arginine (1.149 mM; Sigma), L-lysine (0.219 mM;

Sigma), and 10% of complete RPMI levels of L-leucine (0.038 mM; Sigma). Media also contained 10% dialyzed HyClone FBS, 25 mM HEPES (Invitrogen) and phenol red (Sigma). After pulsing cells, 2 x 10^6 cells were lysed in RIPA buffer in the presence of protease and phosphatase inhibitors and supernatants were frozen for the zero chase time point. Remaining cells were washed in PBS and resuspended in the aforementioned media but with 100% complete RPMI levels of L-leucine (0.382 mM) at 1 x 10^6 cells per mL. At each specified chase time point, 2 x 10^6 cells were lysed and the supernatant collected. Samples were stored at -20˚. Secreted and intracellular IgG antibodies were purified from supernatant and lysate samples respectively using protein G agarose beads (Santa Cruz Biotechnology). Precipitates were subjected to SDS-PAGE in reducing conditions and transferred to PVDF membranes since fluorography of membranes enhances the detection of radioactive proteins over dried gels (Lucher et al., 1988; Symington et al., 1981; Gershoni et al., 1983). PVDF membranes were rocked for 30 minutes in 2 M sodium salicylate (Sigma), a fluor which improves [^{3}H] detection, prior to fluorography at -80˚ for 1 - 14 days. Pulsing cells for 30 minutes with [^{3}H]-leucine was sufficient to detect leucine incorporated antibody in the lysate and supernatant, however for a stronger signal, a one hour pulse was chosen for future wildtype vs. *Prkaa1*$^{\Delta/\Delta}$ experiments (**Fig. 2.4B**). To determine molar amounts of [^{3}H]-leucine incorporated into antibody, membranes were stained with Ponceau S Solution (Sigma) to visualize samples, which were excised with a razor blade and subjected to liquid scintillation counting using a Beckman Coulter LS 6500. [^{3}H]-leucine incorporation was calculated after determining the counting efficiency of the instrument. To ensure that loss of AMPK did not alter leucine uptake and therefore change the opportunity to be incorporated into

antibody, day 7 cultures were seeded as above for one hour with [^{3}H]-leucine and counts per minute were determined after lysates were subjected to liquid scintillation counting (**Fig. 2.4C**).

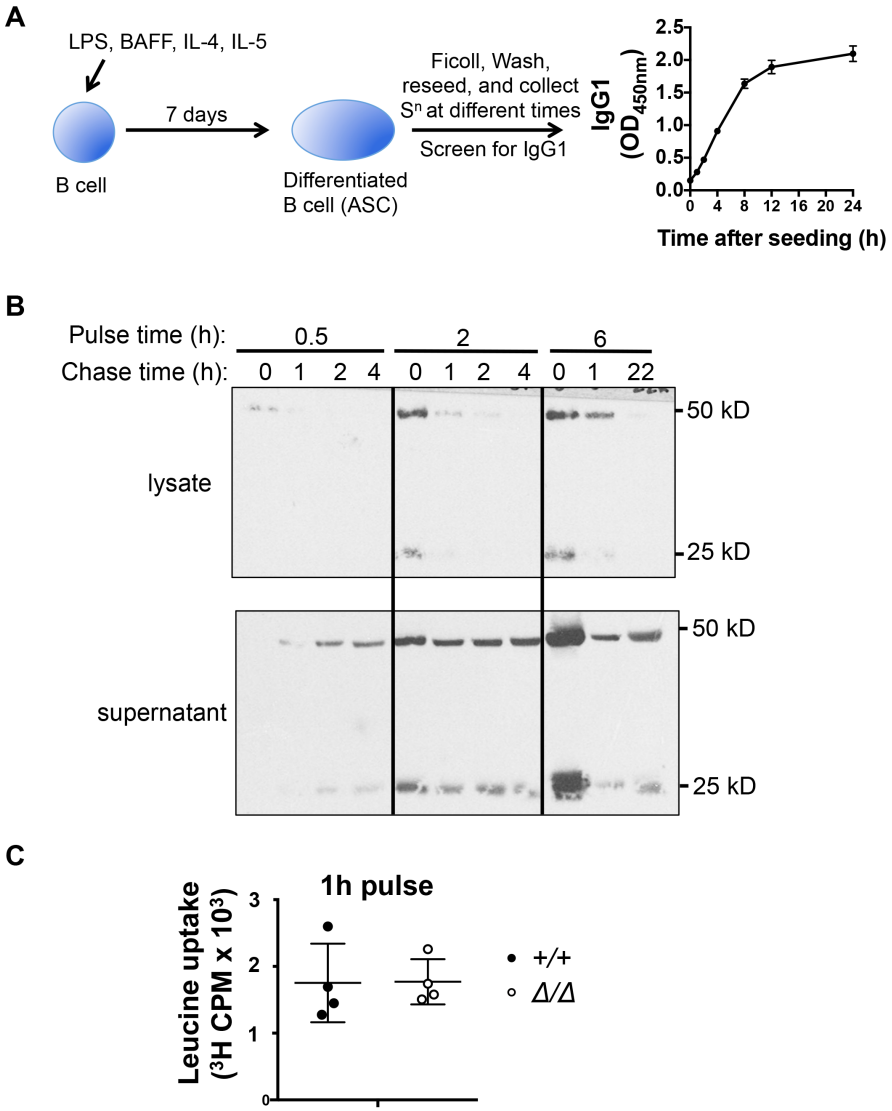

Figure 2.4 Antibody synthesis occurs within 30 minutes in differentiated plasma cells. (A) Schematic to differentiate naïve B cells into plasma cells after seven days of culture with LPS, BAFF, IL-4, and IL-5. Day 7 cultures (>60% B220^{lo}CD138^{+}) were subjected to Ficoll step gradient centrifugation, washed, and reseeded at 5 x 10^4 in 100 µL of fresh media. Right panel, relative concentration of IgG1 in supernatant collected at indicated time points after seeding as determined by ELISA. (B) Salicylate fluorography of wildtype day 7 protein G precipitated lysates and supernatants after pulsing with [^{3}H]-leucine and chasing at indicated time points. (C) [^{3}H]-leucine uptake after one hour pulse in wildtype (●) and *Prkaa1*$^{\Delta/\Delta}$ (○) day 7 differentiated cells.

Immunoblots

Unless otherwise indicated, all immunoblots depict relative protein from whole B cell extracts derived from splenocytes of 2- or 8-day cultures with LPS, BAFF, and 4-OHT at 5 x 10^6 per mL. For immunoblotting for AMPK targets after glucose starvation in Chapter 3, 2-day LPS blasts were washed and reseeded in glucose-free RPMI (Invitrogen) supplemented with 10% dialyzed HyClone FBS (Thermo Scientific) for the specified amount of time. Cells were washed twice in cold PBS and lysed in RIPA buffer (Sigma catalog # 0278) in the presence of phosphatase inhibitor (Thermo Scientific) and a protease inhibitor cocktail (Sigma). Twenty to one hundred micrograms of cell lysates were resolved by SDS-PAGE, transferred to PVDF membranes, and immunoblotted for AMPKα, phospho-S6 (S235/236), total S6, phospho-ACC (S79), total ACC, phospho-ULK1 (S317), total ULK1, phospho-4E-BP1, total 4E-BP1, and/or LC3 using monoclonal rabbit antibodies purchased from Cell Signaling Technology. Gls1 protein in Chapter 5 was detected using KGA-Specific polyclonal antibody (Proteintech). Actin (Santa Cruz Biotechnology) was detected on all blots as a loading control. Immunoblots were visualized using Odyssey Imaging system (Li-Cor) after incubation with secondary reagents, anti-rabbit IgG-680, or anti-mouse IgG-800 (Invitrogen).

Seahorse assays

Oxygen consumption rate (OCR) and extracellular acidification rate (ECAR) were measured using an XFe96 extracellular flux analyzer (Seahorse Bioscience). In Chapter 3, 5 x 10^5 two-day LPS and BAFF activated B cells were seeded per well of a Cell-Tak (5 μg/mL; Corning) coated plate. In Chapter 5, 2.5 x 10^5 two day LPS, BAFF, IL-4, and

IL-5 activated B cells were seeded per well. Glycolytic and mitochondrial stress tests were performed as previously described (Raybuck et al., 2018, Caro-Maldonado et al., 2014). Maximum respiration, spare respiratory capacity, glycolysis, glycolytic capacity, and glycolytic reserve were calculated using formulas derived from the Seahorse platform.

Glucose Uptake

Equal numbers of cells were incubated at 37˚C for 15 minutes in glucose uptake buffer (8.1 mM Na_2HPO_4, 1.4 mM KH_2PO_4, 2.6 mM KCl, 136 mM NaCl, 0.5 mM $MgCl_2$, 0.9 mM $CaCl_2$, pH 7.4) to deplete intracellular glucose stores as in (Cho et al., 2011). Samples were incubated in triplicate (10^6 per sample) with 1 µCi of 2-[1,2-^{3}H]-deoxyglucose (20 Ci/mmol; PerkinElmer) in glucose uptake buffer for 4 min at room temperature and immediately spun through a layer of bromododecane into a layer of 20% perchloric acid/8% sucrose to stop the reaction and separate cells from unincorporated 2-[3H]-deoxyglucose. Recovered cell lysates separated from the supernatant were counted by liquid scintillation.

Immunocytochemistry

LPS blasts (5 x 10^5 cells from 2-day or 8-day cultures) in 0.5 mL were seeded on poly-D-lysine coated coverslips in a 24 well plate and stained with 100 nM MitoTracker Deep Red for 20 min at 37˚ before centrifugation to ensure cellular adherence to coverslips. Coverslips were incubated overnight with anti-B220 or CD138-PE and either anti-LC3, anti-ULK1 or anti-Lamp1 using rabbit monoclonal antibodies (Cell Signaling Technology) after methanol fixation and blocking in 1% BSA in PBST. Coverslips then

were mounted onto slides using ProLong Gold anti-fade reagent (Invitrogen) after incubation with secondary antibody anti-rabbit IgG 488 (Invitrogen) to visualize rabbit antibodies using an Olympus FV-1000 fluorescent confocal microscope. LC3-puncta were assessed using ImageJ. Co-localization of lysosomes and mitochondria, as an indicator of mitophagy, was determined using Just Another Co-localization Plugin (JACoP) in ImageJ as in Onnis et al. (Onnis et al., 2018). Manders' coefficient represents the percentage of mitochondrial pixels (blue channel) that overlay Lamp1 or ULK1 pixels (green channel) where 0 = no co-localization; 1 = 100% co-localization.

CHAPTER 3

AMPK IS CRITICAL FOR MITOCHONDRIAL FUNCTION AND HOMEOSTASIS IN B CELLS AND IS ESSENTIAL FOR HUMORAL MEMORY

The work presented in this chapter is modified from a publication in Journal of Immunology (Brookens et al., 2020)

I. Abstract and Significance

Emerging evidence indicates that metabolic programs regulate B cell activation and antibody responses. However, the metabolic mediators that support the durability of the memory B cell population are not fully elucidated. Adenosine monophosphate-activated protein kinase (AMPK) is an evolutionary conserved serine/threonine kinase that integrates cellular energy status and nutrient availability to intracellular signaling and metabolic pathways. In Chapter 3, I use genetic mouse models to show that loss of AMPKα1 in B cells led to a weakened recall response associated with a decline in the population of memory-phenotype B cells. AMPKα1-deficient memory B lymphocytes exhibited aberrant mitochondrial activity, decreased mitophagy, and increased lipid peroxidation. Moreover, loss of AMPKα1 in B lymphoblasts was associated with decreased mitochondrial spare respiratory capacity. Collectively, my findings fit a model in which AMPKα1 in B cells supports recall function of the memory B cell compartment by promoting mitochondrial homeostasis and longevity.

II. The B cell lineage has cell-type specific metabolic characteristics

B cell activation, proliferation, and differentiation are accompanied by metabolic adaptations to meet energetic and biosynthetic demands. Cell cycle progression and cell-type specific functions are highly interconnected with cell size (Miettinen et al., 2017). B cell subsets specialize in various key functions, influencing both cellular metabolism and size. Consistent with published data (Jellusova et al., 2017), germinal center B cells (GCB: $B220^+$ IgD^- $GL7^+$ Fas^+), which accumulate biomass to support rapid division, are larger than naïve B cells ($B220^+$ IgD^+) or memory B cells (MBC: $B220^+$ IgD^- $CD38^+$) as determined by forward scatter (FSC-A) using flow cytometry (**Fig. 3.1A**). Plasmablasts and plasma cells, collectively called antibody secreting cells (ASC: IgD^- $CD138^+$ $TACI^+$) are relatively larger cells which support the expanded endoplasmic reticulum and Golgi apparatus for the manufacture of large glycosylated antibodies. Interestingly, ASCs in the bone marrow, which can be long-lived (> decades) and manufacture large quantities antibody, were larger in size compared to splenic ASCs, which are mostly short-lived (< 3 days) and produce antibody on a smaller scale (Benner et al., 1981; Sze et al., 2000; Lam et al., 2016).

Carbohydrates, amino acids, and fatty acids provide a carbon source for energy and biosynthetic building blocks. While glucose is critical for ribonucleotide generation in activated B cells, ASCs use glucose mostly for the glycosylation of antibodies (Waters et al., 2018; Lam et al., 2016). To determine differences in glucose uptake in B lineage cells, splenocytes were stained *ex vivo* with fluorescently labeled glucose analog 2-(*N*-Nitrobenz-2-oxa-1,3-diazol-4-yl)Amino)-2-Deoxyglucose (2-NBDG) two weeks after immunization with hapten-carrier protein NP-ova. Though there are several caveats in

equating 2-NBDG uptake to glucose uptake (Sinclair et al., 2020), the mean fluorescence intensity of 2-NBDG was elevated in antigen-specific GCB and MBC compared to the naïve B cell population (**Fig. 3.1B**). Interestingly, ASCs had the highest level of 2-NBDG uptake compared to other B lineage subsets.

Mitochondria regulate multiple aspects of cellular metabolism including energy generation and providing TCA intermediates for downstream biosynthesis and epigenetic modifications. Mitochondrial content and mitochondrial-derived ROS (mtROS), measured by Mitotracker Green and MitoSOX respectively, were enhanced in GCB and MBC compared to naïve B cells (**Fig. 3.1C,D**). Interestingly, unlike with 2-NBDG uptake, ASCs had less mitochondrial content and mtROS compared to antigen-experienced GCB and MBC subsets. The observation that plasma cells have the highest level of glucose uptake but the lowest mitochondrial activity compared to GCB and naïve B cells was also observed in a recent study (Haniuda et al., 2020).

Mammalian target of rapamycin complex 1 (mTORC1), a protein complex that integrates nutrient sensing, protein synthesis, and cell size, is essential for robust GCB, and the differentiation and function of MBC and ASC populations (Raybuck et al., 2018; Jones et al., 2016). mTORC1 activity measured by phospho-S6 MFI by flow cytometry was increased in GCB, MBC and ASC relative to naïve B cells with the highest levels of phospho-S6 in GCB and ASC (**Fig 3.1E**). In sum, different B cell subsets are unique in cell size, glucose uptake, mitochondrial status, and mTORC1 activity.

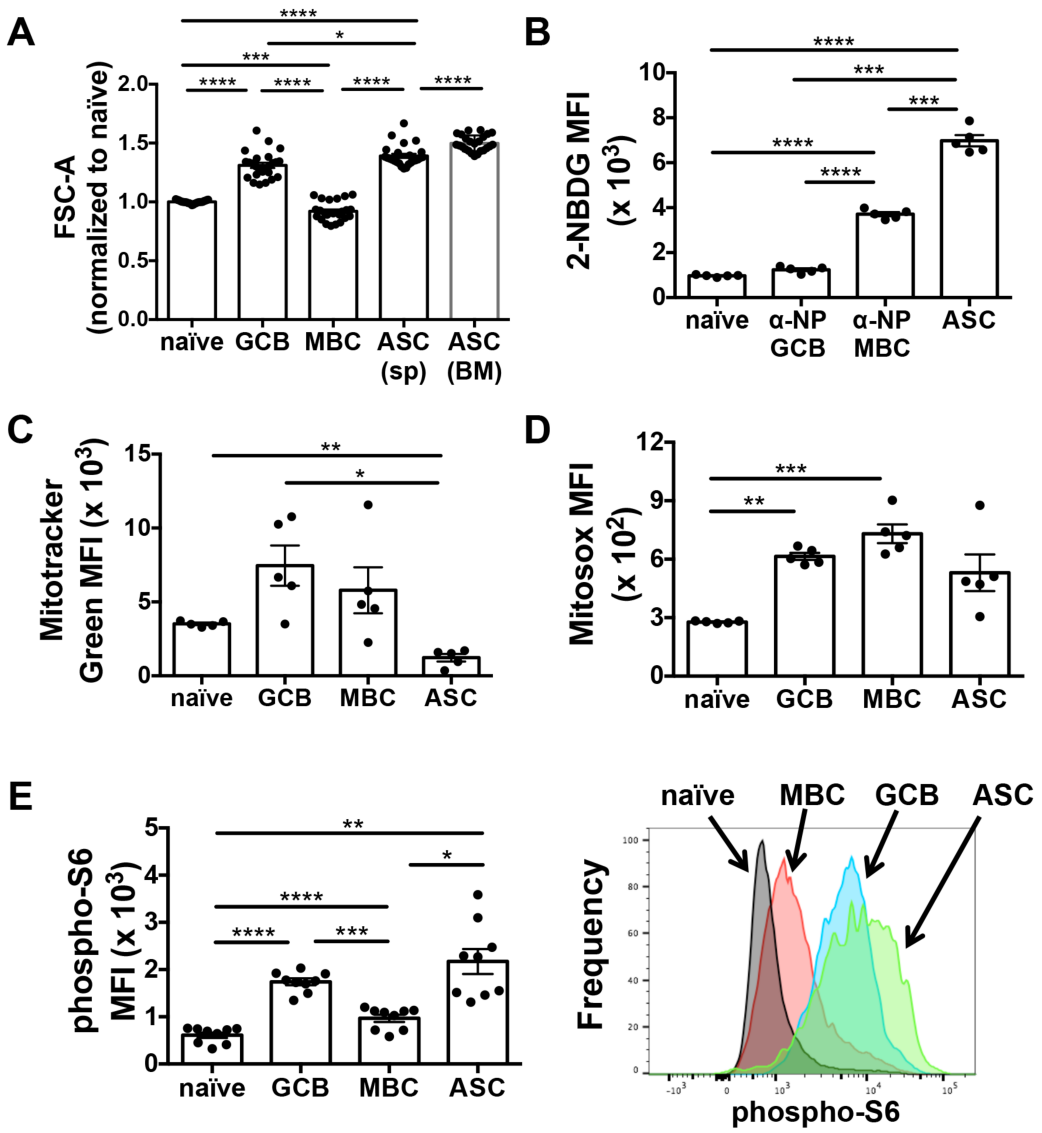

Figure 3.1 The B lineage has varying metabolic attributes. (A) Relative cell size of splenic naïve B cells ($B220^+IgD^+$), GCB ($B220^+IgD^-GL7^+Fas^+$), MBC ($B220^+IgD^-CD38^+$), and splenic and bone marrow ASC ($IgD^-CD138^+TACI^+$) as determined by forward scatter (FSC-A) measured using flow cytometry. (n = 25 wildtype mice from seven independent experiments). (B) *Ex vivo* uptake of fluorescently labeled glucose analog 2-NBDG by splenic naïve, ASC, NP-specific GCB and MBC from wildtype mice immunized with NP-ova two weeks prior. (n = 5 mice from one independent experiment). (C) Mitochondrial mass and (D) Mitochondrial derived ROS (mtROS) of splenic naïve, GCB, MBC, and ASC determined by MitoTracker Green or Mitosox dyes and flow cytometry. (n = 5 mice from one independent experiment). (E) Phospho-S6 expression in naïve, GCB, MBC, and ASCs determined by flow cytometry (left panel, MFI quantification; right panel, representative plot). (n = 9 wildtype mice from two independent experiments). Each symbol represents an individual mouse; mean ± SEM is displayed. * $p < 0.05$, ** $p < 0.01$, *** $p < 0.001$, **** $p < 0.0001$ (one-way repeated measures ANOVA (A-E).

To further investigate the effects of B cell differentiation into ASC on cellular metabolism, I cultured wildtype splenic B cells *in vitro* for up to 8 days with LPS, BAFF, IL-4, and IL-5. LPS, or lipopolysaccharide, is a mitogen that signals through Toll-like Receptor 4 on murine B cells. BAFF, or B-cell-activating factor belonging to the TNF family, is a fundamental survival factor for B cells. IL-4 and IL-5 signaling in B cells lead to gene regulation that induces class-switch recombination to IgG1 and plasma cell differentiation, respectively. As naïve B cells differentiate into ASC, they gradually lose expression of B220 and increase expression of CD138, also known as syndecan-1 (**Fig. 3.2A**). mTORC1 signaling, determined by phospho-S6 expression by Western Blot was enhanced in day 8 cultures (~60% $CD138^+$ $B220^{lo}$) compared to day 2 cultures (< 2% $CD138^+$ $B220^{lo}$) suggesting that ASC have more mTORC1 activity compared to early-activated B cells (**Fig. 3.2B**).

To compare mitochondrial mass and respiration in $B220^+$ cells vs. differentiated ASC ($CD138^+$ $B220^{lo}$) from the same culture, day 4 samples were analyzed, which have substantial frequencies of both populations at this time point (Fig. 3.2C,D,F). Analogous to *ex vivo* data in Fig. 3.1C, ASC generated *in vitro* have reduced mitochondrial content, respiration, and mtROS when compared to activated B cells as determined by Mitotracker Green, Mitotracker Deep Red, and MitoSOX respectively (**Fig. 3.2C,D**). Unlike Mitotracker Green, which has a thiol-reactive chloromethyl moiety that binds free thiols in the mitochondrial matrix regardless of membrane potential, Mitotracker Deep Red is retained only in actively respiring mitochondria and is sensitive to depolarization (Doherty et al., 2017; Xiao et al., 2016). Visually, mitochondria exhibited smaller and dimmer Mitotracker Deep Red signal in $CD138^+$ ASCs compared to $B220^+$ cells from day 8

cultures (**Fig. 3.2E**). Consistent with data shown here, reduced Mitotracker staining in $CD138^+$ cells was also evident in a previous study, which further provided evidence that activated $mtROS^{lo}$ B cells are fated for plasma cell differentiation (Jang et al., 2015). Furthermore, $CD138^+$ cells exhibited more disperse punctate mitochondria parallel to observations in IL-2 differentiated $CD8^+$ T effector cells (Buck et al., 2016) suggesting mitochondrial remodeling is linked to plasma cell differentiation. Despite decreased mitochondrial activity in ASC, the relative proportion of respiring mitochondria to total mitochondria, coined mitochondrial quality, is enhanced in ASC compared to activated B cells in day 4 cultures (**Fig. 3.2F**) (Tsui et al., 2018). It is conceivable that less mtROS in ASC compared to activated B cells results in less oxidative damage rendering better mitochondrial quality (Pickles et al., 2018). All together, data in Figure 3.1 and 3.2 are supportive of dynamic metabolic programs throughout the B lymphocyte lineage. These findings are summarized in Table 3.1.

B cell subset	Cell size	Glucose uptake	mTORC1	Mitochondrial mass	mtROS
naive	+	+	+	+	+
GCB	++	++	+++	++	++
MBC	+	++	++	++	++
ASC	+++	++++	++++	+	+

Table 3.1 Relative metabolic parameters in B-2 lineage cells after immunization.

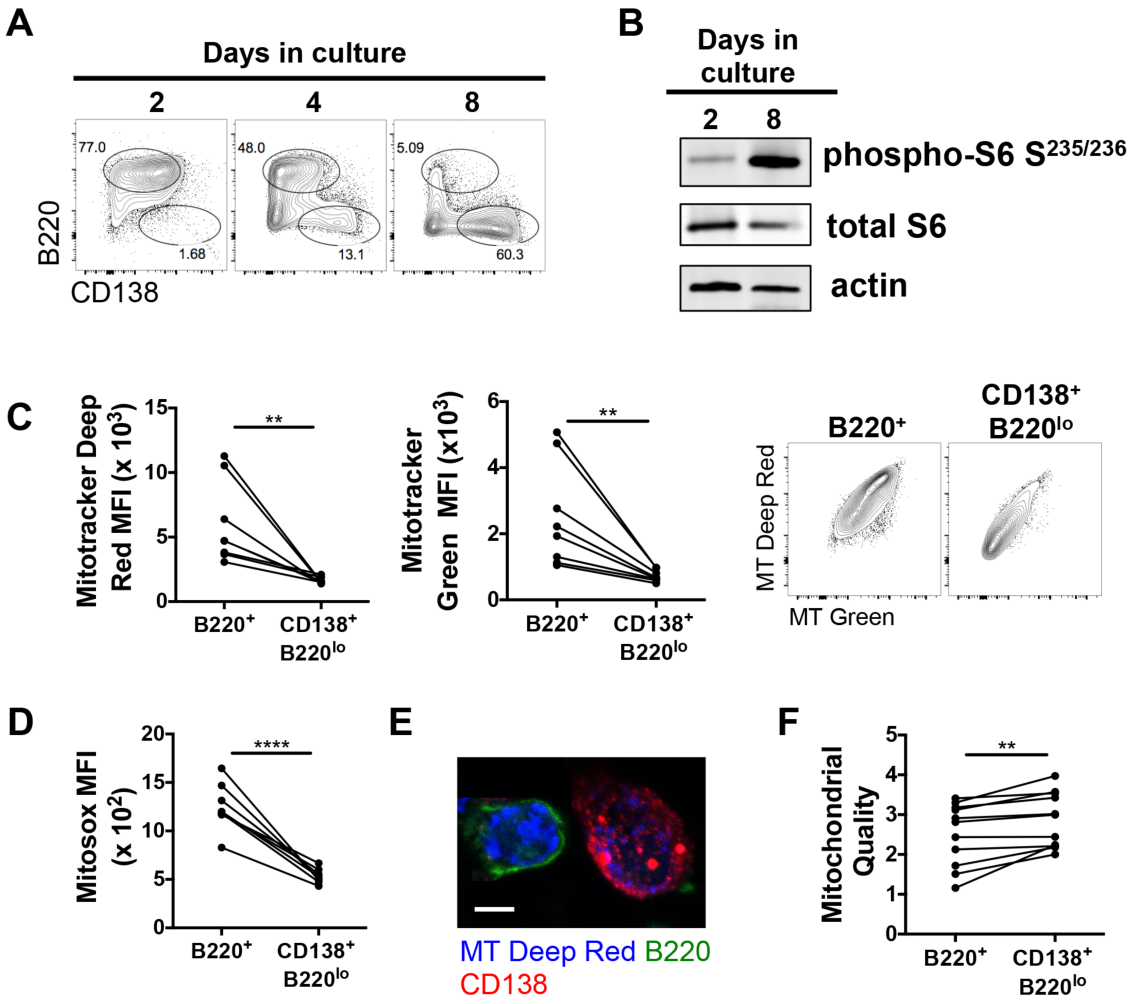

Figure 3.2 B cell differentiation into plasma cells induces increased mTORC1 signaling and decreased mitochondrial function. (A) Representative flow plots depicting the frequency of B cells ($B220^{+}$) and plasma cells ($B220^{lo}$ $CD138^{+}$) on days 2, 4, and 8 after treatment of wildtype splenic B cells with LPS, BAFF, IL-4, and IL-5. (B) Immunoblot of phospho-S6, total S6, and actin from lysates collected on days 2 and 8 of culture. (C) Mitochondrial respiration, left panel, and total mitochondrial mass, middle panel, of wildtype B cells and plasma cells on day 4 of culture as determined by the MFI of MitoTracker Deep Red or MitoTracker Green, respectively. Right panel, representative plot of Mitotracker Green vs. Mitotracker Deep Red in B cells and plasma cells. (D) mtROS of B cells and plasma cells on day 4 of culture as determined by MFI of MitoSOX dye. (E) Immunofluorescence of day 8 culture after staining with Mitotracker Deep Red (blue), B220 (green), and CD138 (red). Scale bar, 5μm. (F) Mitochondrial Quality of wildtype B cells and plasma cells calculated as the ratio of actively respiring mitochondria (MitoTracker Deep Red MFI) over total mitochondrial mass (MitoTracker Green MFI) on day 4 of culture. Each pair represents a day 4 culture from n = 8 individual mice from three independent experiments. ** $p < 0.01$, **** $p < 0.0001$ (paired Student's t-test C-E).

III. AMPKα1 is expressed in B cells and is critical for optimal mitochondrial function

In addition to cell-intrinsic alterations in the metabolic programs required to support the B lineage at various stages, cell-extrinsic factors like activation signals and nutrient availability can alter B cell metabolism. Different tissues and micro-anatomical sites where B cell activation, GC, and antibody synthesis occur have various nutrient and oxygen availability (Tsentalovich et al., 2020; Cho et al., 2016; Jellusova et al., 2017). Regulation of metabolism that supports both the diverse requirements in the B lymphocyte lineage and supports the adaptations necessary to face nutrient-limiting microenvironments is not yet fully elucidated.

Adenosine monophosphate-activated protein kinase (AMPK) is a conserved serine/threonine kinase that restores cellular energy homeostasis in metabolically stressful conditions (Garcia et al., 2017). At the onset of my thesis, AMPK had already been shown to be critical for primary effector $CD4^+$ and $CD8^+$ T cell responses to influenza as well as $CD8^+$ T cell memory responses to Listeria monocytogenes-OVA (Blagih et al., 2015; Rolf et al., 2013). I sought to test the role of AMPK in immunity conferred by the B lineage or humoral responses.

In metabolically stressful conditions, such as low glucose availability, upstream liver kinase B1 (LKB1) phosphorylates the threonine-172 residue of the catalytic subunit of AMPK, essential for its activation (Hawley et al., 1996; Shaw et al., 2004). Activated AMPK in turn phosphorylates multiple downstream targets, the most notable being an inhibitory phosphorylation on acetyl-CoA carboxylase (ACC) which otherwise promotes fatty acid synthesis (Munday et al., 1988). A simplified cartoon depiction of AMPK signaling is

illustrated in Fig 1.6. Glucose withdrawal led to increased pACC ^{S79} expression in day 2 LPS and BAFF cultured cells (**Fig 3.3A**). Alternatively, AMPK activation can be induced by Ca^{2+}/calmodulin-dependent kinase kinase β (CAMKKβ) independent of metabolic stress (Fig 1.6) (Hawley et al., 2005; Tamás et al., 2006). In parallel to evidence of Ca^{2+}-induced phosphorylation of AMPK in T cells by crosslinking the TCR (Tamás et al, 2006), BCR crosslinking with anti-IgM led to elevated AMPK activity indicated by elevated pACC ^{S79} expression (**Fig 3.3B**). Data indicate that AMPK signaling turns on in response to both low nutrient availability and anti-BCR activation in B cells.

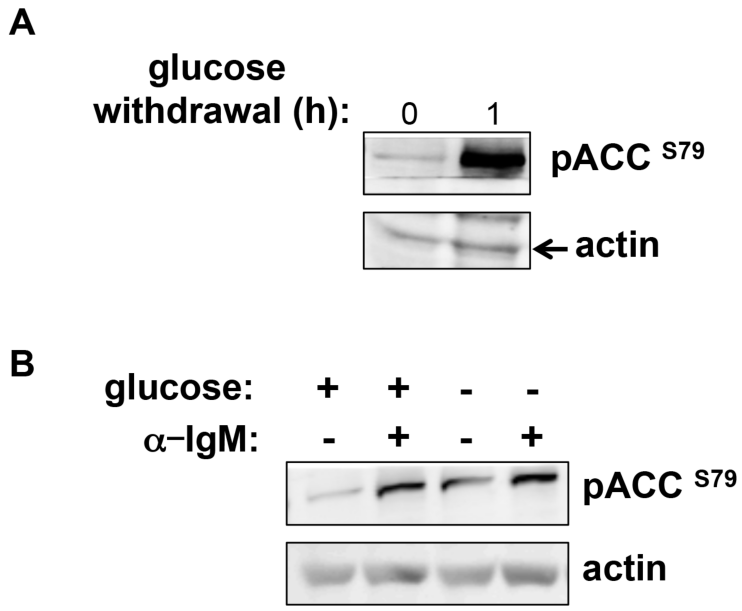

Figure 3.3 Expression of AMPK target pACC S^{79} is induced by glucose starvation and BCR cross-linking. (A) Immunoblot for pACC S^{79} after 2-day LPS/BAFF activated wildtype B cells were deprived of glucose for one hour. (B) Immunoblot for pACC S^{79} after 2-day α-IgM/BAFF activated wildtype B cells were deprived of glucose for 2h and reactivated with α-IgM for an additional hour. Data are representative of four (A) or two (B) independent experiments.

Previous studies have provided evidence that AMPKα1, encoded by *Prkaa1*, is the only isoform of the essential catalytic subunit of AMPK expressed in B cells (Mayer et al., 2008; Waters et al., 2019; Faubert et al., 2013). Thus, to generate mice with a conditional B cell-specific deletion of AMPK, I crossed *Prkaa1* floxed mice to transgenic animals expressing a hydroxytamoxifen-inducible Cre recombinase under the control of the huCD20 promoter (huCD20-CreER^{T2}) (Fig. 2.2). This B lineage-restricted promoter is

active from the pre-B to mature B cell stage (Ahuja et al., 2007). AMPKα protein expression was undetectable in LPS-activated B lymphoblasts from tamoxifen-injected *Prkaa1*$^{f/f}$ huCD20-CreER^{T2} mice when compared to *Prkaa1*$^{+/+}$ huCD20-CreER^{T2} controls (**Fig. 3.3**). Since there was no detectable band in *Prkaa1*$^{\Delta/\Delta}$ cells with the AMPKα antibody which detects both AMPKα1 and α2 catalytic isoforms, I conclude that only AMPKα1 is substantially expressed in B cells and that loss AMPKα1 did not lead to compensatory induction of AMPKα2.

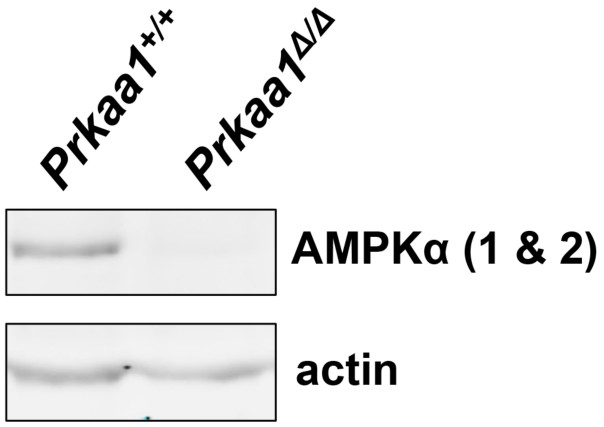

Figure 3.4 The AMPKα1 isoform is expressed in B cells. Immunoblot for AMPKα (1 and 2) and actin expressed in 2-day LPS-activated B cells purified from *Prkaa1*$^{+/+}$ and *Prkaa1*$^{\Delta/\Delta}$ mice. Data are representative of immunoblots from n = 3 vs. 3 mice.

In light of the role of AMPK as a regulator of intermediary metabolism and mitochondrial function, I next tested metabolic performance of activated B cells that were AMPKα1-sufficient or -deficient. Extracellular flux analyses revealed no changes in any aspect of the extracellular acidification rate (ECAR) with the loss of AMPKα1 (**Fig. 3.5A**). In contrast, analyses of the oxygen consumption rate (OCR), before and after treatment with different mitochondrial stressors, determined that mitochondrial oxidative phosphorylation was impaired in AMPKα1-deficient B cells (**Fig. 3.5B**). Basal respiration, represented by the OCR values before the addition of ATP synthase V inhibitor oligomycin, was not significantly altered by the loss of AMPKα1. However, loss

of AMPKα1 led to defects in maximal and spare respiratory capacity (**Fig. 3.5C**). The OCR derived from the function of the electron transport chain as the OCR levels were dependent on complex I and III inhibitors rotenone and antimycin A. Taken together, these data indicate that AMPKα1 in activated B cells promotes the establishment or maintenance of optimal respiratory function of mitochondria.

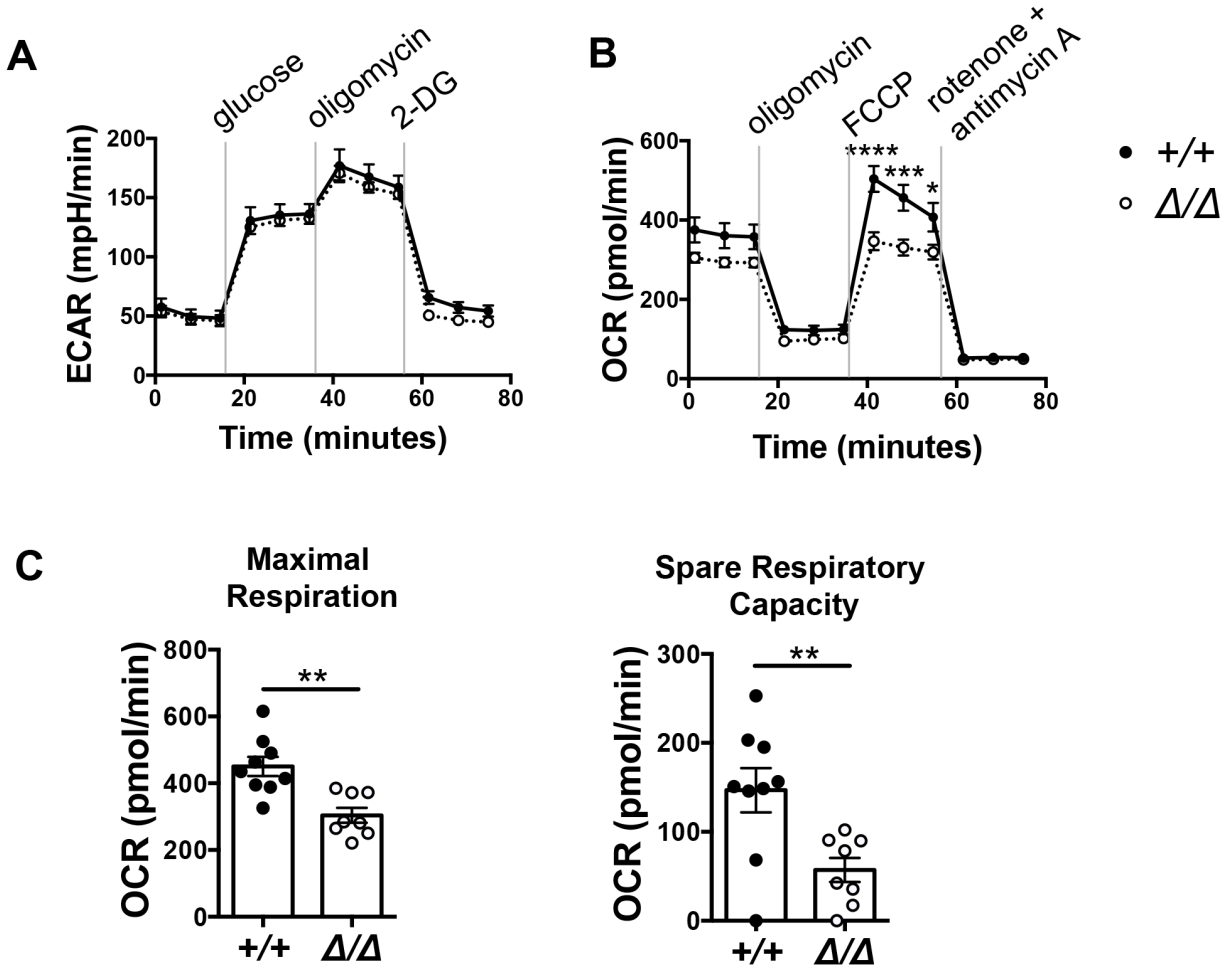

Figure 3.5 AMPK is essential for optimal mitochondrial respiration in activated B cells. (A) Glycolytic and (B) Mitochondrial stress tests after *Prkaa1*$^{+/+}$ or *Prkaa1*$^{\Delta/\Delta}$ B cells were activated with LPS and BAFF for 2 days. (C) Maximal respiration, left panel, and spare respiratory capacity, right panel, were calculated by Agilent Seahorse XF Cell Mito Stress Test Report Generator. Filled circles (●) represent n = 9 wildtype mice and open circles (○) represent n = 8 *Prkaa1*$^{\Delta/\Delta}$ mice from three independent experiments; SEM is displayed. * $p < 0.05$, ** $p < 0.01$, *** $p < 0.001$ (two-way ANOVA with Sidak's multiple comparisons (B), or Student's t-test (C)).

IV. AMPK is dispensable for generating GCB but important for mitochondrial quality in GCB

I next set out to test the role of AMPK on B cell function over the course of an immune response. One would expect that GCB, which are activated through the BCR and are possibly competing for limited nutrients, would require AMPK signaling to mitigate metabolic stress. To test the reliance of AMPK on GCB formation, I immunized tamoxifen-treated huCD20-CreER^{T2} mice (*Prkaa1*$^{+/+}$ or *Prkaa1*$^{f/f}$) with hapten-carrier NP-KLH followed by boosting after three weeks and analyses of NP-specific humoral responses one week after the booster immunization (**Fig. 3.6A**). Surprisingly, but consistent with a relatively recent study (Waters et al., 2019), I observed no difference in total or NP-specific germinal center B cells (B220^{+} IgD^{-} GL7^{+} Fas^{+} NP^{+}) in mice with AMPKα1-deficient B cells (**Fig. 3.6B-D**) suggesting that AMPK is unessential for the generation of GCB.

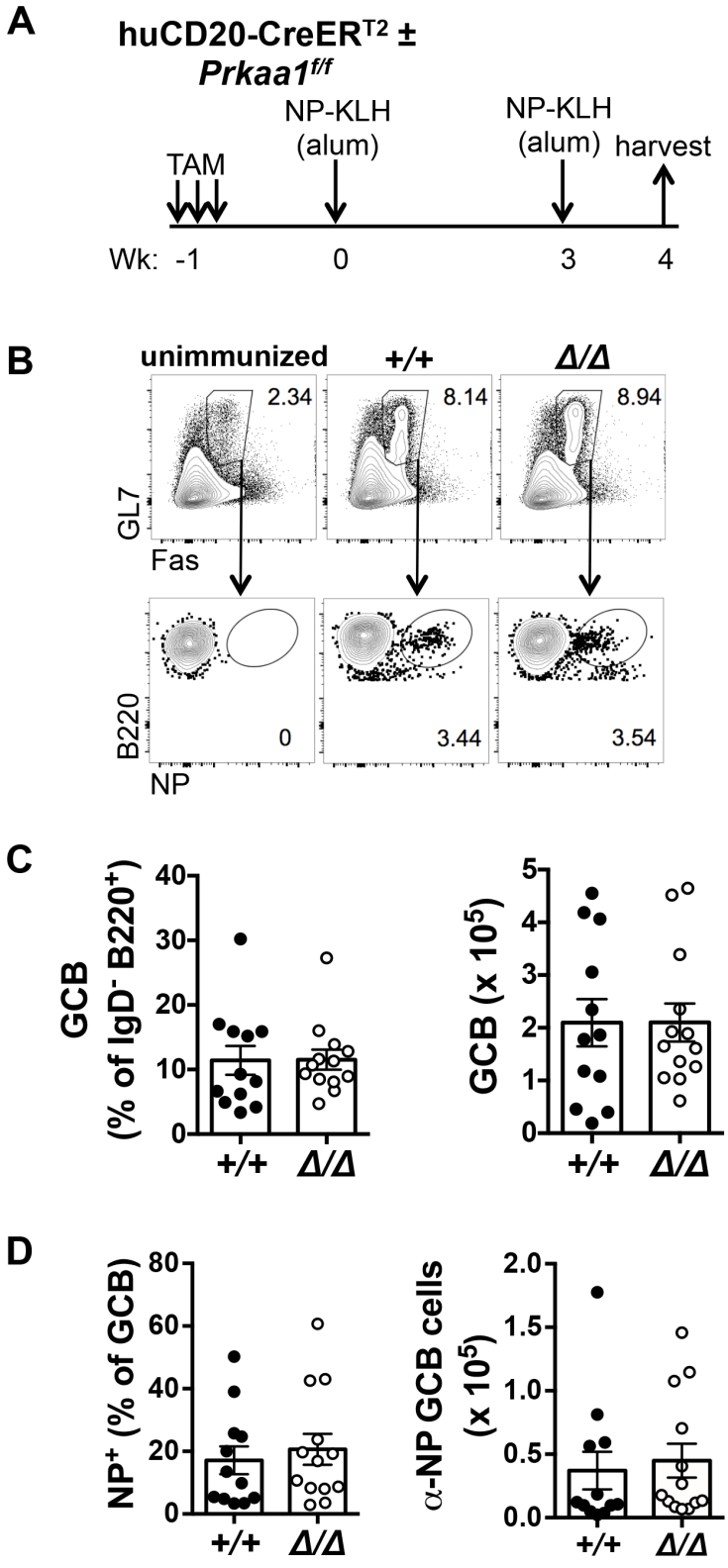

Figure 3.6 AMPK is dispensable for generating GCB. (A) Schematic of immunization strategy with NP-KLH using mice harboring a tamoxifen-inducible Cre under control of a B lineage restricted promoter, huCD20. Mice were treated with three doses of tamoxifen to induce B-cell specific deletion of *Prkaa1* and then immunized and boosted three weeks later with NP-KLH. Mice were harvested one week post boost to monitor primary B cell responses. (B) Representative flow plots depicting frequencies of GCB ($B220^+$ $GL7^+$ Fas^+) from the Dump negative gate (Dump: CD11b, CD11c, F4/80, Gr1, 7-AAD, IgD) and NP^+ GCB in unimmunized, *Prkaa1*$^{+/+}$, or B cell-specific *Prkaa1*$^{Δ/Δ}$ mice. (C) Frequency and total number of GCB in the spleen of *Prkaa1*$^{+/+}$ or B cell-specific *Prkaa1*$^{Δ/Δ}$ mice. (D) Frequency and total number of antigen specific GCB in the spleen of *Prkaa1*$^{+/+}$ or B cell-specific *Prkaa1*$^{Δ/Δ}$ mice. Data represent the mean ± SEM of n = 12 wildtype and n = 13 *Prkaa1*$^{Δ/Δ}$ mice from four independent experiments.

Despite normal GCB numerically, actively respiring mitochondria and mitochondrial content were impaired in both *Prkaa1*$^{\Delta/\Delta}$ GCB cells and nonGCB (B220^{+} GL7^{-}) compared to wildtype as foreshadowed by the impaired OCR in activated *Prkaa1*$^{\Delta/\Delta}$ B cells shown in Fig 3.5B (**Fig 3.7A**). Furthermore, *Prkaa1*$^{\Delta/\Delta}$ GCB had proportionally more dysfunctional mitochondria than wildtype, as determined by the Mitochondrial Quality calculation using the ratio of MFI dyes as described in Fig. 3.2 (**Fig. 3.7B**). Defects in mitochondrial quality coincided with increased MitoSOX staining in the *Prkaa1* $^{\Delta/\Delta}$ GCB population (**Fig. 3.7C**).

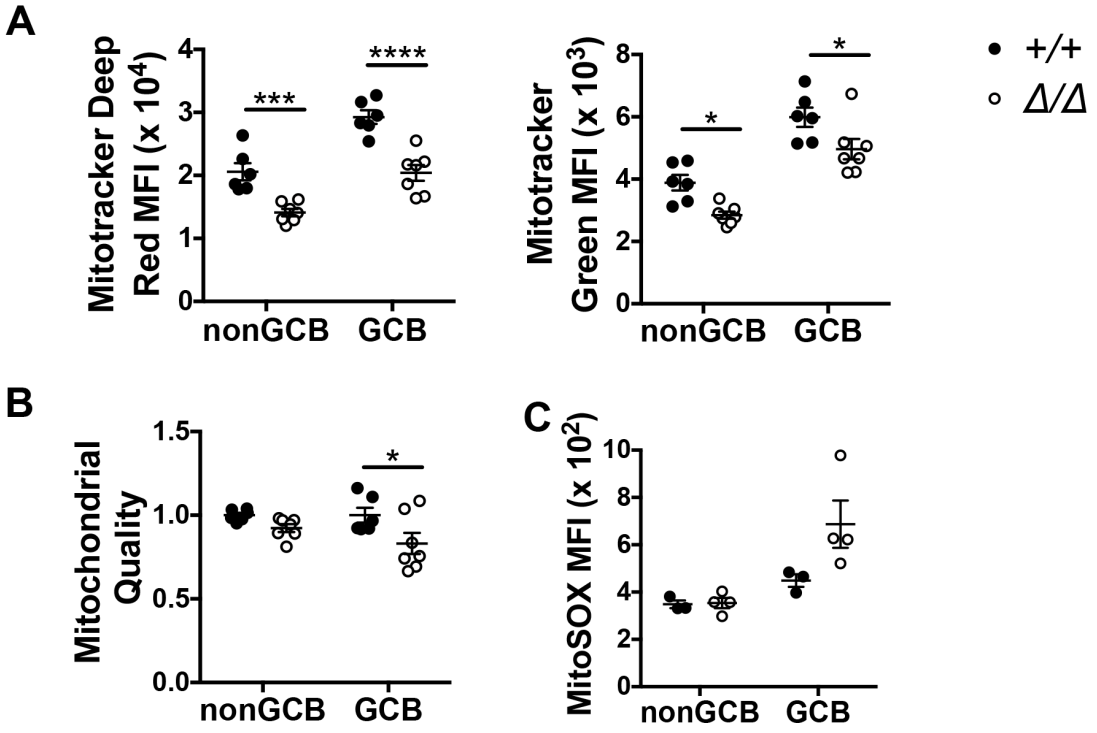

Figure 3.7 AMPK maintains mitochondrial quality in GCB. (A) Mitochondrial respiration, left panel, and mitochondrial mass, right panel, in GCB (B220^{+} GL7^{+}) and nonGCB (B220^{+} GL7^{-}) of *Prkaa1*$^{+/+}$ and *Prkaa1*$^{\Delta/\Delta}$ after immunization strategy depicted in Fig. 3.6A. (B) Relative mitochondrial quality of GCB and nonGCB of *Prkaa1*$^{+/+}$ and *Prkaa1*$^{\Delta/\Delta}$ calculated as a ratio of Mitotracker Deep Red to Mitotracker Green and normalized to wildtype nonGCB values as an indicator of relative levels of dysfunctional mitochondria. (C) mtROS of nonGCB and GCB in *Prkaa1*$^{+/+}$ and *Prkaa1*$^{\Delta/\Delta}$ mice. Data represent two independent experiments using a total of n = 6 *Prkaa1*$^{+/+}$ and n = 7 *Prkaa1*$^{\Delta/\Delta}$ mice. * $p < 0.05$, *** $p < 0.001$, **** $p < 0.0001$. (two-way repeated measures ANOVA with Sidak's multiple comparisons (A-B)).

V. AMPK dampens initial generation of MBC but promotes longevity in MBC likely by supporting mitophagy

A prior study also provided evidence that a B cell-specific deletion of AMPKα1 driven by CD19-Cre had no effect on GC (Waters et al., 2019). However, the impact of AMPKα1 on other outcomes of the GC, including the generation and maintenance of memory remain unexamined. After the immunization strategy depicted in Fig. 3.6A, induced loss of AMPKα1 from mature B cells led to increased frequencies of total splenic memory phenotype B cells (M_{phen}BC: $B220^+$ IgD^- $CD38^+$) and modestly increased total M_{phen}BC compared to wildtype controls (**Fig. 3.8A**). The frequency and total number of antigen-specific M_{phen}BC ($B220^+$ IgD^- $GL7^-$ $CD38^+$ NP^+) in the spleen were two-fold increased in number in *Prkaa1*$^{\Delta/\Delta}$ mice compared to wildtype mice (**Fig. 3.8B**). I further examined whether AMPKα1 differentially supported the generation of functionally distinct M_{phen}BC subsets distinguished by PD-L2 and CD80 expression (Zuccarino-Catania et al., 2014; Weisel et al., 2017; Tomayko et al., 2010). The double-positive ($CD80^+$ $PD\text{-}L2^+$) population, which makes up ~5-10% of total M_{phen}BC, are approximately 5 times more likely than other M_{phen}BC subsets to be $IgG1^+$. The double-negative ($CD80^-$ $PD\text{-}L2^-$) M_{phen}BC population, which makes up the majority (>85%) of total M_{phen}BC, are >90% IgM^+ (Weisel et al., 2017; Tomayko et al., 2010). (**Fig. 3.8C**). Interestingly, hapten-binding double-negative $CD80^-$ $PD\text{-}L2^-$ M_{phen}BC in *Prkaa1*$^{\Delta/\Delta}$ mice were increased two-fold in the absence of AMPKα1 with no alterations in double positive $CD80^+$ $PD\text{-}L2^+$ M_{phen}BC suggesting different degrees AMPK involvement in the two M_{phen}BC subsets (**Fig. 3.8D**). Although I cannot exclude a contribution of renewed proliferation of M_{phen}BC after the boost, I infer that AMPK dampened the initial M_{phen}BC

population size, particularly double negative CD80$^-$ PD-L2$^-$ M_{phen}BC, after a short-term prime/boost immunization strategy.

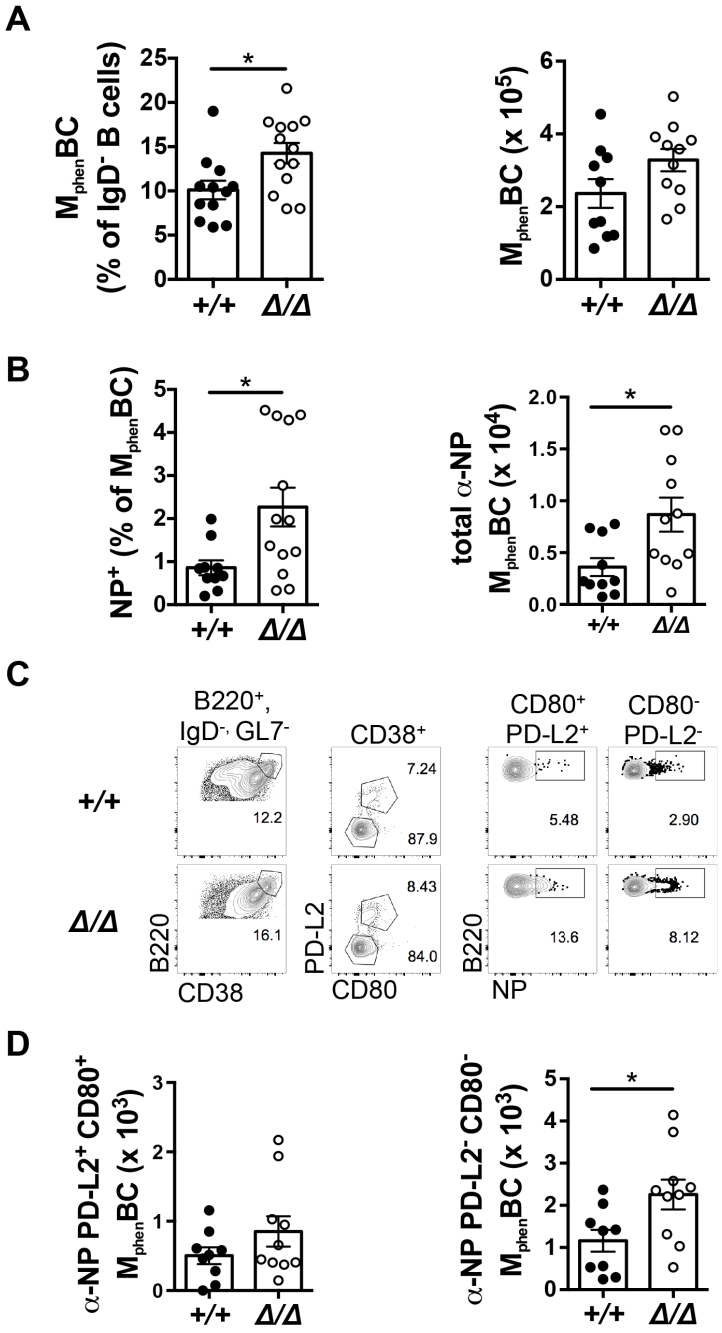

Figure 3.8 Loss of AMPK leads to elevated M_{phen}BC produced during the GCB reaction. (A) Representative flow plots depicting frequencies of phenotypical memory B cells (M_{phen}BC: B220$^+$ CD38$^+$) from the B220$^+$, Dump negative gate (Dump: CD11b, CD11c, F4/80, Gr1, 7-AAD, IgD, GL7, CD4, CD8) and NP$^+$ M_{phen}BC subset populations CD80$^+$ PD-L2$^+$ and CD80$^-$ PD-L2$^-$ in *Prkaa1*$^{+/+}$ and *Prkaa1*$^{Δ/Δ}$ mice after immunization regimen depicted in Fig. 3.6A. Frequency and absolute number of splenic (B) M_{phen}BC, (C) NP$^+$ M_{phen}BC, and (D) NP$^+$ CD80$^+$ PD-L2$^+$ M_{phen}BC or NP$^+$ CD80$^-$ PD-L2$^-$ M_{phen}BC in *Prkaa1*$^{+/+}$ and *Prkaa1*$^{Δ/Δ}$ mice. Data represent the mean ± SEM of at least n = 9 wildtype and n = 9 *Prkaa1*$^{Δ/Δ}$ mice from three independent experiments. * p < 0.05 (Student's t-test (B-D)).

Memory B cells (MBC), generated during primary responses, can live for decades recirculating in the blood and secondary lymphoid tissues (Crotty et al., 2003; Gourley et al., 2004; Weisel et al., 2017; Zotto et al., 2021). To test the role of AMPK on the long-term maintenance of MBC subsets, I immunized *Prkaa1*$^{+/+}$*mb1*-Cre and *Prkaa1*$^{f/f}$*mb1*-Cre mice with NP-KLH and tracked the frequency of NP^{+} M$_{phen}$BC in the peripheral blood over time (**Fig. 3.9A**). The potent B lineage specific *mb1*-Cre transgene allowed me to overcome the technical barrier relating to new B cell production after tamoxifen treatments in the huCD20-CreER^{T2} mice (Hobeika et al., 2006). This mode of excision, which starts as early as the pro-B cell stage, is constitutive and tamoxifen-independent. Recall that lack of AMPKα1 throughout B lymphoid ontogeny had no discernable effect on the pre-immune B cell populations of *Prkaa1*$^{f/f}$ *mb1*-Cre mice (Fig. 2.3A,B). Consistent with the initial increase in total splenic M$_{phen}$BC after immunization in the huCD20-CreER^{T2} model depicted in Fig. 3.8B, the frequency of NP^{+} M$_{phen}$BC in the peripheral blood of *Prkaa1*$^{f/f}$ *mb1*-Cre mice was on average 2-fold higher than in wildtype mice 3 weeks after immunization (**Fig. 3.9B**). However, by six weeks the relative frequency of total circulating *Prkaa1*$^{\Delta/\Delta}$ NP^{+} M$_{phen}$BC declined relative to wildtype levels of NP^{+} M$_{phen}$BC and lessened to below wildtype levels by nine weeks. The gradual decline in NP^{+} M$_{phen}$BC population over time in *Prkaa1*$^{\Delta/\Delta}$ mice was driven specifically by the wane in the CD80^{-} PD-L2^{-} M$_{phen}$BC population (**Fig 3.9C**). Minimal change over time was observed in the *Prkaa1*$^{\Delta/\Delta}$ NP^{+} CD80^{+} PD-L2^{+} M$_{phen}$BC population relative to wildtype (**Fig 3.9D**). These data support the concept that AMPK supports the longevity of the MBC population, specifically double negative MBC, which is the subset

critical for repopulating the germinal center upon re-exposure to antigen (Zuccarino-Catania et al., 2014).

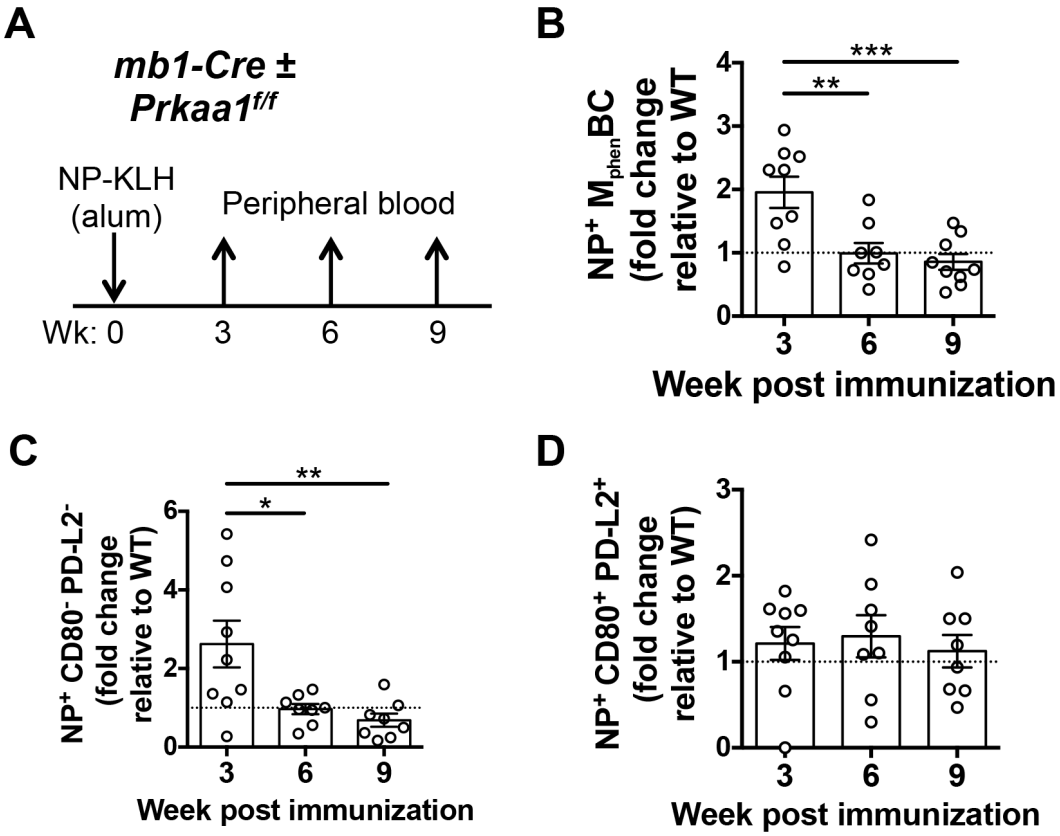

Figure 3.9 Loss of AMPK leads to a decline in the circulating M_{phen}BC population over time. (A) Schematic of the immunization strategy using mice with mb1-integrated Cre such that Cre is constitutively expressed exclusively in B cells from the pro-B cell stage. Mice were immunized with NP-KLH and bled every three weeks to track the fate of circulating NP-specific M_{phen}BC over time by flow cytometry. (B) Fold change of NP^+ cells in the peripheral blood of *Prkaa1*$^{\Delta/\Delta}$ mice relative to wildtype mice (dashed line) from the (B) total M_{phen}BC gate, (C) $CD80^+$ $PD\text{-}L2^+$ M_{phen}BC gate, and (D) $CD80^-$ $PD\text{-}L2^-$ M_{phen}BC gate at weeks 3, 6, and 9 post immunization. Dashed line indicates the relative average of the wildtype values. Data represent the mean of the fold change ± SEM of n = 9 *Prkaa1*$^{\Delta/\Delta}$ mice relative to n = 7 *Prkaa1*$^{+/+}$ mice from two independent experiments. * $p < 0.05$, ** $p < 0.01$, *** $p < 0.001$ (one-way ANOVA with Tukey's multiple comparisons (B) and (D)).

While there are several studies that track antigen-specific T cells in the peripheral blood of mice (Zotto et al., 2021; Blagih et al., 2015), there was only one precedent that I could find where circulating memory B cells after immunization were screened as in Fig. 3.9 (Blink et al., 2005). To confirm that *Prkaa1*$^{\Delta/\Delta}$ mice harbor a decreased MBC population several weeks after immunization in the spleen, I immunized *mb1*-Cre mice (*Prkaa1*$^{f/f}$ and *Prkaa1*$^{+/+}$) with NP-KLH, analogous to Fig. 3.6A, except mice were harvested eight weeks after the booster immunization (**Fig. 3.10A**) instead of one. The frequency of NP^{+} cells from the M_{phen}BC population and the total number of NP^{+} MBC was markedly reduced in the spleen of *Prkaa1*$^{\Delta/\Delta}$ mice compared to wildtype (**Fig. 3.10B**) with most of the defect driven by the double negative CD80^{-} PD-L2^{-} M_{phen}BC population (**Fig. 3.10C**). Data in figures 8, 9, and 10 demonstrate that AMPK in B cells dampens the initial generation of MBC after immunization but is critical for the longevity of this population. Hence, AMPK in MBC protects against a “live fast, die young” phenotype. Specifically, AMPK activation supports the long-term persistence of the majority of the MBC population.

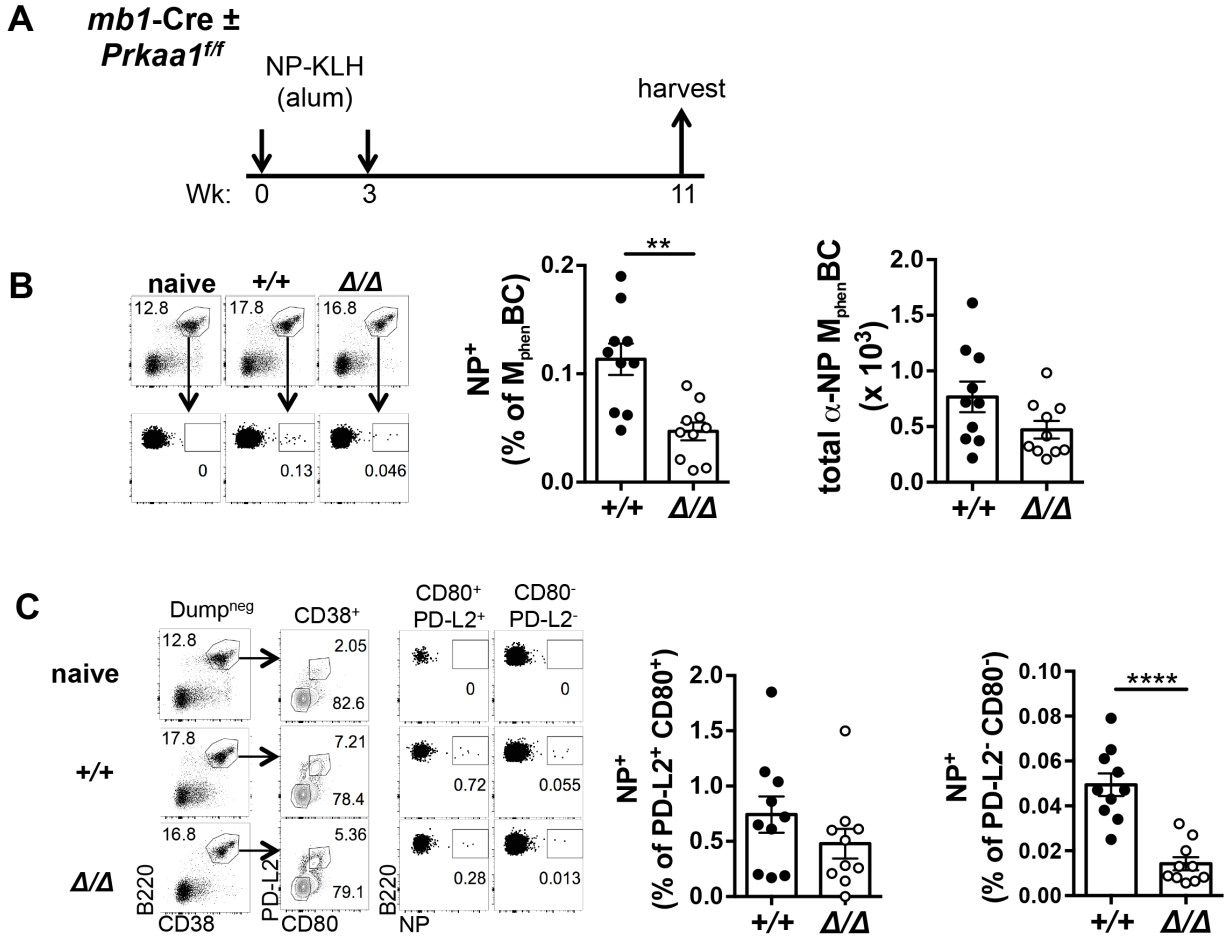

Figure 3.10 AMPK promotes the long-term maintenance of the PD-L2$^-$ CD80$^-$ MBC population. (A) Immunization strategy using *mb1-Cre* mice depicting immunization with NP-KLH, a booster immunization at week 3, followed by harvest eight weeks post boost to test long-term persistence of the MBC population. Representative flow plots and quantification depicting frequency of splenic NP$^+$ cells from the (B) total M_{phen}BC gate and the (C) CD80$^+$ PD-L2$^+$, left panel, or CD80$^-$ PD-L2$^-$, right panel, MBC subset gates in *Prkaa1*$^{+/+}$ and *Prkaa1*$^{\Delta/\Delta}$ mice at the harvest time point. The mean ± SEM is displayed where each dot represents one mouse with a total of n = 10 *Prkaa1*$^{+/+}$ and n = 10 *Prkaa1*$^{\Delta/\Delta}$ from three independent experiments. ** $p < 0.01$, **** $p < 0.0001$ (Student's t-test (B) and (C)).

AMPK regulates many aspects of intracellular metabolism including supporting autophagy, the degradation and recycling of cellular components (Tamargo et al., 2018). Autophagy supports the survival of memory B cells (Chen et al., 2014; Chen et al., 2015). Therefore, I hypothesized that the decline in the M_{phen}BC population observed in B cell-specific AMPKα1-deficient mice was due to a defect in autophagy in the B lineage. Surprisingly, however, the ability of LPS-activated B cells to form LC3-puncta indicative of autophagosome formation after glucose starvation was no different in AMPKα1-deficient B cells compared to controls (**Fig. 3.11A,B**). Furthermore, LC3-I conversion into the faster migrating LC3-II upon glucose starvation was independent of AMPKα1 expression (**Fig 3.11C**). Thus, LPS-activated B cells appear able to undergo glucose starvation-induced autophagy by an AMPKα1-independent mechanism. Finally, normal frequencies and sizes of LC3-puncta were visualized in freshly purified bone marrow plasma cells of tamoxifen-treated *Prkaa1*$^{f/f}$*Rosa26*-CreER^{T2} mice (**Fig. 3.11D**) further supporting that autophagy occurs in the B lineage even in the absence of AMPKα1. Collectively, data in Fig. 3.11 suggest that B lineage cells can induce AMPKα1-independent autophagy, potentially by non-canonical pathways (Codogno et al., 2012).

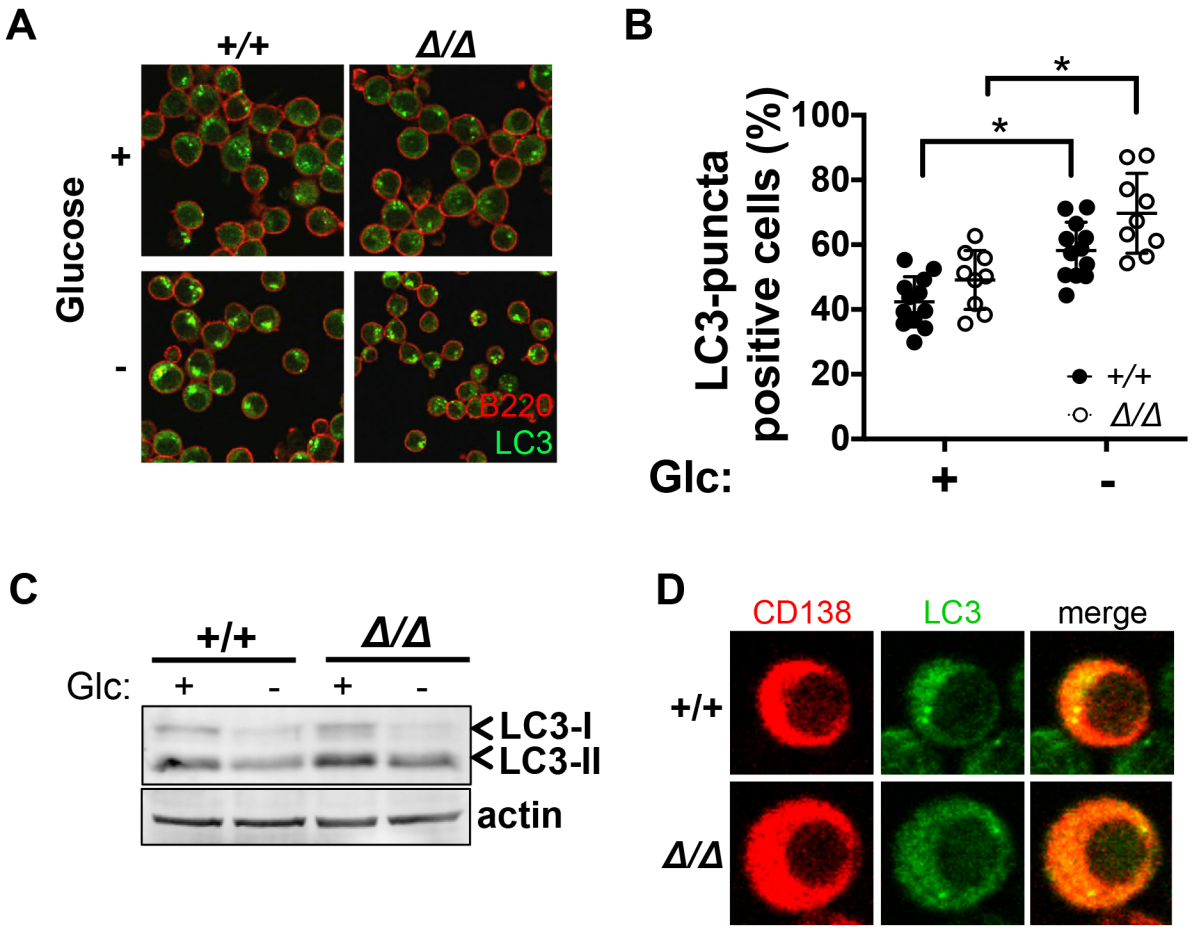

Figure 3.11 Loss of AMPK leads to no defect in autophagy upon glucose deprivation. (A) Representative immunofluorescence image of 2-day LPS/BAFF-treated cells after reseeding for 3h in glucose-sufficient or –deficient media followed by staining with antibodies recognizing B220 (red) and LC3 (green). (B) Immunofluorescence quantification of the frequency of cells containing LC3 puncta using ImageJ "Find Maxima" feature. Data represent three independent experiments with n = 4 *Prkaa1*$^{+/+}$ mice and n = 3 *Prkaa1*$^{\Delta/\Delta}$ mice where each value represents a field. (C) Immunoblot for LC3 after 3h incubation of *Prkaa1*$^{+/+}$ and *Prkaa1*$^{\Delta/\Delta}$ LPS blasts in glucose-sufficient or –deficient media. Data represent three independent experiments. (D) LC3 immunofluorescence staining of *ex vivo* bone marrow plasma cells from tamoxifen treated Rosa26-Cre-ER^{T2} mice. Data represent two independent experiments. * $p < 0.05$ (Student's t-test (B)).

To determine the mechanisms underpinning poor MBC survival in Prkaa1$^{\Delta/\Delta}$ mice, I revisited the mitochondrial defect observed in *Prkaa1*$^{\Delta/\Delta}$ GCB and LPS-activated B cells (Fig. 3.5 & 3.7). Several studies have linked mitochondrial homeostasis to both cellular and organismal survival, reviewed in (Akbari et al., 2019). To monitor respiration

vs. mitochondrial content as an indicator of dysfunctional mitochondria over time, I activated wildtype and *Prkaa1*$^{\Delta/\Delta}$ B cells with LPS, IL-4, IL-5, and BAFF and stained cells with Mitotracker dyes before flow cytometry analysis (Fig 3.12). In parallel to basal respiration of 2-day LPS blasts (Fig. 3.5B), there was no substantial defect in the relative respiration in day 2 or day 6 *Prkaa1*$^{\Delta/\Delta}$ B220^{+} cells as determined by Mitotracker Deep Red MFI values (**Fig 3.12A**). However, total mitochondrial mass in the B220^{+} gate, as determined by relative Mitotracker Green MFI values, was enhanced in day 6 *Prkaa1*$^{\Delta/\Delta}$ B cells suggesting an accumulation of mitochondria over time (**Fig. 3.12B**). Increased mitochondrial mass but unaltered respiration in day 6 *Prkaa1*-null B cells signified the accumulation of dysfunctional mitochondria (**Fig. 3.12C**). In parallel to an accumulation of mitochondrial mass, mtROS in *Prkaa1*$^{\Delta/\Delta}$ B cells was also enhanced compared to wildtype by day 6 (**Fig. 3.12D**). These data are consistent with a model where AMPKα1 in B cells is important for the clearance of ineffective mitochondria, as characterized for erythrocytes (Zhu et al., 2014).

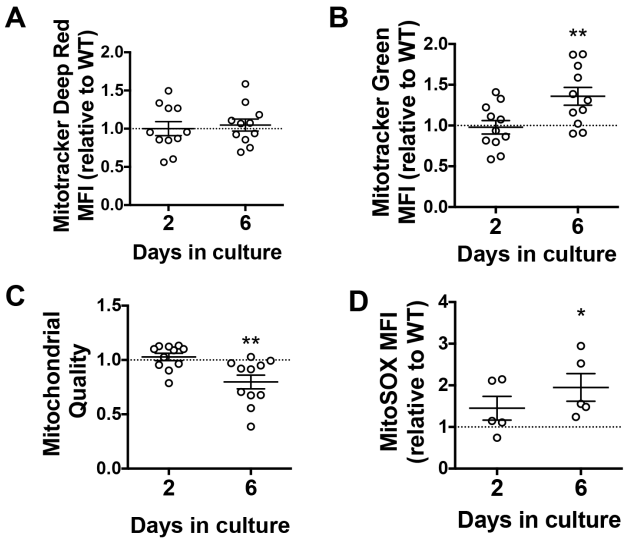

Figure 3.12 AMPK is critical for B cell mitochondrial homeostasis *in vitro*. Relative MFI values for (A) mitochondrial respiration (MitoTracker Deep Red) and (B) mitochondrial mass (MitoTracker Green) in the B220^{+} gate on days 2 and 6 after activation of *Prkaa1*$^{+/+}$ and *Prkaa1*$^{\Delta/\Delta}$ B cells with LPS, BAFF, IL-4, and IL-5. (C) Mitochondrial quality, calculated as the ratio of the MFI value for MitoTracker Deep Red and the MFI values for MitoTracker Green. (D) Relative MFI values for mtROS of B220^{+} cells on days 2 and 6 of culture. Data represent the mean ± SEM of 10 wildtype and n = 11 *Prkaa1*$^{\Delta/\Delta}$ mice from four independent experiments (A-C) or 5 vs. 5 from two independent experiments (D). * $p < 0.05$, ** $p < 0.01$ (Student's t-test (B-D)).

I next tested if the defect in mitochondrial homeostasis applied to the phenotypically-defined memory B cell population, i.e., M_{phen}BC. To obtain sufficient numbers of cells, mitochondrial parameters were analyzed by flow cytometry using total rather than NP-specific M_{phen}BC ($B220^+$ $GL7^-$ IgD^- $CD38^+$) 7-10 weeks after immunization of *mb1*-Cre mice (*Prkaa1*$^{f/f}$ vs. *Prkaa1*$^{+/+}$) with NP-KLH (**Fig. 3.13A**, left panel). Actively respiring mitochondria were modestly decreased in the AMPKα1-deficient M_{phen}BC, whereas total mitochondrial mass was unchanged compared to *mb1*-Cre controls (Fig. 3.13A, right panel). The ratio of mitochondrial membrane potential to total mitochondrial mass (**Fig. 3.13B**), indicative of mitochondrial quality, was diminished in AMPKα1-deficient M_{phen}BC. These data indicate that AMPKα1 supports mitochondrial quality maintenance in phenotypically defined memory B cells.

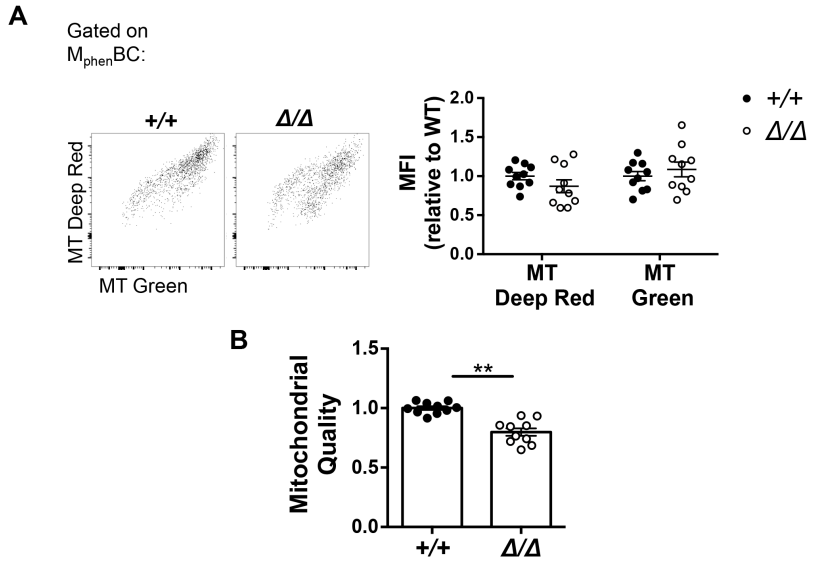

Figure 3.13 AMPK supports mitochondrial quality in MBC. (A) Left panel, representative flow plots of mitochondrial mass (MitoTracker Green) vs. respiring mitochondria (MitoTracker Deep Red) in M_{phen}BC ($B220^+$ $CD38^+$ IgD^-) after immunization strategy illustrated in Fig. 3.10A. Right panel, Quantification of MitoTracker Deep Red and MitoTracker Green MFI values of M_{phen}BC normalized to wildtype. (B) Mitochondrial quality of M_{phen}BC, an indicator of the proportion of functional mitochondria relative to the total, is calculated as the normalized ratio of MitoTracker Deep Red MFI to MitoTracker Green MFI. Data represent the mean ± SEM of 10 wildtype and n = 10 *Prkaa1*$^{Δ/Δ}$ mice from three independent experiments. ** $p < 0.01$ (Student's t-test (B)).

AMPK phosphorylates multiple downstream targets that support different aspects of mitochondrial homeostasis and quality, including mitochondrial biogenesis and mitophagy, i.e., the selective degradation of mitochondria (Herzig et al., 2018). As I observed no defect in overall autophagy in the mutant B cells (Fig. 3.11), I explored whether AMPK was essential for mitophagy in LPS-activated B cells. Unc-51 like kinase (ULK1), a substrate of AMPK, is involved in the initiation of canonical autophagy and is essential for mitophagy (Kim et al., 2011; Wu et al., 2014; Tian et al., 2015; Laker et al., 2017). LPS-activated wildtype B cells increased phosphorylation of the S317 site of ULK1, a target of AMPK, after 2 h of glucose starvation (**Fig. 3.14A**). Induction of ULK1 (S317) phosphorylation due to glucose withdrawal was dependent on AMPKα1 expression. Once activated in a manner dependent in part on AMPK-mediated phosphorylation, ULK1 migrates to the mitochondria and triggers a signaling cascade that leads to the recruitment of LC3 machinery and fusion with the lysosome (Wu et al., 2014; Tian et al., 2015). To test if AMPKα1 enhances ULK1-Mitochondria colocalization in B cells, I assessed in LPS-activated B cells the association of mitochondria with ULK1, by confocal imaging after 24h in a hypoxic chamber (pO_2 = 1%). As expected, co-localization analyses revealed that the percentage of $ULK1^+$ mitochondria was enhanced in hypoxia-experienced B cells compared to B cells grown in normoxia (pO_2 = 21%), however AMPK-deficiency dampened the ULK1-Mitotracker association (**Fig. 3.14B**). These data indicate that AMPK plays a role in targeting ULK1 for recruitment to the mitochondria, an essential first step in mitophagy.

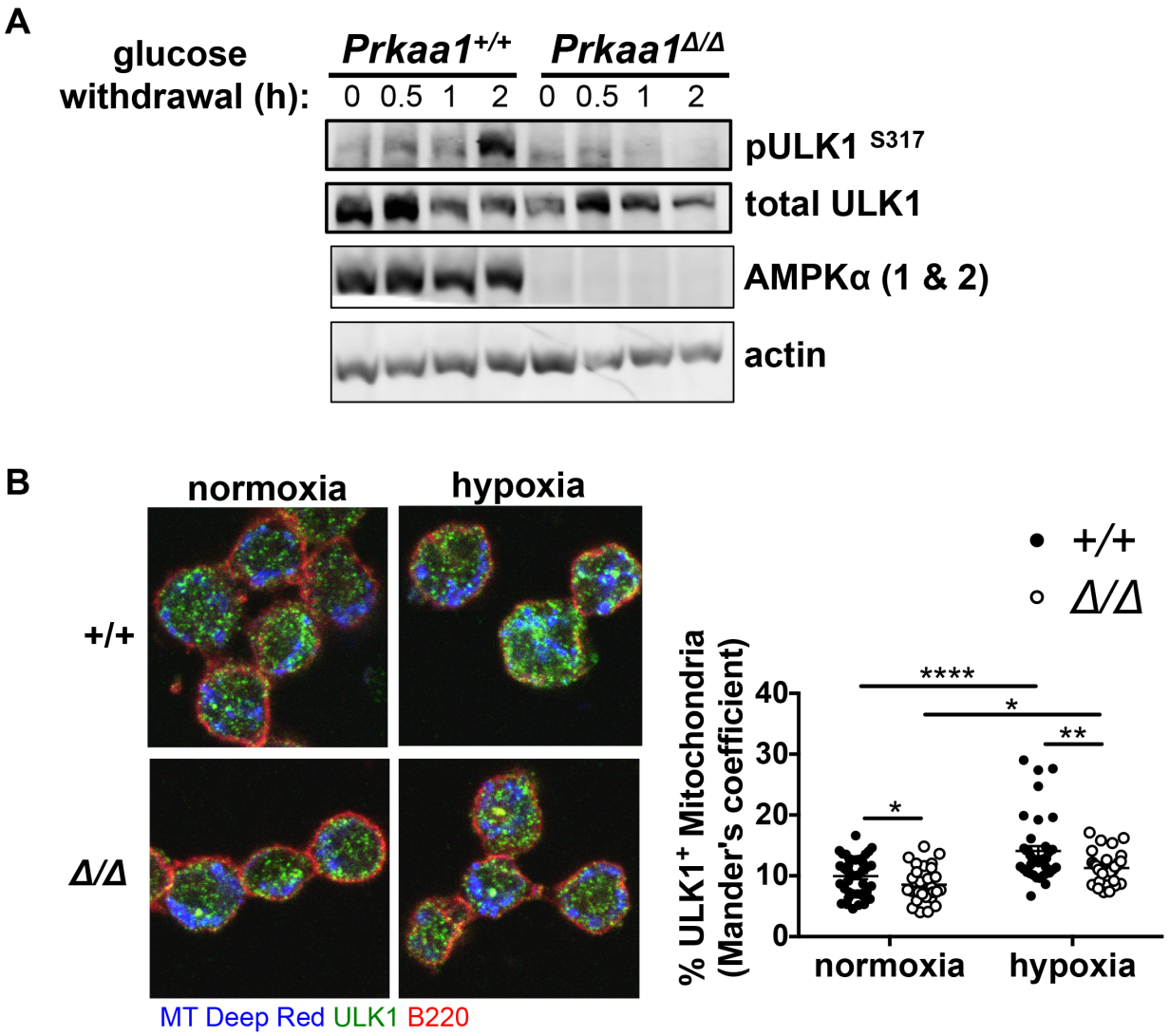

Figure 3.14 AMPK targets ULK1 and promotes ULK1-mitochondrial co-localization in metabolically stressful *in vitro* conditions. (A) Immunoblot of pULK1^{S317}, an AMPK target that initiates mitophagy, after glucose deprivation in day 2 LPS-activated *Prkaa1*$^{+/+}$ and *Prkaa1* $^{\Delta/\Delta}$ B cells. Data is representative of three independent experiments (A) or n = 3 *Prkaa1*$^{+/+}$ and n = 3 *Prkaa1* $^{\Delta/\Delta}$ mice. (B) Left panel, representative immunofluorescence of 1-day LPS-activated *Prkaa1*$^{+/+}$ and *Prkaa1* $^{\Delta/\Delta}$ B cells and subsequent 24h incubation in a 21% or 1% oxygen chamber; Mitotracker Deep Red (blue), ULK1 (green), B220 (red). Right panel, quantification of ULK1-MitoTracker co-localization quantified by the Mander's coefficient determined using the JACop plugin in ImageJ. Data is representative of two independent experiments where each dot represents a field with 10 fields per mouse; n = 4 *Prkaa1*$^{+/+}$ and n = 4 *Prkaa1* $^{\Delta/\Delta}$. * $p < 0.05$, ** $p < 0.01$, **** $p < 0.0001$ (two-way ANOVA with Sidak's multiple comparisons (B)).

As further evidence of a defect in mitophagy in AMPK-deficient B cells, the frequencies of Lamp1^{+} mitochondria, indicative of mitochondrial fusion to the lysosome, were diminished in *Prkaa1*-null LPS blasts and sorted MBC (**Fig. 3.15A,B**). Collectively, these findings support a model in which AMPKα1 promotes mitochondrial clearance and quality control in B cells, likely due to a requirement for ULK1 phosphorylation at S317, and supporting mitochondrial function.

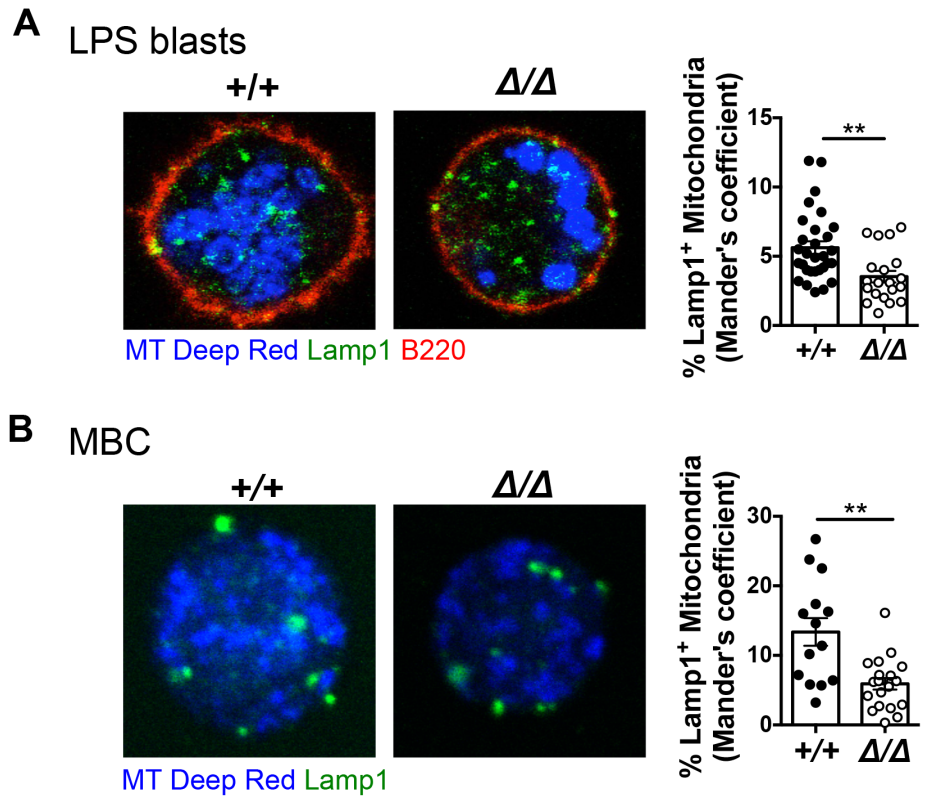

Figure 3.15 AMPK promotes mitophagy in LPS blasts and MBC. (A) Representative immunofluorescence (left panel) and quantification (right panel) of *Prkaa1*$^{+/+}$ and *Prkaa1* $^{\Delta/\Delta}$ 2-day LPS blasts depicting MitoTracker Deep Red (blue) co-localization with Lamp1 (green); B220 (red). Deletion in (A) is driven by 4-OHT treated Rosa26-CreER^{T2}. (B) Representative immunofluorescence (left panel) and quantification (right panel) of flow sorted *Prkaa1*$^{+/+}$ and *Prkaa1* $^{\Delta/\Delta}$ M_{phen}BC (B220^{+} GL7^{-} IgD^{-} CD38^{+}) depicting MitoTracker Deep Red (blue) co-localization with Lamp1 (green). Deletion in (B) is driven by *mb1*-Cre. Data are representative of n = 3 vs. 3 mice where each dot represents one field with 10 fields/mouse; ** $p < 0.01$ (Student's t-test (A,B)).

Levels of mtROS play a key role in many cellular functions including regulating B cell fate and function (Sena et al., 2012, Jang et al., 2015). Consistent with the defect in quality control (Fig. 3.13B), AMPKα1-deficient M_{phen}BC exhibited increased mtROS compared to controls (**Fig. 3.16A**). To test if the increased mtROS observed in AMPKα1-deficient M_{phen}BC was accompanied with changes in lipid peroxidation, I used Bodipy 581/591 C11 and found it to be elevated in AMPKα1-deficient M_{phen}BC (**Fig. 3.16B**). Collectively, these results suggest that AMPKα1 protects memory B cells against excessive oxidative stress and cell death involving lipid peroxidation by promoting to mitophagy and maintaining mitochondrial homeostasis.

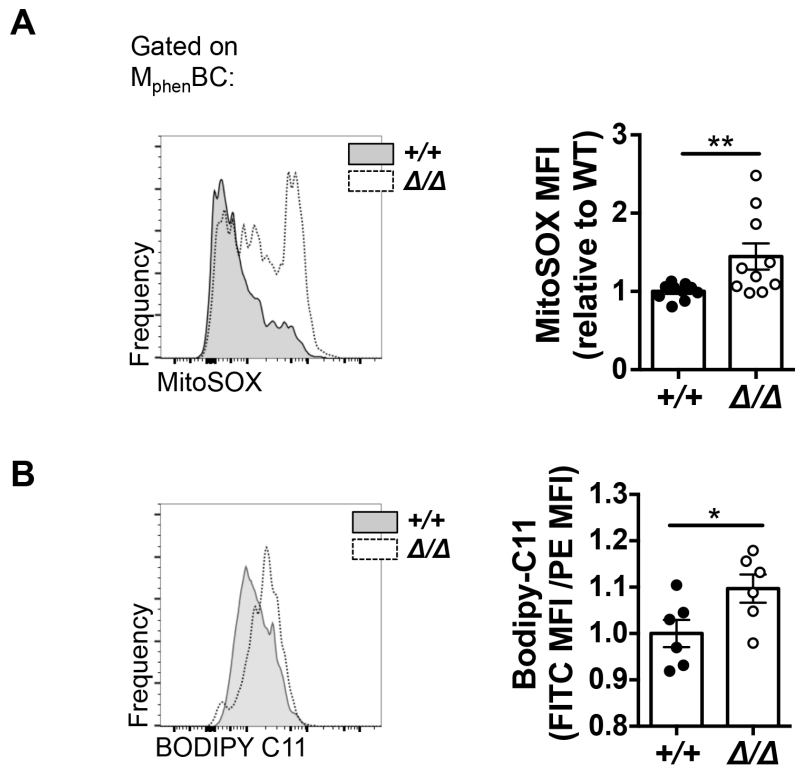

Figure 3.16 Loss of AMPK leads to increased mtROS and lipid peroxidation in MBC. (A) Left panel, representative MitoSOX histogram and quantification (right panel) of M_{phen}BC from *Prkaa1*$^{+/+}$ and *Prkaa1* $^{Δ/Δ}$ mice after immunization strategy depicted in Fig. 3.10A. (B) Left panel, representative BODIPY C11 (which fluoresces in the FL-1 channel upon lipid oxidation) of M_{phen}BC after immunization strategy depicted in Fig 3.10A. Right panel, normalized ratio of FITC (FL-1) MFI to PE (FL-2) MFI of M_{phen}BC after staining with Bodipy 581/591 C11 as a measure of lipid peroxidation. Data are representative of three (A) or two (B) independent experiments with at least six mice in each group. * $p < 0.05$, ** $p < 0.01$ (Student's t-test).

VI. AMPK supports humoral recall

Upon second exposure to antigen, MBC can mount robust secondary responses with fast kinetics. Specifically, double positive $CD80^+$ $PD\text{-}L2^+$ MBC rapidly differentiate into ASC and double negative $CD80^-$ $PD\text{-}L2^-$ MBC re-enter the GC upon subsequent encounter with cognate antigen (Zuccarino-Catania et al., 2014; Weisel et al., 2017). To test if the defect in the long-term maintenance of the MBC population has consequences on recall function, I re-challenged *mb1*-Cre mice (*Prkaa1*$^{f/f}$ vs. *Prkaa1*$^{+/+}$) 14 weeks after a primary immunization (**Fig. 3.17A**). In contrast to the primary response, antigen-specific GC B cells were diminished in re-challenged AMPKα1-deficient mice (**Fig. 3.17B**). The $CD138^+$ $TACI^+$ splenic plasmablast/plasma cell populations (Pracht et al., 2017) also were attenuated in mice harboring AMPKα1-deficient B cells (**Fig. 3.17C**).

To assess the strength of recall responses induced by *Prkaa1*-null $M_{phen}BC$, I measured circulating anti-NP IgM and anti-NP IgG1 in sera collected both immediately prior and a week after re-challenge. For each mouse, a recall effect, or the memory-induced Ab concentration, was calculated (Cho et al., 2013). The change in anti-NP IgM and IgG1 increased substantially less in response to the recall immunization in *Prkaa1*$^{\Delta/\Delta}$ mice compared to *mb1*-Cre controls (**Fig. 3.17D**). These data indicate that recall Ab responses were weaker when B cells lacked AMPKα1. I infer from these data that AMPKα1 supports the longevity of $M_{phen}BC$ which maintains the functional capacity of recall humoral responses.

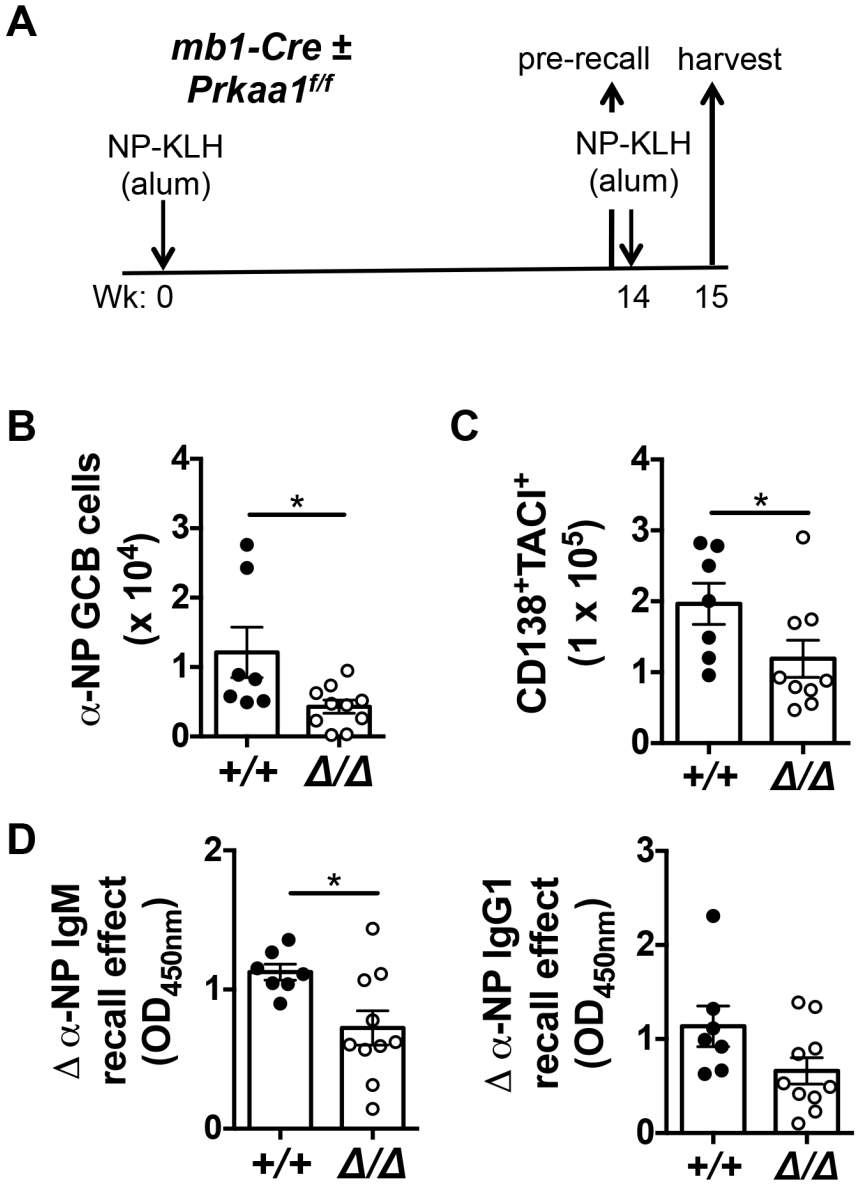

Figure 3.17 AMPK in B cells supports recall humoral responses. (A) Schematic of immunization strategy to test humoral recall in *Prkaa1*$^{+/+}$ and *Prkaa1*$^{\Delta/\Delta}$ mice. Mice were immunized with NP-KLH and rechallenged fourteen weeks later. Mice were harvested one week after rechallenge. Total numbers of splenic (B) NP-specific GCB and (C) CD138^{+}TACI^{+} cells one week after recall immunization. (D) Calculated difference in anti-NP IgM (left panel) and anti-NP IgG1 (right panel) in the sera immediately before and one week after recall immunization, "recall effect". Data represent mean ± SEM from two independent experiments with n = 7 *Prkaa1*$^{+/+}$ and n = 10 *Prkaa1*$^{\Delta/\Delta}$ mice. * $p < 0.05$ (Student's t-test).

Prkaa1$^{f/f}$ *mb1*-Cre mice, used to generate Fig. 3.9, 3.10, 3.12, 3.13, 3.15B, 3.16, and 3.17, harbor B cells that are deficient in AMPKα1 from very early in B lineage development, so that a defect of programming during the primary response might contribute to the finding of weaker recall. To test the role of AMPKα1 after intact primary immunity, I used adoptive transfers with a tamoxifen-inducible system in which *Prkaa1* was deleted after a normal primary response when AMPK is expressed. Naïve B cells (CD45.2$^+$ IgH^b allotype) from *Rosa26*-CreER^{T2} mice (*Prkaa1*$^{f/f}$ or *Prkaa1*$^{+/+}$) were transferred into sub-lethally irradiated CD45.1$^+$ IgH^a allotype-disparate recipients along with helper T cells (a mix of CD4$^+$ T cells from wild-type and OTII transgenic mice). Recipients were then immunized with NP-ovalbumin (NP-ova) and boosted at week 3 to generate primary responses. Tamoxifen injections to induce deletion of *Prkaa1* in the donor B cell population, including M_{phen}BC, were deferred to week nine to allow for unaltered primary immunity. To assess recall responses, mice were re-challenged with NP-ova several months after deletion by tamoxifen (4.5 months), and harvested one week after the recall immunization (**Fig. 3.18A**). PCR products from flow-sorted donor CD45.2$^+$ M_{phen}BC at the time of harvest documented effective deletion of *Prkaa1* in the cells from mice that received *Prkaa1*$^{f/f}$ Rosa26-CreER^{T2} donor B cells (**Fig. 3.18B**). Using allotype-specific detection reagents, donor and recipient anti-NP IgG1 was measured in the sera before and after recall challenge. Compared to mice receiving wild-type CreER^{T2} B cells, mice that received CreER^{T2} *Prkaa1*$^{f/f}$ B cells had weaker donor anti-NP IgG1^b recall responses after re-challenge (**Fig. 3.18C**). In contrast, an internal control of recipient-derived a-allotype Ab found that levels of anti-NP IgG1^a were similar regardless of the donor cell source. Consistent with these serologies after

re-challenge, anti-NP IgG1^{b}-secreting cells and donor-derived CD45.2^{+} CD138^{+} TACI^{+} plasmablasts and plasma cells in the spleen were diminished in mice that received B cells from which AMPKα1 was depleted (**Fig. 3.18D, E**). AMPKα1-deficient donor-derived GCB were also decreased compared to wildtype donor GCB (**Fig. 3.18F**). These data support the conclusion that after a normal primary humoral response is established, the recall capacity of B cells is supported by AMPKα1.

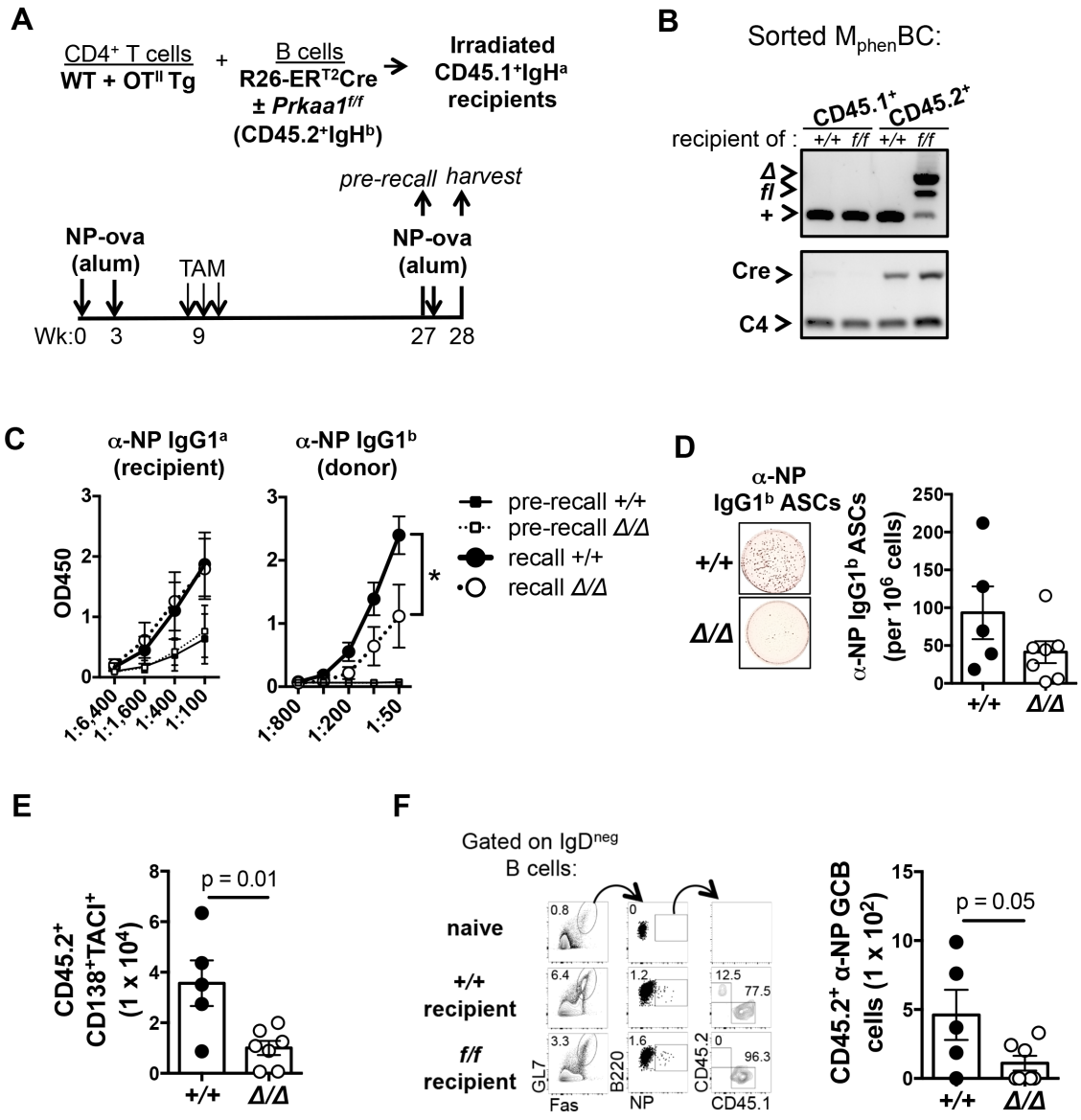

Figure 3.18 Loss of AMPK after a normal primary response leads to later defects in recall function. (A) Experimental design to evaluate the effect of AMPK in $M_{phen}BC$ after a normal primary response. $CD4^+$ T cells (4:1, polygenic and OTII) and $CD45.2^+$ IgH^b B cells from Rosa26-$CreER^{T2}$ (*Prkaa1*$^{f/f}$ or *Prkaa*$1^{+/+}$) mice were transferred into sub-lethally irradiated naïve wild-type allotype-disparate $CD45.1^+$ IgH^a mice prior to immunization with NP-ova. Deletion of *Prkaa1* in $M_{phen}BC$ was induced by tamoxifen injections nine weeks after the initial immunization. Mice were rechallenged 18 weeks thereafter and harvested 1 week after the recall immunization. (B) *Prkaa1* and Cre PCR of DNA from purified splenic $CD45.1^+$ or $CD45.2^+$ $M_{phen}BC$ ($B220^+$ IgD^- $GL7^-$ $CD38^+$). (C) Circulating anti-NP $IgG1^a$ (recipient-derived) and anti-NP $IgG1^b$ (donor-derived) immediately before and one week post rechallenge. (D) Representative wells and quantification of ELISpot analyses depicting numbers of splenic NP-specific $IgG1^b$ ASCs

at time of harvest. (E) Numbers of donor CD45.2$^+$ CD138$^+$ TACI$^+$ plasma cells in the spleen after rechallenge. (F) (Left panel) Representative flow plots depicting frequency of splenic NP-specific germinal center B cells that are recipient-derived (CD45.1$^+$) vs. donor-derived (CD45.2$^+$) after rechallenge. (Right panel) Total number of donor-derived NP-specific germinal center B cells in the spleen after rechallenge. Data represent mean ± SEM with n = 5 *Prkaa1*$^{+/+}$ and n = 7 *Prkaa1* $^{\Delta/\Delta}$ mice. * $p < 0.05$, ** $p < 0.01$ (Student's t-test (E,F)).

VII. Discussion

The orchestration of intracellular metabolic pathways varies to support developmental and functional needs throughout the lifespan of a B lineage cell (Boothby et al., 2017; Jellusova et al., 2017; Egawa et al., 2019; Akkaya et al., 2019). Furthermore, as B cells and their progeny migrate through or take residence in distinct tissues, they likely have the capacity to persist in distinct microenvironments with differing nutrient availability (Boothby et al., 2017; Jellusova et al., 2017). Relatively little is known about the metabolic pathways that support the persistence and function of memory B cells. The energy sensor AMPK regulates multiple aspects of intracellular metabolism. Its overall program favors energy conservation and tilts balance toward catabolism while restraining anabolism in response to declining levels of ATP (Garcia et al., 2017). Here, in Chapter 3 I have shown that AMPK supports the longevity of memory B cells essential for robust recall humoral responses. After the initial population increase, AMPK deficiency resulted in declines in the memory-phenotype B cell population along with the accumulation of dysfunctional mitochondria, decreased mitophagy, increased mitochondrial ROS, and increased lipid peroxidation. The functional impact of these changes was a reduced strength of recall antibody response after rechallenge. A summary of Chapter 3 findings, depicted in **Fig. 3.19**, indicates that AMPK protects the maintenance of the memory B cell population and suggests that this function is achieved at least in part through the regulation of mitochondrial turnover.

Echoing observations in T cells after TCR crosslinking and nutrient-poor conditions, AMPK in B cells is activated upon anti-BCR stimulation and after glucose starvation (Tamás et al., 2006; Blagih et al., 2015; Rolf et al., 2013). Therefore, it is surprising that AMPK is dispensable for the formation of primary germinal centers were B cells are potentially competing for limited nutrients to support extensive proliferation and energy demand (Waters et al., 2019; Brookens et al., 2020). Observed defects in mitochondrial mass and respiration in *Prkaa1*-null GCB did not affect the ability to become a GCB or any downstream outcomes of GC (See Chapter 4 for AMPK in plasma cells). Though p-AMPKα1^{T172} expression increases with B cell activation (Waters et al., 2019), it is speculated that anabolic pathways dominate B cell metabolism during activation and proliferation in GCB and from that perspective AMPK-loss is expected to have minimal effects as Waters *et al.* and our group have observed. Interestingly, the kinetics for p-AMPKα1^{T172} expression after B cell activation parallels with the deceleration of biomass accumulation indicating that p-AMPKα1^{T172} may be important for dampening unlimited cell growth through negative regulation of mTORC1 and other anabolic substrates (Waters et al., 2019).

Immunological memory is a hallmark component of the adaptive immune system whereby long-lived cells of the T and B lineages confer long-lasting protective immunity against re-infection. Though there are some distinctions in the balance of oxidative phosphorylation and glycolysis employed by B and T cells during activation (Caro-Maldonado et al., 2014), such that B lymphoblasts better couple pyruvate generation to the mitochondria than their T cell counterparts, both subsets undergo clonal expansion and generate long-lived quiescent memory populations (Jones et al., 2015; Konjar et al., 2019). Thus, there may be parallels in the metabolic programming between the two lineages. Akin to the role of

AMPK in maintaining CD8 memory T cells (Rolf et al., 2013), the data presented in this chapter indicate that AMPK promotes the persistence of memory-phenotype B cells and their function in humoral recall responses. The finding that AMPK promotes longevity and catabolism in both the B and T cell lineages suggests a conserved function of AMPK in these long-lived memory lymphocytes.

AMPK regulates autophagy, a conserved self-degrading cellular process (Kim et al., 2011). Autophagy is essential for the long-term persistence of both memory B and CD4 T cell populations (Chen et al., 2014, Chen et al., 2015; Murera et al., 2018). Loss of either two autophagy-essential genes, *Atg5* or *Atg7*, was tied to mitochondrial dysfunction and enhanced lipid peroxidation in the B and T cell lineages (Chen et al., 2014; Murera et al., 2018; Pua et al., 2009). It was surprising, therefore, to observe that autophagy after glucose withdrawal was normal for AMPK-deficient B cells despite the expected absence of activating phosphorylation of ULK1. These findings suggest that activated B cells can also induce autophagy via non-canonical, AMPK-independent pathways (Codogno et al., 2012; Martinez-Martin et al., 2017; Raso et al., 2018; Sil et al., 2018). Despite normal formation of LC3 puncta, the defect in ULK1 ^{S317} phosphorylation was associated with a defect in ULK1 recruitment to the mitochondria, and failure to induce mitophagy in AMPK-deficient B cells. In support of our findings, the AMPK-ULK1 axis is reported to be essential for hypoxia- or exercise-induced mitophagy in mouse embryonic fibroblasts and skeletal muscle cells respectively (Tian et al., 2015; Laker et al., 2017). Interestingly, previous studies demonstrating the importance of autophagy in lymphocyte persistence and mitochondrial homeostasis use genetic models by conditional inactivation of *Atg5* or *Atg7*, both of which are involved in multiple autophagy pathways including mitophagy (Codogno et al., 2012; Sil et al., 2018).

Accordingly, the reason memory B cell persistence is promoted by Atg7 may be attributable to multiple upstream pathways and not limited to mitochondrial-specific autophagy activated via AMPKα1.

Our data show that AMPK promotes both the long-term persistence of memory B lymphocytes and mitophagy in B lineage cells. There are substantial antecedents that connect mitochondria to memory B cell persistence (Sandoval et al., 2018). Memory B cell longevity is linked to enhanced expression of mitochondrial pro-survival proteins in the Bcl2 superfamily, both Bcl2 itself (Nuñez et al., 1991) and BH3-only Puma (Clybouw et al., 2011). Furthermore, mitochondrial homeostasis is associated with the persistence of memory B cells (Chen et al., 2014; Sandoval et al., 2018). Mitophagy has also been associated with maintaining memory in a natural killer cell population (O'Sullivan et al., 2015). In that setting, mitophagy likely functioned through clearance of dysfunctional mitochondria, which protected cells from the accumulation of excessive mitochondrial-derived ROS, lipid peroxidation, and cell death. Our findings with AMPK-deficient B cells align with this previous work, in that I observed increased mitochondrial ROS and abnormal function in mitochondrial challenging during metabolic flux analyses. Spare oxidative phosphorylation, or the reserved capacity to amplify respiration in response to increased demand, was impaired in B cells lacking AMPK, similar to the requirement for spare respiratory capacity in promoting memory CD8 T cell longevity (Van der Windt et al., 2012). The types of memory lymphocytes assayed in prior work and ours are known to circulate through blood, tissue, and lymphatics (Tangye et al., 2009; Blink et al., 2005). Accordingly, I speculate that spare respiratory capacity may be critical for memory cells to adapt to substantial differences in these microenvironments and the attendant metabolic stresses as they survey and pass

through distinct tissues.

Activation of the AMPK pathway by metformin has been associated with increased memory B cells and improved antibody responses to influenza vaccine in type II diabetic patients (Diaz et al., 2017). These data may provide insight on the efficacy of drugs that target AMPK to achieve longer lasting humoral responses and improve vaccine design.

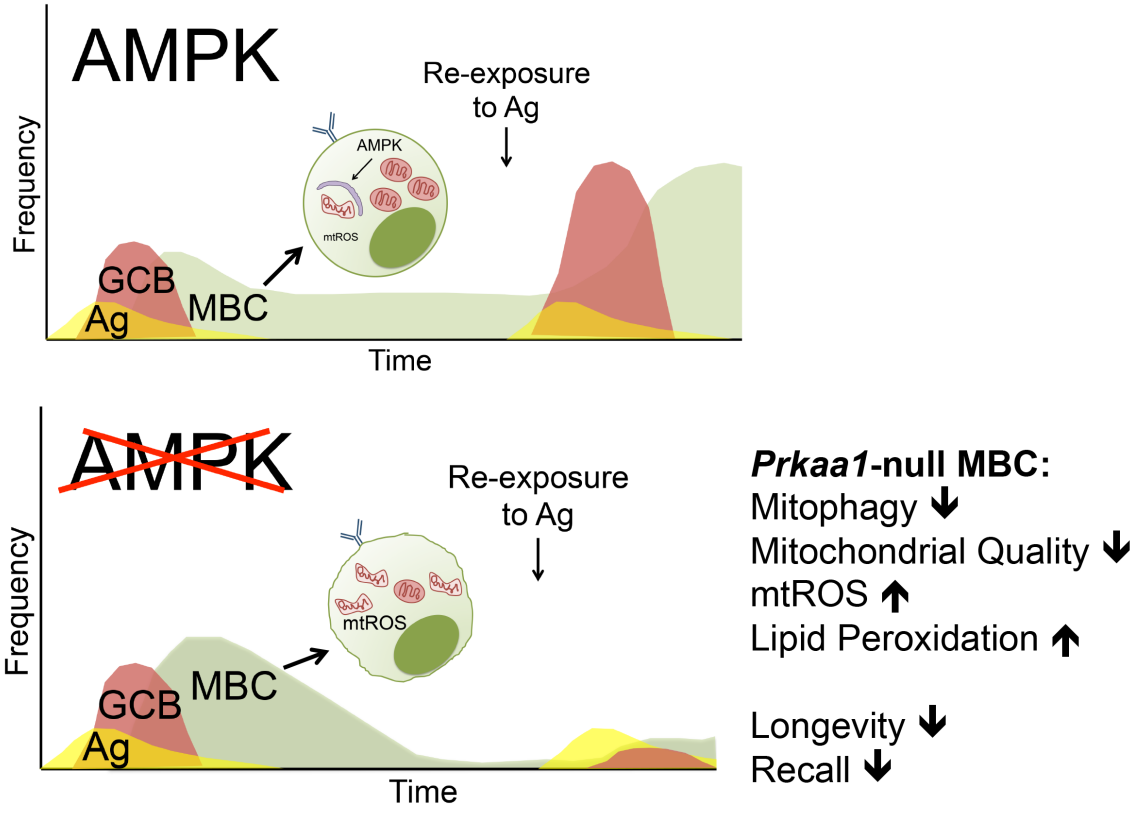

Figure 3.19 AMPK supports humoral recall by promoting mitochondrial homeostasis and persistence of the MBC population. AMPK is dispensable for generating GCB but is critical for the normal production and long-term maintenance of MBC. *Prkaa1*-null MBCs exhibit defective mitophagy, enhanced mtROS, and lipid peroxidation which coincides with their gradual decline over time. Ag – antigen; GCB – germinal center B cell; MBC – memory B cell; mtROS – mitochondrial derived reactive oxygen species. Figure is modified from Brookens et al., 2021.

CHAPTER 4

AMPK REGULATES THE RATE OF ANTIBODY SYNTHESIS THROUGH INHIBITION OF mTORC1

The work presented in this chapter is modified from a publication in Journal of Immunology (Brookens et al., 2020)

I. Abstract and Significance

Plasmablasts and plasma cells, collectively called antibody secreting cells (ASCs), produce hundreds to thousands of glycosylated antibody per second but evidence for the metabolic pathways that support ASC generation, maintenance, and immunoglobulin production are limited. Adenosine monophosphate-activated protein kinase (AMPK) is an evolutionary conserved serine/threonine kinase that integrates cellular energy status and nutrient availability to intracellular signaling and metabolic pathways. In Chapter 4, I used genetic mouse models to show that although AMPK is dispensable for the differentiation of short-lived plasma cells (SLPC) and the persistence of long-lived plasma cells (LLPC), this metabolic sensor dampens antibody synthesis in both subsets by antagonizing mTORC1 activity. Intriguingly, AMPK supported mitochondrial mass and respiration in LLPC but mitochondrial homeostasis was not reliant on AMPK. Collectively, my findings fit a model where AMPK modulates rates of antibody synthesis and shed light on differential mitochondrial dynamics in ASCs in relation to B cells.

II. Introduction

At the time of writing this dissertation, monoclonal antibodies as a treatment to neutralize severe acute respiratory syndrome coronavirus 2 (SARS-CoV-2), which have caused the worldwide pandemic respiratory disease COVID-19, have been of increased public interest (Wang et al., 2020; Chen et al., 2021). The manufacture and secretion of antibodies are the primary function of plasmablasts and plasma cells, which are derived from differentiated B cells. Each plasmablast and plasma cell, collectively called antibody-secreting cells (ASC), produce monoclonal antibodies of a single isotype depending on the activation signals received by the B cell from which they are derived. ASCs are heterogeneous in their lifespan, isotype, antibody rates, and tissue localization. Most ASCs are short-lived plasma cells (SLPC) and secrete antibody before undergoing ER stress-induced apoptosis only a few days following antigen exposure (Auner et al., 2010; Sze et al., 2000). However, a fraction of terminally differentiated ASCs are long-lived and continuously produce immunoglobulin independent of antigen or precursor cells for a lifetime (Manz et al., 1997; Slifka et al., 1998). One of the first sets of evidence of long-lived plasma cells (LLPC) was the presence of antibody specific for the 1918 influenza virus in the sera of people born before 1915; these antibodies still persisted nearly 90 years after the pandemic ended (Yu et al., 2008). Considering that the half-life of immunoglobulins is only hours to days (Vieira et al., 1988), and that plasma cells persist without renewal from precursors (Manz et al., 1997; Slifka et al., 1998), the machinery and metabolic networks that enable a single cell to continuously produce hundreds to thousands of glycosylated antibody per second for decades is impressive (Hibi et al., 1986; Brinkmann et al., 1993). There is evidence of many extrinsic and intrinsic factors that

support the survival and function of LLPCs reviewed in (Khodadadi et al., 2019; Lam et al., 2018). However, how ASC are able to survive despite high metabolic demands is still not fully elucidated.

The B- and T-lymphocyte lineages are closely related and represent the two major branches of adaptive immunity. Most of the focus of metabolic regulation in lymphocytes has been on T cells so educated hypotheses are made about similar pathways in the B-lymphocyte lineage. In parallel to memory T cells, MBC are metabolically quiescent so it is no surprise that AMPK would have an analogous role in promoting survival and mitochondrial homeostasis in both memory subsets as described in Chapter 3 and published previously (Rolf et al., 2013; O'Sullivan et al., 2015; Braverman et al., 2020; Lepez et al., 2020; Pearce et al., 2009). However, plasma cells, a subset of which have the longevity of a memory cell but with the high energy demands of immunoglobulin production, do not have a parallel counterpart in the T cell lineage. Therefore, studying metabolism in these unique populations would reveal important new insights. Recall that ASC are unique in their glucose uptake, mTORC1, and mitochondrial activity compared to other B lineage cells (Fig. 3.1 and 3.2). At the onset of my project, new evidence for the importance of autophagy, glucose uptake, and mitochondrial pyruvate in supporting plasma cell function and longevity emerged (Pengo et al., 2013; Lam et al., 2016; Lam et al., 2018). However, whether AMPK impacts these metabolic processes or independently influences the function or longevity of ASCs is unknown.

III. AMPK is dispensable for generating and maintaining ASC

As in Chapter 3, I used genetic models to test the role of AMPK in ASC. I crossed huCD20-CreER^{T2} mice with mice harboring floxed alleles of *Prkaa1,* which encodes the catalytic subunit of AMPK. Recall *Prkaa1* deletion is restricted to mature B cells after administration of tamoxifen regimen (Fig. 2.2). Though the huCD20 promoter is no longer active in ASC, antigen-specific ASC are derived from B cells that were subjected to *Prkaa1* deletion immediately prior to immunization. To test the role of AMPK in generating ASC in primary responses, *Prkaa1*$^{+/+}$ huCD20-CreER^{T2} wildtype and *Prkaa1*$^{f/f}$ huCD20-CreER^{T2} were injected with tamoxifen to induce deletion, immunized with NP-KLH as indicated, and screened at week 4 to assess humoral responses (**Fig. 4.1A**). Loss of AMPK led to no alterations in the frequency of NP-specific IgM- or IgG1- secreting cells generated in the spleen or bone marrow as determined by ELISpot analysis (**Fig. 4.1B,C**). These data indicate that AMPK is dispensable for not only the generation of primary GCB (Fig. 3.6), but also for numbers of SLPCs.

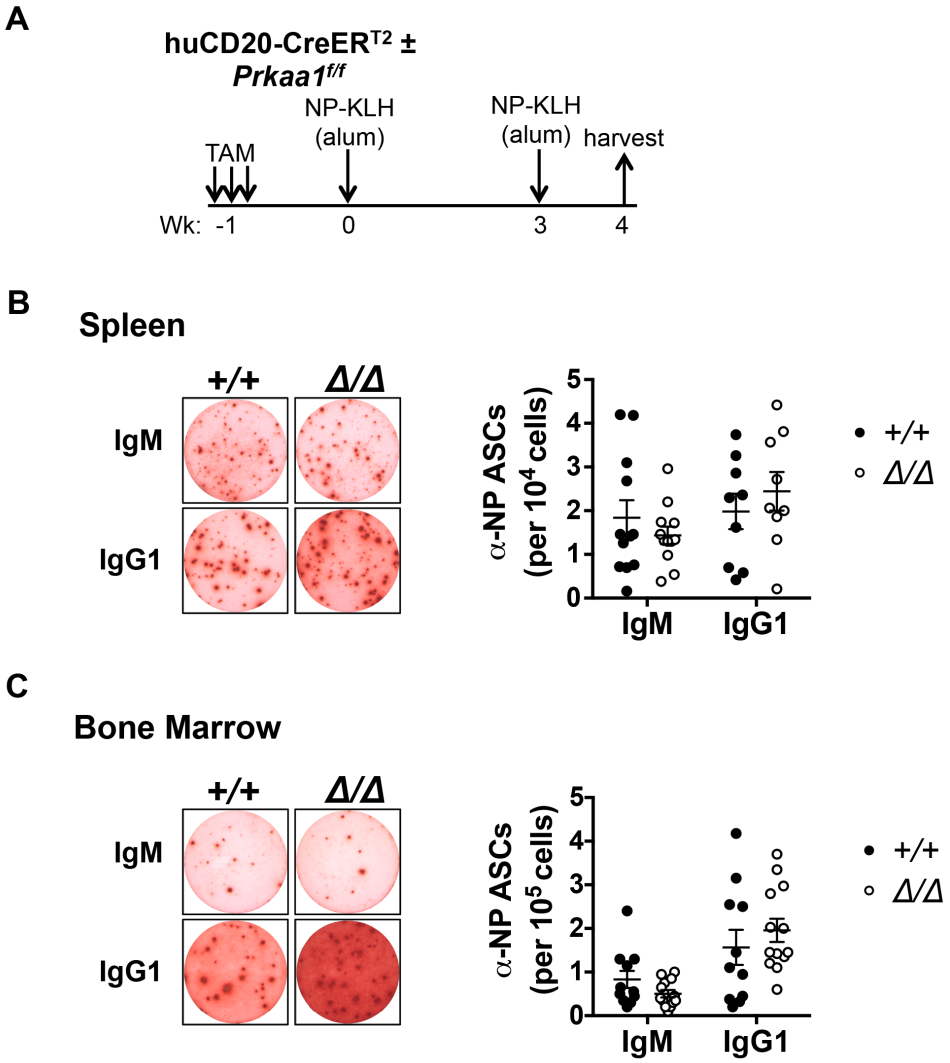

Figure 4.1 AMPK is dispensable for generating antibody secreting cells in response to hapten-carrier immunization. (A) Schematic of immunization strategy with NP-KLH using mice harboring a tamoxifen-inducible Cre under control of a B lineage restricted promoter, huCD20. Mice were treated with tamoxifen to induce B-cell specific deletion of *Prkaa1* and then immunized and boosted three weeks later with NP-KLH. Mice were harvested one week post boost. (B) Left panel, representative ELISpot wells depicting density of splenic NP-specific IgM and IgG1 secreting cells; 5 x 10^5 total splenocytes plated per well. Right panel, numbers of NP-specific IgM and IgG1 secreting cells per 10^4 total splenocytes in *Prkaa1*$^{+/+}$ and *Prkaa1*$^{\Delta/\Delta}$ mice at the time of harvest. (C) Left panel, representative ELISpot wells depicting density of bone marrow NP-specific IgM and IgG1 secreting cells; 2 x 10^6 total bone marrow cells plated per well. Right panel, numbers of NP-specific IgM and IgG1 per 10^5 total marrow cells in *Prkaa1*$^{+/+}$ and *Prkaa1*$^{\Delta/\Delta}$ mice at the time of harvest. Filled circles (●) represent at least n = 9 wildtype mice and open circles (○) represent at least n = 9 *Prkaa1*$^{\Delta/\Delta}$ mice from four independent experiments.

The NP-specific ASC screened for in Figure 4.1 are mostly SLPC, which live and secrete antibodies for only a few days before apoptosis (Auner et al., 2010; Sze et al., 2000). Like MBC, LLPC confer long-term immunity. Though LLPC may be less likely than plasmablasts to express B220 and CD19 surface markers, definitive characteristics that distinguish LLPC from SLPC has been challenging since both have similar transcriptional profiles (Lam et al., 2018). Many groups have simplified the distinction by anatomical location, specifically designating ASC in secondary lymphoid structures as SLPC and those in the bone marrow as LLPC (Lam et al., 2016). Though there are some reports of IgA-secreting LLPC residing in human intestine (Landsverk et al., 2017), many LLPC traffic from secondary lymphoid structures and permanently reside in the bone marrow (Slifka et al., 1998). In addition to identifying LLPC as those ASC in the bone marrow, waiting to screen for LLPC and the antibody they produce at least a couple months post antigen exposure ensures that the ASC population detected are true LLPC.

To assess the role of AMPK in the maintenance of LLPC, I immunized *Prkaa1*$^{+/+}$ *mb1*-Cre and *Prkaa1*$^{f/f}$ mb1-Cre mice with NP-KLH and harvested them eight weeks after the last antigen exposure (**Fig. 4.2A**). Recall that *mb1*-Cre mice have tamoxifen-independent strong excision of *Prkaa1* in the B lineage and its use avoids technical limitations in the inducible huCD20-CreER^{T2} model (Fig. 2.3). The frequency and total number of ASCs defined by CD138^{+} TACI^{+} expressing cells was unchanged in the bone marrow in *Prkaa1*$^{\Delta/\Delta}$ mice as determined by flow cytometry (**Fig. 4.1B**) (Pracht et al., 2017). The frequency of NP-specific IgM- and IgG1- secreting cells was also unaltered in the absence of AMPK (**Fig. 4.1C**). Interestingly, in contrast to the dynamic regulation of

the generation and long-term maintenance of MBC population, AMPK is dispensable for the generation and long-term persistence of ASC.

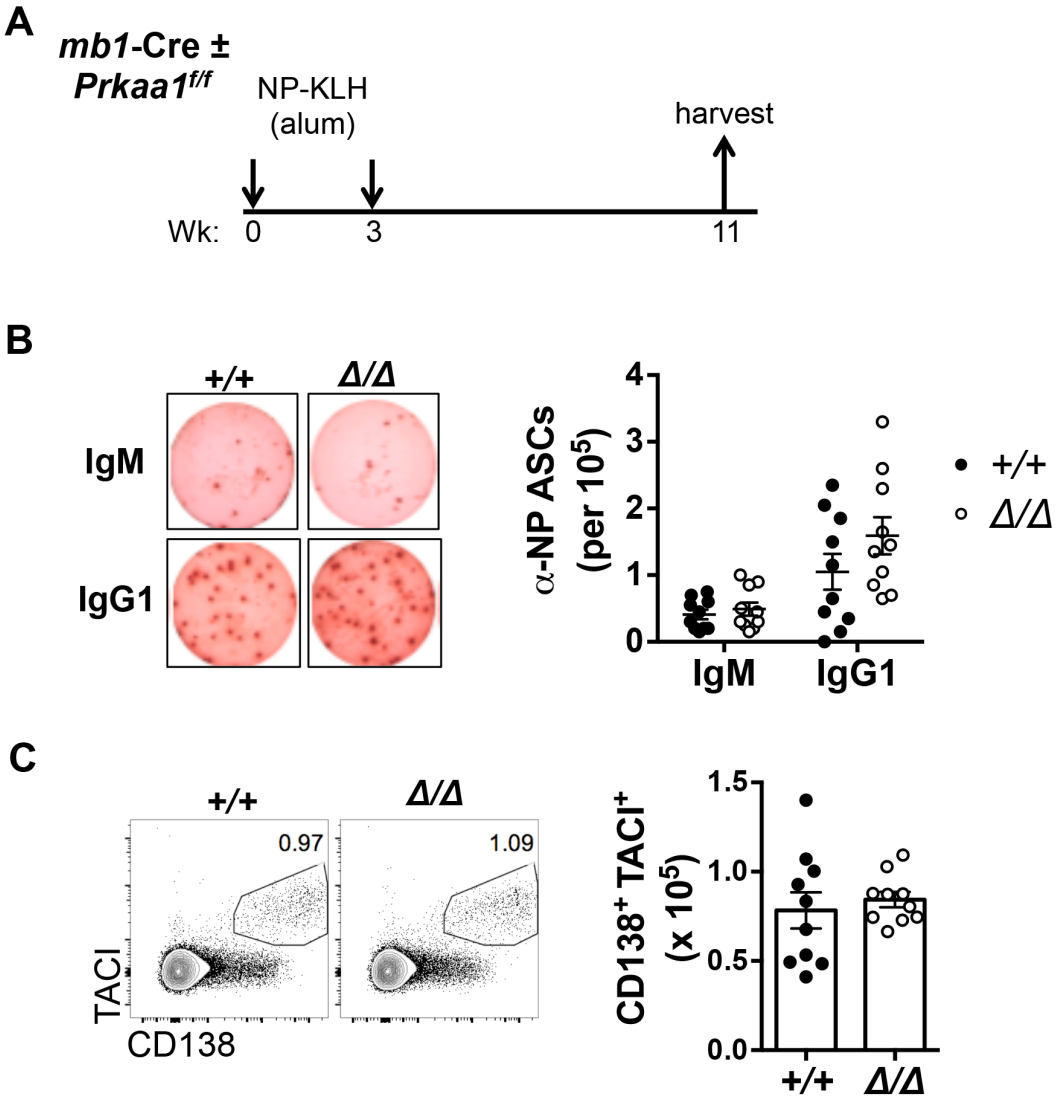

Figure 4.2 AMPK is dispensable for maintaining frequency of long-lived plasma cells. (A) Schematic of the immunization strategy using mice with mb1-integrated Cre such that Cre is constitutively expressed exclusively in the B lineage starting from the pro-B cell stage. Mice were immunized with NP-KLH, boosted at week 3, and harvested eight weeks post boost to screen specifically for long-lived plasma cells that remain long after the peak of the GC response. (B) Representative flow plot and quantification of total $CD138^{+}TACI^{+}$ bone marrow cells. (C) Left panel, representative ELISpot wells depicting density of bone marrow NP-specific IgM and IgG1 secreting cells; 2 x 10^6 total bone marrow cells plated per well. Right panel, numbers of NP-specific IgM and IgG1 per 10^5 total marrow cells in *Prkaa1*$^{+/+}$ and *Prkaa1*$^{\Delta/\Delta}$ mice at the time of harvest. Data represent mean ± SEM of n = 10 *Prkaa1*$^{+/+}$ and 10 *Prkaa1*$^{\Delta/\Delta}$ mice.

As described in Chapter 3, mitochondrial dynamics was dysfunctional in AMPK-deficient MBC coinciding with increased mtROS, lipid peroxidation, and eventual decline in the frequency of the MBC population. However, AMPK confers no defect on SLPC or LLPC numerically (Fig. 4.1 and Fig. 4.2). To assess mitochondrial parameters in AMPK-deficient LLPC, I stained bone marrow cells with Mitotracker dyes before flow cytometric analysis of the $CD138^{+}$ $B220^{lo}$ population. *Prkaa1*$^{\Delta/\Delta}$ bone marrow ASCs had less mitochondrial respiration and mitochondria mass compared to wildtype ASCs as determined by the MFI of Mitotracker Deep Red and Mitotracker Green, respectively (**Fig. 4.3A**). Interestingly, the Mitotacker Deep Red to Mitotracker Green ratio, as an indicator of dysfunctional mitochondria, was unaltered in *Prkaa1*$^{\Delta/\Delta}$ bone marrow ASCs (**Fig 4.3B**). mtROS, as determined by MitoSOX staining, was also unimpaired in ASCs in the absence of AMPK (**Fig 4.3C**). These data indicate that while AMPK does promote mitochondrial mass and respiration in LLPC, the homeostasis of mitochondria, at least in this setting, is independent of AMPK. In contrast to *Prkaa1*$^{\Delta/\Delta}$ MBC, the normal levels of mtROS in *Prkaa1*$^{\Delta/\Delta}$ LLPC coincide with their intact frequencies.

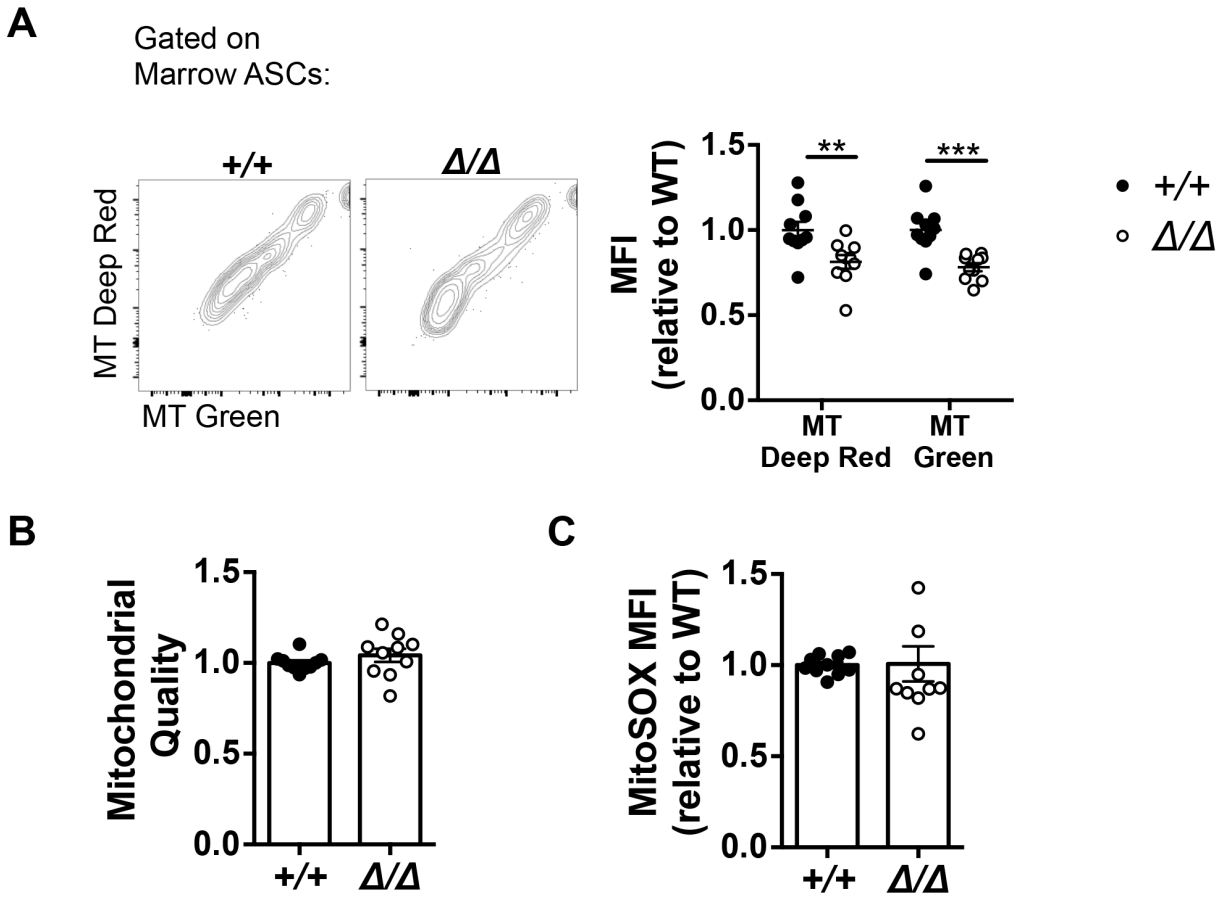

Figure 4.3 Loss of AMPK in ASCs leads to decreased mitochondrial respiration and total mass but is dispensable for mitochondrial homeostasis. (A) Left panel, representative flow plot depicting MFI of mitochondrial mass (MitoTracker Green) vs. respiring mitochondria (MitoTracker Deep Red) in marrow ASCs (ASCs: $B220^{lo}$ $CD138^{+}$) at harvest following immunization strategy illustrated in Fig. 4.2A. Right panel depicts quantification of relative MFI values of MitoTracker Deep Red and MitoTracker Green in ASCs of *Prkaa1*$^{+/+}$ and *Prkaa1*$^{\Delta/\Delta}$ mice. Data are normalized to wildtype MFI values in each experiment. (B) Mitochondrial quality of bone marrow ASCs calculated as the ratio of MitoTracker Deep Red MFI to MitoTracker Green MFI as an indicator of levels of dysfunctional mitochondria. Values are normalized to wildtype values in each experiment. (C) Mitochondrial-derived ROS in bone marrow ASCs measured by flow cytometry after MitoSOX labeling following immunization strategy in Fig. 4.2A. The mean ± SEM is displayed from three independent experiments with n = 10 *Prkaa1*$^{+/+}$ and n = 10 *Prkaa1*$^{\Delta/\Delta}$ mice. ** $p < 0.01$, *** $p < 0.001$ (Student's t-test (A)).

IV. AMPK attenuates antibody synthesis, likely by dampening mTORC1 activity

The primary function of ASCs is immunoglobulin production. To test if loss of AMPK led to changes in antibody production in primary responses, I immunized mice with NP-KLH as in Fig. 4.1A and collected sera weekly to screen for NP-specific IgM and IgG1 (**Fig. 4.4A**). Despite similar numbers of antigen-specific IgM and IgG1 ASCs, there was a substantial increase in circulating anti-NP IgM and IgG1 as early as two weeks after the initial immunization in the absence of AMPK (**Fig. 4.4B,C**).

A critical function of germinal centers is to generate antibody diversity and select high-affinity BCR and antibodies after iterative rounds of mutations and selection (Bozic et al., 2007). The affinity of polyclonal serum antibodies to NP can be determined by ELISA using NP_{27}-BSA and NP_2-PSA antigens. Only high affinity antibodies remain bound to low ratios of NP conjugated to protein. Similar to all-affinity antibodies, loss of AMPK led to an increase in high affinity IgG1 (**Fig 4.4D**). There was no difference in the ratio of NP_2/NP_{27} binding IgG1 indicating AMPK is nonessential for affinity maturation, i.e. antibody quality (**Fig. 4.4E**). Analogous to IgG1, IgG2c NP-binding antibodies of all and high affinities were also enhanced in *Prkaa1*$^{\Delta/\Delta}$ mice (data not shown for the interest of simplicity). Data indicate that although AMPK is dispensable for the frequency of SLPC generated in primary antibody responses, AMPK dampens the overall amount of antigen-specific antibody generated.

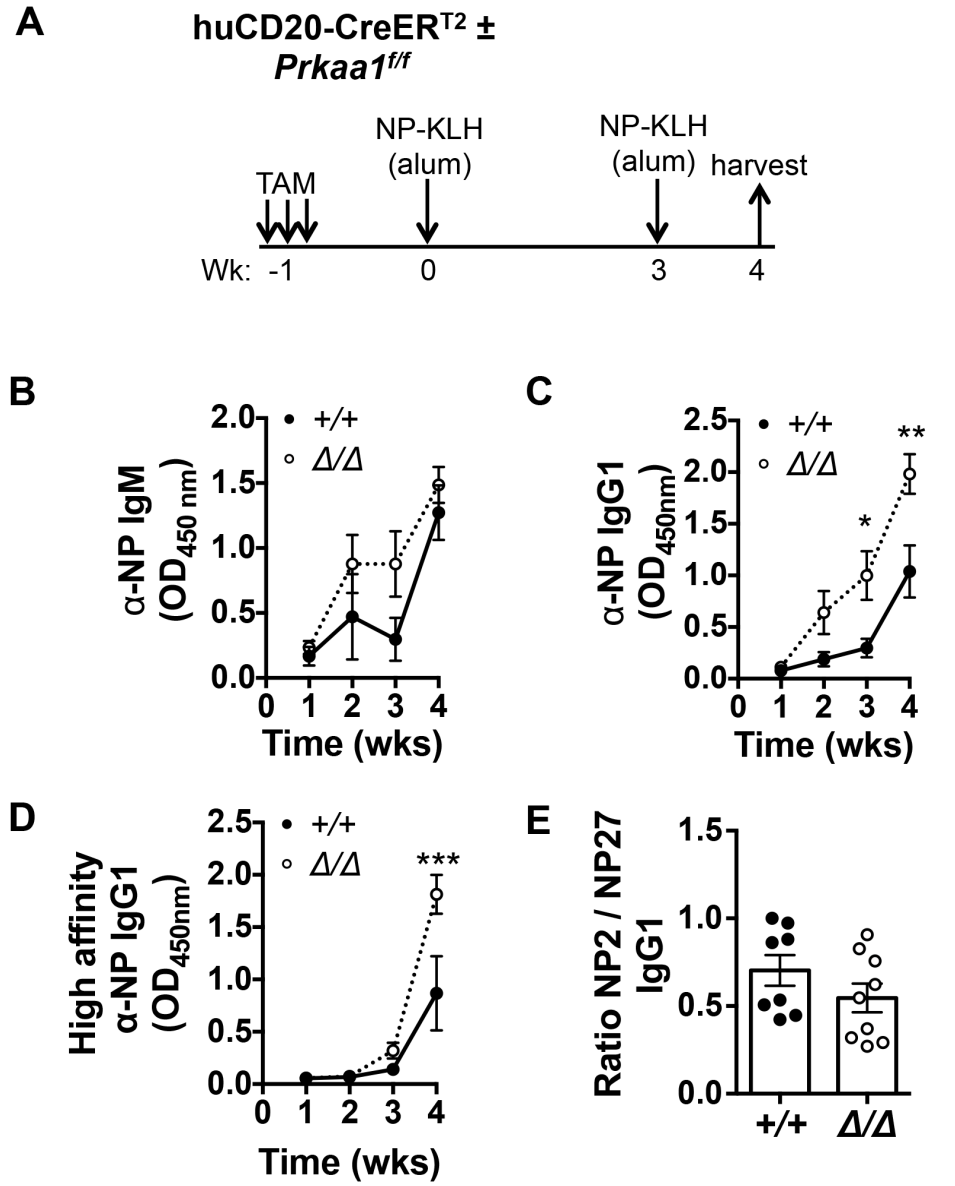

Figure 4.4 Loss of AMPK leads to increased IgG1 primary humoral responses. (A) Schematic of immunization strategy with NP-KLH using mice harboring a tamoxifen-inducible Cre under control of a B lineage restricted promoter, huCD20. Mice were treated with tamoxifen to induce B-cell specific deletion of *Prkaa1* and then immunized and boosted at week three with NP-KLH. Mice were bled to collect sera weekly to monitor primary immune responses. Circulating NP-specific (B) IgM, (C) IgG1, and (D) high affinity IgG1 at weeks 1, 2, 3, and 4 after initial immunization determined by ELISA where sera were diluted in the linear range (1:2,000 for IgM and 1:50,000 for IgG1); week 3 sera was collected immediately before the booster immunization. (E) Affinity maturation depicted by the ratio of week 3 ELISA OD values of NP2 binding IgG1 antibodies (high affinity) to NP27 binding IgG1 antibodies (all affinity). The mean ± SEM is displayed with at least n = 8 Prkaa1$^{+/+}$ mice and n = 9 *Prkaa1*$^{\Delta/\Delta}$ mice in four (B, C) or two independent experiments (D, E). * $p < 0.05$, ** $p < 0.01$, *** $p < 0.001$ (two-way ANOVA with Sidak's multiple comparisons (C, D)).

The most durable humoral immunity is due to antibody continuously produced by the LLPC population that remain long after the antigen has been cleared. Most of what was screened for in Fig. 4.4 was likely derived from SLPC. To determine the role of AMPK in LLPC antibody production, mice were immunized with NP-KLH, boosted at week 3, and harvested eight weeks later as in Fig. 4.2A (**Fig. 4.5A**). NP-specific IgM was unaltered in *Prkaa1*$^{\Delta/\Delta}$ mice compared to wildtype controls (**Fig. 4.5B**). However, similar to primary responses, antigen-specific IgG1 antibody production was enhanced in *Prkaa1*$^{\Delta/\Delta}$ LLPC (**Fig. 4.5C**). All together, AMPK appears to be nonessential for the generation and persistence of ASCs. However AMPK lessens IgG1 production in both SLPC and LLPC.

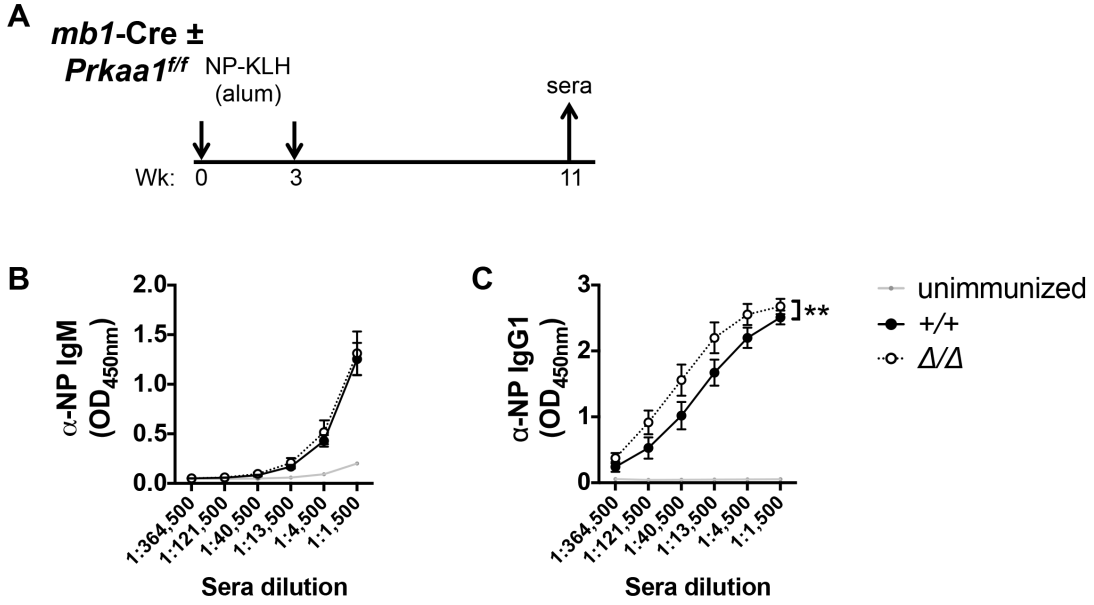

Figure 4.5 AMPK dampens LLPC IgG1 antibody production. (A) Schematic depicting immunization of *mb1-Cre* mice with a hapten-carrier. Mice were immunized with NP-KLH, boosted at week 3, and sera collected eight weeks post boost to screen specifically for the function of long-lived plasma cells that remain long after the peak of the GC response and the demise of short-lived plasma cells. Circulating NP-specific (B) IgM and (C) IgG1 in the sera eight weeks post the booster immunization. Data represent three independent experiments with 10 wildtype and 10 *Prkaa1*$^{\Delta/\Delta}$ mice. ** $p < 0.01$ (Student's paired t-test(C)).

Several models, none mutually exclusive of another, could account for the apparent paradox of persistently higher antibody concentrations in the absence of any increase in ASCs derived from AMPKα1-deficient B cells. First, loss of AMPKα1 in B cells may lead to increased rates of antibody production per ASC. Second, for primary responses, loss of AMPKα1 from B cells might lead to enhanced formation of plasma cells that generate higher circulating antibody but die before time of analysis. To explore these possibilities, I used *in vitro* cultures to test the effect of AMPKα1 on plasma cell differentiation and antibody production. For these *in vitro* studies, B cells purified from tamoxifen-injected *Rosa*26-CreER^{T2} mice (*Prkaa1*$^{f/f}$ or *Prkaa1*$^{+/+}$) were cultured with IL-4 on NB-21.2D9 feeder cells as described (Nojima et al., 2011; Kuraoka et al., 2016). When CD138 and B220 expression were analyzed every three days for nine days of co-culture with the BAFF, CD40L, and IL-21-expressing feeder cells, no differences were observed in the frequency or number of plasma cells (B220^{lo} CD138^{+}) (**Fig. 4.6A**), suggesting that AMPKα1 is dispensable for plasma cell differentiation. To test the effect of B cell AMPKα1 on antibody production throughout the co-culture, IgG1 was measured in supernatants. Despite similar numbers of plasma cells, cultures with AMPKα1-deficient B cells accumulated three-fold higher concentrations of antibody in their supernatants from days six to nine (**Fig. 4.6B**). Thus, consistent with the *in vivo* serologies, loss of AMPKα1 led to an increase in antibody in the supernatant despite comparable plasma cell numbers.

To test if similar frequencies of B220^{lo} CD138^{+} cells translated to similar numbers of functional ASCs, I performed ELISpot analyses on day 9 cultures. These assays detected ~40 IgG1-secreting cells per 500 plated differentiated cells for both AMPKα1-

deficient and -sufficient B cells (**Fig. 4.6C**). Despite similar numbers of IgG1-secreting cells after nine days of co-culture, the mean spot size for AMPKα1-deficient plasma cells was enhanced almost two-fold (**Fig. 4.6D**) suggesting increased antibody per cell.

To obtain enough plasma cells for downstream biochemical assays, I activated and cultured wildtype and AMPKα1-deficient B cells using LPS. The effect of AMPK on LPS activated cells concerning plasma cell differentiation and antibody production mirrors phenotypes of B cells activated on NB.21-2D9 feeder cells but LPS data not shown here for simplicity (if interested, see Brookens et al. 2020, Supplemental Fig. 2C,D). After an 8-day treatment of B cells with LPS, BAFF, IL-4, and IL-5, immunoblots probing whole cell lysates for total immunoglobulin revealed that *Prkaa1*$^{\Delta/\Delta}$ samples exhibited increased heavy and light chain expression compared to wildtype controls (**Fig. 4.6E**). All together, these *in vitro* results indicate that the increase in antibody observed from AMPKα1-deficient ASCs was due to an increase in antibody production on a per cell basis.

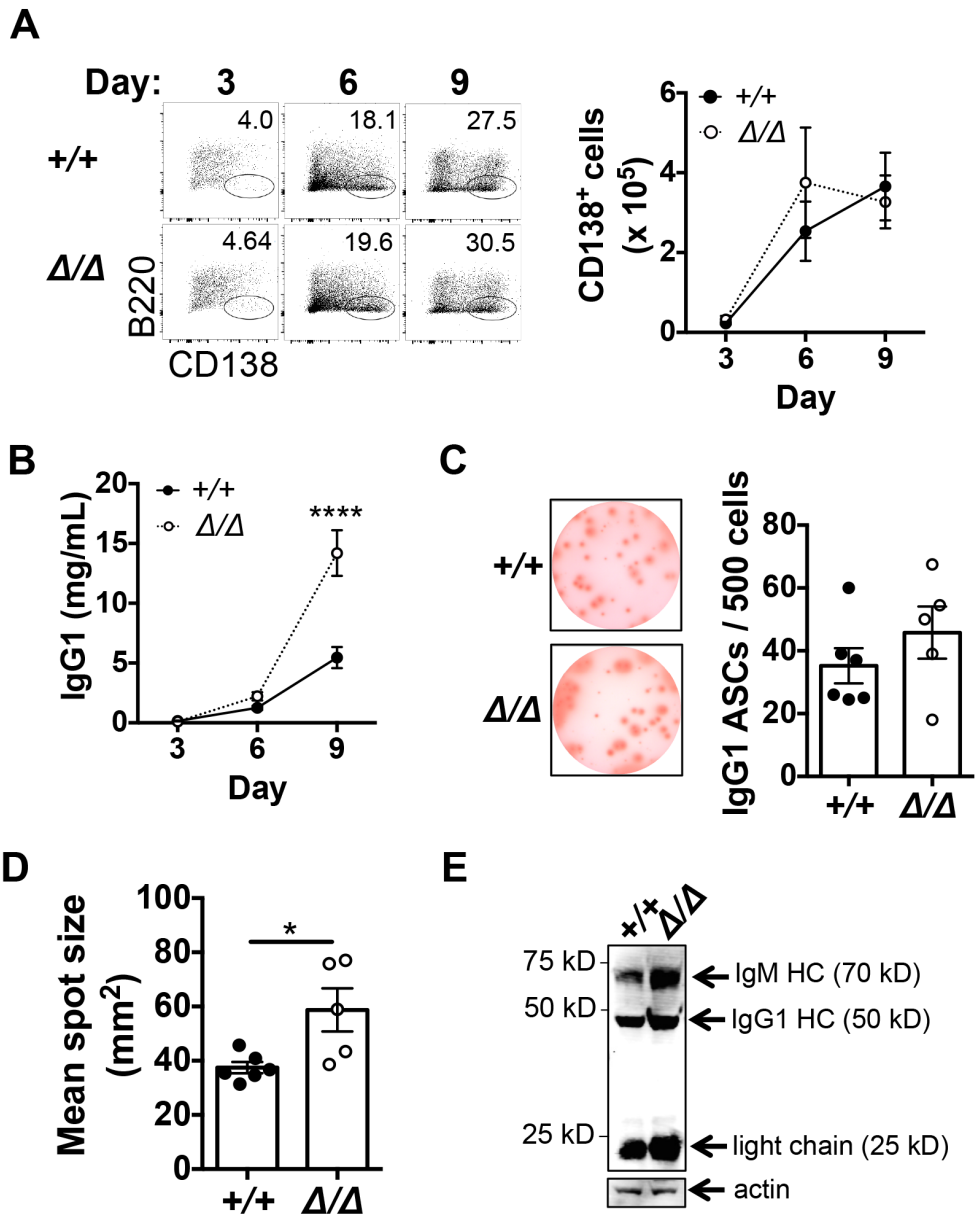

Figure 4.6 AMPK is dispensable for plasma cell differentiation but attenuates antibody production *in vitro*. (A) Representative flow plots (left panel) and total number (right panel) of CD138^{+} B220^{lo} cells on days 3, 6, and 9 during plasma cell differentiation after B cells from Prkaa1$^{+/+}$ or *Prkaa1*$^{\Delta/\Delta}$ mice were co-cultured on NB-21.2D9 feeder cells. (B) Concentration of IgG1 detected in the supernatants collected on days 3, 6, and 9 of co-culture. (C) Representative wells and quantification of ELISpot analysis depicting numbers of IgG1 secreting cells per 500 plated day 9 cultured cells. (D) Mean spot size of IgG1 ASCs from day 9 cultures of Prkaa1$^{+/+}$ or *Prkaa1*$^{\Delta/\Delta}$ mice determined by ELISpot analysis. (E) Expression of immunoglobulin on day 8 lysates after activation with LPS, BAFF, IL-4, and IL-5. Data represent three experiments with 6 vs. 5 mice. * $p < 0.05$, **** $p < 0.0001$ (Two-way ANOVA with Sidak's multiple comparisons test (B), Student's t-test (D)).

To distinguish the role of AMPKα1 on rates of antibody synthesis and/or immunoglobulin secretion, we performed [^{3}H]-leucine pulse-chase analyses after re-plating equal numbers of LPS-differentiated cells. Recall from Fig. 2.4 a brief summary of the pulse-chase optimization and that loss of *Prkaa1* did not alter [^{3}H]-leucine uptake. AMPKα1-deficient cells exhibited increased intracellular and secreted [^{3}H]-leucine labeled immunoglobulin (**Fig. 4.7A,B**). Specifically, AMPKα1-deficient cultures had ~6.5 fmol [^{3}H]-leucine incorporated in antibody after 1h of labeling compared to ~3.5 fmol of wild-type controls (Fig. 4.7A). The similar ratio of secreted to intracellular [^{3}H]-antibody after labeling suggests that the increase in antibody was not due to increased secretion rates (**Fig. 4.7C**). Therefore, increased synthesis was the basis for higher IgG1 production in *Prkaa1*$^{\Delta/\Delta}$ cells. Together, these data demonstrate that AMPKα1 in B cells restrains rates of antibody synthesis in plasma cells.

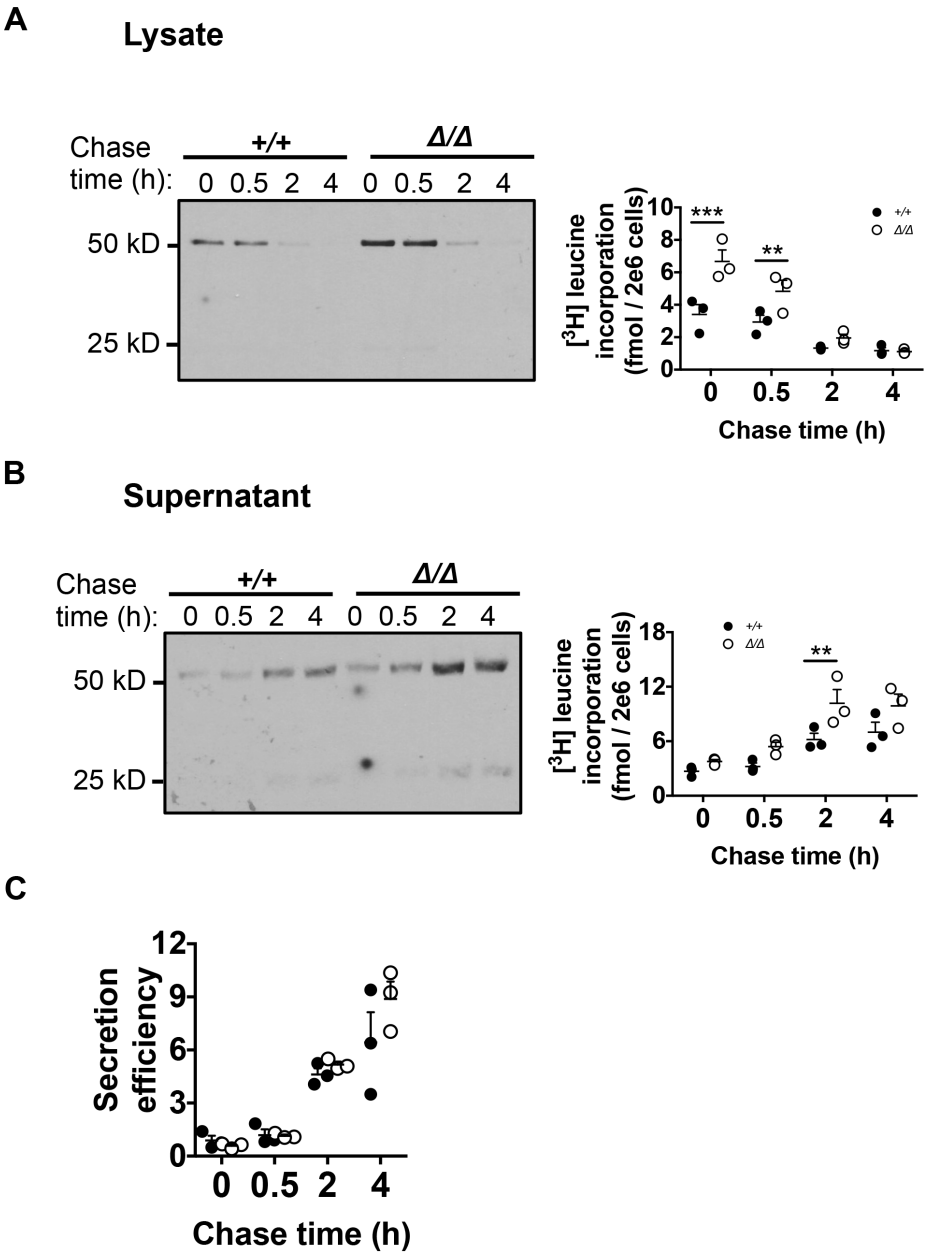

Figure 4.7 AMPK attenuates antibody synthesis. (A) Left panel, representative salicylate fluorography of protein G precipitates from day 7-LPS Prkaa1$^{+/+}$ or *Prkaa1*$^{\Delta/\Delta}$ lysates after one hour of labeling with [^{3}H]-leucine and chased at indicated times. Right panel, quantification of [^{3}H]-leucine incorporated into lysate protein G precipitates, as an indicator of intracellular IgG1. (B) Left panel, representative salicylate fluorography of protein G precipitates from day 7 LPS-culture supernatants with labeling and chase times as in panel (A). Right panel, quantification of [^{3}H]-leucine incorporated into supernatant protein G precipitates, as in indicator of secreted IgG1. (C) Ratio of [^{3}H]-leucine incorporation in the supernatant to incorporation in the lysate as an indicator of secretion efficiency. Data are representative of three independent experiments using n = 3 Prkaa1$^{+/+}$ and 3 *Prkaa1*$^{\Delta/\Delta}$ mice. ** $p < 0.01$, *** $p < 0.001$ (two-way ANOVA with Sidak's multiple comparisons (A, B)).

AMPKα1 inhibits mechanistic target of rapamycin complex 1 (mTORC1) activity both indirectly through the activation of TSC2 and directly by an inhibitory phosphorylation of Raptor, an essential component of mTORC1 (Gwinn et al., 2008). Loss of Raptor in B cells led to poor antibody responses *in vivo* (Raybuck et al., 2018; Jones et al., 2016). To evaluate mTORC1 activity in AMPKα1-deficient B cells, we performed immunoblots for mTORC1 targets using extracts of B lymphoblasts. Consistent with the canonical model, loss of AMPKα1 led to elevated expression of downstream mTORC1 targets, phospho-S6$^{S235/236}$ and phospho-4E-BP1$^{T37/46}$ (**Fig. 4.8A, B**). Similarly, LLPC in *Prkaa1*$^{f/f}$ *mb1*-Cre mice had elevated levels of phospho-S6 compared to wildtype controls after undergoing the immunization strategy illustrated in Fig. 4.2 (**Fig. 4.8C**). Because mTORC1 promotes protein synthesis, the elevated levels of antibody production observed with AMPKα1-deficient plasma cells are consistent with the increase in mTORC1 activity.

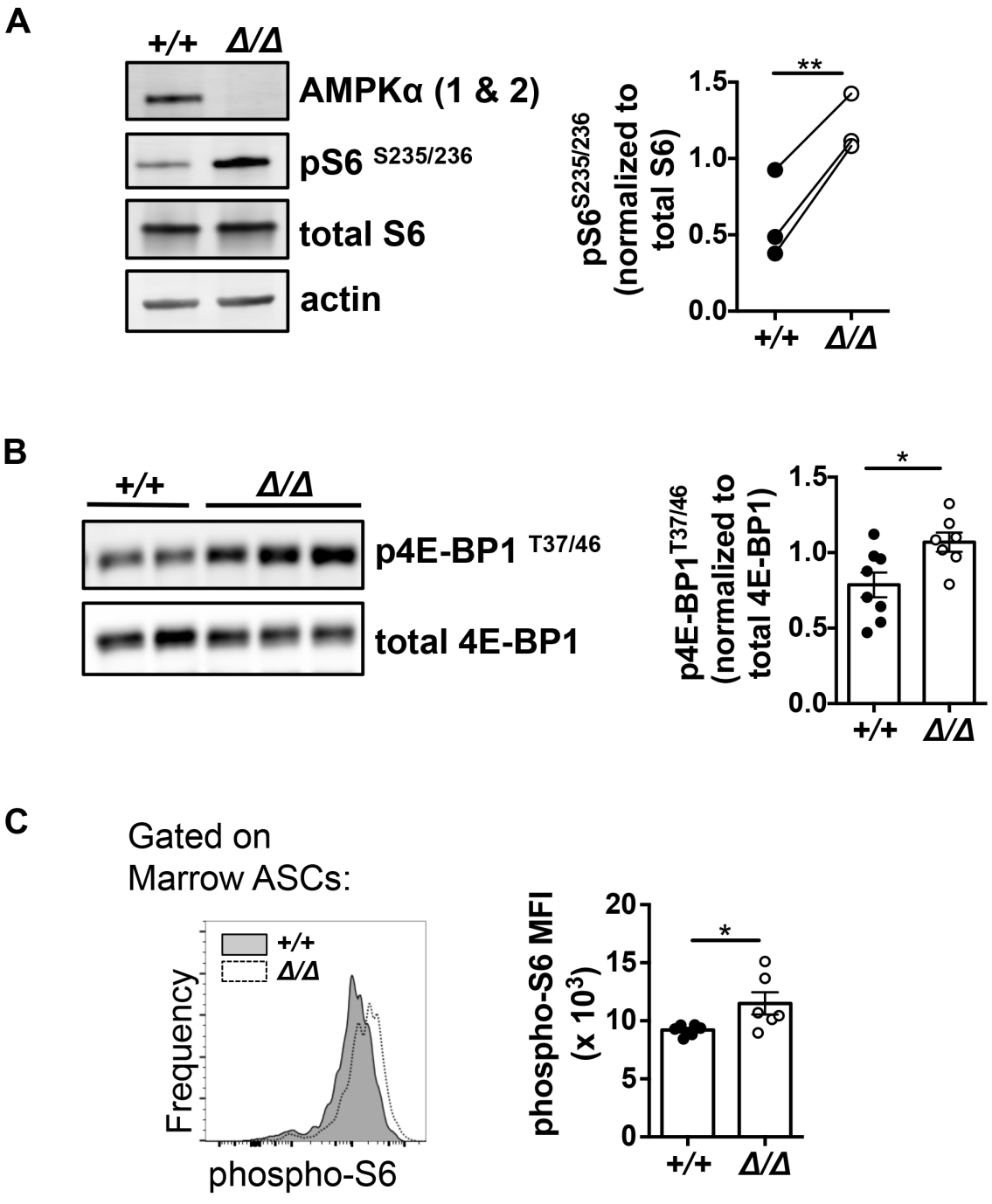

Figure 4.8 Increased mTORC1 signaling in the absence of AMPK in the B lineage. Immunoblot of mTORC1 targets (A) $pS6^{S235/236}$ and (B) $p4E\text{-}BP1^{T37/46}$ in 2-day LPS/BAFF activated $Prkaa1^{+/+}$ and $Prkaa1^{\Delta/\Delta}$ B cells. Expression is quantified in the right panels as the ratio of indicated phospho-protein to the total protein. Values determine using Image J densitometry. Data represent three independent experiments. (C) Representative histogram and quantification of the MFI of phospho-S6 in bone marrow ASCs ($B220^{lo}$ $CD138^{+}$) determined by flow cytometry. Data represent two independent experiments with n = 6 $Prkaa1^{+/+}$ and n = 6 $Prkaa1^{\Delta/\Delta}$ mice. * $p < 0.05$, ** $p < 0.01$ (paired Student's t-test (A,B), Student's t-test (C)).

To test if the increase in antibody produced in *Prkaa1*$^{\Delta/\Delta}$ mice was due to increased mTORC1 activity, I integrated the *Rptor*^{fl} allele to generate *Prkaa1*$^{f/f}$ *Rptor*$^{f/+}$ huCD20-CreER^{T2} mice. Regulatory-associated protein of mTOR (Raptor), encoded by *Rptor* is an adaptor protein essential for mTORC1 activity (Kim et al., 2002). Hemizygous loss of Rptor in B cells led to reduced class-switched antibody responses to immunization compared to wildtype (Cho et al., 2016; Raybuck et al., 2018; Raybuck et al., 2019). huCD20-CreER^{T2} mice harboring wildtype, *Prkaa1*$^{f/f}$, or *Prkaa1*$^{f/f}$ *Rptor*$^{f/+}$ alleles were immunized with NP-KLH after tamoxifen injections to investigate primary antibody responses (**Fig 4.9A**). Consistent with increased mTORC1 activity in *Prkaa1*$^{\Delta/\Delta}$ bone marrow plasma cells, MFI values of phospho-S6 *Prkaa1*$^{\Delta/\Delta}$ splenic ASCs were also enhanced compared to wildtype (**Fig. 4.9B**). However, additional loss of one allele of *Rptor* attenuated phospho-S6 of *Prkaa1*$^{\Delta/\Delta}$ splenic ASCs down to wildtype levels, which coincided with a restoration of wildtype amounts NP-specific IgG1 in the terminal sera (**Fig. 4.9C**). These data indicate that AMPK limits IgG1 production by negative regulation of mTORC1.

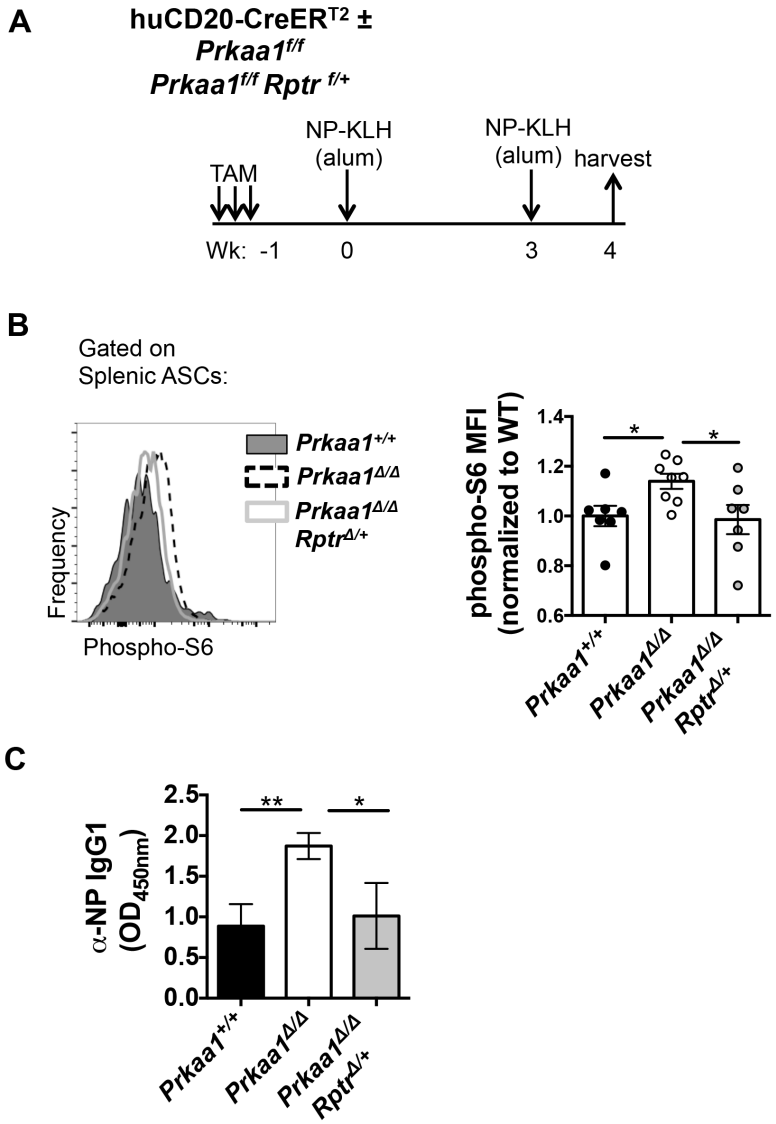

Figure 4.9 AMPK dampens antibody production through down regulation of mTORC1. (A) Schematic of immunization strategy with NP-KLH. HuCD20-*CreER*^{T2} mice were treated with tamoxifen to induce B-cell specific deletion of *Prkaa1* or additional loss of one copy of mTORC1 essential gene *Raptor* (*Rptr*) and then immunized, boosted at week three with NP-KLH, and harvested one week post boost to test primary responses, analogous to Fig 4.4A. (B) Left panel, representative flow plot depicting expression of phospho-S6 in wildtype, *Prkaa1*$^{Δ/Δ}$, and Prkaa1$^{Δ/Δ}$ Rptr $^{Δ/+}$ splenic ASCs (ASCs: B220^{lo} CD138^{+}). Right panel, quantification of phospho-S6 expression represented by relative MFI values in splenic ASCs at the time of harvest. (C) Circulating NP-specific IgM and IgG1 at the week four time point; values are ELISA OD values at the linear portion of the curve (1:2,000 for IgM and 1:50,000 for IgG1). Data are representative of two independent experiments with at least n = 7 wildtype (●), n = 8 *Prkaa1* $^{Δ/Δ}$ (○), and n = 5 Prkaa1$^{Δ/Δ}$ Rptr $^{Δ/+}$ mice (●). * $p < 0.05$, ** $p < 0.01$ (Student's t-test (B,C)).

In parallel to *in vivo* results, hemizygous loss of *Rptor* in *Prkaa1*$^{\Delta/\Delta}$ mice attenuated the IgG1 detected in the supernatant to normal levels after a 7-day culture with LPS, BAFF, IL-4, and IL-5 (**Fig. 4.10A**). The restoration of antibody levels was not due to a decrease in plasma cell frequency in *Prkaa1*$^{\Delta/\Delta}$ *Rptor*$^{\Delta/+}$ cells (**Fig. 4.10B**). mTORC1 regulates multiple targets involved in the translation of ribosomal proteins and translation factors, potentially supporting the synthesis of antibodies in ASCs (Fonseca et al., 2014). To test the effect of *Rptor*$^{\Delta/+}$ on immunoglobulin synthesis in *Prkaa1*$^{\Delta/\Delta}$ ASCs, I pulsed equal numbers of day-7 LPS cultures with [^{3}H]-leucine before salicylate fluorography of membranes with protein G precipitates (**Fig. 4.10C**). *Prkaa1*$^{\Delta/\Delta}$ *Rptor*$^{\Delta/+}$ samples had less [^{3}H]-leucine incorporation into the light and heavy chains of IgG than *Prkaa1*$^{\Delta/\Delta}$ samples as determined by exposed membranes and scintillation counts (**Fig. 4.10D**). All together, the evidence suggests that AMPK limits antibody synthesis by antagonizing mTORC1 activity.

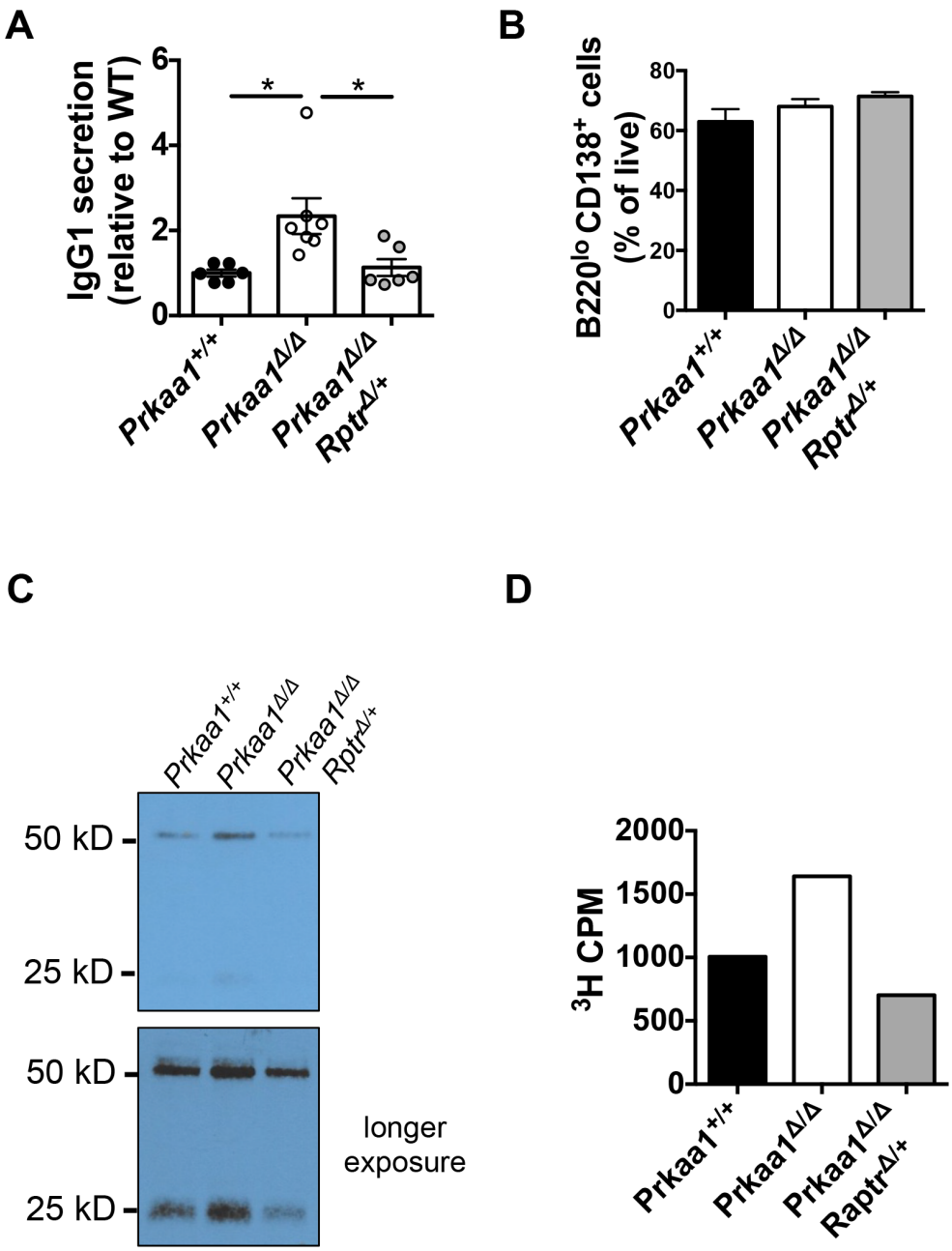

Figure 4.10 AMPK dampens IgG1 synthesis through down regulation of mTORC1. (A) Relative levels of IgG1 detected in the supernatant eight hours after plating 5 x 10^4 cells/100µL of day-7 LPS/BAFF/IL-4/IL-5 cultured Prkaa1$^{+/+}$, *Prkaa1* $^{\Delta/\Delta}$, and *Prkaa1* $^{\Delta/\Delta}$ Rptr $^{\Delta/+}$cells. (B) Frequency of B220^{lo}CD138^{+} cells on day 7 of LPS/BAFF/IL-4/IL-5 culture. (C) Salicylate fluorography of protein G precipitates in lysates following a six-hour of pulse of day-7 cultures with [^{3}H]-leucine. Membranes were subjected to 4 day (upper panel) or 2 week exposure (lower panel). (D) [^{3}H]-leucine incorporation depicted by scintillation counts per minute (CPM). Data in (A) and (B) are representative of n = 6 Prkaa1$^{+/+}$, n = 7 *Prkaa1* $^{\Delta/\Delta}$, and n = 6 *Prkaa1* $^{\Delta/\Delta}$ Rptr $^{\Delta/+}$ mice. * $p < 0.05$ (Student's t-test (A)).

V. Discussion

Short and long-lived plasma cells are critical for the production of antibodies that provide protection against pathogens and their endotoxins. The energetic demands necessary for immunoglobulin synthesis and the microenvironments in which ASCs reside necessitate that this unique cell type has evolved specialized metabolic programs to maintain fitness and function. However, at the time of my thesis, the extrinsic and intrinsic factors that specifically support plasma cell metabolism have only recently garnered attention and many unanswered questions remain. Currently, for every six publications elucidating various aspects of T cell metabolism there is only one on B cells and even fewer concerning plasma cells specifically. Both B and T lymphocytes go through parallel stages of activation, proliferation, and the formation of memory. This mimicry allows for educated hypotheses to be made about critical metabolic processes in B cells from the plethora of new T cell literature. However, there is no corresponding counterpart in the T lineage for LLPC, which unlike memory cells require high rates of protein and glucose metabolism to support the synthesis and glycosylation of antibodies (D'Souza et al., 2019).

Here, in Chapter 4 I have shown that in contrast to MBC, the energy sensor AMPK is dispensable for plasma cell differentiation, the generation of SLPC, and the persistence of LLPC populations. However, this metabolic regulator dampens antibody synthesis in both SLPC and LLPC likely through inhibition of mTORC1. Additionally, contrary to MBC, mitochondrial homeostasis in LLPC is unaltered by my metrics highlighting a stark molecular distinction between MBC and bone marrow plasma cells in their metabolic programming. Chapter 4 findings, summarized in Fig. 4.11, indicate

that rates of antibody synthesis can be manipulated by modulating nutrient sensor activity.

Two studies, one of which was published a few months before my work, concluded that loss of *Prkaa1* in B cells led to no alterations in antibody responses to T-dependent immunization strategies (Mayer et al., 2008; Waters et al., 2019). However, these studies used either germ-line AMPK knockout animals, which have B-cell independent effects of AMPK (Wang et al., 2010; Carroll et al., 2013) or in their discussion authors overlooked their observations on heightened IgM responses in favor of highlighting interesting novel insights on IgD expression (Waters et al., 2019). Here, I used multiple genetic models, (including deletion of *Prkaa1* by Cgamma1-*Cre* (Casola et al., 2006), data not shown for simplicity), and *in vivo* and *in vitro* approaches which all converge to the conclusion that AMPK in the B lineage limits antibody synthesis.

mTORC1 in activated B cells, GCB, and plasma cells have all been shown to be critical for antibody production (Raybuck et al., 2018; Jones et al., 2016; Gaudette et al., 2020). In Chapter 4, I observed enhanced mTORC1 activity in AMPK-deficient LPS activated B cells and in *ex vivo* splenic and bone marrow plasma cells, which corresponded to elevated antibody production. Additional loss of one *Rptor* allele, an essential mTORC1 adaptor protein which has intermediate effects on antibody production when compared to deletion of both Raptor alleles (Raybuck et al., 2018, Raybuck et al., 2019), restored antibody in *Prkaa1*-null cells to normal levels. Thus, my data suggest that AMPK moderates mTORC1 activity in a manner that maintains a biologically appropriate range of mTORC1 signaling that ultimately leads to appropriate levels of antibody generation. Such “Goldilocks mTOR” may be evolutionarily conserved for purposes of maintaining

controlled primary humoral responses as it does in T cell differentiation (Zeng et al., 2017). In keeping with these findings, plasma cell associated transcription factor Blimp-1 was important for the elevated mTORC1 signaling observed in plasma cells with modest reductions in AMPK activity indicating that mTORC1 is the dominant metabolic regulator in these cells (Tellier et al., 2016). I have uncovered that AMPK plays a part in the fine-tuning of mTORC1 during B cell activation and antibody secretion.

Effects of genetic modifications that persistently increased mTORC1 in B cells have been studied in several alternative models (Benhamron et al., 2015; Ci et al., 2015; Ersching et al., 2017). B cell-specific inactivation of *Tsc1,* which encodes a negative regulator of mTORC1 [tuberous sclerosis complex 1 (TSC1)], led to increased Ig synthesis (Benhamron et al., 2015), akin to results shown here with induced loss of AMPKα1. However, another study revealed that inactivation of the *Tsc1* gene led to modestly impaired antibody responses (Ci et al., 2015). Although TSC1 deficiency in B cells also had little impact on GC in this study, Ci *et al.* results did not phenocopy antibody results with the loss of AMPKα1. However, differences between the two perturbations of AMPK and Tsc1 loss may vary because both regulate other pathways in addition to mTORC1 and their loss leads to different degrees of increase in mTORC1 activity. Analogous points apply to findings with a constitutive knock-in of a gain-of-function mutation in an upstream regulator that promotes mTORC1 activity (Ersching et al., 2017).

As discussed in Chapter 3, AMPK and mTORC1 reciprocally regulate canonical autophagy. In a manner mirroring our findings with AMPKα1, Atg5 in B cells was critical for limiting excessive immunoglobulin production by plasma cells (Pengo et al., 2013),

which was attributed to a function in restraining endoplasmic reticulum stress signaling. However, recall that LC3-II conversion was intact in *Prkaa1*-null B cells; specifically, LC3 autophagosome puncta were apparent in $CD138^{+}$ bone marrow cells indicative of vigorous autophagy despite loss of AMPK (Fig. 3.11). Evidence again underscores the importance of non-canonical modes of autophagy in the B lineage, including Rubicon-dependent non-canonical autophagy, which has also been highlighted in GCB in recent studies (Raso et al., 2018; Martinez-Martin et al., 2017). Though AMPK may play a part in promoting overall autophagy, evidence indicates that B cells have alternative mechanisms to bypass the requirement for AMPK in exercising this essential self-degrading process.

Loss of AMPK impaired mitochondrial respiration and mass in LLPC but in contrast to MBC, mtROS and mitochondrial quality were intact which coincides with no defect in longevity. LLPCs have substantial mitochondrial respiratory capacity compared to their short-lived counterparts and require mitochondrial pyruvate and long-chain fatty acids for fuel (Lam et al., 2016). It is unclear how AMPK-deficient LLPCs maintain mitochondrial quality in light of evidence that AMPK is vital for maximal and spare respiratory capacity in B lymphoblasts and mitochondrial homeostasis in MBCs (Chapter 3). Here, I speculate on a few possibilities that may explain the differences in LLPC and MBC and their reliance on AMPK for mitochondrial homeostasis. One possibility is that LLPCs upregulate HIF and HIF related genes to support survival and function in the hypoxic niches of the bone marrow (Schoenhals et al., 2017; Spencer et al., 2014). Ectopic expression of HIF-1α decreased mtROS and mitochondrial genes in a human cell line and protected against oxidative stress (Li et al., 2019). Increased HIF

activation in LLPC may keep mtROS levels at bay, even in the absence of AMPK, as observed here. In support of this hypothesis, loss of AMPKα1 in Eμ-Myc lymphoma cells led to increased HIF-1α expression and a glycolytic signature (Faubert et al., 2013). Furthermore, several groups have reported the reciprocal regulation of HIF and AMPK to combat metabolic stress and redundant targets of both signaling pathways have been identified suggesting that HIF activity in LLPC may compensate for the loss of AMPK (Dengler et al., 2020).

The difference between MBC and LLPC in their reliance of AMPK for mitochondrial homeostasis may also be due to distinctions in mitochondrial regulation in the two subsets. Recall from Fig. 3.1 and 3.2 that wildtype ASCs had less mitochondrial mass, respiration, and mtROS than activated B cells or any other B lineage subsets measured *ex vivo*. Blimp1 transcription factor, which governs plasma cell differentiation, reduces mitochondrial mass and mtROS in these cells (Jang et al., 2015). Plasma cells had less mitochondrial content and mtROS compared to naïve and germinal center *in vivo* in recent study as well (Haniuda et al., 2020). B cells The need for AMPK to turnover accumulating mitochondria in plasma cells may be less critical since plasma cells are more likely to have lower mitochondrial mass and membrane potential than $IgG1^+$ B cells (Jang et al., 2015).

Lastly, ASCs may exhibit decreased mitochondrial mass, respiration, and mtROS than MBC due to cell size. Recall from Chapter 3 that cell size distinguishes ASCs from other cell types in the B lineage and that LLPC in the bone marrow are even larger than SLPC in the spleen, which accommodate expanded endoplasmic reticulum and Golgi machinery. The allometric scaling phenomenon suggests that the biophysical properties

of larger cells and organisms limits metabolism including mitochondrial activity (Miettinen et al., 2017; West et al., 2002; West et al., 2005). The reduced but dispersed mitochondria observed in plasma cells potentially leads to increased fitness for these larger cells with higher energy demands and highlights differential regulation of mitochondria in ASCs compared to other B cell subtypes.

Here, I have provided evidence that AMPK dampens antibody synthesis, which may be a potential target for limiting autoantibody production. Mechanisms that govern sufficient ATP generation in plasma cells to fuel metabolically demanding processes such as antibody synthesis needs to be further explored to better understand how this unique subset maintains fitness.

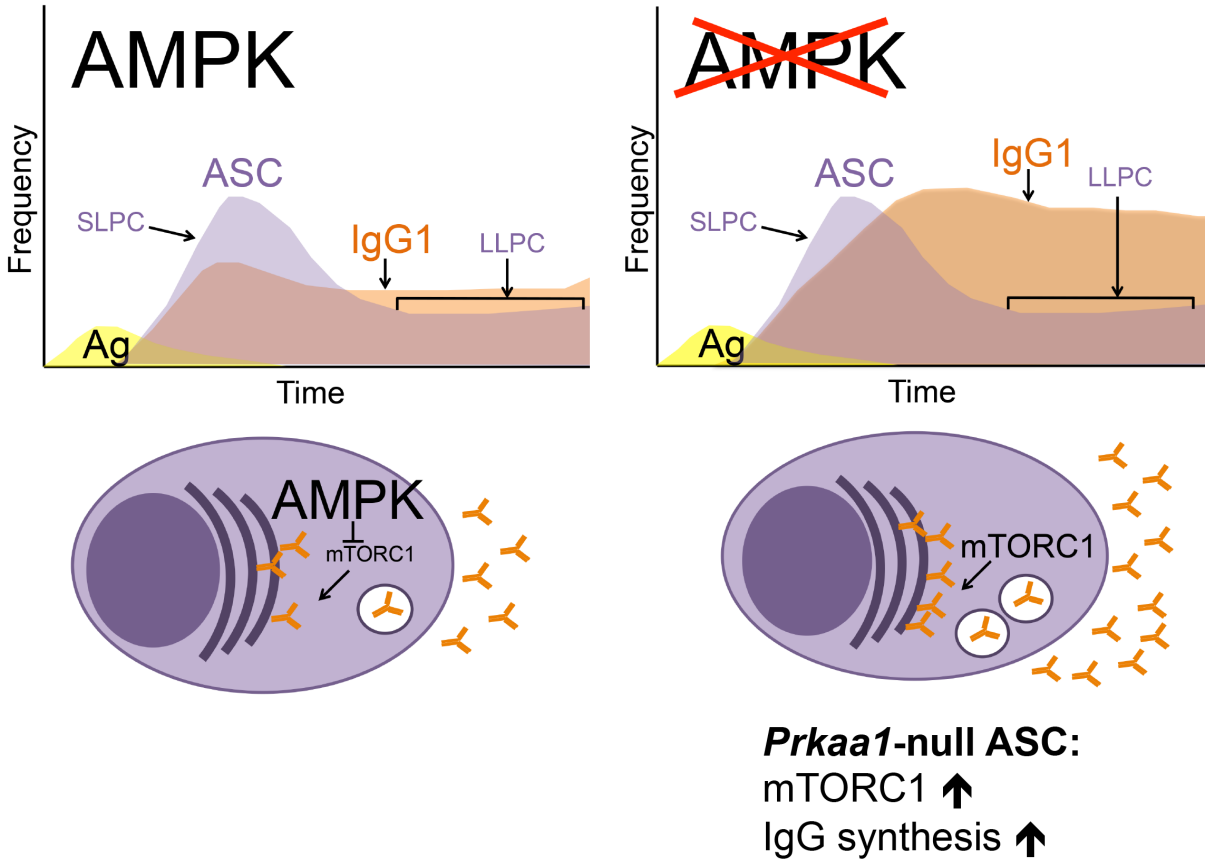

Figure 4.11 AMPK attenuates antibody synthesis. AMPK is dispensable for generating and maintaining ASCs. However *Prkaa1*-null ASCs exhibit increased IgG1 synthesis due to increased mTORC1 signaling indicating that AMPK down-regulates antibody synthesis. Figure is modified from Brookens et al 2021.

CHAPTER 5

GLUCOSE AND GLUTAMINE METABOLISM ARE CRITICAL FOR EFFECTIVE PRIMARY HUMORAL RESPONSES

The work presented in this chapter is unpublished findings concerning glucose metabolism and glutaminolysis in B cells and antibody responses

I. Abstract and Significance

Glucose and glutamine metabolism are critical for supporting B cell activation, differentiation, and antibody production. However, the interplay between the two carbon sources is not clearly elucidated in *in vivo* humoral responses. Glucose has been previously shown to be critical for biosynthesis in activated B cells and important for the glycosylation of antibodies in plasma cells. Previous reports indicate that glutamine supports anaplerotic reactions in activated B cells and plasma cells and promotes plasma cell differentiation *in vitro*. Here in Chapter 5, I used genetic mouse models to disrupt glucose transport and glutaminolysis in the B lineage to show that loss of both Glut1 and Gls1 synergistically attenuate IgG1 class-switching, plasma cell differentiation, and $IgG1^+$ antibody responses highlighting overlapping metabolic pathways from distinct carbon fuels. Additionally, my findings extend previous reports on the essential role for Glut1 and glutamine metabolism on antibody responses and further expand on the role of these pathways in affinity maturation, in fate decisions, and class-switching.

II. Introduction

AMPK regulates a plethora of downstream metabolic pathways including those involving glucose and glutamine metabolism. AMPK downregulated glycolysis in CD3/28 activated T lymphocytes, leukemic T cells, and Eμ-Myc$^+$ lymphoma cells (MacIver et al., 2011; Kishton et al., 2016; Faubert et al., 2013). Enhanced glycolysis in the absence of AMPK is consistent with evidence that AMPK protects against the Warburg effect in some settings (Li et al., 2015; Liu et al., 2020). However, in other settings AMPK promotes glucose (and glutamine) metabolism in T cells (Blagih et al., 2015). *Ex vivo* analysis after rLmOVA-infection revealed that AMPK expressing CD8$^+$ T effector cells had increased expression of glucose transporter Glut1, increased glucose uptake, as well as enhanced expression of glutaminolysis-related genes compared to AMPK-deficient T cells (Blagih et al., 2015). Conversely, low glucose or glutamine conditions lead to AMPK activation to promote energy conservation in lymphocytes and a lymphoma cell line (Rolf et al., 2013; Blagih et al., 2015; MacIver et al., 2011; Faubert et al., 2013). In nutrient poor settings, AMPK supports viability by enabling metabolic plasticity; AMPK in glucose-starved T cells was critical for switching from glycolysis to glutamine-dependent oxidative phosphorylation (Blagih et al., 2015). Due to the role of AMPK on glucose and glutamine metabolism, I sought to focus on glucose and glutamine metabolism specifically in humoral immunity.

B cells have increased glucose and glutamine uptake upon activation or entry into germinal centers (Caro-Maldonado et al., 2014; Cho et al., 2011; Doughty et al., 2006; Dufort et al., 2007; Jellusova et al., 2017; Waters et al., 2018; Masle-Farquhar et al., 2017; Brand et al., 1989; Jayachandran et al., 2018; Haniuda et al., 2020). Molecularly, activated lymphocytes increase activities of the enzymes that metabolize glucose, glutamine, fatty acids, and ketone

bodies. However, glycolytic- and glutaminolysis-related enzymes are quantitatively the most active (Curi et al., 1999; Fitzpatrick et al., 1993). Glycolysis and glutaminolysis provide metabolic intermediates for biosynthetic pathways. Specifically, the glycolytic metabolite glucose-6-phosphate is a precursor to ribose and NADPH, which are essential for nucleotide and fatty acid synthesis respectively. Glycolytic intermediate glycerol 3-phosphate is a precursor for phospholipid synthesis. In activated lymphocyte cultures, most of the glucose is routed to these biosynthetic intermediates to support proliferation while glutamine fuels the TCA cycle after conversion to glutamate and then α-ketoglutarate (Waters et al., 2018; Le et al., 2019; Curi et al., 1999; Fitzpatrick et al., 1993). Alpha-ketoglutarate is also a substrate for histone and DNA demethylases that regulate epigenetic reactions (Nakajima et al., 2014). In addition to anaplerosis and regulation of chromatin accessibility, glutamine is also a source of nitrogen, which is essential for the generation of purines and pyrimidines.

Beyond B cell activation, plasmablasts and plasma cells have unique requirements for glucose and glutamine metabolism (Crawford et al., 1985; Vijay et al., 2020; Lam et al., 2016; Lam et al., 2018; Garcia-Manteiga et al., 2020; Dufort 2014 et al., 2014; Bertolotti et al., 2010). Glutamine was required for plasma cell differentiation *in vitro* (Crawford et al., 1985). Plasmablasts have an increased demand for glutamine compared to GCB after *Plasmodium* infection resulting in competition for this amino acid between B lineage subsets in the spleen (Vijay et al., 2020). Glutamine contributes as an amino acid building block used for immunoglobulin synthesis in plasma cells and provides NADPH necessary for antioxidant responses (Lam et al., 2018; Bertolotti et al., 2010; Garcia-Manteiga et al., 2020). Glucose carbons are used for de novo lipid synthesis used in the expanding ER membranes of plasma cells (Dufort et al., 2014). Furthermore, long-lived plasma cells,

which take up more glucose than their short-lived counterparts, use ~90% of imported glucose for the glycosylation of antibodies (Lam et al., 2016). In Chapter 5, I provide evidence that glucose availability has effects on B cell fate and affinity maturation after germinal center responses. I expand on the role for glutamine metabolism in plasma cell differentiation and IgG1 class-switching. Furthermore, I present new evidence indicating that glutamine and glucose metabolism has redundant functions in antibody responses.

III. Glucose uptake, glycolysis, and mitochondrial function are disrupted in activated Glut1-deficient B cells

To investigate the role of glucose metabolism on B cell responses I crossed *Glut1*$^{f/f}$ mice, a generous donation from Jeff Rathmell, to huCD20-Cre-ER^{T2} mice. *Glut1*$^{f/f}$ huCD20-Cre-ER^{T2} is a tamoxifen-dependent inducible model where Glut1, a glucose transporter, is deleted from mature B cells after tamoxifen injection. Expression of *Slc2a1* mRNA, which encodes for Glut1, was reduced in *Glut1*$^{f/f}$ huCD20-Cre-ER^{T2} B cells compared to *Glut1*$^{+/+}$ huCD20-Cre-ER^{T2} controls after 2-day treatment with LPS, BAFF, and 4-hydroxy-tamoxifen (**Fig. 5.1A**). Lymphocytes express various glucose transporters including Glut1 (Maratou et al., 2007; Caro-Maldonado et al., 2014; Macintyre et al., 2014; Liu et al., 2014; Kojima et al., 2009; Choi et al., 2018). However, loss of Glut1 alone was sufficient to decrease glucose uptake in 2-day LPS-activated B cells after 4-hydroxy-tamoxifen treatment (**Fig. 5.1B**). Furthermore, *ex vivo* uptake of fluorescently labeled glucose analog 2-(*N*-Nitrobenz-2-oxa-1,3-diazol-4-yl)Amino)-2-Deoxyglucose (2-NBDG) was decreased two-fold in CD138^{+} TACI^{+} antibody secreting cells (ASCs) in tamoxifen injected *Glut1*$^{f/f}$ huCD20-Cre-ER^{T2} (*Glut1*$^{\Delta/\Delta}$) mice compared to wildtype ASCs (**Fig.**

5.1C). There are several caveats with equating 2-NBDG uptake to glucose uptake (Sinclair et al., 2020). However, Seahorse analysis also indicated defects in the extracellular-acidification rate (ECAR) as a surrogate for glycolytic functions in 2-day LPS and BAFF activated *Glut1*$^{\Delta/\Delta}$ B cells (**Fig. 5.1D**). Challenging B cells with ATP synthase inhibitor oligomycin did not promote any increases in ECAR in *Glut1*$^{\Delta/\Delta}$ cells suggesting that Glut1 is involved in mitochondrial stress-response pathways (**Fig. 5.1E**). Multiple molecules and metabolic processes can lead to extracellular acidification including lactate, which is one of many downstream metabolites of glycolytic end-product pyruvate (Mookerjee et al., 2015; Gray et al., 2014). Notwithstanding, Glut1 in LPS-activated B cells supported glycolysis, glycolytic capacity, and glycolytic reserve in B cells as interpreted by the Seahorse Agilent platform (**Fig. 5.1 F-H**).

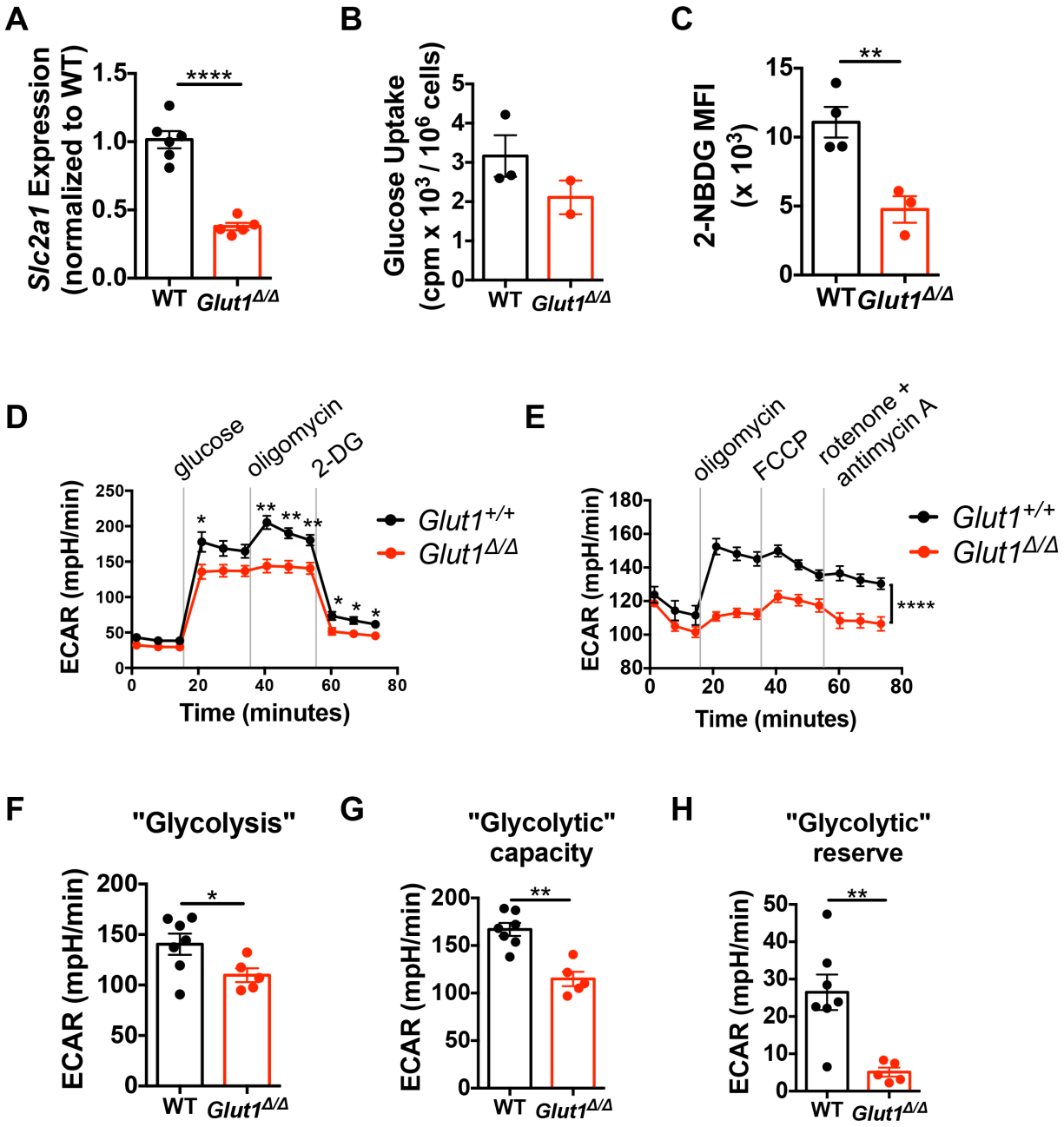

Figure 5.1 Reduced expression of Slc2a1, glucose uptake, and glycolytic function in *Glut1*-deficient B cells. (A) *Slc2a1* expression, encoding for Glut1 in B cells, in 4-hydroxy-tamoxifen treated wildtype and *Glut1*$^{f/f}$ CD20-ER^{T2}Cre 2-day LPS blasts determined by Real Time PCR. (B) 2-[1,2-^{3}H]-deoxy-glucose uptake in 2-day *Glut1*$^{+/+}$ and *Glut1*$^{\Delta/\Delta}$ LPS blasts after depleting intracellular stores by starvation. (C) *Ex vivo* 2-NBDG uptake of splenic CD138^{+}TACI^{+} in *Glut1*$^{+/+}$ and *Glut1*$^{\Delta/\Delta}$ mice. (D) Extracellular acidification rate (ECAR) during Agilent Seahorse Glycolytic Stress Test or (E) Mitochondrial Stress test after *Glut1*$^{+/+}$ or *Glut1*$^{\Delta/\Delta}$ were activated with LPS, BAFF, IL-4, and IL-5 for 2 days. (F) Glycolysis, indicated by glucose induced ECAR, is calculated by

Agilent Seahorse XF Glyco Stress Test Report Generator. (G) Glycolytic capacity, indicated by glucose and oligomycin-induced ECAR; oligomycin is an inhibitor of the ATP synthase. (H) Glycolytic reserve, determined by oligomycin-induced ECAR. In (A-C, F-H) each dot represents a mouse where black circles (●) represent *Glut1*$^{+/+}$ and red circles (●) represent *Glut1*$^{\Delta/\Delta}$. Data in D-H are representative of two independent experiments with n = 7 *Glut1*$^{+/+}$ mice and n = 5 *Glut1*$^{\Delta/\Delta}$ mice. * $p < 0.05$, ** $p < 0.01$, **** $p < 0.0001$ (Student's t-test (A,C), two-way ANOVA with Sidak's multiple comparisons (D), paired Student's t-test (E), Student's t-test (F-H)).

Glucose taken up by activated B cells is used primarily for biosynthetic pathways with very little contribution to oxidative phosphorylation (Doughty et al., 2006; Waters et al., 2018). It was surprising therefore that loss of Glut1 led to defects in the oxygen consumption rate (OCR) of LPS, BAFF, IL-4, and IL-5 activated B cells in the Mitochondrial Stress Test by Seahorse Agilent (**Fig. 5.2A**). Though basal respiration, represented by the OCR values before the addition of ATP synthase inhibitor oligomycin, was not significantly altered by the loss of Glut1, maximal and spare respiratory capacity were impaired in Glut1-deficient B cells compared to wildtype cells (**Fig. 5.2B,C**). These data indicate that Glut1 in activated B cells promotes optimal respiratory function of mitochondria. Taken together, Glut1 in B cells promotes optimal mitochondrial activity and glycolytic function as determined by Seahorse Agilent Technologies.

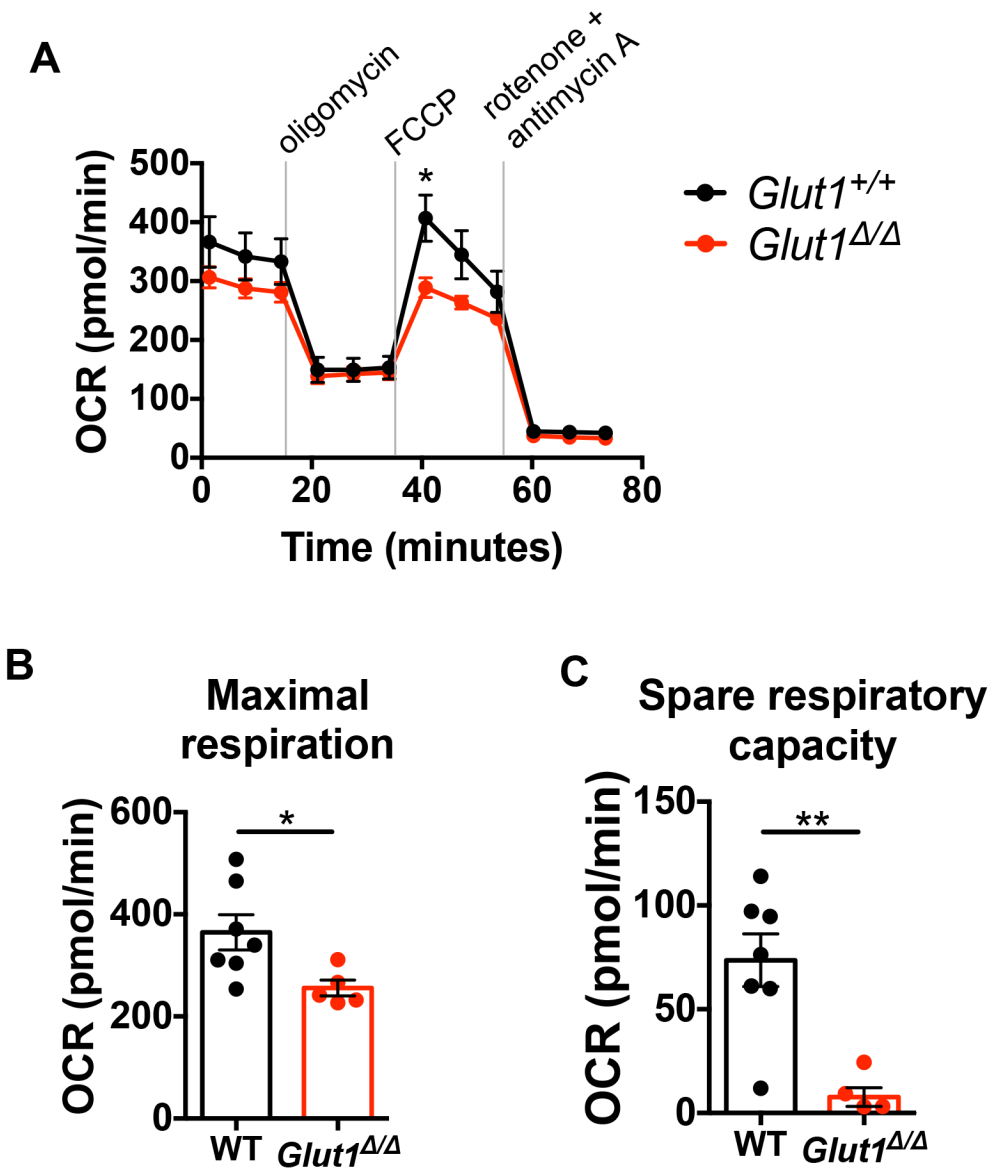

Figure 5.2 *Glut1* is supportive of mitochondrial function in activated B cells. (A) Oxygen consumption rate (OCR) during Agilent Seahorse Mitochondrial Stress test after *Glut1*$^{+/+}$ or *Glut1*$^{\Delta/\Delta}$ were activated with LPS, BAFF, IL-4, and IL-5 for 2 days. (B) Maximal and (C) Spare respiratory capacity calculated by Agilent Seahorse XF Mito Stress Test Report Generator. Data are representative of two independent experiments with n = 7 *Glut1*$^{+/+}$ mice and n = 5 *Glut1*$^{\Delta/\Delta}$ mice. * $p < 0.05$, ** $p < 0.01$, *** $p < 0.001$ (two-way ANOVA with Sidak's multiple comparisons (A), Student's t-test (B,C)).

IV. Glut1-deficiency alters B cell fate decisions favoring MBC over ASC generation

I next sought to determine the effect of Glut1 on primary humoral responses. Loss of Glut1 in B cells driven by CD19-Cre led to decreased antibody responses to NP-chicken gamma globulin (Caro-Maldonado et al., 2014). In this CD19-Cre model, Glut1 is deleted at the pre-B cell stage of B cell development (Rickert et al., 1997) when glucose and glycolysis was reported to be critical (Kojima et al., 2009; Urbanczyk et al., 2018). Consistent with the importance of Glut1 on B cell development, *Glut1*$^{f/f}$ CD19-Cre mice had three-fold less splenic B cells than wildtype mice before immunization (Caro-Maldonado et al., 2014). To test the role of Glut1 specifically on primary B cell responses without the confounding factor of Glut1-loss in immature B cells, I used the huCD20-CreER^{T2} tamoxifen-inducible model to delete floxed alleles of Glut1 from mature B cells immediately before intraperitoneal immunization and boost with NP-ovalbumin (**Fig. 5.3A**).

Germinal center B cells increase glucose uptake as determined by 2-NBDG fluorescence (Recall Fig 3.1B) (Jellusova et al., 2017; Haniuda et al., 2020). Surprisingly, however I found that the frequency and absolute numbers of total and antigen-specific germinal centers were unimpaired in the spleens of *Glut1*$^{\Delta/\Delta}$ mice a week after the booster immunization (**Fig. 5.3B**). Despite no change in GCB, the frequency and number of total and NP-specific phenotypical memory B cells (M_{phen}BC: B220^{+} GL7^{-} IgD^{-} CD38^{+} NP^{+}) was enhanced ~two-fold in *Glut1*$^{\Delta/\Delta}$ mice compared to wildtype (**Fig. 5.3C**). In contrast, *Glut1*$^{\Delta/\Delta}$ mice had defects in the frequency of splenic NP-specific IgG1 ASCs, especially those that bind antigen with high affinity (**Fig. 5.3D**). NP-specific IgM secreting cells in response to NP-ova immunization was unaltered in the absence

of Glut1. Data indicate that Glut1 expression plays a role in regulating B cell fate decisions where its loss tilts the balance toward memory generation. I speculate that decreased glucose uptake in activated B cells of *Glut1*$^{\Delta/\Delta}$ mice leads to $M_{phen}BC$ differentiation and disfavor towards an IgG1-secreting plasma cell fate.

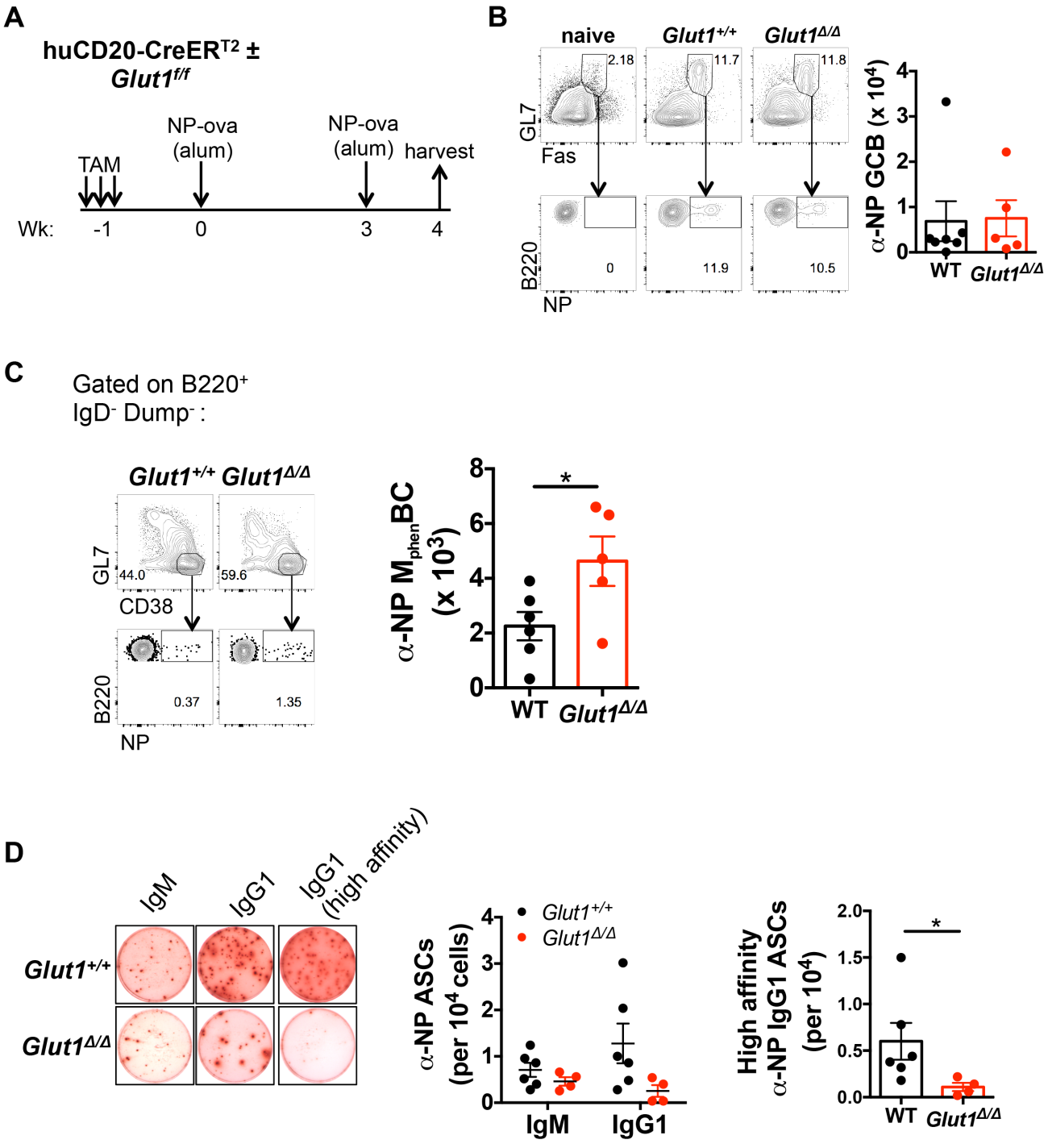

Figure 5.3 *Glut1*-deficient B cells favor the M_{phen}BC over the ASC fate. (A) Schematic depicting immunization strategy with a hapten-carrier to test primary humoral responses in the absence of B cell intrinsic Glut1. Mice were immunized with NP-ova after tamoxifen-induced deletion of *Glut1* from mature B cells. Mice were harvested at week 4 folllowing a booster immunization at week 3. (B) Representative flow plots and quantification depicting frequency and total number of NP-specific GCB from the B220$^+$

IgD$^-$ Dump$^-$ gate (Dump: CD11b, CD11c, F4/80, Gr1, 7-AAD) in naïve, wildtype and *Glut1* $^{\Delta/\Delta}$ mice; (GCB: Fas$^+$ GL7$^+$). (C) Left panel, representative flow plots depicting frequency of M_{phen}BC and NP$^+$ M_{phen}BC (M_{phen}BC: B220$^+$ CD38$^+$) from the B220$^+$ IgD$^-$ Dump$^-$ gate. Right panel, quantification of total number of splenic NP$^+$ M_{phen}BC. (D) Left panel, representative ELISpot wells depicting density of NP-specific IgM, IgG1 ASCs of all and high affinity in the spleen; 5 x 10^5 total splenocytes plated per well. Numbers of all affinity NP-specific IgM and IgG1 secreting cells (middle panel) or high affinity NP-specific IgG1 secreting cells (right panel) per 10^4 total splenocytes in *Glut1*$^{+/+}$ and *Glut1* $^{\Delta/\Delta}$ mice at the time of harvest. Data are representative of n = 7 wildtype and n = 5 Glut1 $^{\Delta/\Delta}$ mice in two independent experiments. * $p < 0.05$ (Student's t-test (C) and Mann-Whitney U test (D)).

V. Glucose metabolism is critical for affinity maturation

Loss of Glut1 in B cells immediately prior to immunization had modest to no defect in circulating IgM and IgG1 that bind to NP after the immunization strategy depicted in Fig. 5.3A (**Fig. 5.4A, B**). One critical function of germinal centers is to generate antibody diversity and select high-affinity (B cell receptors) BCR and antibodies after iterative rounds of mutations and selection (Bozic et al., 2007). The affinity of polyclonal serum antibodies to NP can be determined by ELISA using NP_{27}-BSA and NP_2-PSA where only high affinity antibodies remain bound to low ratios of NP conjugated to protein. Glut1 in B cells was particularly critical for the generation of circulating high affinity NP-specific IgG1 antibody (**Fig. 5.4C**). The 2-fold decrease in the ratio of NP_2/NP_{27} binding IgG1 indicates that Glut1 is essential for affinity maturation, i.e. antibody quality (**Fig. 5.4D**). Take together, Glut1 promotes optimal glycolytic and mitochondrial fitness in activated B cells, balances activated B cell fate decision between M_{phen}BC and ASC fates in primary responses, and is particularly essential for the production of high affinity antibodies. I next sought to elucidate the role of glutamine metabolism in humoral immunity.

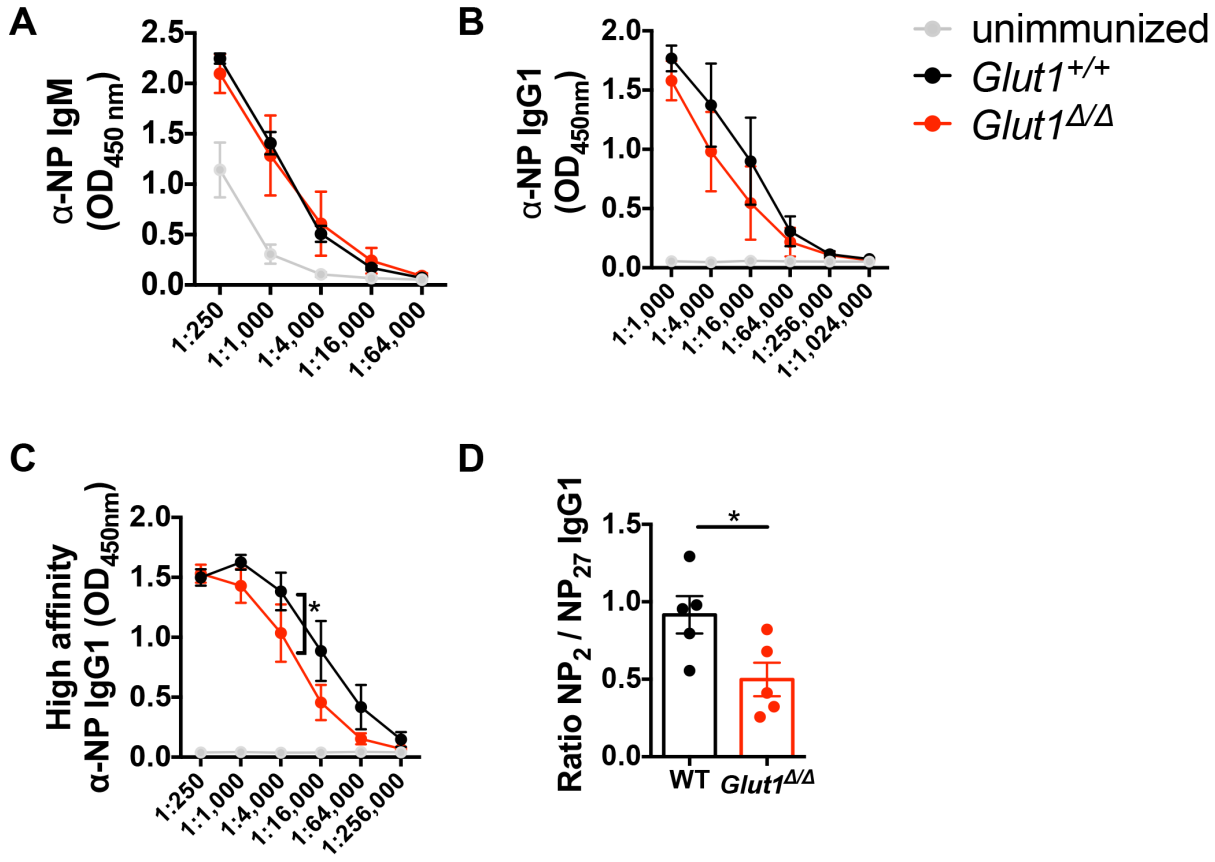

Figure 5.4 *Glut1* in B cells supports affinity maturation. All affinity NP-specific (A) IgM, (B) IgG1, and (C) high affinity NP-specific IgG1 in the sera of *Glut1*$^{+/+}$ and *Glut1*$^{\Delta/\Delta}$ mice at the terminal time point in accordance to the immunization strategy depicted in Fig. 5.4A (D) Affinity maturation calculated by the ratio of ELISA OD values of NP_2 binding IgG1 antibodies (high affinity) to NP_{27} binding IgG1 antibodies at the linear range; ratio calculated at the 1:16,000 dilution. Data are representative of n = 7 wildtype and n = 5 *Glut1*$^{\Delta/\Delta}$ mice in two independent experiments. * $p < 0.05$, **** $p < 0.0001$ (two-way ANOVA (C), Student's t-test (D).

VI. Glutaminolysis in B cells is critical for mitochondrial function and IgG1 humoral responses

Glutamine has been proposed to have an anaplerotic role in activated B cells wherein glutamine is taken up by ASCT2 transporter, converted to glutamate, which is then converted to alpha-ketoglutarate fueling the TCA cycle (Masle-Farquhar et al., 2017; Le et al., 2012; Brand et al., 1989; Waters et al., 2018). Glutamine tracer experiments reveal that glutamine is also incorporated into pyruvate, lactate, alanine, aspartate, and ammonia in proliferating lymphocytes and plasma cells and thus used as a carbon and nitrogen precursor for multiple biosynthetic processes (Brand et al., 1989; Garcia-Manteiga et al., 2011; Lam et al., 2018). However, the role glutamine metabolism in GC responses has not yet been clearly elucidated.

I sought out to investigate the role of glutamine metabolism in humoral immunity by genetically disrupting glutaminolysis, one of the main fates of glutamine, in B cells. Glutaminase 1 (GLS1), first discovered in the kidney in 1958, is a mitochondrial enzyme that catalyzes the deamidation of glutamine to generate glutamate and producing ammonia as a byproduct (Klingman, 1958). Gls1 in the T lymphocyte lineage had distinct roles on $CD4^+$ Th1, Th17 and cytotoxic $CD8^+$ T cells shedding light on the unique demands for glutaminolysis on different T subsets (Johnson et al., 2018). $Gls1^{f/f}$ mice, a generous gift from Jeff Rathmell, were crossed with huCD20-$CreER^{T2}$ mice to generate a tamoxifen-inducible model of Gls1 deletion from mature B cells. Expression of *GLS* mRNA and protein was reduced in *Gls1*$^{f/f}$ huCD20-Cre-ER^{T2} B cells compared to *Gls1*$^{+/+}$ huCD20-Cre-ER^{T2} controls after a 2-day treatment with LPS, BAFF, and 4-hydroxy-tamoxifen to induce deletion (**Fig. 5.5A,B**).

To determine glycolytic and mitochondrial function in Gls1-deficient activated B cells, I subjected 2-day LPS, BAFF, IL-4, IL-5 blasts to Seahorse analysis. *Gls1* was dispensable for lactate production as determined by ECAR (**Fig. 5.5C**). However, because glycolytic end-product pyruvate has multiple fates apart from lactate and glycolytic intermediates can be shunted to multiple pathways, the possibility of alterations in glycolytic flux in $Gls1^{\Delta/\Delta}$ B cells cannot be excluded (Gray et al., 2014). In contrast to no defects in ECAR, oxidative phosphorylation was impaired in $Gls1^{\Delta/\Delta}$ B cells (**Fig. 5.5D**). Specifically, the spare respiratory capacity in $Gls1^{\Delta/\Delta}$ B cells was impaired suggesting that glutaminolysis promotes optimal mitochondrial activity (**Fig. 5.5E**).

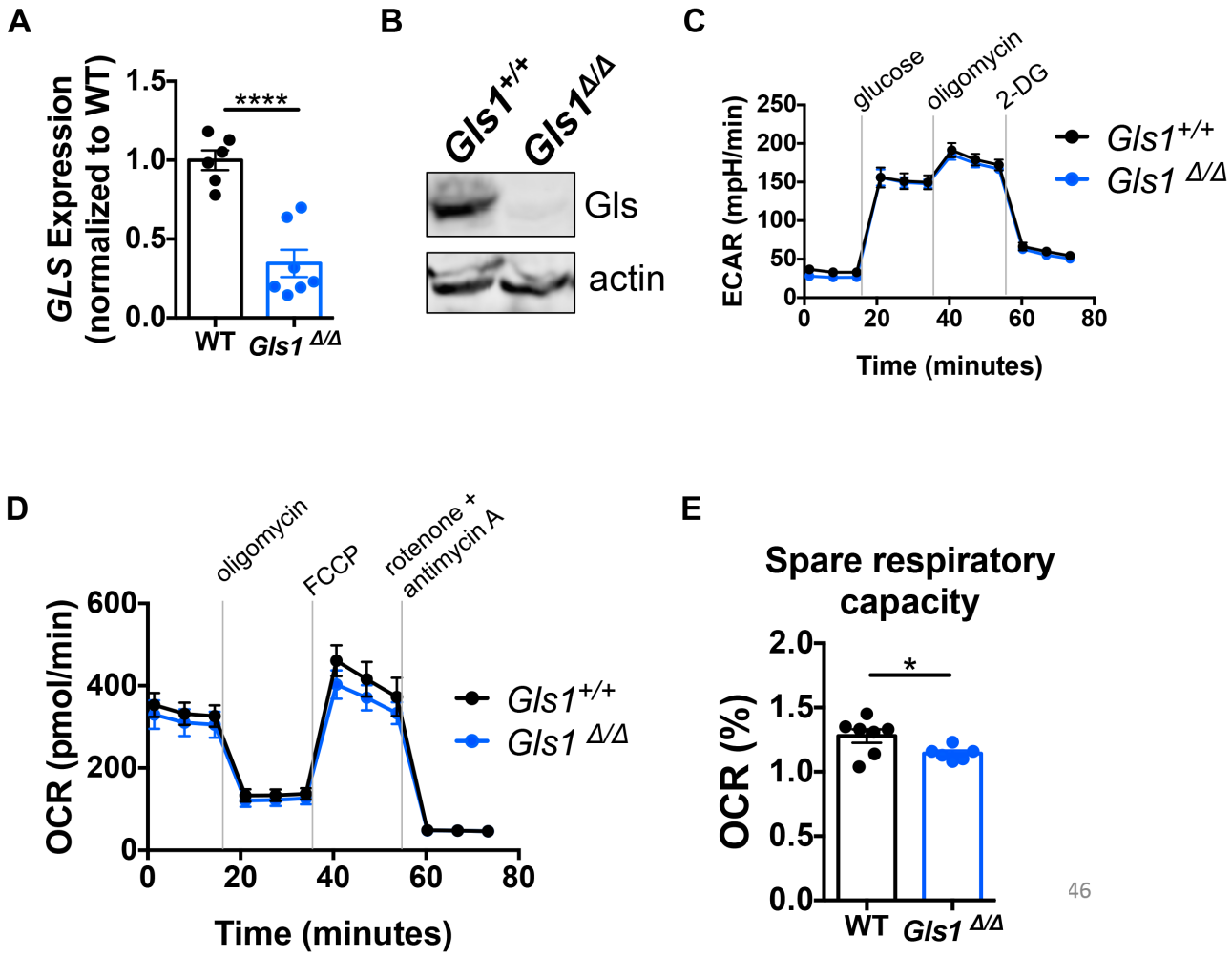

46

Figure 5.5 Glutaminase 1 is critical for maintaining the spare respiratory capacity of mitochondria in B cells. (A) Gls gene expression, encoding for glutaminase 1 in B cells, in 4-hydroxy-tamoxifen treated wildtype and *Gls1*$^{f/f}$ CD20-ER^{T2}Cre 2-day LPS-activated B cells determined by Real Time PCR. Each dot represents a mouse where black circles (●) represent *Gls1*$^{+/+}$ and blue circles (●) represent *Gls1*$^{\Delta/\Delta}$ (B) Representative immunoblot probing for Gls protein in wildtype and *Gls1* $^{\Delta/\Delta}$ B cells after 2-day LPS/BAFF activation. Data is representative of at least 3 independent experiments. (C) Glycolytic and (D) Mitochondrial stress tests after *Gls1*$^{+/+}$ or *Gls1*$^{\Delta/\Delta}$ B cells were activated with LPS, BAFF, IL-4, and IL-5 for 2 days. (E) Spare respiratory capacity of B cells calculated by Agilent Seahorse XF Mito Stress Test Report Generator. * $p < 0.05$, **** $p < 0.0001$ (Student's t-test (A,E).

I investigated the effect of B cell-intrinsic glutaminolysis on primary humoral responses in a lung inflammation model. Wildtype and *Gls1*$^{\Delta/\Delta}$ mice were immunized and boosted a week later with ovalbumin (ova) in alum adjuvant followed by intranasal rechallenge with 7 daily ova inhalations immediately prior to harvest (**Fig. 5.6A**). Similar to Glut1, Gls1 was dispensable for the formation of total GCB in the mediastinal lymph node (**Fig. 5.6B**). However, loss of Gls1 led to a two-fold decrease in the frequency of IgG1^{+} GCB. Additionally, ova-specific IgG1 ASC were reduced in both the lung and bone marrow of *Gls1*$^{\Delta/\Delta}$ mice as determined by ELISpot analysis (**Fig. 5.6C**). The defect in the frequency of ova-specific IgG1 ASC coincided with a decrease in circulating anti-ova IgG1 at the terminal time point (**Fig. 5.6D**). Data indicate that Gls1 is critical for generating effective primary IgG1 responses to ova-antigen in a lung inflammation model.

Uptake of glutamine and other amino acids has been linked to enhanced glutaminolysis and increased mTORC1 signaling and assembly in human cell lines (Nicklin et al., 2009; Durán et al., 2012). High amino acid concentrations and mTORC1 activation have also been shown to be critical for antibody production *in vitro* and primary B cell responses *in vivo* (Raybuck et al., 2019; Raybuck et al., 2018). Here, linking previous studies, genetic reduction in glutaminolysis in B cells led to defects in mTORC1 signaling in the splenic CD138^{+}TACI^{+} ASC population indicated by decreased phospho-S6 MFI determined by flow cytometry (**Fig. 5.6E**). Taken together, glutaminolysis in B cells, critical for optimal mitochondrial spare respiratory capacity, promotes mTORC1 signaling and effective IgG1 primary responses in a lung inflammation model.

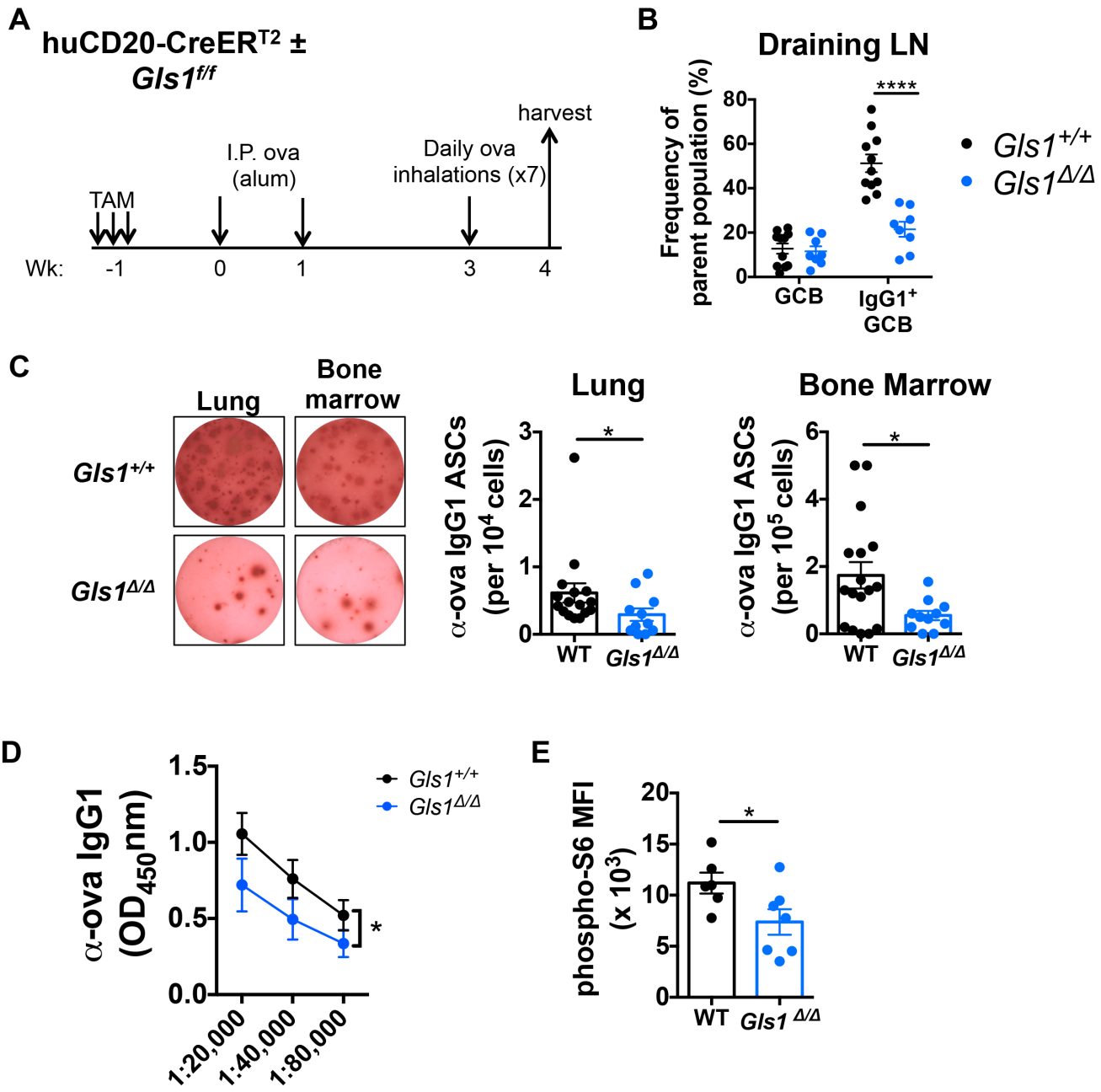

Figure 5.6 *Gls1* is essential for IgG1 antibody responses and mTORC1 signaling *in vivo*. (A) Schematic of immunization strategy to test the role of B cell intrinsic Gls1 in primary humoral responses using *Gls1$^{f/f}$* CD20-ER^{T2}Cre and wildtype mice. Mice were injected with tamoxifen to induce B cell specific deletion of Gls1 followed by two sequential intraperitoneal injections of ovalbumin with alum adjuvant as indicated. Two weeks after the last injection, mice were rechallenged intranasally with ovalbumin daily for seven days immediately prior to harvest. (B) Frequency of GCB and IgG1^{+} GCB cells from the dump (F4/80, CD11c, CD11b, Gr1, IgD) negative gate and the GCB (Fas^{+} GL7^{+}) gate respectively in mediastinal lymph node at the time of harvest. (C) Left panel, density of ova-specific IgG1 ASCs in the lung and bone marrow of wildtype and *Gls1$^{Δ/Δ}$* mice at the time of harvest; 10^{6} lung cells plated per well and 2 x 10^{6} bone marrow cells

plated per well. Middle and right panels, numbers of lung anti-ova IgG1 secreting ASCs and bone marrow cells per 10^4 or 10^5 total cells respectively. (D) Circulating ova-specific IgG1 in the sera of *Gls1*$^{+/+}$ and *Gls1*$^{\Delta/\Delta}$ mice at the time of harvest. Data are representative of five independent experiments with at least n = 12 wildtype mice and n = 12 *Gls1*$^{\Delta/\Delta}$ mice. (E) Phospho-S6 MFI of splenic CD138$^+$ TACI$^+$ of n = 6 *Gls1*$^{+/+}$ and n = 7 *Gls1*$^{\Delta/\Delta}$ mice from two independent experiments. * $p < 0.05$, **** $p < 0.0001$ (Student's t-test (B, C, E), two-way ANOVA (D)).

Glutamine and glucose metabolism intersect and there are multiple examples in the literature where lack of one of these substrates leads to altered reliance on the other in multiple cell types (Stumvoll et al., 1999; Polet et al., 2016; Brand et al., 1989; Blagih et al., 2015; Gebregiworgis et al., 2017; Mazat et al., 2019; Le et al., 2012; Kaadige et al., 2009). To test if loss of glutaminolysis in B cells led to alterations in glucose uptake, I performed glucose uptake assays on 2-day LPS and BAFF activated B cells using radiolabeled 2-DG (**Fig. 5.7A**). Activated *Gls1*$^{\Delta/\Delta}$ B cells exhibited increased glucose uptake compared to wildtype B cells suggesting that disruption in glutamine metabolism leads to a potential compensatory mechanism involving enhanced glucose uptake.

Many groups have reported that glutamine and pyruvate are two of a few substrates that may fuel the TCA cycle in anaplerotic reactions supporting mitochondrial function in immune cells (Le et al., 2012; Brand et al., 1989; Waters et al., 2019; Lam et al., 2018); substrates promoting anaplerosis are reviewed (Brunengraber et al., 2006). Interestingly, consistent with glutaminolysis supporting mitochondrial function, activated *Gls1*$^{\Delta/\Delta}$ B cells had defects in basal OCR when glutamine alone was present in the base media compared to wildtype cells (**Fig. 5.7B**). The addition of glucose and pyruvate to the base media increased the basal OCR in both wildtype and *Gls1*$^{\Delta/\Delta}$ B cells indicating that multiple fuels contribute to oxidative phosphorylation. Furthermore, glucose and pyruvate in the base media rescued the defect in the basal OCR of *Gls1*$^{\Delta/\Delta}$ B cells

compared to glutamine only availability. Taken together, these data suggest that nutrient availability in the microenvironment has consequences on the metabolic activity of B cells. Additionally, though Gls1 enables B cells to have optimal mitochondrial function in nutrient-limited conditions, Gls1-deficiency leads to compensatory mechanisms including increases in glucose uptake.

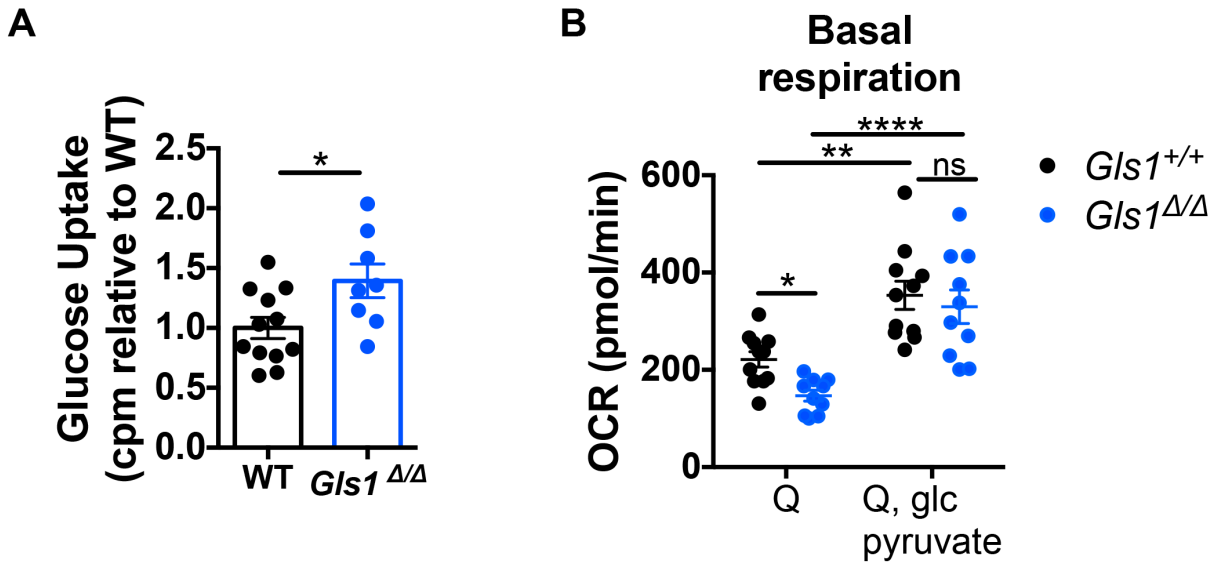

Figure 5.7 Loss of *Gls1* leads to enhanced glucose uptake. (A) 2-[1,2-^{3}H]-deoxy-glucose uptake in 2-day *Gls1*$^{+/+}$ and *Gls1*$^{\Delta/\Delta}$ LPS blasts after depleting intracellular stores by starvation. Each dot represents a replicate from two independent experiments from n = 6 *Gls1*$^{+/+}$ mice and n = 4 *Gls1*$^{\Delta/\Delta}$ mice. (B) Basal OCR of *Gls1*$^{+/+}$ or *Gls1*$^{\Delta/\Delta}$ in base media supplemented with either glutamine (Q) alone or Q, glucose, and sodium pyruvate. Data are representative of three independent experiments with at least n = 7 wildtype mice and n = 5 *Gls1*$^{\Delta/\Delta}$ mice. * $p < 0.05$, ** $p < 0.01$ (two-way ANOVA with Tukey's multiple comparisons (B)).

VII. Glucose and glutamine metabolism synergistically impair class-switching, ASC, and antibody production

I next investigated the interaction between glucose and glutamine metabolism in primary B cell responses by crossing *Gls1*$^{f/f}$ mice and *Glut1*$^{f/f}$ mice to generate *Gls1*$^{f/f}$ *Glut1*$^{f/f}$ huCD20-CreER^{T2} mice, which have a combined deficiency in glutaminolysis and glucose transport by Glut1. To test primary B cell responses with multiple metabolic defects I immunized and boosted wildtype, *Gls1*$^{\Delta/\Delta}$, *Glut1*$^{\Delta/\Delta}$, and *Gls1*$^{\Delta/\Delta}$ *Glut1*$^{\Delta/\Delta}$ mice with NP-ova followed by seven daily ova-inhalations immediately prior to harvest (**Fig. 5.8A**). In this immunization scheme, mice should generate humoral responses to NP and ova, with ova-specific GC responses localized mostly to the lung. Consistent with prior observations in Fig. 5.3B and 5.6B, loss of Gls1, Glut1, or both was dispensable for the generation of GCB in the mediastinal lymph node in this model (**Fig. 5.8B**). However, doubly-deficient *Gls1*$^{\Delta/\Delta}$ *Glut1*$^{\Delta/\Delta}$ mice had little to no ova-specific IgG1 secreting cells in the lung or the bone marrow as determined by ELISpot analysis (**Fig. 5.8C**). The frequency of NP-binding IgG1 secreting cells in the spleen and bone marrow of doubly-deficient *Gls1*$^{\Delta/\Delta}$*Glut1*$^{\Delta/\Delta}$ mice were completely demolished compared to those in mice deficient in Gls1 or Glut1 alone, which exhibited moderately reduced antigen-specific IgG1 secreting cells compared to wildtype mice (**Fig 5.8C,D**). All together, data suggest that glutaminolysis and glucose import in B cells synergistically support the generation of ASCs in humoral immunity.

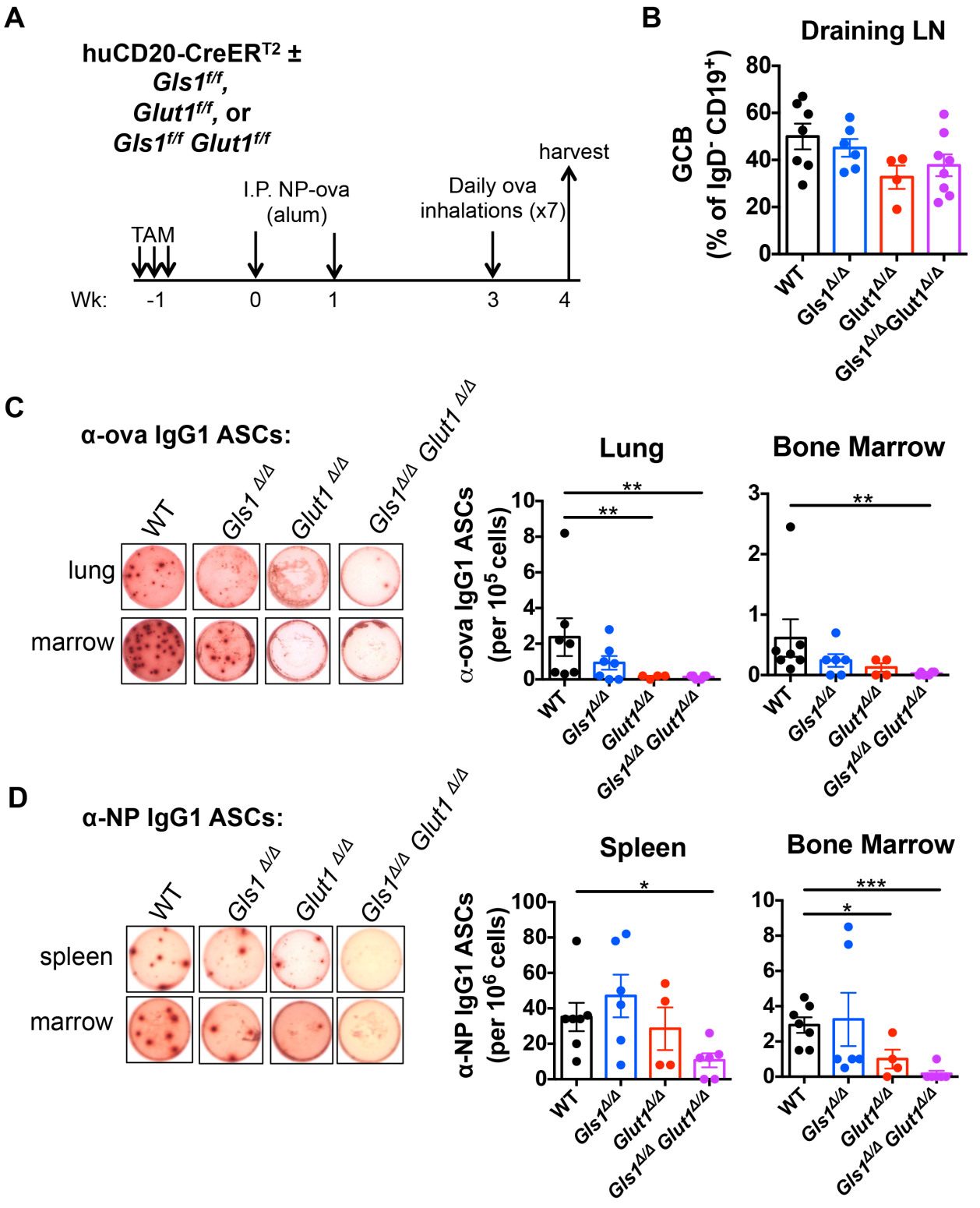

Figure 5.8 Simultaneous loss of both *Glut1* and *Gls1* obliterate the generation of antigen-specific IgG1-secreting plasma cells. (A) Schematic of immunization strategy to test B cell loss of either *Gls1*, *Glut1*, or both in primary humoral responses.

Mice were injected with tamoxifen to induce deletion followed by two sequential intraperitoneal injections of NP-ova with alum adjuvant one week apart. Two weeks following the second injection, mice received daily ova inhalations for seven days immediately prior to harvest. (B) Frequency of GCB in mediastinal lymph node in wildtype, Gls1$^{\Delta/\Delta}$, *Glut1*$^{\Delta/\Delta}$, and *Gls1*$^{\Delta/\Delta}$*Glut1*$^{\Delta/\Delta}$ mice at time of harvest determined by flow cytometry. (C) Left panel, representative ELISpot wells of ova-specific IgG1-secreting cells in the lung and bone marrow of wildtype (●), Gls1$^{\Delta/\Delta}$ (●), *Glut1*$^{\Delta/\Delta}$ (●), and *Gls1*$^{\Delta/\Delta}$*Glut1*$^{\Delta/\Delta}$ (●) mice; 10^6 total lung cells and 2 x 10^6 total bone marrow cells plated per well. Right panel, numbers of ova-specific IgG1 antibody secreting cells in the lung or bone marrow per 10^5 total cells. (D) Left panel, representative ELISpot wells of NP-specific IgG1-secreting cells in the spleen and bone marrow of wildtype, *Gls1*$^{\Delta/\Delta}$, *Glut1*$^{\Delta/\Delta}$, and *Gls1*$^{\Delta/\Delta}$*Glut1*$^{\Delta/\Delta}$ mice; 5 x 10^5 total splenic cells and 2 x 10^6 total bone marrow cells plated per well. Right panel, numbers of NP-specific IgG1 antibody secreting cells in the spleen or bone marrow per 10^6 total cells. Data are representative of two experiments with n = 7 wildtype, n = 6 *Gls1*$^{\Delta/\Delta}$, n = 4 *Glut1*$^{\Delta/\Delta}$, and n = 6 *Gls1*$^{\Delta/\Delta}$*Glut1*$^{\Delta/\Delta}$ mice. * $p < 0.05$, ** $p < 0.01$, *** $p < 0.001$ (Mann-Whitney U test (C,D)).

Consistent with the decrease in the formation of IgG1 secreting cells, combined loss of Gls1 and Glut1 led to ~10 fold reduction in circulating ova-specific IgG1 compared to wildtype mice; mice with genetic loss of either Glut1 or Gls1 alone had intermediate anti-ova IgG1 levels circulating in the sera (**Fig. 5.9A**). NP-specific IgM responses were modestly impaired in *Gls1*$^{\Delta/\Delta}$ *Glut1*$^{\Delta/\Delta}$ mice but this observation did not reach statistical significance (**Fig. 5.9B**). In parallel to anti-ova IgG1 responses, anti-NP IgG1 responses were also reduced ~10 fold in *Gls1*$^{\Delta/\Delta}$ *Glut1*$^{\Delta/\Delta}$ mice compared to wildtype mice (**Fig. 5.9C**). Interestingly, anti-NP responses in *Gls1*$^{\Delta/\Delta}$ mice were normal in contrast to the defect in anti-ova responses compared to wildtype (Fig. 5.8 and 5.9). This observation potentially sheds light on a differential reliance of activated B cells on glutaminolysis depending on the nature of the antigen.

Immunization with NP-ova enables screening for high affinity antibodies. Doubly-deficient *Gls1*$^{\Delta/\Delta}$ *Glut1*$^{\Delta/\Delta}$ mice had ~15 fold reduction in high affinity IgG1 antibody compared to wildtype mice (**Fig. 5.9D**). The ratio of OD values from NP_2 and NP_{27}

ELISAS indicate that affinity maturation with the combined loss of Gls1 and Glut1 was equally inhibited as loss of Glut1 alone (**Fig. 5.9E**). Taken together, these data indicate that loss of Gls1 and Glut1 in B cells synergistically impair the production of IgG1 ASC and IgG1 antibody. Furthermore, analogous to results in Fig. 5.4, it is evident that Glut1 is specifically imperative for the generation high affinity antibodies.

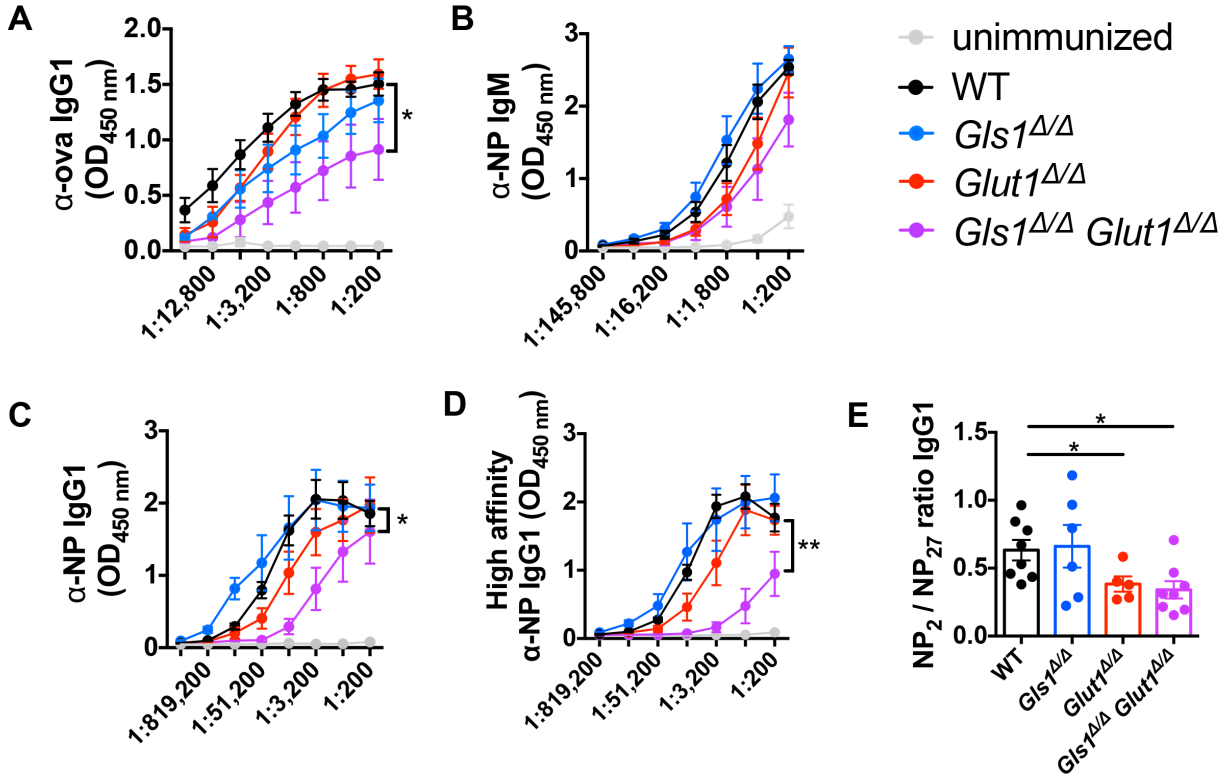

Figure 5.9 Loss of both *Glut1* and *Gls1* synergistically impair IgG1 antibody responses. (A) Ova-specific IgG1 in the sera of wildtype, Gls1$^{\Delta/\Delta}$, *Glut1*$^{\Delta/\Delta}$, and *Gls1*$^{\Delta/\Delta}$*Glut1*$^{\Delta/\Delta}$ mice at the terminal time point after immunization strategy illustrated in Fig 5.10A. (B) NP-specific (B) IgM, (C) IgG1 in the sera of mice at the terminal time point. (D) High affinity NP-specific IgG1 in the sera of mice prior at week 3 of immunization strategy illustrated in Fig. 5.10A. (E) Affinity maturation depicted by the ratio of ELISA OD values of NP_2 binding IgG1 antibodies (high affinity) to NP_{27} binding IgG1 antibodies in the linear range; ratio calculated at the 1:12,800 dilution at the week three time point of the immunization strategy depicted in Fig 5.10A. Data are representative of two independent experiment with n = 8 wildtype, n = 6 *Gls1*$^{\Delta/\Delta}$, n = 5 *Glut1*$^{\Delta/\Delta}$, and n = 8 *Gls1*$^{\Delta/\Delta}$*Glut1*$^{\Delta/\Delta}$ mice. * $p < 0.05$, ** $p < 0.01$, *** $p < 0.001$, (two-way ANOVA with Dunnet's multiple comparisons (A, C, D), Student's t-test (E)).

To confirm defects in class-switching and plasma cell differentiation in the absence of Glut1, Gls1, or both Gls1 and Glut1, I cultured naïve B cells for four days with LPS, IL-4, IL-5, BAFF, and 4-hydroxy-tamoxifen to induce deletion. The frequency of $IgG1^+$ cells in $Gls1^{\Delta/\Delta}$ and $Gls1^{\Delta/\Delta}$ $Glut1^{\Delta/\Delta}$ cultures was 75% and 50% of the $IgG1^+$ population in wildtype cultures, respectively (**Fig. 5.10A**). Loss of Glut1 moderately impacted the frequency of class-switched $IgG1^+$ cells. These data indicate that Gls1 is critical for the generation of $IgG1^+$ cells and additional loss of Glut1 exacerbates this phenotype. The frequency of plasma cells ($B220^{lo}$ $CD138^+$) in both $Gls1^{\Delta/\Delta}$ and $Glut1^{\Delta/\Delta}$ cultures was ~75% of wildtype cultures suggesting both pathways support plasma cell differentiation (**Fig. 5.10B**). However, simultaneous loss of both Gls1 and Glut1 in $Gls1^{\Delta/\Delta}$ $Glut1^{\Delta/\Delta}$ cultures led to only 25% of the plasma cells generated in wildtype cultures. These data are congruent with *in vivo* observations and suggest that glutaminolysis and glucose uptake support the generation of class-switched cells and plasma cell differentiation.

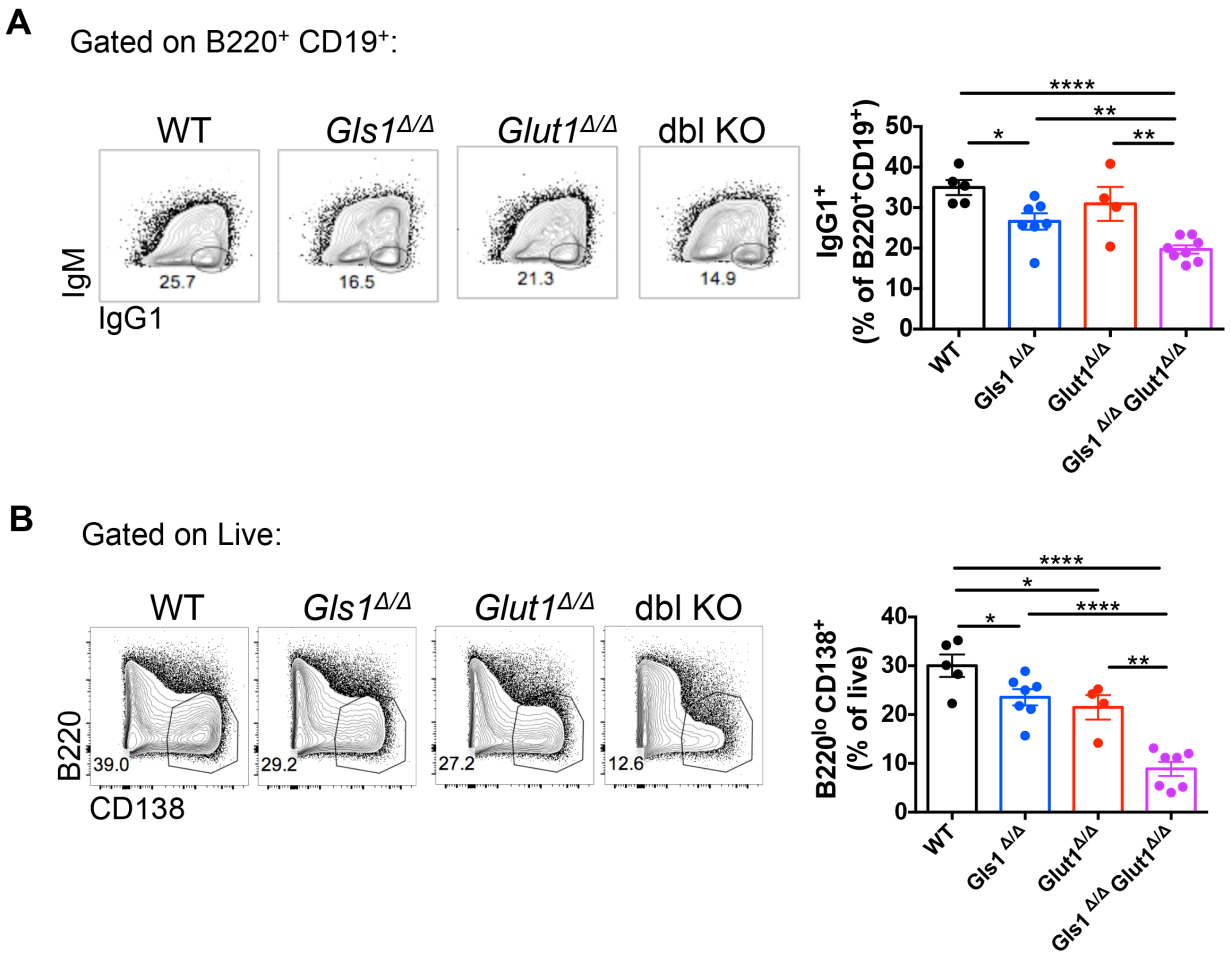

Figure 5.10 *Glut1* and *Gls1* are critical for generating IgG1$^+$ cells and plasma cells *in vitro*. (A) Representative flow plots and frequency of IgG1$^+$ cells from the B cell gate (B220$^+$ CD19$^+$) after 4 days of activation of B cells from wildtype, Gls1$^{\Delta/\Delta}$, *Glut1*$^{\Delta/\Delta}$, and *Gls1*$^{\Delta/\Delta}$*Glut1*$^{\Delta/\Delta}$ mice with LPS, IL-4, IL-5, and BAFF. (B) Representative flow plots and frequency of B220^{lo} CD138$^+$ cells from the viable gate after 4 days of activation of B cells from wildtype, Gls1$^{\Delta/\Delta}$, *Glut1*$^{\Delta/\Delta}$, and *Gls1*$^{\Delta/\Delta}$*Glut1*$^{\Delta/\Delta}$ mice with LPS, IL-4, IL-5, and BAFF. Data are representative of three experiments with n = 5 wildtype, n = 7 Gls1$^{\Delta/\Delta}$, n = 4 *Glut1*$^{\Delta/\Delta}$, and n = 8 *Gls1*$^{\Delta/\Delta}$*Glut1*$^{\Delta/\Delta}$ mice. * $p < 0.05$, ** $p < 0.01$, **** $p < 0.0001$ (Student's t-test).

Class-switching and plasma cell differentiation is a division-linked process. B cells must proliferate before class-switching and differentiation can occer. To test the ability of *Gls1*$^{\Delta/\Delta}$ *Glut1*$^{\Delta/\Delta}$ to proliferate, I labeled wildtype and *Gls1*$^{\Delta/\Delta}$ *Glut1*$^{\Delta/\Delta}$ B cells with Cell Trace Violet before activating them with anti-CD40, IL-4, IL5, and BAFF to induce activation and proliferation. *Gls1*$^{\Delta/\Delta}$ *Glut1*$^{\Delta/\Delta}$ B cells exhibited impaired proliferation compared to wildtype by day 4 of culture (**Fig. 5.11A**). Specifically, the majority of *Gls1*$^{\Delta/\Delta}$ *Glut1*$^{\Delta/\Delta}$ B cells had divided once or twice compared to 4+ divisions in wildtype cells. To test if the defect in class-switching observed in *Gls1*$^{\Delta/\Delta}$ *Glut1*$^{\Delta/\Delta}$ B cells was due to poor proliferation, the frequency of IgG1^{+} cells in each division were compared (**Fig. 5.11B**). Most class-switching to IgG1^{+} cells is observed starting at division 5 in wildtype cultures however *Gls1*$^{\Delta/\Delta}$ *Glut1*$^{\Delta/\Delta}$ cultures had ~50% less IgG1^{+} cells compared to wildtype in divisions 5, 6, and 7. Similarly, plasma cells, which start to emerge around division 5 or 6 in wildtype cultures, were obliterated in *Gls1*$^{\Delta/\Delta}$ *Glut1*$^{\Delta/\Delta}$ cultures (**Fig. 5.11C**). Taken together, glutaminolysis and glucose uptake in B cells promotes proliferation and these processes support class-switching and plasma cell generation independent of division.

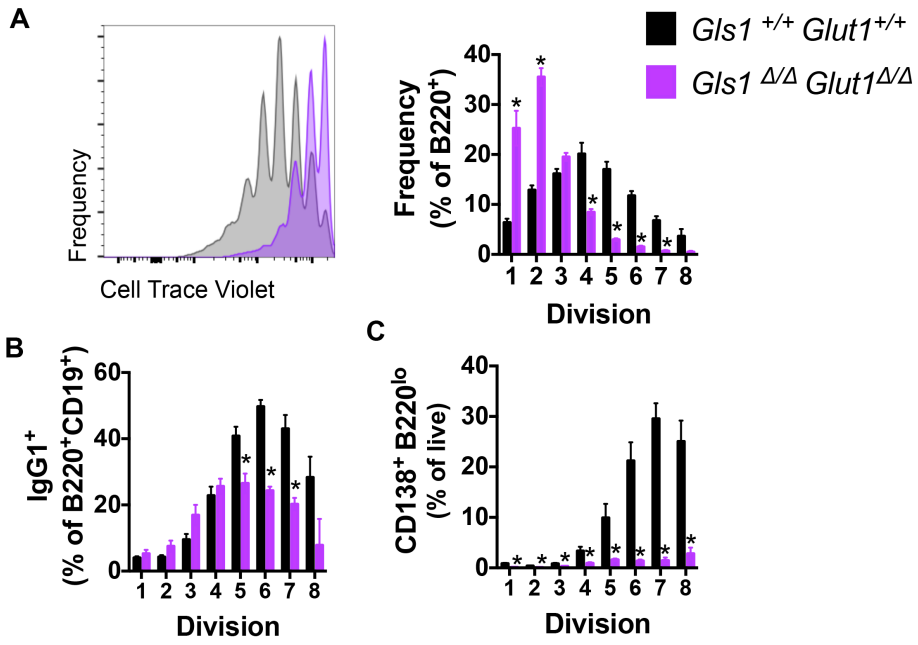

Figure 5.11 *Glut1/Gls1* doubly deficient B cells have impaired proliferation, class switching to IgG1$^+$, and plasma cell differentiation. (A) Proliferation of wildtype and *Gls1*$^{\Delta/\Delta}$*Glut1*$^{\Delta/\Delta}$ B cells after 4-day activation with anti-CD40, IL-4, IL-5, and BAFF indicated by cell trace violet partitioning and measured by flow cytometry; cells were labeled on day 0 with cell trace violet which decreases 2-fold in brightness with each cell division. Right panel, the frequency of cells in each division from the B cell gate of wildtype and *Gls1*$^{\Delta/\Delta}$*Glut1*$^{\Delta/\Delta}$ B cells. Frequency of (B) IgG1$^+$ cells or (C) CD138$^+$ B220^{lo} in each cellular division. Data is representative of n = 4 wildtype and n = 3 *Gls1*$^{\Delta/\Delta}$*Glut1*$^{\Delta/\Delta}$ mice. * $p < 0.001$ (Multiple t-tests A-C)).

VIII. Discussion

Glucose and glutamine are critical carbon and nitrogen sources for activated and proliferating lymphocytes. Here, I present that genetic perturbations in glucose transport and glutaminolysis in B cells impair primary humoral responses. Activated B cells with loss of Glut1, a plasma membrane carrier that mediates passive transport of glucose, led to decreased glucose uptake, ECAR, and OCR. Despite the importance of Glut1 during *in vitro* B cell activation, experiments using a prime and boost immunization strategy, found Glut1 to be dispensable for the frequency of generated GCB. However, Glut1 was critical for the production of high affinity IgG1 ASC and antibodies. Similarly, disrupting the conversion of glutamine to glutamate in activated B cells by genetically deleting glutaminase (Gls1) led to attenuated mitochondrial function, class-switching to IgG1, and anti-ovalbumin IgG1 primary responses despite increases in glucose uptake. Combined loss of both Glut1 and Gls1 led to synergistic defects in IgG1 production in a lung inflammation model indicating that glucose and glutamine metabolic pathways interact to promote optimal humoral primary immunity. A cartoon depiction of key findings in Chapter 5 is represented in **Figure 5.12**.

Glucose utilization in leukocytes was described in canines over a century ago (Levene et al., 1912). Lymphocytes take up glucose following a concentration gradient through a family of Glut transporters, which increase expression upon activation (Maratou et al., 2007; Doughty et al., 2006; Caro-Maldonado et al., 2014; Jayachandran et al., 2018; Dufort et al., 2014). Once taken up, glucose has multiple fates in the B lymphocyte lineage including the generation of nucleotides via the pentose phosphate pathway (PPP), lipid synthesis, fueling the TCA cycle, and the glycosylation of antibodies (Doughty et al., 2006; Waters et al., 2018; Lam et al., 2016, Dufort et al., 2014). Two groups use glucose isotopomer tracing to

demonstrate that a large fraction of glucose is used for nucleotide synthesis in the first 24-48h of anti-CD40/IL-4 or anti-IgM activation (Doughty et al., 2006; Waters et al., 2018). In support of a crucial role for glucose in nucleotide synthesis in transformed B cells, glucose transporter Glut1 was critical for the synthesis of multiple metabolites involved in the PPP and pyrimidine/purine metabolism in BCR-Abl+ B-cell acute lymphoblastic leukemia cells (B-ALL) (Liu et al., 2014). *De novo* nucleotide synthesis is crucial for the proliferation and cell cycle progression of activated T lymphocytes (Quéméneur et al., 2003) and I speculate it to have a similar role in activated B cells. In contrast to T cells, activated B cells undergo DNA alterations in immunoglobulin genes potentially resulting in an even greater demand for free nucleotides. Here, I observe a novel finding that Glut1 is essential for affinity maturation in response to hapten-carrier immunization. Affinity maturation results in a growing pool of B cells and ASCs that express BCR or secrete antibody with enhanced affinity for antigen and is derived from somatic hypermutation (SHM) and selection. SHM, occurring primarily in GCB but also observed in activated B cells outside the GC (William et al., 2002), is the critical mechanism underlying the diversification of immunoglobulin genes involving the introduction of point mutations in the variable region of the immunoglobulin gene followed by DNA repair (Teng et al., 2007). SHM-associated DNA repair in B cells may coincide with an increase flux in glucose through the PPP to support nucleotide synthesis, similar to observations in mouse embryonic fibroblasts (Franklin et al., 2016). Further experiments are needed to test if nucleotides are limiting in Glut1-deficient B cells leading to the observed defects in affinity maturation. Another possibility contributing to poor affinity maturation with Glut1-defiency is that glucose availability influences antibody glycosylation; the ratio of

glucose to N-acetylglucosamine concentrations in the tissue culture medium had severe consequences on antibody affinity in hybridoma cultures due to glycosylation alterations in the hyper-variable region (Tachibana et al., 1997). The mechanism underpinning glucose availability and the generation of antibody diversity with varying affinities, critical for robust humoral responses, needs to be elucidated.

In addition to the PPP for the generation of nucleotides, metabolite tracer analyses indicated that glucose flux through the glycolytic pathway was nearly 70-fold more compared to glucose oxidation through the TCA cycle in anti-IgM stimulated B cells (Doughty et al., 2006). Similarly, Waters and colleagues demonstrated that glucose contributes very few carbon atoms to TCA intermediates in anti-CD40/IL4 activated B cells and postulate that the TCA cycle is fueled mainly by alternative nutrients like lipids or glutamine (Waters et al., 2018). Additionally, long-lived plasma cells (LLPC) used mostly long-chain fatty acids to fuel basal respiration with only little TCA contribution from glucose (Lam et al., 2016). However, the Seahorse analyses presented here indicated that LPS/BAFF activated Glut1-deficient B cells have impaired mitochondrial function suggesting that decreased glucose in *Glut1*$^{\Delta/\Delta}$ is sufficient to affect even the small fraction of glucose that supplies the TCA cycle in the B lineage. In support of glucose contribution to mitochondrial function, anti-CD40/IL-4/anti-IgM activated B cells with knock-in of TAPP 1 and 2 adaptor proteins, had increased Glut1 expression, glucose uptake, and were associated with enhanced glycolytic and mitochondrial function (Jayachandran et al., 2018).

Despite increases in glucose uptake in GCB shown in Chapter 3 and published elsewhere (Jellusova et al., 2017; Haniuda et al., 2020), here, glucose transporter Glut1 was

dispensable for the generation of GCB. Consistent with these observations, a previous study revealed that pre-treatment of mice with glycolytic inhibitor 2-DG led to normal GCB numbers after immunization (Choi et al., 2018). Furthermore, B cells activated *in vitro* with anti-CD40 and IL-4 in glucose-deficient media had no defect in the expression of GCB surface markers Fas and GL7 (Waters et al., 2018). In face of the evidence, it would appear that glucose was dispensable for numbers of GC generated. However, 2-DG has multiple off-target effects and is not B cell specific in the Choi *et al*. study (Urbanczyk et al., 2018; Choi et al., 2018) and *in vitro* cultures used in Waters *et al*. do not capture the physiology of the GC. Other factors to consider are that B cells express other glucose transporters besides Glut1 (Maratou et al., 2007; Caro-Maldonado et al., 2014; Kojima et al., 2009) and the prime/boost immunization strategies used here may mask defects in GC formation since increased antigen exposure has been shown to enhance the potency of humoral responses in other settings (Cirelli et al., 2017). Furthermore, the elevated generation of MBC observed in *Glut1*$^{\Delta/\Delta}$ mice may contribute to reseeding the GC after booster immunizations, concealing any possible defects. However, it is possible that when faced with limitations on glucose-use, GCB are able to adapt and use an alternative fuel like amino acids or fatty acids in the microenvironment. Further studies will be needed to establish the extent of dependence on glucose in generating GC.

One novel finding in this Chapter is that loss of Glut1 led to alterations in the fate decisions of activated B cells. Glut1-deficiency led to an enhanced MBC population and a decrease in ASC generation during primary responses. Evidence of the molecular underpinnings contributing to the imbalance in MBC vs. ASC differentiation in *Glut1*$^{\Delta/\Delta}$ needs to be elucidated, however there are a few hypotheses. As previously mentioned,

Glut1 expression in B cells promoted anabolic pathways like pyrimidine/purine metabolism and hexosamine biosynthetic metabolism while Glut1-defiency led to increases in catabolic pathways like fatty acid oxidation (Liu et al., 2014). By limiting glucose uptake with Glut1$^{\Delta/\Delta}$, activated B cells may be preferentially fated to become MBC because MBC have lower anabolic demands compared to antibody synthesizing ASC. A second possibility is that altered fate decisions in the absence of B cell intrinsic Glut1 may be due to decreased BCR affinity observed in these mice. B cells with BCR that have moderate to high affinity for antigen are more likely to be fated for ASC whereas lower affinity interactions lead to increased production of the MBC population consistent with observations shown here in Glut1-deficient mice (Shinnakasu et al., 2016, Smith et al., 1997; O'Conner et al., 2006). A third possibility is that altered glucose uptake may indirectly influence the degree of mTORC1 activity (Leprivier et al., 2020); decreased mTORC1 signaling in GCB has been associated with increased likelihood to differentiate into MBC (Inoue et al., 2021). Consistent with this study in B cells, proliferating daughter CD8^{+} T cells with relatively higher mTORC1 activity was associated with increased glycolysis and favored differentiation to the effector rather than the memory T cell fate (Pollizzi et al., 2016). The extent to which mTORC1 signaling is affected in *Glut1*$^{\Delta/\Delta}$ B cells is yet to be determined.

I presented that loss of Glut1 immediately prior to immunization *in vivo* or activation *in vitro* had limited plasma cell differentiation and antibody responses overall. ASC have a high demand for glucose. In figure 1 of Chapter 3 I showed that splenic ASC had the highest demand for glucose compared to naïve, GCB, or MBC as determined by 2-NBDG uptake. Similarly, Haniuda and colleagues recently showed that

plasma cells exhibit relatively higher glucose uptake compared to naïve and GCB populations (Haniuda et al., 2020). In ASCs, especially LLPC, 90% of imported glucose is used for antibody glycosylation (Lam et al., 2016). Glycosylation is essential for proper folding and secretion of immunoglobulins (Hickman et al., 1977; Arnold et al., 2007). LLPC, which secrete more antibodies on a per cell basis than SLPC, had higher expression of Glut1 and had increased glucose uptake compared to their short-lived counterparts (Lam et al., 2016). Loss of Glut1 early during B cell development led to a decrease in B cells and downstream antibody responses after immunization (Caro-Maldonado et al., 2014). Here, Glut1 expression is deleted immediately prior to the experiment to specifically test its role in B cell activation and immunization without the confounding variable of the effect of Glut1 in developing B cells. In my work, I present novel evidence that Glut1 expression was specifically important for the generation of ASC and antibody responses, particularly those of high affinity. All together, I have provided evidence that highlights vital, previously unrecognized aspects of the antibody response. Specifically, I have demonstrated that expression of glucose transporter Glut1 influences the balance of MBC and ASC generated after immunization and is critical for affinity maturation.

The discovery of the importance of glutamine in immune cells was first made in the 1980's in the laboratory of Eric Newsholme (Ardawi et al., 1983; Newsholme et al., 1986). It has been reported that an activated B cell depletes glutamine from the media at a rate of more than 10 pM of glutamine per hour (Waters et al., 2018). Additionally, in a murine hybridoma cell line, the rate of glutamine utilization was more than half the rate of glucose indicating the importance of this alternative carbon source (Fitzpatrick et al., 1993). During B cell activation, glutamine is critical for biomass accumulation and anaplerotic

reactions (Waters et al., 2018; Heyse et al., 2015). Similarly, ^{13}C-glutamine tracing experiments in LLPC reveal that glutamine fuels the TCA cycle and contributes to glutamate and aspartate synthesis, potentially necessary for amino acid incorporation into antibodies (Lam et al., 2018). Here, I used a genetic model to disrupt glutaminase 1, which catalyzes the conversion of glutamine to glutamate in the mitochondria of B cells.

It is important to note that glutamine has multiple downstream fates independent of glutaminolysis (Fig 1.2) (DeBerardinis et al., 2010; Yoo et al., 2020). Similar to the role of glucose in *de novo* nucleotide synthesis via PPP, glutamine is also essential for purine and pyrimidine production as it provides a source of nitrogen (Cory et al., 2006). Glutamine along with glucose, acetyl-CoA, and uridine-5'-triphosphosphate, are used for the production of uridine diphosphosphate *N*-acetylglucosamine (UDP-GlcNAc) via the hexosamine pathway, critical for glycosylation and signaling (Marshall et al., 1991). Furthermore, glutamine is involved in the generation of asparagine and other non-essential amino acids in the cytosol (DeBerardinis et al., 2010; Yoo et al., 2020). These cytosolic pathways are all independent of glutaminolysis and therefore it should be stressed that loss of Gls1 is not expected to recapitulate all aspects of glutamine metabolism in B cells.

The findings of my work here demonstrate that genetic disruption of glutaminolysis in B cells leads to a defect in IgG1 class-switching and plasma cell differentiation. While not providing direct or definitive evidence of a need for glutaminolysis, previous work showed that glutamine was essential for plasma cell differentiation *in vitro* (Crawford et al., 1985). Moreover, a recent report provided evidence that plasmablasts have an increased appetite for glutamine over GCB during *in vivo*

responses to *Plasmodium* infection (Vijay et al., 2018). Similarly, pre-treatment of mice with glutaminolysis inhibitor 6-Diazo-5-oxo-L-norleucine (DON) led to decreased IgG1 responses to a T-dependent antigen (Choi et al., 2018). However in this setting, there were also defects in GCB not observed in my studies, suggesting that glutaminolysis may also be critical for T follicular helper cells.

A detailed molecular mechanism underpinning the importance of glutaminolysis in anti-ova IgG1$^+$ B cell responses is yet to be elucidated. Glutamine, glutaminolysis, and mTORC1 signaling, the latter critical for primary humoral responses, are all tightly interconnected (Nicklin et al., 2009; Durán et al., 2012; Csibi et al., 2013; Ni et al., 2019; Raybuck et al., 2018). Here loss of Gls1 led to diminished mTORC1 signaling, which correlated with the observed defect in IgG1$^+$ antibody responses both *in vitro* and *in vivo*. Another hypothesis linking Gls1 to antibody responses is that glutamine metabolism provides the NADPH necessary to serve as an anti-oxidant in plasma cells (Garcia-Manteiga et al., 2011; Bertolotti et al., 2010). In addition to NADPH as an anti-oxidant, glutamine and glutamate are precursors of glutathione, critical for the defense against free radicals and oxidants important for immunological functions (Muri et al., 2019; Dröge et al., 2000). Finally, the role of glutamine metabolism in anaplerotic reactions in B cells is evident here since activated *Gls1*$^{\Delta/\Delta}$ B cells had defects in OCR. Another possible mechanism involves the role of glutaminolysis in the generation of α-KG, which acts as a cofactor to histone demethylases resulting in modified gene expression (Teperino et al., 2010). Glutaminase inhibition differentially affected levels of histone trimethylation and gene expression in Th1 and Th17 CD4$^+$ cell subsets (Johnson et al., 2018). Loss of Gls1 in B cells could lead

to altered gene expression important for plasma cell differentiation and IgG1 class switching.

Glucose and glutamine metabolic pathways intersect (Mazat et al., 2019). In B cells, two groups independently observed that glutamine contribution to TCA cycle intermediates was inversely proportional to the concentration of glucose in the media indicating overlapping functions (Le et al., 2012; Brand et al., 1989). Here, I observed that basal OXPHOS of wildtype B cells increased when glucose, pyruvate, and glutamine were in the base media compared to glutamine alone. ECAR was similarly enhanced in wildtype cells with the addition of pyruvate and glucose. Therefore, nutrient availability dictates metabolic properties of B cells as they sense and fine-tune signaling pathways to rely on various available carbon and nitrogen sources. Accordingly, even though multiple reports conclude that glucose is used primarily for biosynthesis while glutamine is used primarily for fueling the TCA cycle in lymphocytes, glucose and glutamine metabolism may overlap and compensate for one another when one of the two nutrients are limiting to B cells or plasma cells. Here, loss of both Gls1 and Glut1 had synergistic defects in the production of $IgG1^+$ ASC and IgG1 production *in vitro* and *in vivo*.

Interestingly, B cells from double knock out mice had poor proliferation *in vitro* yet there was no substantial defect in the frequency of GCB generated *in vivo*. One possibility is that perturbations in Gls1 and Glut1 in GCB lead to increased dependence on fatty acids as a carbon and energy source to maintain GC size (Cho et al., 2011; Weisel et al., 2020). Different phenotypes observed *in vivo* vs. *in vitro* systems establish the need to determine the composition of the nutrient milieu available in the microenvironment of

tissues, which differs substantially from tissue culture media conditions (Ackermann et al., 2019).

All together, in Chapter 5 I presented evidence that supports and expands on previous reports establishing that glucose uptake and glutamine metabolism support B cell and plasma cell functions. Novel findings include the requirement for a threshold of glucose import to generate high affinity antibodies and that levels of glucose uptake influence differentiation fate decisions of activated B cells *in vivo*. Additionally, while glutamine has already been reported to be critical in B cell responses, genetic inhibition of glutaminolysis reveals new insights on the role of this aspect of glutamine metabolism in class-switching. Furthermore, perturbations of both glucose and glutamine metabolism in the B lineage are detrimental to humoral responses compared to a defect in only one pathway, suggesting that B cells adapt to alternative carbon sources for optimal fitness and robust humoral immunity.

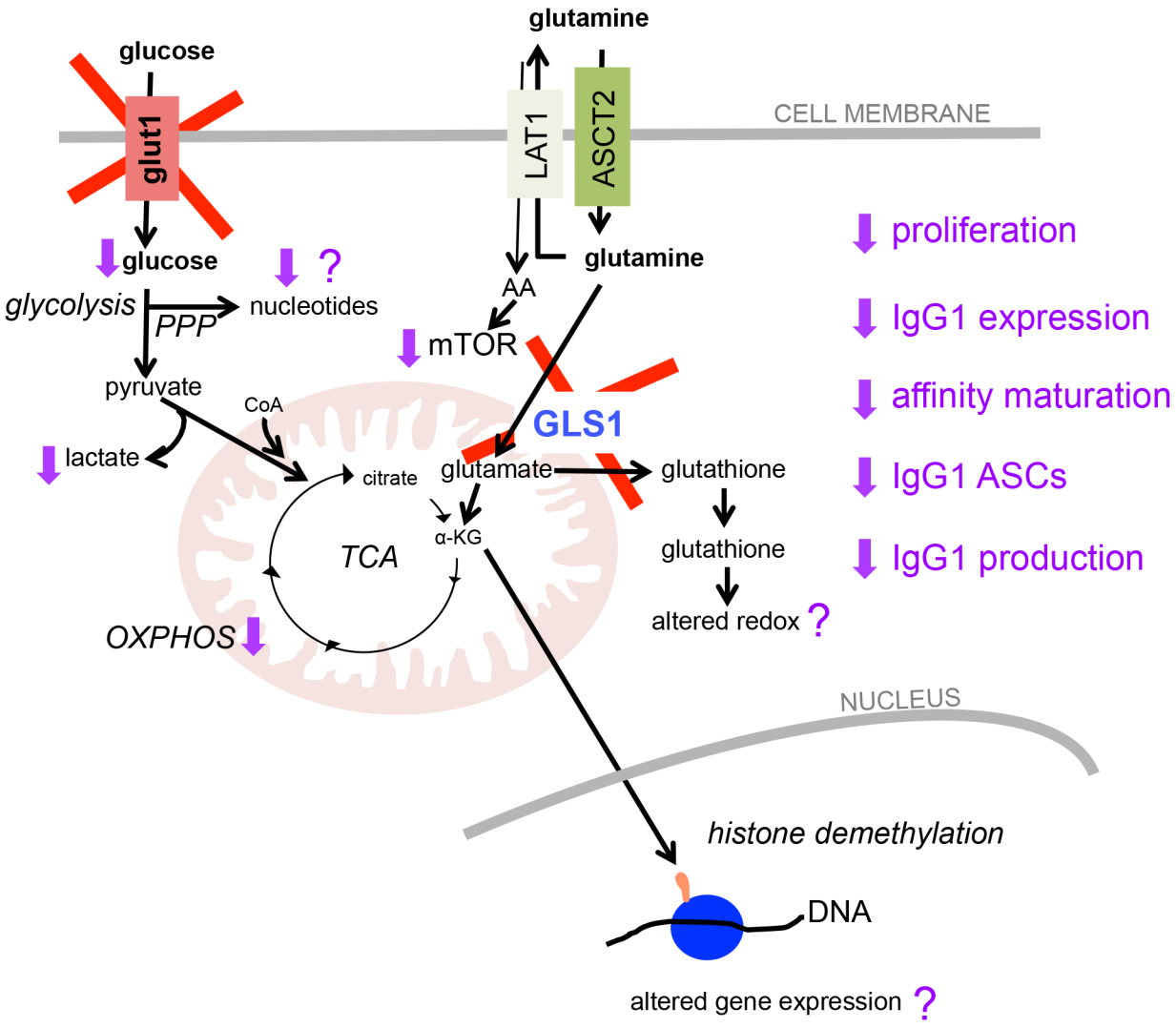

Figure 5.12 Working model: glucose transporter Glut1 and glutaminase (Gls1), an enzyme that catalyzes the conversion of glutamine to glutamate, are critical for primary humoral responses. Combined loss of Glut1 and Gls1 led to defects in glucose uptake, ECAR and OCR, which coincides with major impairments in proliferation and class-switching *in vitro* and defects in affinity maturation and IgG1 antibody production *in vivo*. Hypotheses linking metabolic perturbations to B cell phenotypes include decreased glucose flux through the PPP, decreased redox due to decreased glutathione and NADH generation, decreased fuels feeding the TCA cycle, and altered gene expression regulated by demethylases and limiting cofactor α-KG. Figure design inspired by Jin et al., 2015.

CHAPTER 6

DISCUSSION

Understanding the metabolic pathways critical for the B lymphocyte lineage is key to the development of therapeutic strategies against aberrant B cell or antibody responses and improving vaccination design (Pålsson-McDermott et al., 2020; Piranavan et al., 2020). Modulation of humoral immunity for human health could include dampening autoantibody production in autoimmune disorders or generating a robust and persistent MBC population for booster immunizations. Key metabolic regulator AMPK has been established as a pro-longevity and anti-aging target in model organisms and promotes the persistence of different tissues including in the T lymphocyte lineage (Burkewitz et al., 2014; Rolf et al., 2013). This thesis work is the first to show that AMPK is critical for the longevity of a subset in the B lymphocyte lineage. In this dissertation, I uncovered the importance of AMPK in the persistence of the MBC population specifically supporting optimal mitochondrial performance and homeostasis. Thus, AMPK in the B lineage was critical for effective recall responses, a hallmark feature of the adaptive immune response and the basis of vaccination. In contrast to the MBC population, my findings shed light on the interesting finding that AMPK was conversely dispensable for the persistence of LLPC, highlighting stark molecular distinctions between the two long-lived populations. I also demonstrated that the rate of antibody synthesis in both SLPC and LLPC could be modulated by the balance between levels of mTORC1 and AMPK activity.

Though other groups have observed the necessity of glucose and glutamine metabolism in lymphocyte survival and function, here I provide new insights specific to the B lineage. In regards to primary responses, I provide new evidence that expression of glucose transporter Glut1 alters the balance in the generation GC outcomes after immunization, specifically favoring ASC over MBC differentiation. Glut1 expression during the GC stage is also especially critical for affinity maturation. Additional findings indicate that the import of glucose by Glut1 and glutaminolysis in B cells have overlapping redundant downstream pathways that support humoral immunity. Key findings of my thesis work are illustrated in **Fig. 6.1**. Here in Chapter 6, I discuss the limitations of the work presented in this dissertation, explore remaining unanswered questions, and consider implications of my findings.

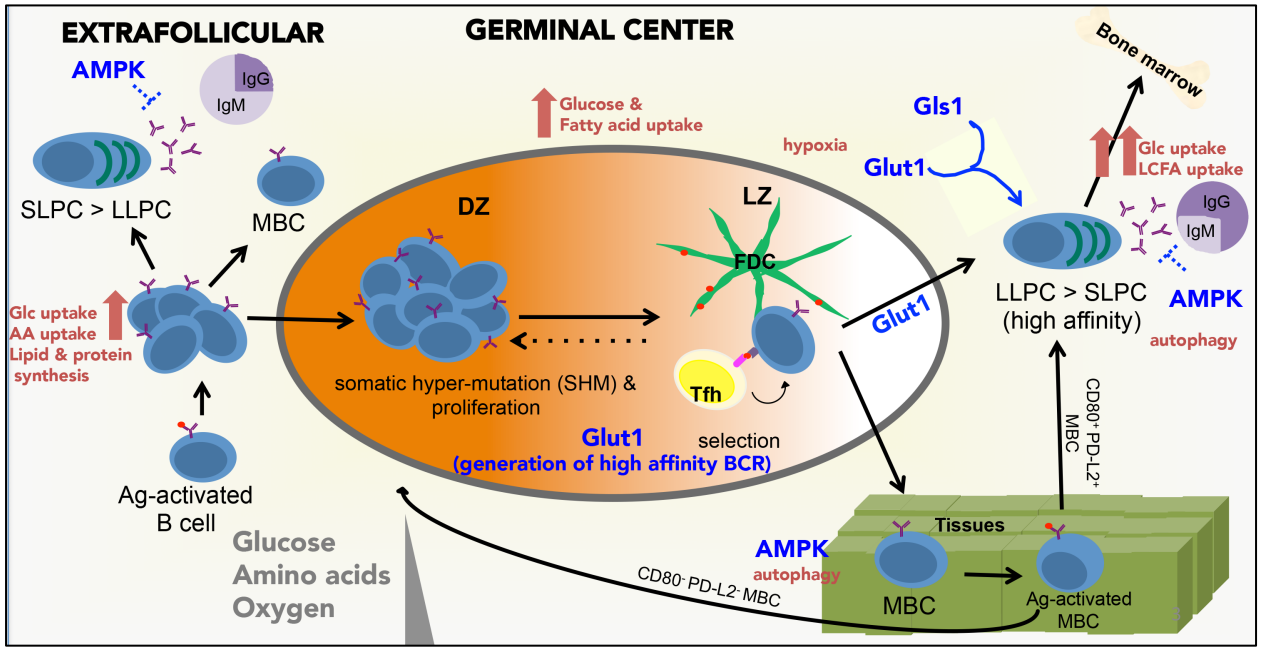

Figure 6.1. Summary of key findings. AMPK dampens antibody responses and promotes longevity in the memory B cell compartment. Glucose transporter, Glut1, is critical for the generation of high affinity antibodies and for the generation of antibody secreting cells. Gls1 and Glut1 synergistically promote effective plasma cell differentiation and antibody production.

I. Nutrient milieu and metabolite shunting

Regulation of metabolic pathways in lymphocytes involves the integration of nutrient availability with cellular intrinsic demands. Though glycogen and fatty acid stores fuel metabolic processes in lymphocytes (Yunis et al., 1964, Pacella et al., 2018), the microenvironment is the primary source of nutrients used to meet the cell's energetic and metabolic demands (Wasinski et al., 2014). Understanding the concentrations of nutrients with high resolution in micro-anatomical locations like the GC or niches in the bone marrow where LLPC reside are critical for identifying important metabolites necessary for survival and function of different subsets. The studies presented in this dissertation, among others, reveal that B lymphocytes exhibit a great deal of metabolic plasticity depending on nutrient availability. Specifically, in Chapter 5, two-fold increases in OCR and ECAR were observed when media was supplemented with glucose, glutamine, and pyruvate compared to glutamine alone. In addition, loss of both Glut1 and Gls1 expression led to severe defects in antibody production compared to genetic loss of either gene alone indicating flexibility in nutrient utilization. This leads me to question the following: To what degree are nutrients limiting *in vivo* in the GC and how much competition is there for preferential carbon and nitrogen sources? Can nutrient concentrations in the local milieu be modified to influence GC outcomes and ASC function?

Reliance on AMPK in lymphocytes for *in vitro* survival was only evident in nutrient-poor or metabolically challenging conditions (Mayer et al., 2008; Blagih et al., 2015; Brookens et al., 2020). The observation in Chapter 3 that AMPK was dispensable for the generation of GCB, MBC, and ASC raises the question of nutrient distribution in the

local milieu and whether or not essential metabolites are present at rate limiting concentrations in the follicles and other tissues where subsets reside. New evidence has emerged in the cancer field where rather than nutrient competition between tumor cells and infiltrating immune cells in the tumor microenvironment, both populations of cells have intrinsic programs that dictate preferred levels and types of nutrient uptake (Reinfeld, Madden et al., 2021). This phenomenon was coined nutrient partitioning. Assessing the availability and utilization of metabolites *in vivo* at cellular resolution in tissues where GC, MBC, ASC reside will shed light on how and whether modulating the microenvironment improves humoral responses and provides a potential avenue for targeting autoantibody producing ASC.

One major limitation of these studies is the assessment of glycolytic flux using ECAR measured by Seahorse analysis. There are at least two complications with equating ECAR to glycolytic function. The first is that ECAR is reported to be a surrogate measurement of lactic acid production, which is one of multiple fates of glycolytic end-product pyruvate. Glycolytic flux resulting in pyruvate entry into the TCA cycle or glycolytic intermediates shunted into other pathways, for instance, would not be captured in this assay. Secondly, multiple substrates apart from lactate can lead to acidification of the media leading to misinterpretation of data (Arnett et al., 1994; Sakano et al., 1997). Isotope tracer analyses would be better suited for measuring the extent of glucose carbons into glycolytic intermediates.

II. AMPK regulation of mitochondrial homeostasis

AMPK was critical for optimal mitochondrial fitness in the B lymphocyte lineage. However, the molecular mechanisms linking AMPK signaling to mitochondrial function in B cells are lacking. *In vitro* activated *Prkaa1*$^{\Delta/\Delta}$ B cells had decreased spare respiratory capacity compared to wildtype B cells. Reserved capacity has been linked to defects in succinate dehydrogenase which serves both as a component of the electron transport chain (complex II) and the TCA cycle (Pfleger et al., 2015). AMPK has been shown to regulate complex II via Pparα in rat cardiac myocytes (Pfleger et al., 2015). In this study, higher reserved capacity was associated with better viability and less ROS production after AMPK activation, analogous to my observations in MBC. This finding highlights a potential mechanistic link underpinning the correlation of spare respiratory capacity and the longevity of the MBC population.

Loss of AMPK coincided with increased mtROS and lipid peroxidation in MBC. I would have loved to test if injection of general antioxidant N-acetyl cysteine (NAC) or mitochondria-targeted antioxidant MitoQ rescues mitochondrial dysfunction, MBC persistence, and recall responses in AMPK-deficient mice. These studies would link observations in mitochondrial homeostasis in MBC with persistence of this population.

In addition to defects in mitochondrial function in LPS activated *Prkaa1*$^{\Delta/\Delta}$ B cells by Seahorse analysis, GCB, MBC, and LLPC populations all exhibited a decrease in Mitotracker Deep Red staining indicating defects in respiration. The molecular mechanisms underpinning these observations are also not uncovered by my thesis work. Apart from ULK1, critical for mitophagy, AMPK directly targets peroxisome proliferator-activated receptor gamma coactivator 1-alpha (PGC1α) and mitochondrial

fission factor (MFF) which are master regulators of mitochondrial biogenesis and an initiator mitochondrial fission after forming a complex with GTPase Drp1, respectively (Herzig et al., 2018). Therefore, in addition to promoting mitophagy through ULK1, AMPK may initiate mitochondrial generation and remodeling in B lineage subsets by directly targeting PGC1α and MFF, respectively. Though all *Prkaa1*$^{\Delta/\Delta}$ subsets had defects in respiration as determined by Mitotracker Deep Red, only the frequency of the MBC population was affected, specifically declining over time, suggesting that mitochondrial homeostasis is essential particularly for MBC longevity. I speculate the gradual decline in MBC was due to prolonged oxidative stress from mtROS in MBC, consistent with the oxidative stress theory of aging. This theory postulates that the steady accumulation of ROS over time leads to damage of macromolecules and is associated with age-related illnesses (Lin et al., 2003). Two weeks, the average duration of the GC, may be too short a time to accumulate enough mtROS to observe oxidative-related cell death in GCB compared to the months that MBC build-up mtROS leading to lipid peroxidation and cell death in these studies.

Surprisingly and in contrast to MBC, *Prkaa1*$^{\Delta/\Delta}$ bone marrow LLPC had no alterations in mtROS or mitochondrial quality, despite a decrease in respiration and total mitochondrial mass. In other words, *Prkaa1*$^{\Delta/\Delta}$ LLPC had equitably less mitochondrial mass and respiration and no alterations in mtROS. This distinction between LLPC and MBC alludes to distinct regulation pathways of mitochondrial homeostasis and oxidative stress in these two subsets. Indeed, in Chapter 3, I showed that *in vitro* derived CD138^{+} ASC had decreased mtROS and increased mitochondrial quality compared to B220^{+} B cells suggesting plasma cell differentiation involves mitochondrial remodeling. Metabolic

regulators, not limited to AMPK, have dynamic levels of activity at different stages in the B lineage. Sensors and transcription factors including mTORC1, sirtuins, HIF-1α, c-Myc, PPAR, and SREBP can all influence mitochondrial metabolism and may have different levels of activity in ASC and MBC (Ghirotto et al., 2019). Loss of AMPK may be dispensable for mitochondrial turnover and longevity in LLPC due to compensatory pathways orchestrated by other metabolic regulators with altered activity in this subset. For example, plasma cell differentiation entails reshaping of antioxidant responses involving several partially redundant redox pathways (Bertolotti et al., 2010; Muri et al., 2019). Enhanced redox systems in ASC may enable for better clearance of mtROS in *Prkaa1*$^{\Delta/\Delta}$ LLPC compared to *Prkaa1*$^{\Delta/\Delta}$ MBC.

In a series of elegant studies, autophagy-essential protein Atg7 was reported to be associated with mitochondrial clearance and was essential for the long-term persistence of MBC (Chen et al., 2014; Chen et al., 2015). Similarly, autophagy protein Atg5 was critical for mediating long-term survival and ER stress in plasma cells (Pengo et al., 2013). Canonical autophagy is downstream from AMPK activation so it was surprising that autophagy was intact in *Prkaa1*$^{\Delta/\Delta}$ activated B cells. This observation is the first to highlight, of which I am aware, that MBC and ASC can use non-canonical forms of autophagy consistent with observations in GCB (Raso et al., 2018; Martinez-Martin). Multiple pathways to autophagy underscore the redundant functions in cells to establish robust metabolic fitness.

III. Distinct reliance of AMPK in subset populations

AMPK was particularly critical for the persistence of the $CD80^-$ $PD\text{-}L2^-$ MBC population with less detectable function in the smaller (< 10% of total MBC) $CD80^+$ $PD\text{-}L2^+$ MBC population. Additionally, AMPK preferentially modulated IgG antibody responses with modest impact on IgM antibody production. These distinctions highlight molecular distinctions within subsets. Antigen-engaged IgG1 and IgM BCR are distinct in their signaling patterns and distribution in the cell membrane, which may coincide with differences in metabolic regulation (Liu et al., 2010). Furthermore, ASC differ in their transcriptional program depending on antibody isotype, which influences function and survival (Higgins et al., 2019). Understanding the regulation of metabolic pathways that distinguish isotypes and MBC subsets will further allow for more targeted approaches improving B cell-mediated immunity.

IV. Downstream of glutaminase and antigen-dependent immunity

In Chapter 5, I provided evidence that glutaminolysis in B cells was critical for spare respiratory capacity, class-switching, and plasma cell differentiation. However, the molecular mechanisms leading to this phenotype was not elucidated. Glutaminolysis involves the conversion of glutamine to glutamate, which has multiple fates. Glutamate is catalyzed by glutamate dehydrogenase resulting in TCA substrate α-ketoglutarate (α-KG). As a TCA cycle metabolite, αKG is involved in ATP production, reducing equivalent (NADH) generation, and providing TCA intermediates for amino acid synthesis. αKG is also directly involved in epigenetic regulation and signaling which influence gene expression (Zdzisińska et al., 2017). One possible mechanism is that α-KG

alters methylation of genes associated with class-switching and plasma cell differentiation. In addition to conversion to α-KG, glutamate serves as a precursor to glutathione (GSH), a tripeptide of glutamate, cysteine, and glycine. GSH and the generation of NADH both contribute to redox homeostasis by maintaining intracellular levels of ROS. Treatment of cancer cell lines with dimethyl α-KG (DMKG), a nontoxic cell permeable α-KG, and a complex I inhibitor led to transcriptional reprogramming and cell death (Sica et al., 2019). Next steps would include elucidating possible transcriptional changes induced by α-KG that would lead to defects in class-switching and plasma cell differentiation.

Interestingly, my findings reveal that the reliance on glutaminolysis was higher in anti-ova IgG1$^+$ compared to anti-NP IgG1$^+$ responses *in vivo*. Experiments need to be done to distinguish the requirement for glutaminoylsis in antibody responses against a carrier protein but dispensable for a small hapten molecule. However, this finding is reminiscent of the immunodominance phenomenon, which is the observation that different epitopes on complex antigens elicit varied responses usually due to differences in antigen processing (Kim et al., 2014). Several hypotheses in understanding the variables that influence epitope selection have been considered including antigen structure (Maric et al., 2001), antigen protease-sensitivity (Delamarre et al., 2006), duration of antigen presentation (Lazarski et al., 2005), cognate naïve T-cell frequency (Moon et al., 2007), and strength of TCR affinity to the MHC class II: peptide complex (Kedl et al., 2003). My finding that Gls1 in B cells is differentially required for responses specific to different antigens inspires the hypothesis that glutaminolysis may play a role in aspects of B cell antigen presentation to Tfh cells in the GC. Though metabolism important for the

activation of professional antigen presentation cells has been studied at length (Jennelle et al., 2016), the metabolic processes that specifically regulate antigen processing and presentation is limiting. As a start, important links have been described between B cell antigen presentation and autophagy (Crotzer et al., 2009; Pérez et al., 2016) and NADPH oxidase (Gardiner et al., 2013).

This thesis work is novel because it tests for the effect of Glut1 immediately before activation without the confounding factor of the important role for Glut1 in B cell development (Caro-Maldanado et al., 2014). Expression of glucose transporter Glut1 was critical for affinity maturation and played a role in GC outcomes. Glut1 expression was critical for purine/pyrimidine synthesis in B-ALL cells (Liu et al., 2014). Therefore, nucleotides may be limiting for SHM, a process requiring DNA repair mechanisms and a prerequisite to affinity maturation, in the absence of Glut1 expression. This observation supports the past time of revisiting older studies describing mechanisms behind immunological processes and making hypotheses about links to metabolism. p53, which is essential for guarding against genomic instability during SHM in B cells (Ramiro et al., 2006), may be regulated in part by metabolic pathways as observed in mouse embryonic fibroblasts (Franklin et al., 2016). Lastly, obliteration of plasma cell generation and antibody responses in the absence of both Gls1 and Glut1 indicates interacting pathways in glucose and glutamine metabolism suggesting that the plasticity of B cell fuel preference needs to be considered if seeking a metabolic target.

V. Exploiting B cell metabolism

I introduced this dissertation with commentary concerning exploiting metabolic pathways for cancer, immune disorders, and improving vaccine responses. Given the data in Chapter 3, it is conceivable that AMPK activation would lead to better MBC and recall antibody responses. Consistent with my studies, IgM^+ human $CD27^+$ MBC have elevated mitochondrial activity and $pAMPK^{T172}$ expression compared to mature naïve B cells (Mensah et al., 2018). Furthermore, metformin treatment, which indirectly activates AMPK, is associated with increased MBC and improved Ab responses to influenza vaccine in type II diabetic patients (Diaz et al., 2017). Increased expression of memory markers were observed in human CD4+ T cells after genetically inducing AMPK expression (Braverman et al., 2020). However, treating mice with metformin derivative IMI56 during acute lymphocytic choriomeningitis virus infection unexpectedly led to decreased memory T cell differentiation (Son et al., 2019). In this setting, it is important to consider the timing of AMPK activation as authors administered treatment during the proliferation phase of immunization. Though AMPK may support some subsets of MBC such as the IgM^+ MBC, enhanced $pAMPK^{T172}$ in IgD^- $CD27^-$ late/exhausted human MBC was associated with senescence and the inability to respond to CpG activation (Frasca et al., 2019).

More broadly, it is important to consider temporal regulation in metabolic pathways. Treatment with rituximab is commonly used as a therapy to target CD20 expressing B cells (Hofmann et al., 2018) while numerous proteasome inhibitors target plasma cells in autoimmune disease (Hiepe et al., 2016). Targeting the dynamic metabolic

pathways in the B lymphocyte lineage provides a new opportunity for the treatment of autoimmune disorders and enhancing antibody responses to vaccines.

REFERENCES

1. Abbott RK, Thayer M, Labuda J, Silva M, Philbrook P, Cain DW, et al. Germinal center hypoxia potentiates immunoglobulin class switch recombination. J Immunol 2016; 197: 4014-4020.
2. Ackermann T, Tardito S. Cell culture medium formulation and its implications in cancer metabolism. Trends Cancer 2019; 5: 329-332.
3. Ahluwalia GS, Grem JL, Hao Z, Cooney DA. Metabolism and action of amino acid analog anti-cancer agents. Pharmacol Ther 1990; 46: 243-71.
4. Ahmadian M, Duncan RE, Jaworski K, Sarkadi-Nagy E, Sul HS. Triacylglycerol metabolism in adipose tissue. Future Lipidol 2007; 2: 229-237.
5. Ahuja A, Shupe J, Dunn R, Kashgarian M, Kehry MR, Shlomchik MJ. Depletion of B cells in murine lupus: efficacy and resistance. J Immunol. 2007; 179: 3351-61.
6. Akbari M, Kirkwood TBL, Bohr VA. Mitochondria in the signaling pathways that control longevity and health span. Ageing Research Reviews 2019; 54: 1-18.
7. Akkaya M, Pierce SK. From zero to sixty and back to zero again: the metabolic life of B cells. Curr Opin Immunology 2019; 57:1-7.
8. Akkaya M, Traba J, Roesler AS, Miozzo P, Akkaya B, Theall BP. Second signals rescue B cells from activation-induced mitochondrial dysfunction and death. Nat Immunol 2018; 19: 871-884.
9. Alkhatib Y, Rahman ZA, Kuriakose P. Clinical impact of metformin in diabetic diffuse large B-cell lymphoma patients: a case-control study. Leuk Lymphoma 2017; 58: 1130-34.
10. Altman BJ. Stine ZE, Dang CV. From Krebs to clinic: glutamine metabolism to cancer therapy. Nat Rev Cancer 2016; 16: 619-634.
11. Ardawi MSM, Newsholme EA. Glutamine metabolism in lymphocytes of the rat. Biochemical Journal 1983; 212: 835-842.
12. Arnett TR, Boyde A, Jones SJ, Taylor ML. Effects of medium acidification by alteration of carbon dioxide or bicarbonate concentrations on the resorptive activity of rat osteoclasts. JBMR 1994; 9: 375-379.
13. Arnold JN, Wormald MR, Sim RB, Rudd PM, Dwek RA. The impact of glycosylation on the biological function and structure of human immunoglobulins. Annual Rev Immunol 2007; 25: 21-50.
14. Auner HW, Beham-Schmid C, Dillon N, Sabbattini P. The life span of short-lived plasma cells is partly determined by a block on activation of apoptotic caspases acting in combination with endoplasmic reticulum stress. Blood 2010; 116: 3445-55.
15. Balendiran GK, Dabur R, Fraser D. The role of glutathione in cancer. Cell Biochem Funct 2004; 22: 343-52.
16. Baumgarth N. A hard(y) look at B-1 cell development and function. J Immunol 2017; 199: 3387-3394.
17. Becher B, Waisman A, Lu L. Conditional gene-targeting in mice: problems and solutions. Immunity; 2018; 48: 835-836.

18. Beg ZH, Allmann DW, Gibson DM. Modulation of 3-hydroxy-3-methylglutaryl coenzyme A redutase activity with cAMP and with protein fractions of rat liver cytosol. Biochem Biophys Res Comm 1973; 54: 1362-1369.
19. Benhamron S, Pattanayak SP, Berger M, Tirosh B. mTOR activation promotes plasma cell differentiation and bypasses XBP-1 for immunoglobulin secretion. Mol Cell Biol. 2015; 35: 153-166.
20. Benner R, Hijmans W, Haaijman JJ. The bone marrow: the major source of serum immunoglobulins, but still a neglected site of antibody formation. Clin Exp Immunol 1981; 46: 1-8.
21. Berod L, Friedrich C, Nandan A, Freitag J, Hagemann S, Harmrolfs K, et al. De novo fatty acid synthesis controls the fate between regulator T and T helper 17 cells. Nat Med 2014; 20: 1327-33.
22. Bertolotti M, Tim S, Garcia-Manteiga JM, Masciarelli S, Kim YJ, Kang MH, et al. B- to plasma-cell terminal differentiation entails oxidative stress and profound reshaping of the antioxidant responses. Antioxid Redox Signal 2010; 13: 1133-44.
23. Berton MT, Vitetta ES. IL-4-induced expression of germline γ1 transcripts in B cells following cognate interactions with T helper cells. Int Immunol 1992; 4: 387-396.
24. Blagih J, Coulombe F, Vincent EE, Dupuy F, Galicia-Vázquez G, Yurchenko E, et al. The energy sensor AMPK regulates T cell metabolic adaptation and effector responses in vivo. Immunity 2015;. 42: 41-54.
25. Blair D, Dufort FJ, Chiles TC. Protein kinase Cβ is ciritical for the metabolic switch to glycolysis following B cell antigen receptor engagement. Biochem J 2012; 448: 165-169.
26. Blink EJ, Light A, Kallies A, Nutt S, Hodgkin PD, Tarlinton DM. Early appearance of germinal center-derived memory B cells and plasma cell in blood after primary immunization. J Exp Med 2005; 201: 545-554.
27. Boothby MR, Hodges E, Thomas JW. Molecular regulation of peripheral B cells and their progeny. Gene Dev 2019; 33: 26-48.
28. Boothby MR, Raybuck A, Cho SH, Stengel KR, Hiebert S, Li J. Generalizing about GC (hypoxia): dys- & dat-informatica. Under review 2021.
29. Boothby MR, Rickert RC. Metabolic regulation of the immune humoral response. Immunity 2017; 46: 743-755.
30. Bortnick A, Allman D. What is and what should always have been: long-lived plasma cells induced by T-cell independent antigens. J Immuol 2013; 15: 5913-18.
31. Bozic B, Cucnik S, Kveder T, Rozman B. Affinity and avidity of autoantibodies. Autoantibodies 2007; 2: 21-28.
32. Brand K, Fekl W, von Hintzenstern J, Langer K, Luppa P, Schoerner C. Metabolism of glutamine in lymphocytes. Metabolism 1989; 38: 29-33.
33. Braverman EL, Dobbs A, Monlish D, Byersdorfer. Increasing AMPK activity in human T cells enhances memory subset formation without sacrificing in vitro expansion. Blood 2020; 136: 38-39.
34. Briney B, Inderbitzin A, Joyce C, Burton DR. Commonality despite exceptional diversity in the baseline human antibody repertoire. Nature 2019; 566: 393-397.

35. Brinkman V, Heusser CH. T cell-dependent differentiation of human B cells into IgM, IgG, IgA, or IgE plasma cells: high rate of antibody production by IgE plasma cells, but limited clonal expansion of IgE precursors. Cell Immunol 1993; 152:323-32.
36. Brookens SK, Boothby MR. AMPK metabolism in the B lineage modulates humoral responses. Immunometabolism 2021; 3: 1-9.
37. Brookens SK, Cho SH, Basso PJ, Boothby MR. AMPKα1 in B cells dampens primary antibody responses yet promotes mitochondrial homeostasis and persistence of B cell memory. J Immunol 2020; 205: 3011-22.
38. Brunengraber H, Roe CR. Anaplerotic molecules: current and future. J Inherit Metab Dis 2006; 29: 327-31.
39. Buck MD, O'Sullivan D, Geltink RK, Curtis JD, Chang C, Sanin DE, et al. Mitochondrial dynamics controls T cell fate through metabolic programming. Cell 2016; 166: 63-76.
40. Bultot L, Guinas B, Wilamowitz-Moellendorff AV, Maisin L, Vertommen D, Hussain N, et al. AMP-activated protein kinase phosphorylates and inactivates glycogen synthase. Biochem J 2012; 443: 193-203.
41. Burkewitz K, Zhang Y, Mair WB. AMPK at the Nexus of energetics and aging. Cell Metab 2014; 20: 10-25.
42. Campàs C, Lopez JM, Santidrián AF, Barragán M, Bellosillo B, Colomer D, et al. Acadesine activates AMPK and induces apoptosis in B-cell chronic lymphocytic leukemia cells but not in T lymphocytes. Blood 2003; 1010: 3674-80.
43. Caro-Maldonado A, Wang R, Nichols AG, Kuraoka M, Milasta S, Sun LD, et al. Metabolic reprogramming is required for the antibody production that is suppressed in anergic but exaggerated in chronically BAFF-exposed B cells. J Immunol. 2014; 192: 3626-36.
44. Carroll KC, Viollet B, Suttles J. AMPKα1 deficiency amplifies proinflammatory myeloid APC activity and CD40 signaling. J Leukoc Biol. 2013; 94: 1113-21.
45. Casola S, Cattoretti G, Uyttersprot N, Koralov SB, Seagal J, Hao Z, et al. Tracking germinal center B cells expressing germ-line immunoglobulin gamma1 transcripts by conditional gene targeting. PNAS 2006; 103: 7396-401.
46. Cerutti, A, Cols M, Puga I. Marginal zone B cells: virtues of innate-like antibody producing lymphocytes. 2013; 13: 118-132.
47. Chang CH, Qiu J, O'Sullivan, Buck MD, Noguchi T, Curtis JD, et al. Metabolic competition in the tumor microenvironment is a driver of cancer progression. Cell 2015; 162: 1229-1241.
48. Chen M, Hong MJ, Sun H, Wang L, Shi X, Gilbert BE, et al. Essential role for autophagy in the maintenance of immunological memory against influenza infection. Nature Medicine 2014; 20: 503-510.
49. Chen M, Kodali S, Jang A, Kuai L, Wang J. Requirement for autophagy in the long-term persistence but not initial formation of memory B cells. J Immunol. 2015; 194: 2607-15.
50. Chen P, Nirula A, Heller B, Gottlieb R, Boscia J, Morris J. SARS-CoV-2 neutralizing antibody LY-CoV555 in outpatients with Covid-19. N Engl J Med 2021; 384: 229-237.

51. Cheung PC, Salt IP, Davies SP, Hardie DG, Carling D. Characterization of AMP-activated protein kinase γ-subunit isoforms and their role in AMP binding. Biochem J 2000; 346: 659–669.
52. Cho SH, Ahn AK, Bhargava P, Lee CH, Eischen CM, McGuinness O, et al. Glycolytic rate and lymphomagenesis depend on PARP14, an ADP ribosyltransferase of the B aggressive lymphoma (BAL) family. PNAS 2011; 108: 15972-77.
53. Cho SH, Raybuck A, Wei M, Erickson J, Nam KT, Cox RG, et al. B cell-intrinsic and -extrinsic regulation of antibody responses by PARP14, an intracellular (ADP-ribosyl) transferase. J Immunol 2013; 191: 3169-3178.
54. Cho SH, Raybuck AL, Stengel K, Wei M, Beck TC, Volanakis E, et al. Germinal centre hypoxia and regulation of antibody qualities by a hypoxia response system 2016; 537: 234-237.
55. Choi SC, Titov AA, Abboud G, Seay HR, Brusko TM, Roopenian DC, et al. Inhibition of glucose metabolism selectively targets autoreactive follicular helper T cells. Nat Communications 2018; 9: 1-13.
56. Ci X, Kuraoka M, Wang H, Carico Z, Hopper K, Shin J, et al. TSC1 promotes B cell maturation but is dispensable for germinal center formation. Plos One. 2015; 10:1-17.
57. Cirelli KM, Crotty S. Germinal center enhancement by extended antigen availability. Curr Opin Immunol 2017; 47: 64-69.
58. Clybouw C, Fischer S, Auffredou MT, Hugues P, Alexia C, Bouillet P, et al. Regulation of memory B-cell survival by the BH3-only protein Puma. Blood 2011; 118: 4120-28.
59. Codogno P, Mehrpour M, Proikas-Cezanne T. Canonical and non-canonical autophagy: variations on a common theme of self-eating? Molecular Cell Biology. 2012; 13: 7-12.
60. Cohen AS, Geng L, Zhao P, Fu P, Fu A, Schulte ML, et al. Combined blockade of EGFR and glutamine metabolism in preclinical models of colorectal cancer. Tranl Oncol 2020; 13: 1-10.
61. Cory JG, Cory AH. Critical roles of glutamine as nitrogen donors in purine and pyrimidine nucleotide synthesis: asparaginase treatment in childhood acute lymphoblastic leukemia. In vivo 2006; 20: 587-590.
62. Crawford J, Cohen HJ. The essential role of L-glutamine in lymphocyte differentiation in vitro. J Cell Physiol 1985; 124: 275-82.
63. Crotty S, Felgner P, Davies H, Glidewell J, Villarreal L, Ahmed R. Cutting edge: long-term B cell memory in humans after smallpox vaccination 2003; 171: 4969-73.
64. Crotzer VL, Blum JS. Autophagy and its role in MHC-mediated antigen presentation. J Immunol 2009; 182: 3335-3341.
65. Csibi A, Fendt SM, Li C, Poulogiannis G, Choo AY, Chapski DJ, et al. The mTORC1 pathway stimulates glutamine metabolism and cell proliferation by repressing SIRT4. Cell 2013; 153: 840-854.
66. Curi R, Newsholme P, Pithon-Curi TC, Pires-de-Melo M, Garcia C, Homem-de-Bittencourt PI, et al. Metabolic fate of glutamine in lymphocytes, macrophages

and neutrophils. Brazilian Journal of Medical and Biological Research 1999; 32: 15-21.
67. Cyster JG, Allen CDC. B cell responses: cell interaction dynamics and decisions. Cell 2019; 177: 524-540.
68. D'Souza L, Bhattacharya D. Plasma cells: you are what you eat. Immunological Reviews 2019; 288: 161-177.
69. DeBerardinis RJ, Cheng T. Q's next: the diverse functions of glutamine in metabolism, cell biology and cancer. Oncogene 2010; 29: 313-324.
70. DeBerardinis RJ, Thompson. Cellular metabolism and disease: what do metabolic outliers teach us? Cell 2012; 148: 1132-1144.
71. Delamarre L, Couture R, Mellman I, Trombetta ES. Enhancing immunogenicity by limiting susceptibility to lysosomal proteolysis. J Exp Med 2006; 203: 2049-55.
72. Dengler F. Activation of AMPK under hypoxia: many roles leading to Rome. International Journal of Molecular Sci 2020; 21: 1-15.
73. Diaz A, Romero M, Vazquez T, Lechner S, Blomberg BB, Frasca D. Metformin improves in vivo and in vitro B cell function in individuals with obesity and type-2 diabetes. Vaccine. 2017;35:2694-2700.
74. Diaz-Muñoz MD, Bell SE, Fairfax K, Monzon-Casanova E, Cunningham AF, Gonzalez-Porta M, et al. The RNA-binding protein HuR is essential for the B cell antibody response. Nat Immunol 2015; 16: 415-425.
75. Doherty E and Perl A. Measurement of mitochondrial mass by flow cytometry during oxidative stress. React Oxyg Species 2017; 4: 275-83.
76. Doughty CA, Bleiman BF, Wagner DJ, Dufort FJ, Mataraza JM, Roberts MF, et al. Antigen receptor-mediated changes in glucose metabolism in B lymphocytes: role of phosphatidylinositol 3-kinase signaling in the glycolytic control of growth. Blood 2006; 107: 4458-65.
77. Dröge W, Breitkreutz R. Glutathione and immune function. Proc Nutr Soc 2000; 59: 595-600.
78. Dufort FJ, Bleiman BF, Gumina MR, Blair D, Wagner DJ, Roberts MF, et al. Cutting edge: IL-4 mediated protection of primary B lymphocytes from apoptosis via Stat6-dependent regulation of glycolytic metabolism. J Immunol 2007; 179:4953-57.
79. Dufort FJ, Gumina MR, Ta NL, Tao Y, Heyse SA, Scott DA. Glucose-dependent de Novo Lipogenesis in B lymphocytes. A requirement for ATP-citrate lyase in lipopolysaccharide-induced differentiation. 2014; 289: 7011-7024.
80. Durán RV, Oppliger W, Robitaille AM, Heiserich L, Skendaj R, Gottlieb E. Glutaminolysis activates Rag-mTORC1 signaling. Mol Cell 2012; 47: 349-358.
81. Eagle H. Nutrition needs of mammalian cells in tissue culture. Science 1955; 122: 501-514.
82. Efeyan A, Comb WC, Sabatini DM. Nutrient sensing mechanisms and pathways. Nature 2015; 517: 302-310.
83. Egawa T and Bhattacharya D. Regulation of metabolic supply and demand during B cell activation and subsequent differentiation. Curr Opin Immunology 2019; 57: 8-14.
84. Elsner RA, Shlomchik MJ. Germinal center and extrafollicular B cell responses in vaccination, immunity, and autoimmunity. Immunity 2020; 53: 1136-1150.

85. Ersching J, Efeyan A, Mesin L, Jacobsen JT, Pasqual G, Grabiner BC, et al. Germinal center selection and affinity maturation require dynamic regulation of mTORC1 kinase. Immunity. 2017;46:1045-1058.
86. Faubert B, Boily G, Izreig S, Griss T, Samborska B, Dong Z, et al. AMPK is a negative regulator or the Warburg effect and suppresses tumor growth in vivo. Cell Metab 2013; 17: 113-24.
87. Fitzpatrick L, Jenkins HA, Butler M. Glucose and glutamine metabolism of a murine B-lymphocyte hybridoma in batch culture. Applied Biochemistry and Biotechnology 1993; 43: 93-116.
88. Fonseca BD, Smith EM, Yelle N, Alain T, Bushell M, Pause A. The ever-evolving role of mTOR in translation. Seminars in Cell & Developmental Biol 2014; 102-12.
89. Foretz M, Guihard S, Leclerc J, Fauveau V, Couty J, Andris F, et al. Maintenance of red blood cell integrity by AMP-activated protein kinase α1 catalytic subunit. FEBS Letters 2010; 584: 3667-71.
90. Forthal DN. Functions of antibodies. Microbiol Spectr 2014; 2: 1-17.
91. Foyer CH. Redox homeostasis and antioxidant signaling: a metabolic interface between stress perception and physiological responses. Plant Cell 2005; 17: 1866-1875.
92. Franchina DG, Grusdat M, Brenner D. B-cell metabolic remodeling and cancer. Trends in Cancer 2017; 12: 1-13.
93. Franklin DA, He Y, Leslie PL, Tikunov AP, Fenger N, Macdonald JM, et al. p53 coordinates DNA repair with nucleotide synthesis by suppressing PFKFB3 expression and promoting the pentose phosphate pathway. Sci Reports 2016; 6: 1-13.
94. Frasca D, Diaz A, Romero M, Blomberg. Human peripheral late/exhausted memory B cells express a senescent-associated secretory phenotype and preferentially utilize metabolic signaling pathways. Exp Gerontol 2017; 87: 113-120.
95. Frasca D, Diaz A, Romero M, Thaller S, Blomberg BB. Metabolic requirements of human pro-inflammatory B cells in aging and obesity. Plos One. 2019;7:1-21.
96. Fuchs-Tarlovsky V. Role of antioxidants in cancer therapy. Nutrition 2013; 29: 15-21.
97. Fullerton MD, Galic S, Marcinko K, Sikkema S, Pulinilkunnil T, Chen ZP, et al. Single phosphorylation sites in Acc1 and Acc2 regulate lipid homeostasis and the insulin-sensitizing effects of metformin. Nat Med 2013; 12: 1649-54.
98. Garcia D and Shaw RJ. AMPK: mechanisms of cellular energy sensing and restoration of metabolic balance. Molecular Cell. 2017; 66: 789-800.
99. Garcia-Manteiga JM, Mari S, Godejohann M, Spraul M, Napoli C, Cenci S, et al. Metabolomics of B to plasma cell differentiation. 2011; 10: 4165-76.
100. Gardiner GJ, Deffit SN, McLetchie S, Pérez L, Walline CC, Blum JS. A role for NADPH oxidase in antigen presentation. Front Immunol 2013; 4: 1-6.
101. Gaudette BT, Jones DD, Bortnick A, Argon Y, Allman D. mTORC1 coordinates an immediate unfolded protein response-related transcriptome in activated B cells preceding antibody secretion. Nature Communications 2020; 723: 1-16.

102. Gebregiworgis T, Purohit V, Shukla SK, Tadros S, Chaika NV, Abrego J, et al. Glucose limitation alters glutamine metabolism in MUC1-overexpressing pancreatic cancer cells. J Proteome Res 2017; 16: 3536-46.
103. Gershoni JM and Palade GE. Protein blotting: Principles and applications. Analytical Biochemistry. 1983; 131: 1-15.
104. Ghirotto B, Terra FF, Câmara NOS, Basso PJ. Sirtuins in B lymphocytes metabolism and function. World J Exp Med 2019; 9: 1-13.
105. Ghoneum A, Abdulfattah AY, Warren BO, Shu J, Said N. Redox homeostasis and metabolism in cancer: a complex mechanism and potential targeted therapeutics. Int J Mol Sci 2020; 21: 1-28.
106. Gordan JD, Thompson CB, Simon MC. HIF and c-Myc: sibling rivals for control of cancer cell metabolism and proliferation. Cancer Cell 2007; 12: 108-113.
107. Gourley TS, Wherry EJ, Masopust D, Ahmed R. Generation and maintenance of immunological memory. Seminars in Immunol 2004; 16: 323-333.
108. Gray LR, Tompkins SC, Taylor EB. Regulation of pyruvate metabolism and human disease. Cell Mol Life Sci 2014; 71: 2577-2604.
109. Green DR, Galluzzi L, Kroemer G. Metabolic control of cell death. Science 2014; 345: 1-25.
110. Gross MI, Demo SD, Dennison JB, Chen L, Chernov-Rogan T, Goyal B. Antitumor activity of the glutaminase inhibitor CB-839 in triple negative breast cancer. Small Mol Therapeutics 2014; 13: 890-901.
111. Guerra VA, Burger JA, Borthakur GM, Jabbour E, Pemmaraju N, Kadia TM. Interim analysis of a phase II study of the glutaminase inhibitor telaglenastat (CB-839) in combination with azacitidine in advanced myelodysplastic syndrome (MCD). Blood 2019; 134: 567.
112. Guo M, Price MJ, Patterson DG, Barwick BG, Haines RR, Kania AK, et al. EZH2 represses the B cell transcriptional program and regulates antibody-secreting cell metabolism and antibody production. J Immunol 2018; 200: 1039-52.
113. Gwinn DM, Shackelford DB, Egan DF, Mihaylova MM, Mery A, Vasquez DS, et al. AMPK phosphorylation of raptor mediates a metabolic checkpoint. Mol Cell. 2008; 30: 214-226.
114. Haniuda K, Fukao S, Kitamura D. Metabolic reprogramming induces germinal center B cell differentiation through Bcl6 locus remodeling. Cell Reports 2020; 33: 1-14.
115. Hawley SA, Davison M, Woods A, Davies SP, Beri RK, Carling D, et al. Characterization of the AMP-activated protein kinase kinase from rat liver and identification of threonine 172 as the major site at which it phosphorylates AMP-activated protein kinase. J Biol Chem. 1996;271:27879-87.
116. Hawley SA, Pan DA, Mustard KJ, Ross L, Bain J, Edelman AM, et al. Calmodulin-dependent protein kinase kinase-beta is an alternative upstream kinase for AMP-activated protein kinase. Cell Metab 2005; 2: 9-19.
117. Herzig S, Shaw RJ. AMPK: guardian of metabolism and mitochondrial homeostasis. Nat Rev Mol Cell Biol 2018; 19: 121-135.
118. Heyse S, Connolly T, Chiles T. The regulation and role of L-glutamine in B-cell activation. FASEB 2015; 29: meeting abstract.

119. Hibi T, Dosch HM. Limiting dilution analysis of the B cell compartment in the human bone marrow. Eur J Immunol 1986; 16:139-145.
120. Hickman S, Kulczycki A, Lynch RG, Kornfeld S. Studies of the mechanism of tunicamycin inhibition of IgA and IgE secretion by plasma cells. J Biol Chem 1977; 252: 4402-4408.
121. Hiepe F, Radbruch A. Plasma cells as an innovative target in autoimmune disease with renal manifestations. Nat Rev Nephr 2016; 233: 232-240.
122. Higgins BW, McHeyzer-Williams LJ, McHeyzer-Williams MG. Programming isotype-specific plasma cell function. Trends Immunol 2019; 40: 345-357.
123. Hobeika E, Thiemann S, Storch B, Jumaa H, Nielsen PJ, Pelanda R, et al. 2006. Testing gene function early in the B cell lineage in mb1-cre mice. PNAS 2006; 103: 13789-94.
124. Hoffman AE, Demanelis K, Fu A, Zheng T, Zhu Y. Association of AMP-activated protein kinase with risk and progression of non-Hodgkin lymphoma. Cancer Epidemiol Biomarkers Prev 2013; 22: 736-44.
125. Hoffman W, Laddis FG, Chalasani G. B cells, antibodies, and more. Clin J Am Soc Nephrol 2016; 7: 137-154.
126. Hofmann K, Clauder AK, Manz RA. Targeting B cells and plasma cells in autoimmune diseases. Frontiers in Immunol 2018; 9: 1-17.
127. Houde VP, Donzelli S, Sacconi A, Galic S, Hammill JA, Bramson JL, et al. AMPKβ1 reduces tumor progression and improves survival in p53 null mice. Mol Oncol 2017; 11: 1143-55.
128. Hua H, Kong Q, Zhang H, Wang J, Luo T, Jiang Y. Targeting mTOR for cancer therapy. J Hematology & Oncology 2019; 12: 1-19.
129. Inoue T, Shinnakasu R, Kawai C, Ise W, Kawakami E, Sax N, et al. Exit from germinal center to become quiescent memory B cells depends on metabolic reprogramming and provision of a survival signal. J Exp Med 2021; 218: e20200866.
130. Ivy JL. Muscle glycogen synthesis before and after exercise. Sports Med 1991; 11: 6-19.
131. Jang K, Mano H, Aoki K, Hayashi T, Muto A, Nambu Y, et al. Mitochondrial function provides instructive signals for activation-induced B-cell fates. Nat Communications 2015; 1-13.
132. Jayachandran N, Mejia EM, Sheikholeslami K, Sher AA, Hou S, Hatch GM, et al. TAPP adaptors control B cell metabolism by modulating the phosphatidylinositol 3-kinase signaling pathway: a novel regulatory circuit preventing autoimmunity. J Immunol 2018; 201: 406-416.
133. Jellusova J. Metabolic control of B cell immune responses. Curr Opin Immunol 2020; 63: 21-28.
134. Jellusova J and Rickert RC. A brake for B cell proliferation: appropriate responses to metabolic stress are crucial to maintain B cell viability and prevent malignant outgrowth. Bioessays 2017; 1-9.
135. Jellusova J, Cato MH, Apgar JR, Ramezani-Rad P, Leung CR, Chen C, et al. Gsk3 is a metabolic checkpoint regulator in B cells. Nature Immunol 2017; 18: 303-312.

136. Jennelle LT, Dandekar AP, Magoro T, Hahn YS. Immunometabolic signaling pathways contribute to macrophage and dendritic cell function. Crit Rev Immunol 2016; 36: 379-394.
137. Jeon SM, Hay N. The double-edged sword of AMPK signaling in cancer and its therapeutic implications. Arch Pharm Res 2015; 38: 346-57.
138. Jin L, Alesi GN, Kang S. Glutaminolysis as a target for cancer therapy. Oncogene 2015; 35: 3619-3625.
139. Johnson MO, Wolf MM, Madden MZ, Andrejeva G, Sugiura A, Contreras DC, et al. Distinct regulation of Th17 and Th1 cell differentiation by glutaminase-dependent metabolism. Cell 2018; 175: 1780-95.
140. Jones DD, Gaudette BT, Wilmore JR, Chernova I, Bortnick A, Weiss BM, et al. mTOR has distinct functions in generating versus sustaining humoral immunity. J Clin Investigation 2016; 126: 4250-61.
141. Jones DD, Wilmore JR, Allman D. Cellular dynamics of memory B cell populations: IgM+ and IgG+ memory B cells persist indefinitely as quiescent cells. J Immunol. 2015; 195: 4753-59.
142. Kaadige MR, Looper RE, Kamalanaadhan S, Ayer DE. Glutamine-dependent anapleurosis dictates glucose uptake and cell growth by regulating MondoA transcriptional activity. PNAS 2009; 106: 14878-83.
143. Kedl RM, Kappler JW, Marrack P. Epitope dominance, competition and T cell affinity maturation. Curr Opin Immunol 2003; 15: 120-127.
144. Kelly B, O'Neill LAJ. Metabolic reprogramming in macrophages and dendritic cells in innate immunity. Cell Research 2015; 25: 771-784.
145. Khalsa JK, Chawla AS, Prabhu SB, Vats M, Dhar A, Dev G. Functionally significant metabolic differences between B and T lymphocyte lineages. Immunol 2019; 158: 104-120.
146. Khodadadi L, Cheng Q, Radbruch A, Hiepe F. The maintenance of memory plasma cells. Frontiers in Immunol 2019; 10: 1-15.
147. Kim A, Hartman IZ, Poore B, Boronina T, Cole RN, Song N, et al. Divergent paths for the selection of immunodominant epitopes from distinct antigenic sources. Nat Commun 2014; 5: 1-16.
148. Kim D, Sarbassov DD, Ali SM, King JE, Latek RR, King JE, et al. mTOR interacts with raptor to form a nutrient-sensitive complex that signals to the cell growth machinery. Cell 2002; 110: 163-175.
149. Kim J, Kundu M, Viollet B, Guan K. AMPK and mTOR regulate autophagy through direct phosphorylation of Ulk1. Nature Cell Biology 2011; 13: 132-141.
150. Kishton RJ, Barnes CE, Nichols AG, Cohen S, Gerriets VA, Siska PJ, et al. AMPK is essential to balance glycolysis and mitochondrial metabolism to control T-ALL cell stress and survival. Cell Metabolism 2016; 23: 649-662.
151. Klingman JD, Handler P. Partial purification and properties of renal glutaminase. J Biol Chem 1958; 232: 369-380.
152. Kojima H, Kobayashi A, Sakurai D, Kanno Y, Hase H, Takahashi R, et al. Differentiation stage-specific requirement in hypoxia-inducilbe factor-1α-regulated glycolytic pathway during murine B cell development in bone marrow. J Immunol 2009; 184; 154-163.

153. Konjar S, Veldhoen M. Dynamic metabolic state of tissue resident CD8 T cells. Front Immunol 2019; 10: 1-10.
154. Koo SH, Flechner L, Qi L, Zhang X, Screaton RA, Jeffries S et al. The CREB coactivator TORC2 is a key regulator of fasting glucose metabolism. Nature 2005; 437: 1109–11.
155. Kuraoka M, Schmidt AG, Nojima T, Feng F, Watanabe A, Kitamura D, et al. Complex antigens drive permissive clonal selection in germinal centers. Immunity. 2016; 44: 542-552.
156. Laker RC, Drake JC, Wilson RJ, Lira VA, Lewellen BM, Ryall KA, et al. Ampk phosphorylation of Ulk1 is required for targeting of mitochondria to lysosomes in exercise-induced mitophagy. Nat Commun 2017; 8: 1-13.
157. Lalor PA, Nossal GJ, Sanderson RD, McHeyzer-Williams MG. Functional and molecular characterization of single, (4-hydroxy-3-nitrophenyl-acetyl (NP)-specific, IgG1+ B cells from antibody-secreting and memory B cell pathways in the C57BL/6 immune response to NP. Eur J Immunol 1992; 11: 3001-3011.
158. Lam WY, Becker AM, Kennerly KM, Wong R, Curtis JD, Llufrio EM, et al. Mitochondrial pyruvate import promotes long-term survival of antibody-secreting plasma cells Immunity 2016; 19: 60-73.
159. Lam WY, Bhattacharya D. Metabolic links between plasma cell survival, secretion, and stress. Trends in Immunol 2018; 38; 19-27.
160. Lam WY, Jash A, Yao C, D'Souza L, Wong R, Nunley RM, et al. Metabolic and transcriptional modules independently diversify plasma cell lifespan and function. Cell Rep 2018; 24: 2479-92.
161. Landsverk OJ, Snir O, Casado RB, Richter L, Mold JE, Réu P. Antibody-secreting plasma cells persist for decades in human intestine. J Exp Med 2017; 309-317.
162. Lazarski CA, Chaves FA, Jenks SA, Wu S, Richards KA, Weaver JM, et al. The kinetic stability of MHC class II: peptide complexes is a key parameter that dictates immunodominance. Immunity 2005; 23: 29-40.
163. Le A, Lane AN, Hamaker M, Bose S, Gouw A, Barbi J, et al. Glucose-independent glutamine metabolism via TCA cycling for proliferation and survival in B-cells. Cell Metab 2012; 15: 110-121.
164. Le A, Udupa S, Zhang C. The metabolic interplay between cancer and other diseases. Trends in Cancer 2019; 5: 809-821.
165. Leclerc I, Lenzner C, Gourdon L, Vaulont S, Kahn A, Viollet B. Hepatocyte nuclear factor-4 alpha involved in type 1 maturity-onset diabetes of the young is a novel target of AMP-activated protein kinase. Diabetes 2001; 50: 1515–21.
166. Lee JY, Kim WK, Bae KH, Lee SC, Lee EW. Lipid metabolism and ferroptosis. Biology (Basel) 2021; 184: 1-16.
167. Lee K, Heffington L, Jellusova J, Nam KT, Raybuck A, Cho S, et al. Requirement for Rictor in homeostasis and function of mature B lymphoid cells. Blood 2013; 122: 2369-79.
168. Lee SY, Moon SJ, Kim EK, Seo HB, Yang, EJ, Son HJ, et al. Metformin suppresses systemic autoimmunity in Roquinsan/san mice through inhibiting B cell differentiation into plasma cells via regulation of AMPK/mTOR/STAT3. J Immunol 2017; 198: 2661-2670.

169. Lepez A, Pirnay T, Denanglaire S, Perez-Morga D, Vermeersch M, Leo O. Long-term homeostatic T cell proliferation is driven by AMPK-dependent regulation of oxygen reactive species. Sci Reports 2020; 10: 1-14.
170. Leprivier G, Rotblat B. How does mTOR sense glucose starvation? AMPK is the usual suspect. Cell Death Discovery 2020; 27: 1-5.
171. Levene PA, Meyer GM. The action of leucocytes on glucose. J Biol Chem 1912; 361-70.
172. Li H, Zhou Y, Li L, Li S, Long D, Chen X, et al. HIF-1α protects against oxidative stress by directly targeting mitochondria. Redox Biology 2019; 25: 1-15.
173. Li N, Huang D, Lu N, Luo L. Role of the LKB1/AMPK pathway in tumor invasion and metastasis in cancer cells. Oncol Rep 2015; 34:2821-26.
174. Li X, Egervari G, Wang Y, Berger SL, Lu Z. Regulation of chromatin and gene expression by metabolic enzymes and metabolites. Nat Reviews Mol Cell Biol 2018; 19: 563-578.
175. Liberti MV, Locasale JW. The Warburg effect: how does it benefit cancer cells? Trends Biochem Sci 2016; 41: 211-218.
176. Lin MT, Beal MF. The oxidative damage theory of aging. Clin Neuro Res 2003; 2: 305-315.
177. Ling NXY, Kaczmarek A, Hoque A, Davie E, Ngoei KRW, Morrison KR. mTORC1 directly inhibits AMPK to promote cell proliferation under nutrient stress. Nat Metabolism 2020; 2: 41-49.
178. Liu G, Summer R. Cellular metabolism in lung health and disease. Annu Rev Physiol 2019; 81: 403-428.
179. Liu T, Kishton RJ, Macintyre AN, Gerriets VA, Xiang H, Liu X, et al. Glucose transporter 1-mediated glucose uptake is limiting for B-cell lymphoblastic leukemia anabolic metabolism and resistance to apoptosis. 2014; 5: 1-13.
180. Liu W, Meckel T, Tolar P, Sohn HW, Pierce SK. Intrinsic properties of immunoglobulin IgG1 isotype-switched B cell receptors promote microclustering and the initiation of signaling. Immunity 2010; 32: 778-789.
181. Liu Y, Bai F, Liu N, Zhang B, Qin F, Tu T, et al. Metformin improves lipid metabolism and reverses the Warburg effect in a canine model of chronic atrial fibrillation. BMC Cardiovascular Disorders 2020; 20: 1-9.
182. Lucher LA and Lego T. Use of water soluble-fluor sodium salicylate for fluorographic detection of tritium in thin-layer chromatograms and nitrocellulose blots. Analytical Biochemistry. 1988; 178: 327-330.
183. Luengo A, Gui DY, Vander Heiden MG. Targeting metabolism for cancer therapy. Cell Chem Biol 2017; 24: 1161-1180.
184. Ma EH, Poffenberger MC, Wong AHT, Jones RG. The role of AMPK in T cell metabolism and function. Curr Opin Immunol 2017; 46: 45-52.
185. Ma EH, Verway MJ, Johnson RM, Roy DG, Steadman M, Hayes S, et al. Metabolic profiling using stable isotope tracing reveals distinct patterns of glucose utilization by physiologically activated CD8+ T cells. Immunity 2019; 51: 856-870.
186. Macintyre AN, Gerriets VA, Nichols AG, Michalek RD, Rudolph MC, Deoliveira D, et al. The gluocose transporter Glut1 is selectively essential for CD4 T cell activation and effector function. Cell Metab. 2014; 20: 61-72.

187. Macintyre AN, Rathmell JC. Activated lymphocytes as a metabolic model for carcinogenesis. Cancer Metab 2013; 1: 1-12.
188. MacIver NJ, Blagih J, Saucillo DC, Tonelli L, Griss T, Rathmell JC, et al. The liver kinase B1 is a central regulator of T cell development, activation, and metabolism. J Immunol 2011; 187: 4187-98.
189. MacLennan ICM. Germinal centers. Annu Rev Immunol 1994: 12: 117-139.
190. MacLennan ICM, Johnson GD, Liu YJ, Gordon J. The heterogeneity of follicular reactions. Germinal Centres 1991: 142; 253-257.
191. Mafra ACP, Dias SMG. Several faces of glutaminase regulation in cells. Cancer Research 2019; 79: 1302-1304.
192. Manz RA, Thiel A, Radbruch A. Lifetime of plasma cells in the bone marrow. Nature 1997; 388: 133-134.
193. Maratou E, Dimitriadis G, Kollias A, Boutati E, Lambadiari V, Mitrou P, et al. Glucose transporter expression on the plasma membrane of resting and activated white blood cells. Eur J Clin Invest 2007; 37: 282-290.
194. Maric M, Arunachalam B, Phan UT, Dong C, Garrett WS, Cannon KS, et al. Defective antigen processing in GILT-free mice. Science 2001; 294: 1361-1365.
195. Marshall S, Bacote V, Traxinger RR. Discovery of a metabolic pathway mediating glucose-induced desensitization of the glucose transport system. J Biol Chem 1991; 266: 4706-4712.
196. Martinez-Martin N, Maldonado P, Gasparrini F, Frederico B, Aggarwal S, Gaya M. A switch from canonical to noncanonical autophagy shapes B cell responses. Science 2017; 355: 641-647.
197. Masle-Farquhar E, Bröer A, Yabas M, Enders A, Bröer S. ASCT2 (SLC1A5)-deficient mice have normal B-cell development, proliferation, and antibody production. Frontiers in Immunol 2017; 8: 1-11.
198. Mayer A, Denanglaire S, Viollet B, Leo O, and Andris F. AMP-activated protein kinase regulates lymphocyte responses to metabolic stress but is largely dispensable for immune cell development and function. Euro J Immunol 2008; 38: 948-956.
199. Mazat J, Ransac S. The fate of glutamine in human metabolism. The interplay with glucose in proliferating cells. Metabolites 2019; 81: 1-22.
200. Mendoza P, Martinez-Martin N, Bovolenta ER, Reyes-Garau D, Hernansanz-Agustin P, Delgado P, et al. R-Ras2 is required for the germinal center formation to aid B cells during energetically demanding processes. Sci Signal 2018; 11: 1-15.
201. Mensah FF, Armstrong CW, Reddy V, Bansal AS, Berkovitz S, Leandro MJ, et al. CD24 expression and B cell maturation shows a novel link with energy metabolism: potential implications for patients with myalgic encephalomyelitis/chronic fatigue syndrome. Front Immunol. 2018; 9: 1-14.
202. Meric-Bernstam F, Lee RJ, Carthon BC, Iliopoulos O, Mier JW, Patel MR. CB-839, a glutaminase inhibitor, in combination with cabozantinib in patients with clear cell and papillary metastatic renal cell cancer: results of a phase I study. Renal Cell Cancer 2019; 37: 549.
203. Metallo CM, Vander Heiden MG. Understanding metabolic regulation and its influence on cell physiology. Mol Cell 2013; 49: 388-398.

204. Michalek RD, Gerriets VA, Jacobs SR, Macintyre AN, MacIver NJ, Mason EF, et al. Cutting edge: distinct glycolytic and lipid oxidative metabolic programs are essential for effector and regulator CD4+ T cell subsets. J Immunol 2011; 186: 3299-303.
205. Miettinen TP and Björklund M. Mitochondrial function and cell size: an allometric relationship. Trends in Cell Biology 2017; 27: 393-402.
206. Mihaylova MM, Shaw RJ. The AMPK signaling pathway coordinates cell growth, autophagy and metabolism. Nature Cell Biol 2011; 13: 1016-23.
207. Mihaylova MM, Vasquez DS, Ravnskjaer K, Denechaud PD, Yu RT, Alvarez JG et al. Class IIa histone deacetylases are hormone-activated regulators of FOXO and mammalian glucose homeostasis. Cell 2011: 145: 607-621.
208. Montero AJ, Jassem J. Cellular redox pathways as a therapeutic target in the treatment of cancer. Drugs; 2011; 30: 1385-1396.
209. Mookerjee SA, Goncalves RL, Gerencser AA, Nicholls DG, Brand MD. The contributions of respiration and glycolysis to extracellular acid production. BBA Bioenergetics 2015; 1847: 171-81.
210. Moon JJ, Chu HH, Pepper M, McSorley SJ, Jameson SC, Kedl RM, et al. Naïve $CD4^+$ T cell frequency varies for different epitopes and predicts repertoire diversity and response magnitude. Immunity 2007; 27: 203-13.
211. Munday MR, Campbell DG, Carling D, Hardie DG. Identification by amino acid sequencing of three major regulatory phosphorylation sites on rat acetyl-CoA carboxylase. Eur J Biochem 1988; 175: 331-338.
212. Murera D, Arbogast F, Arnold J, Bouis D, Muller S, F. Gros. CD4 T cell autophagy is integral to memory maintenance. Sci Rep 2018; 8: 1-13.
213. Muri J, Thut H, Heer S, Krueger CC, Bornkamm GW, Bachmann MF, et al. The thioredoxin-1 and glutathione/glutaredoxin-1 systems redundantly fuel murine B-cell development and responses. Eur J Immunol 2019; 49: 709-723.
214. Nakajima H, Kunimoto H. TET2 as an epigenetic master regulator for normal and malignant hematopoiesis. Cancer Sci 2014; 105: 1093-99.
215. Newsholme P, Curi R, Gordon S, Newsholme EA. Metabolism of glucose and glutamine, long-chain fatty acids and ketone bodies by murine macrophages. Biochemical Journal 1986; 239: 121-125.
216. Nguyen DC, Joyner CJ, Sanz I, Lee FE. Factors affecting early antibody secreting cell maturation into long-lived plasma cells. Front Immunol 2019; 10: 1-15.
217. Ni F, Yu WM, Li Z, Graham DK, Jin L, Kang S, et al. Critical role of ASCT2-mediated amino acid metabolism in promoting leukaemia development and progression. Nat Metab 2019; 1: 390-403.
218. Nicklin P, Bergman P, Zhang B, Triantafellow E, Wang H, Nyfeler B, et al. Bidirectional transport of amino acids regulates mTOR and autophagy. Cell 2009; 136: 521-534.
219. Nojima T, Haniuda K, Moutai T, Matsudaira M, Mizokawa S, Shiratori I, et al. In-vitro derived germinal centre B cells differentially generate memory B or plasma cells in vivo. Nature Communications. 2011; 465: 1-11.
220. Nuñez G, Hockenbery D, McDonnell TJ, Sorensen CM, Korsmeyer SJ. Bcl-2 maintains B cell memory. Nature 1991; 353: 71-73.

221. O'Conner B, Vogel LA, Zhang W, Loo W, Shnider D, Lind EF, et al. Imprinting the fate of antigen-reactive B cells through the affinity of the B cell receptor. J Immunol 2006; 177: 1-21.
222. O'Neill LAJ, Kishton RJ, Rathmell JC. A guide to immunometabolism for immunologists. Nat Rev Immunol 2016; 16: 553-565.
223. O'Sullivan TE, Johnson LR, Kang HH, Sun JC. BNIP3- and BNIP3L-mediated mitophagy promotes the generation of natural killer cell memory. Immunity 2015; 43: 331-342.
224. Onnis A, Cianfanelli V, Cassioli C, Samardzic D, Pelicci PG, Cecconi F. The pro-oxidant adaptor p66SHC promotes B cell mitophagy by disrupting mitochondrial integrity and recruiting LC3-II. Autophagy 2018; 14: 2117-38.
225. Pacella I, Procaccini C, Focacetti C, Miacci S, Timperi E, Faicchia D, et al. Fatty acid metabolism complements glycolysis in the selective regulatory T cell expansion during tumor growth. PNAS 2018; 115: 6546-6555.
226. Pålsson-McDermott EM, O'Neill LAJ. Targeting immunometabolism as an anti-inflammatory strategy. Cell Res 2020; 30: 300-314.
227. Patel CH, Leone RD, Horton MR, Powell JD. Targeting metabolism to regulate immune responses in autoimmunity and cancer. Nat Rev Drug Discovery 2019; 18: 669-688.
228. Pavlova NN, Thompson CB. The emerging hallmarks of cancer metabolism. Cell Metab 2016; 23: 27-47.
229. Pearce EL, Pearce EJ. Metabolic pathways in immune cell activation and quiescence. Immunity 2013; 38: 633-643.
230. Pearce EL, Poffenberger MC, Chang CH, Jones RG. Fueling immunity: insights into metabolism and lymphocyte function. Science 2013; 342: 1-9.
231. Pearce EL, Walsh MC, Cejas PJ, Harms GM, Shen H, Wang LS, et al. Enhancing CD8 T-cell memory by modulation fatty acid metabolism. Nature 2009; 460: 103-107.
232. Pengo N, Scolari M, Oliva L, Milan E, Mainoldi F, Raimondi A, et al. Plasma cells require autophagy for sustainable immunoglobulin production. Nature Immunology. 2013; 14: 298-305.
233. Pérez L, McLetchie S, Gardiner GJ, Deffit SN, Zhou D, Blum JS. LAMP-2C inhibits MHC Class II presentation of cytoplasmic antigens by disrupting chaperone-mediated autophagy. 2016; 196: 2457-65.
234. Pfleger J, He M, Abdellatif M. Mitochondrial complex II is a source of the reserve respiratory capacity that is regulated by metabolic sensors and promotes cell survival. Cell Death and Disease 2015; 6: 1-14
235. Pickles S, Vigié P, Youle RJ. Mitophagy and quality control mechanisms in mitochondrial maintenance. Current Biology 2018; 28: 170-185.
236. Piranavan P, Bhamra M, Peri A. Metabolic targets for treatment of autoimmune diseases. Immunometabolism 2020; 2: 1-26.
237. Pircher A, Treps L, Bodrug N, Carmeliet P. Endothelial cell metabolism: a novel player in atherosclerosis? Basic principles and therapeutic opportunities. Atherosclerosis 2016; 253: 247-257.
238. Polet F, Martherus R, Corbet C, Pinto A, Feron O. Inhibition of glucose metabolism prevents glycosylation of the glutamine transporter ASCT2 and

promotes compensatory LAT1 upregulation in leukemia cells. Oncotarget 2016; 19: 46371-83.
239. Pollizzi KN, Sun IH, Patel CH, Lo YC, Oh MH, Waickman AT, et al. Asymmetrical inheritance of mTORC1 kinase activity during division dictates CD8+ T cell differentiation. Nat Immunol 2016; 17: 704-711.
240. Porporato PE, Filigheddu N, Pedro JM, Kroemer G, Galluzzi L. Mitochondrial metabolism and cancer. Cell Research 2017; 28: 265-280.
241. Pracht KJ, Meinzinger P, Daum SR, Schulz D, Reimer M, Hauke E. A new staining protocol for detection of murine antibody-secreting plasma cell subsets by flow cytometry. Eur J Immunol 2017; 47: 1389-92.
242. Pua HH, Guo J, Komatsu M, He YW. Autophagy is essential for mitochondrial clearance in mature T lymphocytes. J Immunol. 2009; 182: 4046-55.
243. Puchowicz MA, Bederman IR, Comte B, Yang D, David F, Stone E. Zonation of acetate labeling across the liver: implications for studies of lipogenesis by MIDA. AM J Physiol 1999; 277: 1022-1027.
244. Quéméneur L, Gerland LM, Flacher M, Ffrench M, Revillard JP, Genestier L. Differential control of cell cycle, proliferation, and survival of primary T lymphocytes by purine and pyrimidine nucleotides. J Immunol 2003; 170: 4986-95.
245. Rabinowitz JD, White E. Autophagy and Metabolism. Science 2010; 330: 1344-48.
246. Rao E, Zhang Y, Zhu G, Hao J, Persson XMT, Egilmez NK, et al. Deficiency of AMPK in CD8+ T cells suppresses their anti-tumor function by inducing protein phosphatase-mediated cell death. Oncotarget 2015; 6: 7944-58.
247. Raso F, Sagadiev S, Du S, Gage E, Arkatkar T, Metzler G, et al. αv Integrins regulate germinal center B cell responses through noncanonical autophagy. J Clin Investigation 2018; 128: 4163-78.
248. Raybuck AL, Cho S, Li J, Rogers MC, Lee K, Williams CL, et al. B cell-intrinsic mTORC1 promotes germinal center-defining transcription factor gene expression, somatic hypermutation, and memory B cell generation in humoral immunity. J Immunol 2018; 200: 2627-39.
249. Raybuck AL, Lee K, Cho SH, Li J, Thomas JW, Boothby MR. mTORC1 as a cell-intrinsic rheostat that shapes development, preimmune repertoire, and function of B lymphocytes. FASEB J 2019; 33: 13202-215.
250. Reinfeld BI, Madden MZ, Wolf MM, Chytil A, Bader JE, Muir A, et al. Cell-programmed nutrient partitioning in the tumour microenvironment. Nature 2021; 1-7.
251. Rickert RC, Roes J, Rajewsky K. B lymphocyte-specific, Cre-mediated mutagenesis in mice. Nucleic Acids Res 1997; 25: 1317-18.
252. Roco JA, Mesin L, Binder SC, Nefzger C, Gonzalez-Figueroa P, Canete PF, et al. Class-switch recombination occurs infrequently in germinal centers. Immunity 2019; 51: 337-350.
253. Rolf J, Zarrouk M, Finlay DK, Foretz M, Viollet B, Cantrell DA. AMPKα1: a glucose sensor that controls CD8 T-cell memory. Eur J Immunol 2013; 43: 889-96.

254. Sakano K, Kiyota S, Yazak Y. Acidification and alkalinization of culture medium by Catharanthus roseus cells. Plant Cell Physiol 1997; 38: 1053-1059.
255. Salminen A, Kaarniranta K, Kauppinen A. AMPK and HIF signaling pathways regulate both longevity and cancer growth: the good news and the bad news about survival mechanisms. Biogerontology 2016; 17: 655-680.
256. Sandoval H, Kodali S, and Wang J. Regulation of B cell fate, survival, and function by mitochondria and autophagy. Mitochondrion 2018; 41: 58-65.
257. Schatz DG, Oettinger MA, Baltimore D. The V(D)J recombination activating gene, RAG-1. Cell 1989; 59: 1035-1048.
258. Schmidt-Supprian, M. and Rajewsky, K. Vagaries of conditional gene targeting. Nat Immunol 2007; 8: 665-668.
259. Schoenhals M, Jourdan M, Bruyer A, Kassambara A, Klein B, Moreaux J. Hypoxia favors the generation of human plasma cells. Cell Cycle 2017; 16: 1104-17.
260. Schuiveling M, Vazirpanah N, Radstake TR, Zimmerman M, Broen JC. Metformin, a new era for an old drug in the treatment of immune mediated disease? Curr Drug Targets 2018; 19: 945-959.
261. Sena LA, Chandel NS. Physiological roles of mitochondrial reactive oxygen species. Mol Cell 2012; 48: 158-167.
262. Shackelford DB, Shaw RJ. The LKB1-AMPK pathway: metabolism and growth control in tumour suppression. Nat Rev Cancer 2009; 9: 563-575.
263. Shaw RJ, Kosmatka M, Bardeesy N, Hurley RL, Witters LA, DePinho Ra, et al. The tumor suppressor LKB1 kinase directly activates AMP-activated kinase and regulates apoptosis in response to energy stress. PNAS 2004; 101: 3329-35.
264. Shinnakasu R, Inoue T, Kometani K, Moriyama S, Adachi Y, Nakayama M, et al. Regulated selection of germinal-center cells into the memory B cell compartment. Nat Immunol 2016; 17: 861-869.
265. Shlomchik MJ, Weisel F. Germinal center selection and the development of memory B and plasma cells. Immunol Reviews 2012; 247: 52-63.
266. Sica V, Pedro JM, Izzo V, Pol J, Pierredon S, Enot D, et al. Lethal poisoning of cancer cells by respiratory chain inhibition plus dimethyl α-ketoglutarate. Cell Reports 2019; 27: 820-834.
267. Sil P, Muse G, Martinez J. A ravenous defense: canonical and non-canonical autophagy in immunity. Curr Opin Immunol 2018; 50: 21-31.
268. Sinclair LV, Barthelemy C, Cantrell DA. Single cell glucose uptake assays: a cautionary tale. Immunometabolism 2020; 2: 1-13.
269. Singh A, Gu J, Yanamadala V, Czuczman MS, Hernandez-Ilizaliturri FJ. Metformin lowers the mitochondrial potential of lymphoma cells and its use during front-line rituximab-based chemo-immunotherapy improves the clinical outcome of diffuse large B-cell lymphoma. Blood 2013; 122: 1825.
270. Slifka MK, Ahmed R. Long-term humoral immunity against viruses: revisiting the issue of plasma cell longevity. Immunity 1998; 8:363-72.
271. Smith KG, Light A, Nossal GL, Tarlinton DM. The extent of affinity maturation differs between the memory and antibody-forming cell compartments in the primary immune response. EMBO J 1997; 16: 2996-3006.

272. Son J, Cho YW, Woo YJ, Baek YA, Kim EJ, Cho Y, et al. Metabolic reprogramming by the excessive AMPK activation exacerbates antige-specific memory CD8+ T cell differentiation after acute lymphocytic choriomeningitis virus infection. Immune Netw 2019; 19: 1-11.
273. Song S, Matthias PD. The transcriptional regulation of germinal center formation. Font Immunol 2018; 9: 1-9.
274. Spencer JA, Ferraro F, Roussakis E, Klein A, Wu J, Runnels JM, et al. Direct measurement of local oxygen concentration in the bone marrow of live animals. Nature 2014; 508: 269-273.
275. Stapleton D, Mitchelhill KI, Gau G, Widmer J, Michell BJ, Teh T, et al. Mammalian AMP-activated protein kinase subfamily. J Biol Chem 1996; 271: 611-614.
276. Stoppani J, Hildebrandt AL, Sakamoto K, Cameron-Smith D, Goodyear LJ, Neufer PD. AMP-activated protein kinase activates transcription of the UCP3 and HKII genes in rat skeletal muscle. AM J Physiol Endocrinol Metab 2002; 283: 1239-48.
277. Stuani L, Sabatier M, Sarry JE. Exploiting metabolic vulnerabilities for personalized therapy in acute myeloid leukemia. MBC Biol 2019; 17: 1-17.
278. Stumvoll M, Perriello G, Meyer C, Gerich J. Role of glutamine in human carbohydrate metabolism in kidney and other tissues. Kidney International 1999; 55: 778-792.
279. Sukumar M, Liu J, Ji Y, Subramanian M, Crompton JG, Yu Z, et al. Inhibiting glycolytic metabolism enhances CD8+ T cell memory and antitumor function. J Clin Invest 2013; 123: 4479-88.
280. Symington J, Green M, and Brackmann K. Immunoautoradiographic detection of proteins after electrophoretic transfer from gels to diazo-paper: analysis of adenovirus encoded proteins. PNAS. 1981; 78: 177-81.
281. Sze DM, Toellner KM, de Vinuesa CG, Taylor DR, MacLennan IC. Intrinsic constraint on plasmablast growth and extrinsic limits of plasma cell survival. J Exp Med 2000; 192: 813-822.
282. Tachibana H, Kim J, Shirahata S. Building high affinity human antibodies by altering glycosylation ion the light variable region in N-acetylglucosamine-supplemented hybridoma cultures. Cytotechnology 1997; 23: 151-159.
283. Takemori T, Kaji T, Takahashi Y, Shimoda M, Rajewsky K. Generation of memory B cells inside and outside germinal centers. Eur J Immunol 2014; 44: 1258-1264.
284. Tamargo-Gómez I, Mariño G. AMPK: regulation of metabolic dynamics in the context of autophagy. Int J of Mol Sci 2018; 19: 1-16.
285. Tamás P, Hawley SA, Clarke RG, Mustard KJ, Green K, Hardie DG, et al. Regulation of the energy sensor AMP-activated protein kinase by antigen receptor and Ca2+ in T lymphocytes. J Exp Med 2006; 203: 1665-1670.
286. Tangye SG and Tarlinton DM. Memory B cells: effectors of long-lived immune responses. Eur J Immunol 2009; 39: 2065-2075.
287. Taylor EB, An D, Kramer HF, Yu H, Fujii NL, Roeckl KS, et al. Discovery of TBC1D1 as an insulin-, AICAR-, and contraction-stimulated signaling nexus in mouse skeletal muscle. J Biol Chem 2008; 283: 9787-96.

288. Tellier J, Shi W, Minnich M, Liao Y, Crawford S, Smyth GK, et al. Blimp-1 controls plasma cell function through the regulation of immunoglobulin secretion and the unfolded protein response. Nat Immunol 2016; 17: 323-330.
289. Teng G, Papavasiliou FN. Immunoglobulin Somatic Hypermutation. Annual Review of Genetics 2007; 41: 107-120.
290. Teperino R, Schoonjans K, Auwerx J. Histone methyl-transferases and demethylases; can they link metabolism and transcription? Cell Metab 2010; 12: 321-327.
291. Tesi A, Pretis S, Furlan M, Filipuzzi M, Morelli MJ, Andronache A, et al. An early Myc-dependent transcriptional program orchestrates cell growth during B-cell activation. EMBO reports 2019; 20: 1-14.
292. Thornton C, Snowden MA, Carling D. Identification of a novel AMP-activated protein kinase beta subunit isoform that is highly expressed in skeletal muscle. J Biol Chem 1998; 273: 12443-50.
293. Tian W, Li W, Chen Y, Yan Z, Huang X, Zhuang H, et al. Phosphorylation of ULK1 by AMPK regulates translocation of ULK1 to mitochondria and mitophagy. FEBS Letters 2015; 589: 1847-54.
294. Tomayko MM, Steinel NC, Anderson SM, and Shlomchik. MJ. Cutting edge: hierarchy of maturity of murine memory B cell subsets. J. Immunol 2010; 181: 27-38.
295. Tripathi SC, Fahrmann JF, Vykoukal JV, Dennison JB, Hanash SM. Targeting metabolic vulnerabilities of cancer: small molecule inhibitors in clinic. Cancer Rep 2018; 2: 1-15.
296. Tsentalovich YP, Zelentsova EA, Yanshole LV, Yanshole VV, Odud IM. Most abundant metabolites in tissues of freshwater fish pike-perch (Sander lucioperca) Sci Reports 2020; 10: 1-12.
297. Tsui C, Martinez-Martin N, Gaya M, Maldonado P, Llorian M, Legrave NM, et al. Protein kinase C-β dictates B cell fate by regulating mitochondrial remodeling, metabolic reprogramming, and heme biosynthesis. Immunity 2018; 48: 1144-59.
298. Urbanczyk S, Stein M, Schuh W, Jäck HM, Mougiakakos D, Mielenz D. Regulation of energy metabolism during B lymphocyte development. Int J Mol Sci 2018; 19: 1-16.
299. Van der Windt GJ, Everts B, Chang C, Curtis JD, Freitas TC, Amiel E, et al. Mitochondrial respiratory capacity is a critical regulator of CD8+ T cell memory development. Immunity 2012; 36: 68-78.
300. Verbist KC, Guy CS, Milasta S, Liedmann S, Kaminski MM, Wang R, et al. Metabolic maintenance of cell asymmetry following division in activated T lymphocytes. Nature 2016; 21: 389-93.
301. Victora GD, Nussenzweig MC. Germinal centers. Annu Rev Immunol 2012; 30: 429-457.
302. Vieira P, Rajewsky K. The half-lives of serum immunoglobulins in adult mice. Eur J Immunol 1988; 18: 313-316.
303. Vijay R, Guthmiller JJ, Sturtz AJ, Surette FA, Rogers KJ, Sompallae RR, et al. Infection-induced plasmablasts are a nutrient sink that impairs humoral immunity to malaria. Nat Immunol 2020; 21: 790-801.

304. Waickman AT, Powell JD. mTOR, metabolism, and the regulation of T-cell differentiation and function. Immunol Rev 2012; 249: 43-58.
305. Walsh NC, Waters LR, Fowler JA, Lin M, Cunningham CR, Brooks DG, et al. LKB1 inhibition of NF-κB in B cells prevents T follicular helper cell differentiation and germinal center formation. EMBO Rep 2015; 16: 753-68.
306. Wan Z, Chen X, Chen H, Ji Q, Chen Y, Wang J. The activation of IgM- or isotype-switched IgG- and IgE-BCR exhibits distinct mechanical force sensitivity and threshold. eLife 2015; 4: 1-24.
307. Wang C, Li W, Drabek D, Okba N, Haperen R, Osterhaus A. A human monoclonal antibody blocking SARS-CoV-2 infection. Nat Communications 2020; 2251: 1-6.
308. Wang S, Dale GL, Song P, Viollet B, and Zou M. AMPKα1 deletion shortens erythrocyte life span in mice. J Biol Chem 2010; 285: 19976-85.
309. Wang YP, Li JT, Qu J, Yin M, Lei QY. Metabolite sensing and signaling in cancer. J Biol Chem 2020; 295: 11938-11946.
310. Warburg O, Gawehn K, Geissler AW. [Metabolism in leukocytes] Z Naturforsch B 1958; 13B: 515-516.
311. Warburg O. On the origin of cancer cells. Science 1956; 123: 309-314.
312. Wasinski F, Gregnani MF, Ornellas FH, Bacurau AVN, Câmara NO, Araujo RC, et al. Lymphocyte glucose and glutamine metabolism as targets of the anti-inflammatory and immunomodulatory effects of exercise. Mediators of Inflammation 2014; 2014: 1-10.
313. Waters LR, Ahsan FM, Hoeve J, Hong JS, Kim DN, Minasyan A, et al. Ampk regulates IgD expression but not energy stress with B cell activation. Scientific Reports. 2019; 9: 1-14.
314. Waters LR, Ahsan FM, Wolf DM, Shirihai O, Teitell MA. Initial B cell activation induces metabolic reprogramming and mitochondrial remodeling. iScience 2018; 5: 99-109.
315. Webster I, Friedrich OS, Lochner A, Huisamen B. AMP kinase activation and glut4 translocation in isolated cardiomyocytes. Cardiovasc J Afr 2010; 21: 72-78.
316. Weisel F, Shlomchik M. Memory B cells of mice and humans. Annu Rev Immunol. 2017; 35: 255-84.
317. Weisel FJ, Mullett SJ, Elsner RA, Menk AV, Trivedi N, Luo W, et al. Germinal center B cells selectively oxidize fatty acids for energy while conducting minimal glycolysis. Nat Immunol 2020; 21: 331-342.
318. West GB, Brown JH. The origin of allometric scaling laws in biology from genomes to ecosystems: towards a quantitative unifying theory in biological structure and organization. J Exp Biol 2005; 208: 1575-92.
319. West GB, Woodruff WH, Brown JH. Allometric scaling of metabolic rate from molecules and mitochondria to cells and mammals. PNAS 2002; 99: 2473-78.
320. William J, Euler C, Christensen S, Shlomchik MJ. Evolution of autoantibody responses via somatic hypermutation outside of germinal centers. Science 2002; 297: 2066-2070.
321. Wise DR, Thompson CB. Glutamine addiction: a new therapeutic target in cancer. Trends Biochem Sci 2010; 35: 427-433.

322. Wolpaw AJ, Dang CV. Exploiting metabolic vulnerabilities of cancer with precision and accuracy. 2017; 28: 201-212.
323. Woodland RT, Fox CJ, Schmidt MR, Hammerman PS, Opferman JT, Korsmeyer SJ, et al. Multiple signaling pathways promote B lymphocyte stimulator dependent B-cell growth and survival. Blood 2008; 111: 750-60.
324. Wu N, Zheng B, Shaywitz A, Dagon Y, Tower C, Bellinger G, et al. AMPK-dependent degradation of TXNIP upon energy stress leads to enhanced glucose uptake via GLUT1. Mol Cell 2013; 49: 1167-75.
325. Wu W, Tian W, Hu Z, Chen G, Huang L, Li W, et al. ULK1 translocates to mitochondria and phosphorylates FUNDC1 to regulate mitophagy. EMBO Reports 2014; 15: 566-575.
326. Xiao B, Deng X, Zhou W, Tan E. Flow cytometry-based assessment of mitophagy using mitotracker. Front Cell Neurosci 2016; 10: 1-4.
327. Yamaguchi S, Katahira H, Ozawa S, Nakamichi Y, Tanaka T, Shimoyama T. Activators of AMP-activated protein kinase enhance GLUT4 translocation and its glucose transport activity in 3T3-L1 adipocytes. Am J Physiol Endocrinol Metab. 2005; 289: 643-649.
328. Yoo HC, Yu YC, Sung Y, Han JM. Glutamine reliance in cell metabolism. Exp & Mol Medicine 2020; 52:1496-1516.
329. Yu X, Tsibane T, McGraw PA, House FS, Keefer CJ, Hicar MD, et al. Neutralizing antibodies derived from the B cells of 1918 influenza pandemic survivors. Nature 2008; 455: 532-536.
330. Yuan HX, Xiong Y, Guan KL. Nutrient sensing, metabolism, and cell growth control. Mol Cell 2013; 49: 379-387.
331. Yunis AA, Arimura GK. Enzymes of glycogen metabolism in white blood cells. Cancer Res 1964; 24: 489-492.
332. Zdzisińska B, Żurek A, Kandefer-Szerszeń. Alpha-ketoglutarate as a molecule with pleiotropic activity: well-known and novel possibilities of therapeutic use. Archivum Immunologiae et Therapiae Experimentalis 2017; 65: 21-36.
333. Zeng H, Chi H. mTOR signaling in the differentiation and function of regulatory and effector T cells. Curr Opin Immunol 2017; 46: 102-111.
334. Zhang CS, Hawley SA, Zong Y, Li M, Wang Z, Gray A. Fructose-1,6-bisphosphate and aldolase mediate glucose sensing by AMPK. Nature 2017; 548: 112-116.
335. Zheng D, MacLean PS, Pohnert SC. Knight JB, Olson AL, Winder WW et al. Regulation of muscle GLUT4 transcription by AMP-activated protein kinase. J Appl Physiol 2001; 91: 1073-1083.
336. Zhu H, Foretz M, Xie Z, Zhang M, Zhu Z, Xing J, et al. PRKAA1/AMPKα1 is required for autophagy-dependent mitochondrial clearance during erythrocyte maturation. Autophagy 2014; 10: 1522-34.
337. Zotto GD, Principi E, Antonini F, Baratto S, Panicucci C, Bruno C, et al. Comprehensive phenotyping of peripheral blood T lymphocytes in healthy mice. Cytometry A 2021; 99: 243-250.
338. Zuccarino-Catania GV, Sadanand S, Weisel FJ, Tomayko MM, Meng H, Kleinstein SH, et al. CD80 and PD-L2 define functionally distinct memory B cell

subsets that are independent of antibody isotype. Nat Immunology 2014; 15: 631-637.